



6-2022

Channeling Influence on Noise and Aerodynamic Performance of NACA 0012 Airfoil as a Possible Solution of Wind Turbines Noise

Hussein Khudhayer Mohammad
Western Michigan University

Follow this and additional works at: <https://scholarworks.wmich.edu/dissertations>



Part of the [Aerodynamics and Fluid Mechanics Commons](#)

Recommended Citation

Mohammad, Hussein Khudhayer, "Channeling Influence on Noise and Aerodynamic Performance of NACA 0012 Airfoil as a Possible Solution of Wind Turbines Noise" (2022). *Dissertations*. 3855.

<https://scholarworks.wmich.edu/dissertations/3855>

This Dissertation-Open Access is brought to you for free and open access by the Graduate College at ScholarWorks at WMU. It has been accepted for inclusion in Dissertations by an authorized administrator of ScholarWorks at WMU. For more information, please contact wmu-scholarworks@wmich.edu.



CHANNELING INFLUENCE ON NOISE AND AERODYNAMIC PERFORMANCE OF NACA 0012 AIRFOIL AS A POSSIBLE SOLUTION OF WIND TURBINES NOISE

Hussein Khudhayer Mohammad, Ph.D.

Western Michigan University, 2022

This work numerically and experimentally investigates the effect of using channels inside airfoils on the noise level as a possible resolution for aerodynamic noise generated by wind turbines. The work also investigates aerodynamic performance and turbulence around the employed airfoils. The results reveal that some of the samples show some improvement in reducing the aerodynamic noise. The reduction of the aerodynamic noise is explained as the trailing edge blowing injection that reduces the wake momentum deficit of the blade and reduces the pressure fluctuation which is responsible for noise production. Particularly, the angles of channel inclination with respect to the cord was the dominant factor that reduces the aerodynamic noise generated by wind turbines. Previous studies of supersonic channels show an increase in lift and decrease in drag. In this study, different sizes and directions of channels were created inside the NACA 0012 airfoil and have been tested under subsonic flow. The effect of these channels was investigated on both drag (D) and lift (L) coefficients experimentally and numerically. The channels were made at three different diameter sizes of 0.05, 0.08, and 0.1 inches and with four inclination angles of -1, 0, 2, and 3 degrees with respect to the chord. The results show an increase in drag coefficients and decrease in lift coefficients for all the channeled samples compared to the regular unchanneled airfoil, hence decreasing the ratio (L/D). In this study, with subsonic flow, the skin friction drag (viscous drag) is dominant, therefore the drag increases with the channels because it increased the skin friction area (wetted area) compared to the airfoil without channels.

This work is significant, especially for those people who live close to wind turbine farms, as this work deals with aerodynamic noise around the wind farms.

CHANNELING INFLUENCE ON NOISE AND AERODYNAMIC PERFORMANCE OF
NACA 0012 AIRFOIL AS A POSSIBLE SOLUTION OF WIND TURBINES NOISE

by

Hussein Khudhayer Mohammad

A dissertation submitted to the Graduate College
in partial fulfillment of the requirements
for the degree of Doctor of Philosophy
Mechanical and Aerospace Engineering
Western Michigan University
June 2022

Doctoral Committee:

Dr. Bade Shrestha, Ph.D., Chair
Dr. Koorosh Naghshineh, Ph.D.
Dr. Tianshu Liu, Ph.D.
Dr. Viktor Kilchyk, Ph.D.

Copyright by
Hussein Khudhayer Mohammad
2022

ACKNOWLEDGEMENTS

I would like to thank God for the perseverance, the diligence, and the opportunity to complete my work and earn my Ph.D. Degree. I would like to express my deepest gratitude to my advisor, Dr. Bade Shrestha, for his encouragement, support, and guidance, including the constructive feedback and discussions. I would like to thank the committee members, Dr. Liu Tianshu and Dr. Viktor Kilchyk, for their valuable efforts and useful direction, and Dr. Koorosh Naghshineh for providing me the necessary equipment and advice. I would like to thank Dr. Parviz Merati for allowing me to use his lab for my experimental work, and a special thanks to Latif Eyada Ibraheem for his collaboration and helping me with hot-wire anemometry. I would like to thank Alexa Nussio from the WMU Writing Center for her writing expertise and suggestion. I would also like to thank the volunteers, including Mustafa Kamal and Jonathan Gallee. Finally, I'd like to thank my wife, my children, and the rest of my family for always standing by me.

Hussein Khudhayer Mohammad

TABLE OF CONTENTS

ACKNOWLEDGEMENTS	ii
LIST OF TABLES	vii
LIST OF FIGURES	viii
CHAPTER	
1. INTRODUCTION	1
1.1 Introduction.....	1
1.2 Objective.....	6
2. LITERATURE REVIEW	7
2.1 Background.....	7
2.2 Sources of the aerodynamic noise in wind turbines.....	7
2.3 Noise reduction	10
2.4 Annoyance and health issues	15
2.5 Turbulence	17
2.6 Lift and Drag.....	18
3. THEORETICAL BACKGROUND	25
3.1 Introduction.....	25
3.2 Wind energy.....	26
3.3 Wind power.....	26
3.4 Wind profile power law	27
3.5 Basic acoustics	27
3.5.1 Sound properties.....	28
3.5.2 Physical description of the sound.....	28
3.5.2.1 Sound pressure level.....	28
3.5.2.2 Sound intensity level	29
3.5.2.3 Sound power level	30
3.5.2.4 Sound propagation and directivity	30
3.6 Some concepts of wind turbine.....	32
3.6.1 Actuator disc concept	33
3.7 Noise sources from wind turbines.....	36
3.7.1 Mechanical noise.....	36

Table of Contents—Continued

CHAPTER		
3.7.2	Aerodynamic noise.....	37
3.7.2.1	Low frequency noise	38
3.7.2.2	Turbulent inflow noise	39
3.7.2.3	Airfoil self-noise	40
4.	EXPERIMENTAL AND NUMERICAL WORK	43
4.1	Experimental work.....	43
4.1.1	The wind tunnel.....	43
4.1.2	The quiet room designing.....	44
4.1.3	Wind tunnel testing area (quiet room).....	48
4.1.4	Noise measurements.....	54
4.1.4.1	The microphones set up.....	54
4.1.5	Wind tunnel testing procedure	59
4.1.6	Test samples	60
4.1.6.1	NACA 0012 airfoil.....	60
4.1.7	Force measurements	62
4.1.7.1	Force balance.....	62
4.1.8	Velocity and turbulence measurements.....	65
4.1.8.1	The hot-wire anemometer	65
4.2	Method of numerical simulation.....	67
4.2.1	Computational domains.....	67
4.2.2	Grid-independent convergence (GIC).....	68
4.2.3	Turbulence model and governing equations	69
5.	THE RESULTS	72
5.1	Noise results.....	72
5.1.1	Background noise.....	72
5.1.2	Velocity influence	73
5.1.3	Angle of attack influence:	77
5.1.4	Channel influence.....	81
5.1.4.1	Channel direction influence	82
5.1.4.2	Diameter size Influence.....	83

Table of Contents—Continued

CHAPTER

- 5.1.5 Tonal noise 84
- 5.2 Force Results..... 86
 - 5.2.1 Calibration setup 86
 - 5.2.2 Lift results 90
 - 5.2.2.1 Influence of the Channel direction 90
 - 5.2.2.2 Influence of channels size 91
 - 5.2.3 Drag..... 92
 - 5.2.3.1 Influence of the Channel angle..... 92
 - 5.2.3.2 Influence of diameter size 93
 - 5.2.4 Lift/Drag..... 94
 - 5.2.4.1 Influence of the Channel angle..... 94
 - 5.2.4.2 Influence of diameter size 95
- 5.3 Turbulence Measurements 98
 - 5.3.1 Hot wire levels 98
 - 5.3.2 Turbulence Intensity measurements..... 99
- 5.4 Comparison between experimental and numerical results..... 101
 - 5.4.1 Noise results 101
 - 5.4.2 Force results: 101
- 5.5 Pressure fluctuation..... 102
- 5.6 The correlation between the noise and Turbulence intensity..... 107
 - 5.6.1 The correlation between the noise from microphone and Turbulence intensit. 107
 - 5.6.2 The correlation between the data ($1/v^2$) and Turbulence intensity..... 109
- 6. CONCLUSION AND FUTURE STUDIES 111
 - 6.1 Conclusion 111
 - 6.2 Recommendations and future studies: 113
- REFERENCES 114
- APPENDICES 120
 - A: Noise results 120
 - B: Force results 129
 - C: Turbulence results..... 145

Table of Contents—Continued

APPENDICES

D: Numerical results	151
E: Airfoil design	157
F: 2D design of the wind tunnel and quiet chamber	161
G: Arduino Code	162
H: Airfoil NACA0012 points from airfoil tools generator.....	165

LIST OF TABLES

1. Operational wind power capacity worldwide	3
2. Sound power level emitted from the wind turbine.....	25
3. Comparison of the Predictions of Lift and Drag Coefficients	70
4. A-weighting adjustments for one octave center frequencies for all the samples in flow velocity 15 m/s.	76
5. A-weighting adjustments for one octave center frequencies for all the samples in flow velocity 10 m/s AOA 10°.	76
6. A-weighting adjustments for one octave center frequencies for all the samples in flow velocity 5 m/s.	77
7. Overall SPL for all samples in flow velocities 5, 10, 15 m/s.....	77
8. overall SPL for all samples for AOA 5, 10 15 V 10 m/s.....	81
9. The result of lift calibration	87
10. The result of drag calibration.....	87
11. The results of drag and lift coefficients for different samples in flow velocity 5 m/s.....	89
12. The losing percentage in drag and lift channeled airfoils comparing to regular (V=5 m/s)...	97
13. Experimental and numerical results for overall noise.....	101
14. Experimental and numerical results of Lift and Drag Coefficients for some samples	102
15. The correlation between the noise (overall 0-10000 Hz) and turbulence intensity	108
16. The correlation between the turbulence intensity and overall noise data come from the pressure ($1/v^2$).....	110

LIST OF FIGURES

1. Operational wind power capacity worldwide	4
2. A-weighted sound power levels in one third octave bands for turbines 2.5, 5, and 10 MW	8
3. The correlation between turbulence intensity and sound pressure level [Steven Buck].....	8
4. NACA 0012 noise versus angle of attack for different Reynolds numbers.....	9
5. Leading edge and trailing edge feathers of the owl	10
6. The one-third-octave band frequency spectrum of flight noise.	11
7. Trailing edge air injection and supply	11
8. Aerodynamic noise generated from the airfoil at various angles of attack.....	12
9. Using porous material on the trailing edge [Geyer et al].....	13
10. Trailing edge noise level of airfoils with different extents of the porous material, as a function of Strouhal number. Black dots: non porous airfoil, AOA = 0°	14
11. Non-flat plate type trailing edge serrations [Chong et al].....	15
12. SPL for indoor (blue) and outdoor (red) noise.....	16
13. Drag coefficient vs angle of attack for no-channel and channel airfoils in: Mach=2.4 and h=12 km for laminar flow	19
14. Drag coefficient vs angle of attack for no-channel and channel airfoils in: Mach=2.4 and h=12 km for turbulent flow	20
15. Sphere cone with a channel in the leading edge.	21
16. Artificially blunted leading edge (ABLE) airfoils	21
17. The airfoil details	32
18. Axial velocity and pressure development before and after the rotor	34
19. Flow around a cylindrical wind turbine tower	39
20. Size of the turbulent eddies and blade loading	40
21. Kind of airfoil self-noise.....	41

List of Figures—Continued

22. The geometry of 1 cubic meter chamber size with 13 and 26 cm diameter outlet	44
23. The counter of velocity magnitude in (m/s) for both of the two chambers	45
24. The velocity vectors magnitude for both of the two chambers.....	46
25. The geometry of 9 cubic meter chamber size with 13 and 26 cm diameter outlet	46
26. The counter of velocity magnitude in (m/s) for both of the two chambers	47
27. The velocity vectors magnitude for both of the two chambers.....	47
28. Quiet crea modeled in AutoCAD in 3D.....	49
29. The plywood used to build the structure of the walls and ceiling	50
30. Middle opening section was where the wind tunnel generator would be placed.....	51
31. The first layer of foam (Volara Foam).....	52
32. The second layer of foam (Wedge Foam).....	52
33. The third layer of foam to add further protection from exterior noises	53
34. Quiet Room Completed	54
35. The microphones set up	55
36. ½ inch Infrasound Microphone System Outline Drawing	57
37. ½” Microphones being calibrated by Larson Davis CAL200.....	57
38. NI-9234 C-Series Sound and Vibration Input Module	58
39. NI-9162 CDAQ USB Chassis.....	59
40. Digital Manometer	60
41. The unchanneled airfoil 3D and 2D views	61
42. Airfoil with channel direction 3 degrees and diameter size 0.1 inch 3D and 2D views.....	62
43. Picture of NACA 0012.....	62
44. The force balance designed by solid works program.....	63

List of Figures—Continued

45. The force balance ready to measure the forces	64
46. The calibration set up of the force balance	64
47. The hot-wire anemometer setup.....	65
48. 2D designing of the hot wire and microphones setup.....	66
49. The hot-film calibration curve for the hot-film probe used in the velocity tests	66
50. Regular airfoil’s entire domain	67
51. a) Regular airfoil’s entire domain. b) Airfoil surface zoomed in. c) Airfoil boundary layer zoomed in. d) Channeled airfoil D=0.1 inch.	68
52. Variation of the flow parameters of all the tested samples.....	68
53. The background noise with no airflow for the different location of microphones	72
54. The background noise with 5 m/s flow velocity for the different location of microphones for unchanneled sample.....	73
55. SPL vs. Freq. for Unchanneled sample for Velocities 5,10, 15 m/s	74
56. SPL vs. Freq. for A0 D0.05 sample for Velocities 5,10, 15 m/s	74
57. SPL vs. Freq. for A0 D0.08 sample for Velocities 5,10, 15 m/s	74
58. SPL vs. Freq. for A0 D0.01 sample for Velocities 5,10, 15 m/s	74
59. SPL vs. Freq. for A-1 D0.05 sample for Velocities 5,10, 15 m/s.....	74
60. SPL vs. Freq. for A-1 D0.08 sample for Velocities 5,10, 15 m/s.....	74
61. SPL vs. Freq. for A2 D0.05 sample for Velocities 5,10, 15 m/s	75
62. SPL vs. Freq. for A2 D0.08 sample for Velocities 5,10, 15 m/s	75
63. SPL vs. Freq. for A2 D0.01 sample for Velocities 5,10, 15 m/s	75
64. SPL vs. Freq. for A3 D0.05 sample for Velocities 5,10, 15 m/s	75
65. SPL vs. Freq. for A3 D0.08 sample for Velocities 5,10, 15 m/s	75
66. SPL vs. Freq. for A3 D0.1 sample for Velocities 5,10, 15 m/s	75

List of Figures—Continued

67. SPL vs. Freq. for Unchanneled sample for AOA 5,10, 15	78
68. SPL vs. Freq. for A3 D0.1 sample for AOA 5,10, 15.....	78
69. SPL vs. Freq. for A3 D0.08 sample for AOA 5,10, 15.....	78
70. SPL vs. Freq. for A3 D0.05 sample for AOA 5,10, 15.....	78
71. SPL vs. Freq. for A2 D0.1 sample for AOA 5,10, 15.....	79
72. SPL vs. Freq. for A2D0.08 sample for AOA 5,10, 15.....	79
73. SPL vs. Freq. for A2 D0.05 sample for AOA 5,10, 15.....	79
74. SPL vs. Freq. for A-1D0.08 sample for AOA 5,10, 15	79
75. SPL vs. Freq. for A-1D0.05 sample for AOA 5,10, 15	80
76. SPL vs. Freq. for A0 D0.1 sample for AOA 5,10, 15.....	80
77. SPL vs. Freq. for A0 D0.08 sample for AOA 5,10, 15.....	80
78. SPL vs. Freq. for A0 D0.05 sample for AOA 5,10, 15.....	80
79. Overall sound for all samples vs. AOA	81
80. SPL vs. Freq. for D0.1 sample for different Angles at 10 m/s velocity.....	82
81. SPL vs. Freq. for D0.05 sample for different Angles at 10 m/s velocity.....	82
82. SPL vs. Freq. for D0.08 sample for different Angles at 10 m/s velocity.....	82
83. SPL vs. Freq. for A3 sample for different Diameters at 10 m/s velocity	83
84. SPL vs. Freq. for A2 sample for different Diameters at 10 m/s velocity	83
85. SPL vs. Freq. for A-1 sample for different Diameters at 10 m/s velocity	84
86. SPL vs. Freq. for A0 sample for different Diameters at 10 m/s velocity	84
87. Noise spectrum for unchanneled sample	85
88. Noise spectrum for the sample A3.....	85

List of Figures—Continued

89. Noise spectrum for the sample A2.....	85
90. Noise spectrum for the sample A0.....	85
91. Noise spectrum for the sample A-1	86
92. The calibration data of the lift forces.....	87
93. The calibration data of the drag forces	88
94. Cl vs. AOA for D0.1 samples for different angle directions	90
95. Cl vs. AOA for D0.08 samples for different angle directions	90
96. Cl vs. AOA for D0.05 samples for different angle directions	90
97. Cl vs. AOA for A0 sample for different Diameters.....	91
98. Cl vs. AOA for A-1 sample for different Diameters	91
99. Cl vs. AOA for A2 sample for different Diameters.....	91
100. Cl vs. AOA for A3 sample for different Diameters.....	91
101. Cd vs. AOA for D0.1 sample for different angles	92
102. Cd vs. AOA for D0.08 sample for different angles	92
103. Cd vs. AOA for D0.05 sample for different angles	92
104. Cd vs. AOA for A0 sample for different Diameters.....	93
105. Cd vs. AOA for A-1 sample for different Diameters.....	93
106. Cd vs. AOA for A2 sample for different Diameters.....	93
107. Cd vs. AOA for A3 sample for different Diameters.....	93
108. Cl/Cd vs. AOA for D0.1 sample for different angles	94
109. Cl/Cd vs. AOA for D0.08 sample for different angles	94
110. Cl/Cd vs. AOA for D0.05 sample for different angles	95

List of Figures—Continued

111. Cl/Cd vs. AOA for A0 sample for different Diameters	95
112. Cl/Cd vs. AOA for A-1 sample for different Diameters.....	95
113. Cl/Cd vs. AOA for A2 sample for different Diameters	96
114. Cl/Cd vs. AOA for A3 sample for different Diameters	96
115. The levels of the set of data measured around the airfoil.	99
116. Turbulence intensity for samples A3 at Z=0	99
117. Turbulence intensity for samples A2 at Z=0	99
118. Turbulence intensity for samples A0 at Z=0	100
119. Turbulence intensity for samples A-1 at Z=0	100
120. Fluctuation of $(1/v^2)$ for the sample A3 D0.1 vs. unchanneled.....	104
121. Fluctuation of $(1/v^2)$ for the sample A3 D0.08 vs. unchanneled.....	104
122. Fluctuation of $(1/v^2)$ for the sample A3 D0.05 vs. unchanneled.....	104
123. Fluctuation of $(1/v^2)$ for the sample A2 D0.1 vs. unchanneled.....	105
124. Fluctuation of $(1/v^2)$ for the sample A2 D0.08 vs. unchanneled.....	105
125. Fluctuation of $(1/v^2)$ for the sample A2 D0.05 vs. unchanneled.....	105
126. Fluctuation of $(1/v^2)$ for the sample A0 D0.1 vs. unchanneled.....	106
127. Fluctuation of $(1/v^2)$ for the sample A0 D0.08 vs. unchanneled.....	106
128. Fluctuation of $(1/v^2)$ for the sample A0 D0.05 vs. unchanneled.....	106
129. Fluctuation of $(1/v^2)$ for the sample A-1 D0.08 vs. unchanneled	107
130. Fluctuation of $(1/v^2)$ for the sample A-1 D0.05 vs. unchanneled	107
131 Visualization for the correlation between the turbulence and the overall noise (0-10000Hz)	109
132 Visualization for the correlation between the turbulence and the overall noise	110

CHAPTER 1

INTRODUCTION

1.1 Introduction

With today's heavy and increasing dependence on fossil fuels, a dependable alternative energy source is demanded. Fossil fuels power nearly all aspects of daily living such as producing electricity for residential homes, fuel for vehicle transportation, power for industry, and countless others. This tremendous use results in negative impacts on the environment such as an increase in CO₂ levels causing the earth's temperature to rise and poisonous emissions that are harmful to both the environment and human health. In addition to the poor byproducts of fossil fuel use, the resource is finite, thus giving it an expiration date for its total depletion [1] [2]. Wind energy provides renewable and clean power with almost no drawbacks for its usage; however, there are downsides to wind turbines. One particular downside is a consequence of the rotating blades, which is the amount of noise they generate.

With advancements and incorporation of technology in modern day living, the demand for energy has increased dramatically in the last decades worldwide. Fossil fuel is considered the main source of energy and provides about 85% of total global energy [3]. Since the industrial revolution, numerous changes have occurred. While the resulting technological innovations have dramatically improved the quality of life, there has also been a significant increase in the concentration of greenhouse gasses in the atmosphere. This has led to a global increase in average temperatures compared to the pre-industrial era. A significant component of the increasing greenhouse gasses results from the combustion of fossil fuels that release carbon dioxide along with other greenhouse gasses such as carbon monoxide, methane, and nitrous oxides. As greenhouse gasses build up in

the atmosphere, they negatively affect the earth by allowing UV radiation from the sun while preventing heat transfer out of the atmosphere. This gradually results in the global temperature rising over time [4]. In addition to the negative effects of fossil fuels on the environment and pollution, fossil fuels will be depleted in a few decades. For this reason, the world has begun to implement other sources of energy, that go by many names such as alternative, renewable, or sustainable energy. Alternative energy comes from sources that replenish themselves, such as wind, solar, hydroelectric, and geothermal [5].

As the world looks for alternative sources of energy to fossil fuel, renewable energy is expected to be the dominant source of energy in the future. Wind turbines are one of the main devices that provide clean energy, however, wind turbines are noise generators that can be very annoying, and especially for people who live close to wind turbine farms. During the last decades, many researchers have attempted to solve or reduce this problem especially due to the sharp increase of farms that have grown fast to catch up to the increasing demand for clean energy [1].

Wind energy essentially comes from the sun, which is considered the only source of energy on earth. The sun's core creates solar energy that streams from the sun to the earth and is then converted to various types of energy on earth such as wind, heat, and light. Wind is generated from the movements of air from one area on earth to another because of the difference in pressure between these two areas. Humans have used wind power for thousands of years, as early as 3400 B.C. ancient Egyptians used wind to sail and traverse the oceans, as well as the ancient Chinese around 4000 B.C. Other than sailing, wind energy has also long been used in windmills, and by children to raise kites [5].

Wind power is considered one of the main sources of renewable energy on the market today. Given its increasingly ubiquitous presence across the globe, wind turbines are especially

impacting our everyday lives and environments. In the past, people used wind energy in many different ways including transportation across the oceans by sailing ships, pumping water by windmills, and grinding grains [5]. Table (1) and Figure (1) shows operational wind power capacity worldwide [6]. The global market has nearly quadruple in size over the past decade, reaching capacity of wind turbine plants to 743 GW by the end of 2020 (Figure 1), establishing itself as a most cost-effective and resilience power resources in the world. In addition, to achieve the ambitious goal of net zero by 2050, the world needs to be installing wind turbine power three times faster over the next decade to avoid the worst climate change impact.

Table 1. Operational wind power capacity worldwide

MW onshore	New installation 2019	Total installation 2019	New installation 2020	Total installation 2020
Total onshore	54,634	620,967	86,932	707,396
Americas	13,437	148,081	21,750	169,758
USA	9,143	105,436	16,193	122,275
Canada	597	13,413	165	13,577
Brazil	745	15,352	2,297	17,750
Mexico	1,281	6,215	574	6,789
Argentina	931	1,604	1,014	2,618
Chile	526	2,145	684	2,829
Other Americas	214	3,817	823	3920
Africa, Middle East	830	6,454	823	7,277
Egypt	262	1,452	13	1,465
Kenya	0	338	0	338
South Africa	0	1,980	515	2,465
Other Africa	568	2,684	295	3009
Asia-Pacific	28,626	283,780	52,546	336,286
China	24,292	229,384	48,940	278,324
India	2,377	37,506	1,119	38,625
Australia	837	6,199	1097	7296
Pakistan	50	1,239	48	1,287
Japan	274	3,857	551	4,373
South Korea	191	1,420	100	1515
Vietnam	160	388	125	513
Philippines	0	427	0	427
Thailand	322	1,538	0	1538
Other-Asia	123	1,822	566	2,388
Europe	11,741	182,651	11,813	194,075
Germany	1,078	53,913	1,431	55,122
France	1,336	16,643	1,318	17,946
Sweden	1,588	8,804	1,007	9,811
United Kingdom	629	13,617	115	13,731
Turkey	686	8,056	1,224	9,280
Other Europe	6,424	81,618	6,718	88,185
MW Offshore	New installation 2019	Total installation 2019	New installation 2020	Total installation 2020
Total offshore	6,243	29,232	6,068	35,293
Europe	3,627	21,901	2,936	24,837
United Kingdom	1,765	9,723	483	10,206
Germany	1,111	7,491	237	7,728
Belgium	370	1,556	706	2,262
Denmark	374	1,703	0	1,703
Netherlands	0	1,118	1493	26,11
Other Europe	8	310	17	327
Asia-Pacific	2,616	7,301	3,120	10,414
China	2,493	6,936	3,060	9,996

South Korea	0	73	60	136
Other Asia	123	292	0	242
Americas	0	30	12	42
USA	0	30	12	42

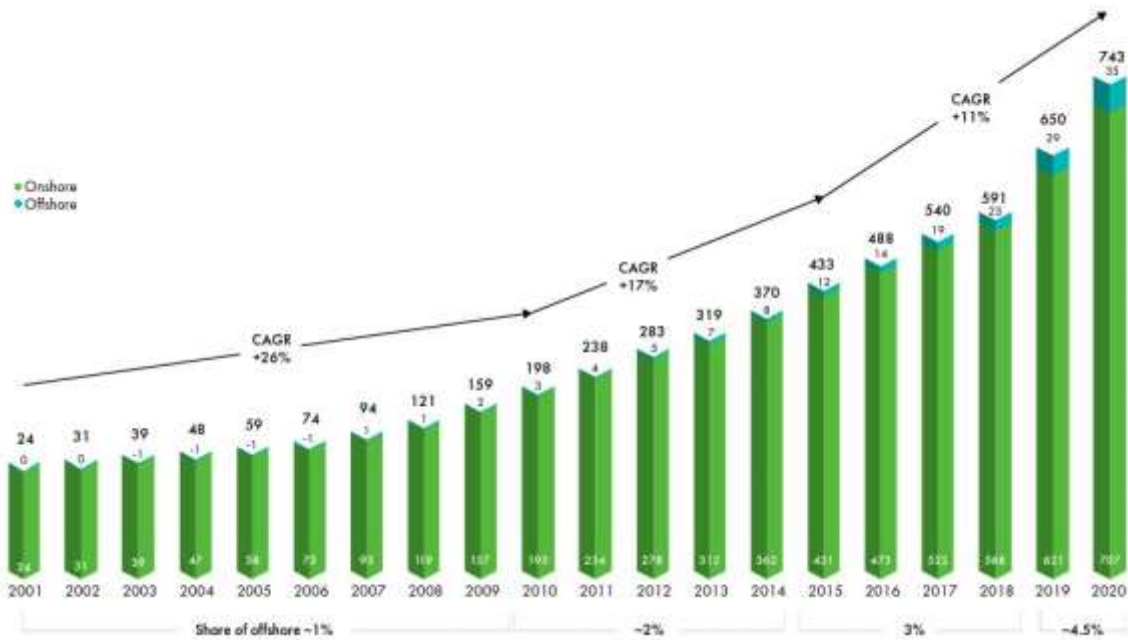


Figure 1. Operational wind power capacity worldwide

As the pollution increases rapidly these days due to the combustion of fossil fuel, renewable energy is the most reliable source of clean energy. Wind energy is one of the most important sources of renewable energy. As the number of wind farms increases to meet the world’s energy needs, the noise emitted from these turbines also increases. This noise is considered one of the drawbacks of the wind turbines that people complain about in the areas near these farms [7]. This study focuses on this problem and tries to create a possible solution that could make wind energy more reliable.

This study aims to find a way to reduce the aerodynamic noise from wind turbines precisely and from any airfoil generally. For this purpose, a novel idea was introduced that could reduce the aerodynamic noise around the moving airfoil. This idea is simply drilling small channels inside the airfoils to stabilize the air flow around the blades and reduce the aerodynamic noise.

The dissertation contains five chapters:

Chapter one is an introduction that focuses on energy in general and renewable energy specifically. The chapter will also give a brief review of wind energy and using wind turbines as a significant source of renewable energy. Chapter two is a literature review. This chapter explores the previous studies that focus on the wind turbine noise and the noise sources from wind turbines and the way the researchers used to resolve this problem. The literature review also shows the studies that have a direct relation with this study such as acoustics, aerodynamic performance, turbulence intensity that have been done in same way or same conditions of this study. Chapter three is a theoretical background, this chapter contains all the mathematical equations that the study deals with. Chapter four is the experimental and numerical setup, this chapter shows all the work that has been done to complete the study. This chapter has two sections: experimental and numerical. Experimental work includes using a quiet chamber to create a quiet environment, acoustics equipment, force balance, turbulence anemometer are explained in the first section. The second section is the numerical study, where ANSYS fluent was used for the simulation and explained in this chapter. Chapter five is the results, this chapter shows: acoustics, forces, turbulence, and numerical results. In this chapter, the noise results are discussed first, the acoustic results cover all the factors that have an impact on the noise emitted from wind turbines. The force results discussed show the aerodynamic performance of the wind turbines. The turbulence results are discussed and show how they are related to the acoustics results. Next, the experimental and numerical results are compared, and finally turbulence results are correlated to the acoustics results. The last chapter is conclusion and future studies; this chapter summarizes the all of the results and gives recommendations for future studies.

1.2 Objective

In finding alternative renewable energy sources for the future, wind turbines are one of the main devices that provide clean energy but have the potential to emit noise. The purpose of this study is to reduce the aerodynamic noise of wind turbines, using NACA 0012 airfoils. The objective of this research is to numerically and experimentally investigate the following:

- 1- Study of the effect of using channels inside airfoils on the noise level as a possible resolution for aerodynamic noise reduction in wind turbines.
- 2- Study the effect of these channels on the aerodynamic performance of the airfoil drag and lift.
- 3- Study the turbulence and turbulence intensity around the tested airfoil and study the change that could occur due to the existence of the channel.
- 4- Correlate the results of the turbulence intensity with the results of the aerodynamic noise of the different airfoils.
- 5- Make a comparison between the experimental results and numerical results for both acoustic results and force results.

CHAPTER 2

LITERATURE REVIEW

2.1 Background

The world is looking for alternative sources of energy to fossil fuel. Renewable energy will be one of the most important sources of energy in the future. Wind turbines are one of the main sources that could offer a clean and continuous energy source, but despite all that has been mentioned, wind turbines could be a source of noise — it is annoying, especially for people who live close to wind turbine farms. During the last several decades, many researchers have tried to solve this problem or reduce it, especially when the number of farms starts to increase to meet the increasing demand for energy.

2.2 Sources of the aerodynamic noise in wind turbines

According to many researchers, the noise can be generated from different sources on the surface of the wind turbine or around it. The low frequency noise is considered one of these sources. This type of noise is generated by the flow interaction that comes from the blades and the tower [8]

Henrik Moller et al. [9] measured low frequency noise from large wind turbines. He collected data for 48 large and small wind turbines. The data was measured inside ten rooms in standard living houses, in addition to the data collected outside. The results revealed a relationship between the frequency and turbine size; as the turbine size increases, the frequency of the source decreases. The study assigned the significance of this kind of noise to the difficulty of attenuating it. Figure (2) shows the A-weighted sound power levels in one third octave bands for turbines 2.5, 5, and 10 MW.

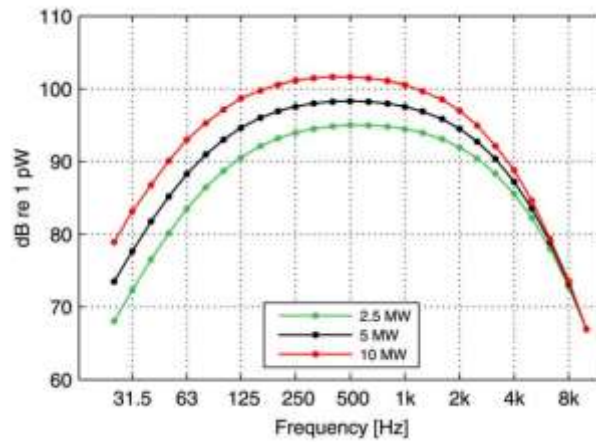


Figure 2. A-weighted sound power levels in one third octave bands for turbines 2.5, 5, and 10 MW

Turbulent inflow noise is the second main source of wind turbine noise. Steven Buck et al. [10] studied the turbulent inflow noise experimentally on a full-scale wind turbine with a 108 m diameter and 2.3 MW capacity. The purpose of the study was to assess the effect of inflow turbulence on wind turbine noise. Fifty hours of sound data were collected by 12 microphones mounted at different angles. The results showed a high correlation between turbulence intensity and noise levels. Figure (3) shows the correlation between turbulence intensity and sound pressure level.

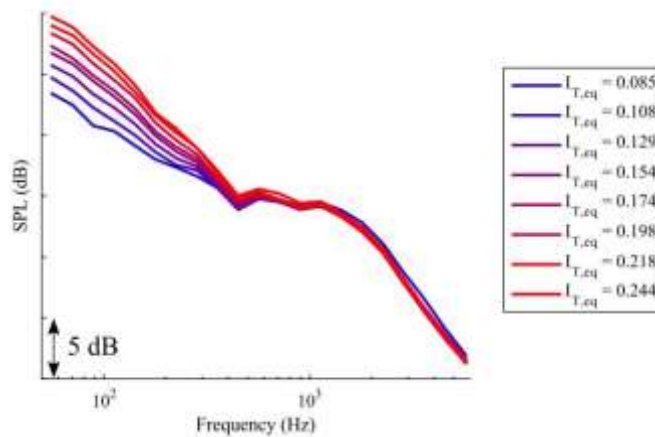


Figure 3. The correlation between turbulence intensity and sound pressure level [Steven Buck]

Airfoil self-noise is the third main source of aerodynamic noise. This type of noise occurs as a result of interaction between the blades and its boundary layer. Airfoil self-noise could be classified into several different noises, depending on the location of this interaction, such as: Turbulent Boundary Layer Trailing Edge Noise (TBLTE), Laminar Boundary Layer Vortex Shedding Noise (LBLVS), Separation-Stall Noise (SEP), Trailing Edge Bluntness Vortex Shedding Noise (TEBVS), and Tip Vortex Noise (TIP) [7].

Van Treuren et al. [11] investigated the noise generation on four different small-scale wind turbine airfoils: NACA0012, NACA 4412, S823, and E387. The collected sound pressure level SPL for wide range of angle of attack was from -10 degree to 25 degree and for different Reynolds numbers from 50,000 to 200,000. The results showed that the noise generated from the wake behind the airfoils, and revealed both the angle of attack and Reynolds number have a direct effect on the sound pressure level. Figure (4) shows the relationship between sound pressure level and angle of attack for different Reynolds number for airfoil NACA 0012.

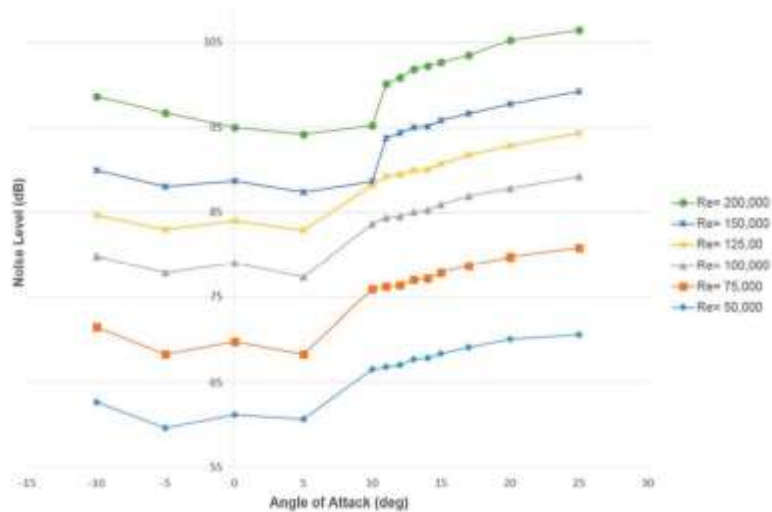


Figure 4. NACA 0012 noise versus angle of attack for different Reynolds numbers

2.3 Noise reduction

One of the most interesting subjects observed by scientists for decades was the silent flight of an owl bird when it hunts its prey. Many researchers investigated this quiet flight to understand the reason behind this secret [12] [13] [14]. These studies showed the differences between the feathers of the owl and some other kinds of birds. In the owl feathers, the leading edge of feathers is serrated, and the trailing edge has fringes and the velvet-like wing back surface. All these features have helped to reduce the noise emitted by an owl. Figure (5) shows the leading edge and trailing edge feathers of the owl, and Figure (6) shows the one-third-octave band frequency spectrum of flight noise [14].

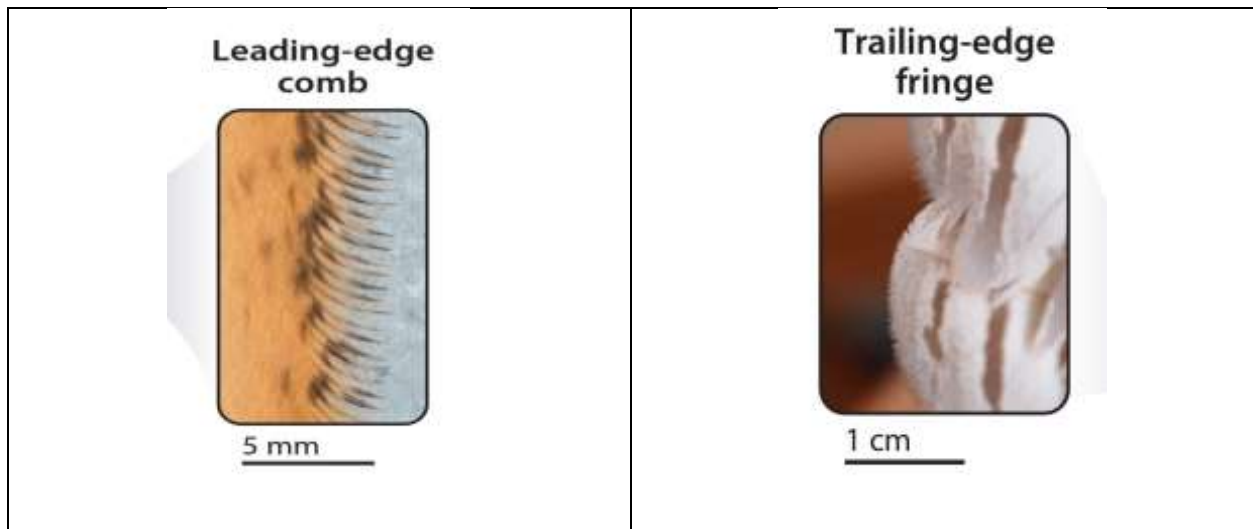


Figure 5. Leading edge and trailing edge feathers of the owl

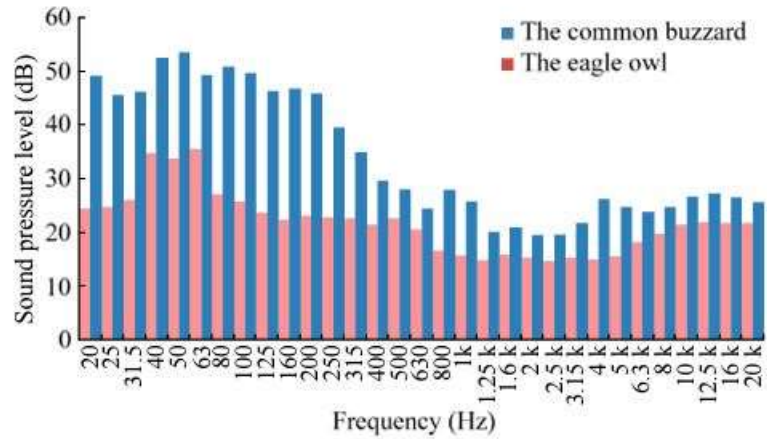


Figure 6. The one-third-octave band frequency spectrum of flight noise.

Brian Fite et al. [15] investigated, experimentally and numerically, the effect of trailing edge flow injection on fan noise and aerodynamic performance. Trailing edge blowing injection was used to reduce the wake momentum deficit of the fan blade. The study concluded that this technique reduced the overall sound power level 2 dB and an average reduction of about 1.5 dB of broadband noise up to 20 kHz. Tone noise was reduced up to 6 dB in the 2 Blade Pass Frequency (BPF) tone at 6700 rpm. The results also indicated that there is no reduction in the aerodynamic performance. Figure (7) shows trailing edge air injection and supply.



Figure 7. Trailing edge air injection and supply

Nakano et al. [16] investigated the tonal noise generation of NACA0018 airfoil. Particle Image Velocimetry (PIV) and liquid-crystal visualization technique were used for the investigation. The study concluded that the tonal noise emission depends on the Angle Of Attack (AOA). For very small angles, the tonal noise generates over pressure surface by the instability of the separating boundary layer, while the tonal noise disappears when angle of attack increases. Figure (8) shows the spectra of aerodynamic noise generated from the airfoil at various angles of attack (0 to 15) degrees.

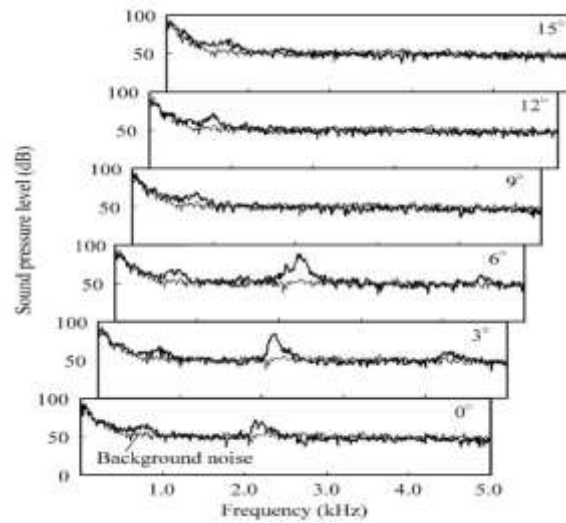


Figure 8. Aerodynamic noise generated from the airfoil at various angles of attack.

Using porous material on the trailing edge, specifically, is a possible approach to reduce the noise. Geyer et al. [17] investigated using several different porous materials with different chord wise extent. An open jet wind turbine was used with a set of microphones to collect the sound data. The aerodynamic performance was measured at the same time. The results concluded that porous trailing edge material reduces the noise with no loss in the aerodynamic performance as the airfoil is non-porous except the trailing edge. Figure (9) shows the geometry of porous material on the trailing edge (s), and Figure (10) shows the third octave band sound pressure levels of the trailing edge noise as a function of chord based Strouhal number. The figure shows different

porous material extent (s/c) cases. The materials used in the study are the porous airfoil made of Porex ($r = 316,500 \text{ Pa s/m}^2$), the porous airfoils made of Recemat ($r = 8,200 \text{ Pa s/m}^2$), and M-Pore Al 45 ppi ($r = 1,000 \text{ Pa s/m}^2$).

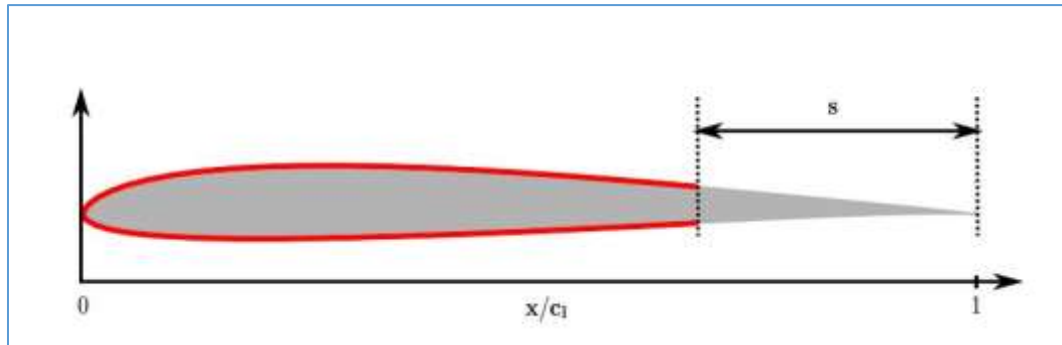


Figure 9. Using porous material on the trailing edge [Geyer et al]

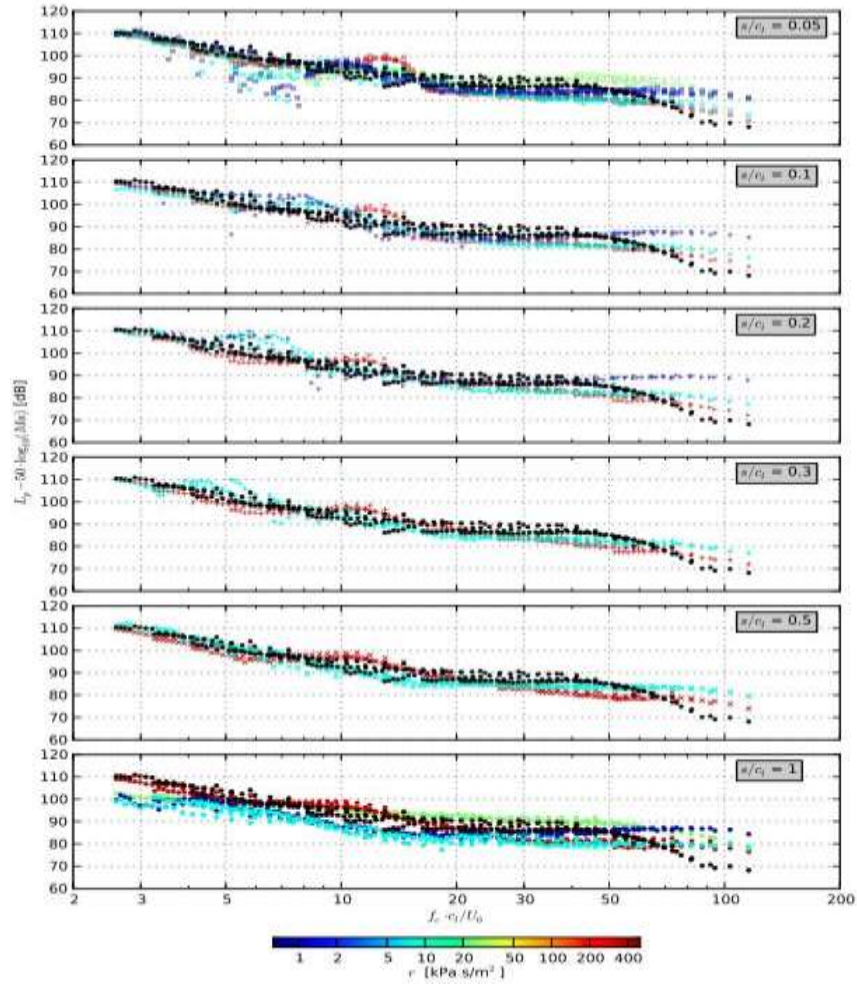


Figure 10. Trailing edge noise level of airfoils with different extents of the porous material, as a function of Strouhal number.
 Black dots: non porous airfoil, AOA = 0°

Chong et al. [18] studied the reduction of self-noise by non-flat plate type trailing edge serrations. In the study, NACA0012 airfoil was used, AOA was 4.2°, and flow velocity was from 20-60 m/s. Three sets of serrated airfoil were used from narrow angle to wide angle serration Figure (11). The study showed there was a reduction in the broadband self-noise between 2 dB to

8 dB, and at the same time, the study showed that the non-flat plate type eliminated the high-frequency noise that exists with flat plate type serration.

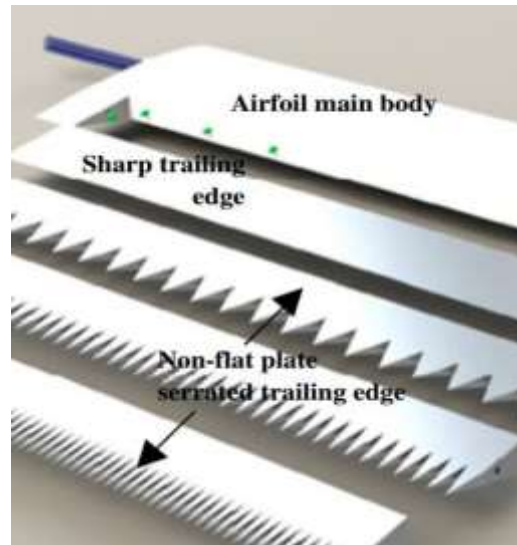


Figure 11. Non-flat plate type trailing edge serrations [Chong et al]

Katinas et al. [19] investigated the wind turbine noise emissions and their impact on the environment. The study concluded that there was a relation between the drop of the noise at specific wind velocity and the background noise. They found that there was an increase in the wind turbine noise level when the velocity of the wind increased. However, there was a decrease in wind turbine noise level when the distance increased from the wind turbine. The results showed that at more than (100m) from the tower, when the wind velocity was (12m/s), the noise emitted from the wind turbine becomes equal to the background noise.

2.4 Annoyance and health issues

Annoyance and health impacts are significant drawbacks of wind turbines. Many researchers studied these issues and provided possible solutions [20].

Felipe A. Fernandez et al. [21] investigated, experimentally and numerically, the inside and outside noise from a wind turbine farm. The results showed that the indoor noise level was significantly higher than outdoor level. Despite the transmission loss of the walls when the doors and windows were closed, the indoor noise level was still higher because of the fluid structure resonance of low frequencies. The study revealed that when the window was open, the structure was working as a large Helmholtz resonator with natural frequency in a low frequency region. The inside noise level increased approximately by 25 dB compared to outdoor noise level. Figure (12) shows the SPL for indoor (blue) and outdoor (red) noise.

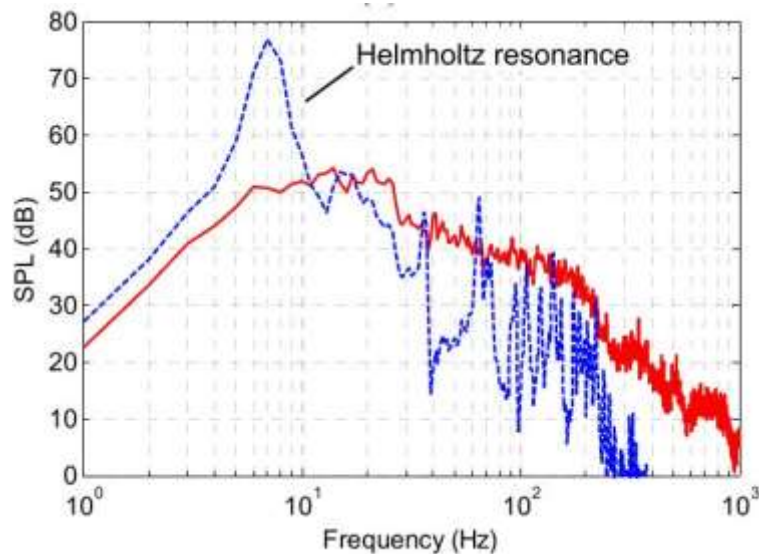


Figure 12. SPL for indoor (blue) and outdoor (red) noise

Chiu et al. [22] studied the effect of low frequency noise that wind turbines produce on heart rate variability in healthy individuals. The study revealed that low frequency noise (20-200 Hz) emitted from wind turbines impacts the heart rate of the residents who live close to wind turbine farms. The study suggested making regulations on the distance that should be maintained between residents and wind turbine farms.

Johannes et al. [23] investigated the methodology of stress psychology with sound measurements. Residents were from Lower Saxony, near where the wind farm is located, and were investigated in two periods (2012, 2014). The investigations showed that 9.9% were strongly annoyed in 2012 and 6.8% in 2014. The study revealed that noise could cause many symptoms, such as anger, bad mood, and sleep difficulties. Other researchers showed the same effects [24] [25].

Daniel Shepherd et al. [26] studied the effect of wind turbine noise with residents who lived close to wind turbine farms. The study was divided into two different areas; these areas were picked to be matched demographically and different only in the distances. The first group, who occupied 56 houses, was located within 2 km of the closest turbine (Turbine group), and the second group, who occupied 250 houses, was located more than 8 km from wind turbines (Comparison group). The results displayed a lower overall quality of life, physical quality of life, and environmental quality of life for the first group (turbine group). The other group (Comparison group) also reported significantly lower sleep quality and rated their environment as less restful. The study suggested that the minimum distance for the wind turbine farms should be at least 2 km from the living areas.

2.5 Turbulence

A theoretical solution was produced by Lighthill to predict the noise generated from the fluid flow and rigid boundaries by solving the equations for motion of gas. Lighthill explained noise as instability waves that contain turbulence fluctuations [27].

Shao-wu LI et al. [28] investigated, numerically and experimentally, effects of turbulence intensity on the flow around NACA 0012 airfoil with a 0.27 m span and 0.1 m chord. Particle Image Velocimetry (PIV) was used to measure the flow around the airfoil. The researchers raised

the turbulence intensity from 0.6% to 6%, and the Reynolds number was 5300. The results showed that both drag and lift coefficients increased by the increasing of turbulence intensity. The study concluded that the airfoil stall did not happen in low turbulence intensity, but it occurred when the turbulence intensity increased.

Acoustical and aerodynamic performances of an open jet wind tunnel were experimentally investigated by T.P. Chong [29] in a noise-controlled chamber. The background noise of the wind tunnel was found to be low for a variable range of exit jet velocity. NACA0012 airfoil was used, and the turbulence intensity level was at 0.1% with 0° and 10° angles of attack. The airfoil was tested in this study for both disturbed and undisturbed boundary layers. Significant high-level noise emitted from the trailing edge of the airfoil was confirmed over a wide range of frequencies.

Buck et al. [30] presented experimental work to show the effects of turbulence on the inflow field of a wind turbine. With wind velocities of 9 m/s and 11.5 m/s, the result showed that the dominant portion of the noise spectrum was in low frequencies, specifically under 400 Hz. Since human hearing is not very sensitive to sound in this range, it is not considered a significant source of the noise.

2.6 Lift and drag

When bodies move through any fluid or even when air moves around static bodies, the interaction will generate aerodynamic forces. The most common forces that researchers care about are the lift and drag around airfoil and blades. Aircraft and wind turbine manufacturers try to increase the lift and decrease the drag as much as they can.

The force that is generated as a result of the aerodynamics has two main components: the force perpendicular to the flow direction is called lift force and is measured by lift coefficient (Cl),

and the force in the same direction of the flow is called drag force and is measured by drag coefficient (C_d) [31][[32].

Many studies focused on these two forces to enhance the ratio (C_l/C_d) by decreasing the drag C_d or increasing the lift C_l .

Ruffin, S. M., Gupta, A., and David Marshall [33] investigated the supersonic channels for an airfoil at Mach = 2.5. The results showed total drag decreased 30% for laminar flow and 20% for the turbulent flow compared to the airfoil without channels. Three different channel designs were used in the study: Sharp-Nose Straight-Channel Airfoil (SNSC), Round-Nose Straight-Channel Airfoil (RNSC), and Round Nose Diverging-Channel Airfoil (RNDC). While airfoil with No Channel (NC) was taken as a baseline. Figures (13) and (14) show the drag coefficient versus angle of attack for no-channel and channel airfoils in, Mach = 2.4 and $h = 12$ km, for laminar flow and turbulent flow in order.

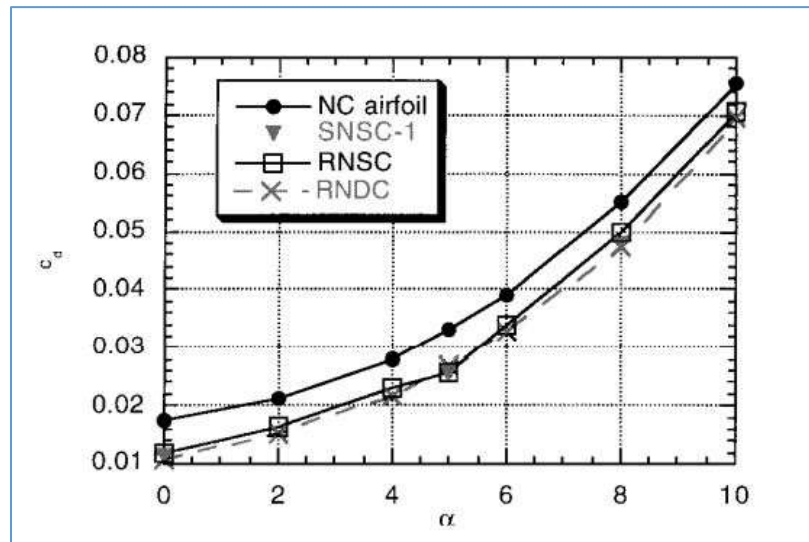


Figure 13. Drag coefficient vs angle of attack for no-channel and channel airfoils in: Mach=2.4 and $h=12$ km for laminar flow

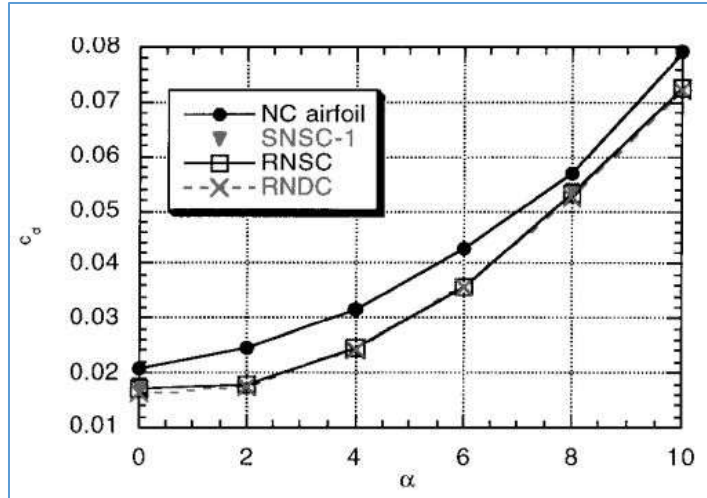


Figure 14. Drag coefficient vs angle of attack for no-channel and channel airfoils in: Mach=2.4 and h=12 km for turbulent flow

The figures above show the effect of the supersonic channels on drag coefficient for different channels compared to the regular airfoil. Both figures show similarity in decreasing the drag coefficient when channels added to the airfoils. The only difference is that in case of laminar flow the channels showed more improvements in the drag compared to the turbulence flow.

Anurag Gupta and Stephen M. Ruffin investigated in two different studies the supersonic channels of an airfoil. The first study [34] focused on a sphere cone with a channel in the leading edge, at Mach=7, at the altitude of 20 km and AOA=5°. The study showed an increasing 25.1 in L/D and revealed that increasing the channel's size, shows improvements in the drag coefficient by up to 20% compared to the sphere cone without a channel. With lifting flight AOA=2, and 10 degrees sphere-cone at Mach=2.25, the study showed more than 30% improvement in L/D. Momentum coefficient improved as well, allowing more controllability for flight. Figure (15) shows the design of sphere cone with a channel in the leading edge.

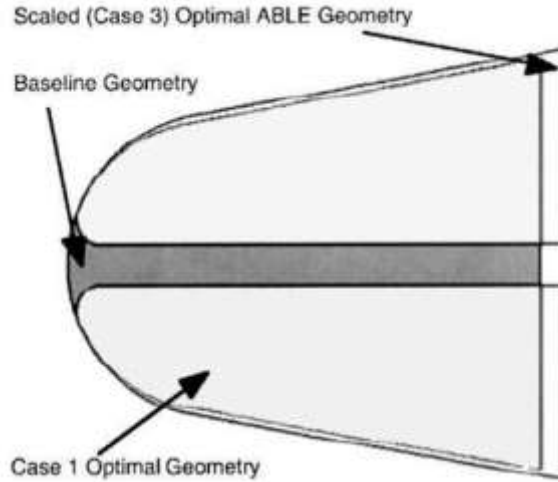


Figure 15. Sphere cone with a channel in the leading edge.

In the second study, Anurag Gupta and Stephen M. Ruffin [35] investigated Artificially Blunted Leading Edge (ABLE) airfoils at Mach=4 and 12km altitude. The geometry of the airfoil was designed to be optimal to reduce the drag to minimum value without increasing the heating rate or decreasing the lift compared to the baseline airfoil. The results show a 19% reduction in the drag coefficient with the same lift and heat transfer. Figure (16) shows the design of artificially blunted leading edge (ABLE) airfoils.

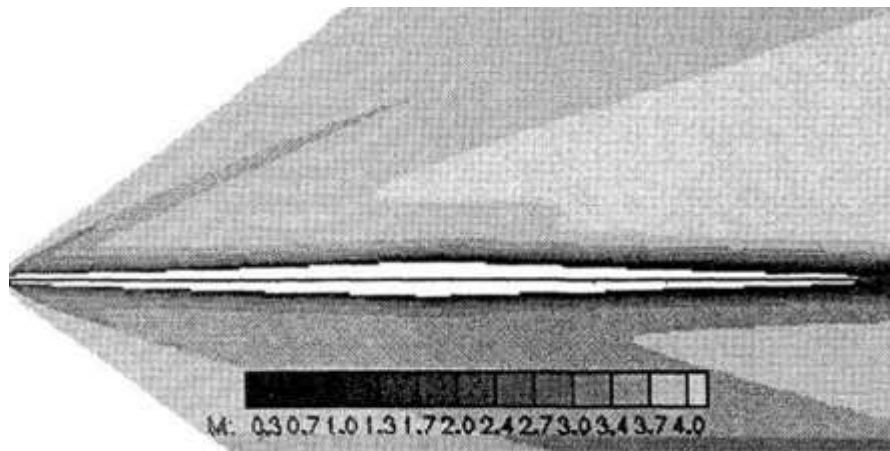


Figure 16. Artificially blunted leading edge (ABLE) airfoils

Giles, D., & Marshall, D. [36] used a diamond shape and supersonic channel design to improve the aerodynamic performance of a NACA 66-206 airfoil. The numerical results showed a 17.2% increase in the lift to drag ratio for airfoils at Mach 2.5, 35,000 ft altitude, and AOA=6°. The experimental results showed a 9% lift to drag ratio increase at the same conditions.

Talluri et al. [37] investigated enhancements of lift and drag on a NACA 0012 airfoil, numerically, and used ANSYS to study the effects of airfoil design on the aerodynamic forces. Three different designs for NACA 0012 were used in this study: the first sample was default, the second sample had flap at 15° and slot at trailing edge, and the third one had gurney flap with flat wedge support. The study revealed an increase in lift coefficient by 1.87 times for the second sample and 1.78 times for the third sample compared with the default NACA 0012 airfoil. On the other hand, the drag coefficient increased for both of the samples as well by 2.22 for the second sample and 1.33 for the third sample compared to the default NACA 0012 airfoil. They recommended the second sample for high lift requirements and sample three for normal lift and low drag applications.

Rong et al. [38] examined the effects of freestream turbulence intensity on the surface-flow regimes. The study employed separation, bubble, leading-edge bubble, turbulent separation, and three-dimensional flow. Also, the corresponding aerodynamic performance, including lift, drag, and stall, of a cantilever NACA 0012 wing model were studied in a wind tunnel. The findings showed that the behavior of the surface flow is closely related to the variations of lift and drag. Also, the intensity of freestream turbulence highly impacts the surface flow and aerodynamic performance.

Arunraj et al. [39] used suction at various points, attempting to increase the lift coefficient by delayed boundary layer separation and to identify the optimum location for suction which

provides maximum lift augmentation. The NACA 0012 airfoil model was used for the experiment. Various suction pressures were conducted experimentally at different locations of the chord length of the airfoil. The outcomes demonstrated that the introduction of suction was highly effective at low suction pressures, and the suction aided in the heat transfer enhancement over the airfoil surface. Moreover, there was no important change in the lift when the suction pressure was increased above 80 kN/m². Also, the results indicated that at a lower angle of attack, the suction was more effective.

Li-Hao et al. [40] investigated flow control of a NACA 0012 airfoil by the dielectric-barrier-discharge plasma actuator on a Gurney flap. All tests were experimentally executed in a wind tunnel. In this study, the lift and drag coefficients and the velocity and vorticity fields were studied by using a dynamic force balance and time-resolved PIV. The present results showed that the lift increased further with a small drag penalty when a dielectric-barrier-discharge plasma actuator was attached to the Gurney flap. The findings also showed that when the plasma actuator was turned on, both lift and drag coefficients were increased. Furthermore, the measurements of the time-resolved near-wake region showed that the plasma forcing shifted the wake downward, reducing its recirculation length. Furthermore, the measurements of Time-resolved of the near-wake region referred that the plasma forcing affects the recirculation length.

Ahmad et al. [41] considered airflow around the NACA 0012 airfoil. Continuum and particle approaches were utilized to measure rarefied supersonic and subsonic gas flow around the airfoil in this investigation. The investigation included three Knudsen numbers over a wide range of flow angles of attack. An agreement was found between the experimental and numerical data when the computed density and surface pressure distributions of particle and continuum approaches in the slip regime were compared. The outcomes predicted that with the decreases of

the Knudsen number, the compressibility of the air stream around the airfoil increases. Also, the outcomes for lift coefficient correspond well with the linearized theory at a low Knudsen number and small angle of attack. However, there was no significant influence with an increase of the Knudsen number on the stall point.

Dong et al. [42] studied the effect of a low Reynolds number on the boundary-layer properties and aerodynamic characteristics of a pitching NACA 0012 airfoil. To show the abrupt increase of lift coefficients in low-Reynolds-number, the boundary layer visualization and static pressure measurements were applied. Moreover, smoke-wire flow visualization was used to visualize the reverse flow and near wake. The lift and pressure drag coefficients were calculated by measuring unsteady pressure through pressure distortion correction. The results showed that the occurrence of boundary-layer events such as laminar separation and transition occurs due to the increase in the Reynolds number.

This chapter was a literature review of the previous studies that focus on the wind turbine noise, the sources of noise from wind turbines, and the method the researchers used to resolve this problem. The chapter also showed the studies that have a direct relation with this study such as acoustics, aerodynamic performance, and turbulence intensity, each having been done in the same way or under the same conditions of this study. The chapter started with a background of the problem of the study. Next, the previous studies that deal with the sources of the aerodynamic noise in wind turbine were covered. Noise reduction studies were mentioned after. Some studies focus on the effects of wind turbine noise on humans, which were explained as annoying or causing health issues. Finally, the previous studies of the turbulence and the aerodynamic forces in the wind turbines were mentioned in this chapter.

CHAPTER 3

THEORETICAL BACKGROUND

3.1 Introduction

Wind energy is one of the main sources of the future's energy. This energy are harvest by wind turbines. Despite of the benefits of the wind turbines, the produced noise during rotation of these turbines affects the people live around the wind farms [43] [44]. In general, the sound generated from these sources is Infrasound and Low Frequency Noise (ILFN), especially in the case of large turbines. Infrasound and low frequency noise are usually less attenuated than high frequency and mid-frequency sounds; ILFN propagates long distances and can penetrate buildings. Noise, due to the wind turbine, is increasing as its size increases. As turbines increases in size, lower frequencies are expected to be emitted from these wind turbines [9]. A. Huskey and J. van Dam studied the acoustic noise emitted from ARE 442 wind turbine, and they recorded the sound power level. Table (2) shows the sound power level emitted from the wind turbine for different wind speed values (from 4-12 m/s [8.9-26.8 mph]) [45].

Table 2 Sound power level emitted from the wind turbine

Wind Speed (m/s)	Wind Speed (mph)	Sound Power Level (dBA)
4	8.9	85.8
5	11.2	85.9
6	13.4	85.2
7	15.6	84.9
8	17.9	87.6
9	20.1	89.9
10	22.4	93.7
11	24.6	96.5
12	26.8	98.2

3.2 Wind energy

Wind energy is one type of energy that is converted from solar energy. Solar energy comes from the sun as a result of nuclear fusion of hydrogen into helium. Small amounts of solar energy fall on the earth, and only 2% of this energy converts to wind energy. However, this small portion of energy is much more than what is needed to power the world. Wind flows from an area with high pressure to another area with low pressure. The movement of the wind is affected by many factors, such as the difference of the temperature, geographical conditions, and Coriolis Effect that happens as a result of self-rotation of the earth [5].

3.3 Wind power

When the particles of air move, they carry kinetic energy. This kinetic energy is converted to electrical energy by wind turbines. If we want to calculate the power that wind could generate, we should start with the kinetic energy formula [5] :

$$E_k = \frac{1}{2} m v^2 \quad \dots\dots\dots (1)$$

Where:

m: the air mass

v: the mean wind speed

The power of the wind, in this case, can be calculated by differentiating the kinetic energy in the wind with respect to time:

$$P = \frac{dE_k}{dt} = \frac{1}{2} \dot{m} v^2 \quad \dots\dots\dots (2)$$

But:

$$\dot{m} = \rho A v \quad \dots\dots\dots (3)$$

So:

$$P = \frac{1}{2} \rho A v^3 \dots\dots\dots (4)$$

Where:

ρ : the air density

A: the swept area of blades

3.4 Wind profile power law

Wind speed changes with height as a result of the roughness on the surface of the earth.

The logarithmic law (the power law) shows the relation between wind speed in a point with the height of this point. This law may be expressed as [46]:

$$\frac{V_1}{V_2} = \left(\frac{Z_1}{Z_2}\right)^p \dots\dots\dots (5)$$

Where:

V_1 = Wind speed at height Z_1

V_2 = Wind speed at height Z_2

$$p = \text{Exponential parameter} = \frac{\ln(V_1/V_2)}{\ln(Z_1/Z_2)}$$

3.5 Basic acoustics

The noise is defined as unwanted sound, therefore some of the sound characteristics and a physical description of the sound will be explained. Sound can be classified as a longitudinal wave; it needs a physical medium to move, so the sound can move in gasses, liquids, and solid mediums, but it is not possible to move in a vacuum. There are three conditions required to hear sound: a source to generate it, a medium to move in, and an ear to hear it [47].

3.5.1 Sound properties

Sound is pressure waves that oscillate in a physical medium, and it has three characteristics: wavelength λ , frequency f , and velocity c . The velocity of sound depends on the type of medium and its physical and chemical properties. For instance, the sound speed in the air in standard conditions (20°C) is 340 m/s, and the speed of sound is always ($c = f \lambda$). Sound behaves as a wave, so it has the properties that other waves have; sound reflects, refracts, attenuates, and can be absorbed. All these cases depend on the mediums that sound moves in [48].

3.5.2 Physical description of the sound

Sound, as mentioned earlier, is a wave that has a frequency. The human ear can recognize this sound if its frequency lies between (20-20,000 Hz). If the wave has a frequency of less than 20 Hz, this wave is called an infrasound wave; on the other hand, if this wave has a frequency of more than 20,000 Hz, the wave is called an ultrasound wave. The unit formerly used to measure the sound is Bel (B); this unit is too large, so the scientists now use decibel (dB) instead. In order to understand the sound well, we have to know some concepts such as sound pressure, sound intensity, and sound power [25].

3.5.2.1 Sound pressure level

The sound pressure level is a logarithm quantity measured relative to a reference value. This reference value represents the threshold of hearing for humans. The response of the human ear is not linear. When the sound pressure doubles, the sound will not be heard twice as high.

Sound Pressure Level (SPL) could be calculated mathematically as [49] [47]:

$$L_p = 10 \log_{10} \left(\frac{P}{P_{ref}} \right)^2 \dots\dots\dots (6)$$

Or:

$$L_p = \text{Log}_{10} \left(\frac{P}{P_{ref}} \right)^2 \dots\dots\dots (7)$$

Where:

L_p : sound pressure level in dB

P : sound pressure in N/M² (Pa)

P_{ref} : the reference sound pressure in air (20*10⁻⁵ Pa)

3.5.2.2 Sound intensity level

The intensity of sound can be defined as the energy transmitted from the source of the sound per the unit of time and unit of area to all the directions. Therefore, the intensity of sound is measured in (W/m²). The intensity of sound is [49] [47]:

$$I = P^2 / (\rho_0 C_0) \dots\dots\dots (8)$$

Sound intensity level in dB is:

$$L_I = 10 \text{Log}_{10} \left(\frac{I}{I_{ref}} \right) \dots\dots\dots (9)$$

where:

I : intensity of sound

I_{ref} : the reference sound intensity in air (10⁻¹² W/m²)

ρ_0 : the mass density of the medium

C_0 : the propagation velocity of the sound waves through the medium

Note that both the sound pressure level and sound intensity level depend on the distance between the source and the receiver.

3.5.2.3 Sound power level

In contrast with sound pressure and sound intensity, the sound power level does not depend on the position from the source, but it depends on the source itself. The power of the source could be calculated from the intensity by the equation [49] [47]:

$$W = 4 \pi I R^2 \dots\dots\dots (10)$$

It could be measured from the pressure as well by the equation:

$$W = \left[\frac{P^2}{(\rho_0 C_0)} \right] * 4\pi R^2 \dots\dots\dots (11)$$

In the same way, the sound power level can be found in dB (L_w) as:

$$L_w = 10 \text{Log}_{10} \left(\frac{W}{W_{ref}} \right) \dots\dots\dots (12)$$

Where:

W_{ref} : the reference sound power in air (10^{-12} W).

R: the distance from the source

3.5.2.4 Sound propagation and directivity

Sound waves spread from a source in all directions through the atmosphere, mainly axially. As the distance between the sound source and measuring device increases, the sound pressure level gradually decreases. In the absence of a reflecting surface, as the distance is doubled, the sound pressure level drops by 6 dB (A). There are many factors that affect sound propagation, such as wind speed and direction, air temperature, and ground or surface damping effect. More specifically, air as a medium carries an absorption coefficient due to its viscosity; reflective surfaces disrupt sound wave paths and diffraction sound waves. Diffraction occurs when a sound

wave travels near solid objects. The region behind the object is known as the shadow zone, which depends on the ratio between the wavelength of the sound and the object's size. Other factors that affect sound propagation include the refraction of the sound wave and the speed and direction of the incident wind on the waves [50].

The directivity of sound refers to the sound waves that spread from the source in different directions according to different levels of pressure. The ratio of the sound intensity at a specific distance in a free field to the sound intensity of a point that has the same distance and power is called the directivity Q_θ then:

$$Q_\theta = (P_{rms}^2)_\theta / (P_{rms}^2) \dots\dots\dots (13)$$

Where:

$(P_{rms}^2)_\theta$: mean square acoustic pressure measured at angle θ and radius r from the source.

P_{rms}^2 : mean square acoustic pressure averaged over the surface of an imaginary sphere of radius r centered on the source, this value could be calculated from:

$$P_{rms}^2 = (1/n) \sum P_i^2 \dots\dots\dots (14)$$

The directivity index ID is defined as:

$$ID_\theta = 10 \text{Log}_{10} Q_\theta = L_{p\theta} - L_p \dots\dots\dots (15)$$

Where:

$L_{p\theta}$: sound pressure level at angle θ and distance r from the source.

L_p : average sound pressure level at radius r from the source; this value can be calculated from the equation:

$$L_p = 10 \text{Log}_{10} [\sum 10^{L_{pi}/10}] - 10 \text{Log}_{10} n \dots\dots\dots (16)$$

Where:

n : number of points measured in an imaginary sphere [50].

3.6 Some concepts of wind turbine

Before going deep into the details of a wind turbine, some concepts need to be defined; wind turbines consist of a rotor, generator, and tower, and the rotor has a number of blades (usually three). Figure (17) shows the terms dealt with in this study of the airfoil.

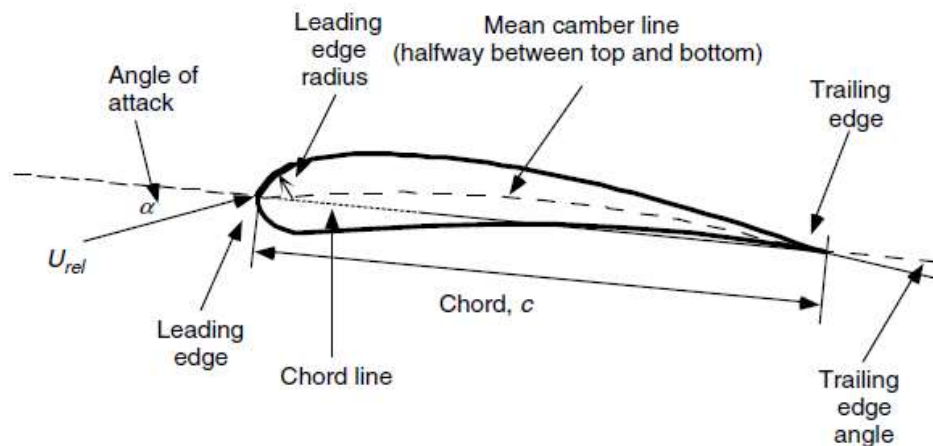


Figure 17. The airfoil details

The most forward point of the airfoil is called the leading edge, and the furthest back point is called the trailing edge. The chord line (c) of the airfoil is a straight line that connects these two points. The mean camber line is the line halfway between the upper and lower surfaces. In most airfoils, the upper surface is longer than the lower surface, and this extra distance will accelerate the flow over the airfoil, increasing the velocity and reducing the pressure at upper surface of the airfoil. This difference in pressure between the upper and lower surfaces will generate force from the lower to the upper surface. Therefore, the upper side is called the suction side, and the lower side is called the pressure side. However, for this study, the NACA 0012 is a symmetric airfoil. Generally in 2D, the force generated has two components: the force perpendicular to the flow

direction is called the lift force (FL), and the force in the same direction of the flow is called the drag force (FD). Lift and drag coefficients, CL and CD, could be defined as:

$$C_L = \frac{F_L}{\frac{1}{2}\rho V_0^2 c} \dots\dots\dots(17)$$

$$C_D = \frac{F_D}{\frac{1}{2}\rho V_0^2 c} \dots\dots\dots(18)$$

Where ρ is the air density, c is the chord length, and V_0 is the flow velocity. Note that the unit for the lift and drag in equations 16 and 17 is force per length (in N/m) [51] [52]

3.6.1 Actuator disc concept

The main function of a wind turbine is to extract the kinetic energy of the incoming flow and convert it into rotation of the blade. The thrust force and power are directly related to the drop of flow velocity upstream and downstream of the rotor. In this section, thrust and power are going to be calculated from mass and momentum conservation law and axial momentum theory.

Figure (18) below shows the flow velocities and pressure before and after the interaction with the blades. At the beginning, the axial induction factor a needs to be defined as a ratio of the reduction of the velocity before and at the blade.

$$a = \frac{V_0 - V}{V_0} \dots\dots\dots(19)$$

Where V_0 is the flow velocity far upstream and V is the flow velocity at the rotor [49] [53].

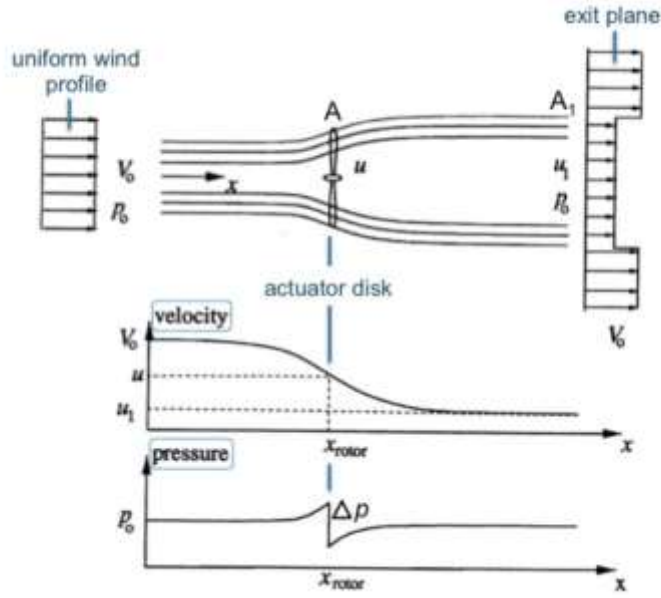


Figure 18. Axial velocity and pressure development before and after the rotor

The thrust can also be defined as the pressure drop across the actuator disc times the area of the rotor.

$$T = \Delta P \cdot A \dots\dots\dots(20)$$

Where T is the thrust, A the area of the rotor.

But:

$$\Delta P = \frac{1}{2} \rho [V_0^2 - V_1^2] \dots\dots\dots(21)$$

Therefore:

$$T = \frac{1}{2} \rho A [V_0^2 - V_1^2] \dots\dots\dots(22)$$

The relation between V , V_0 , and V_1 can be written as:

$$V = \frac{1}{2} [V_0 + V_1] \dots\dots\dots(23)$$

From (19):

$$V = V_0[1 - a] \quad \dots\dots\dots(24)$$

And the wake velocity V_1 can be expressed in term V_0 and a as:

$$V_1 = V_0[1 - 2a] \quad \dots\dots\dots(25)$$

Thrust in terms of a will be:

$$T = \frac{1}{2}\rho AV_0^2 a[1 - 2a] \quad \dots\dots\dots(26)$$

Thrust coefficient can be defined as:

$$C_T = T / [\frac{1}{2}\rho AV_0^2] \quad \dots\dots\dots(27)$$

Then:

$$C_T = 4a[1 - a] \quad \dots\dots\dots(28)$$

The power that extracted from the flow at the rotor is:

$$P = T.V_0 \quad \dots\dots\dots(29)$$

Then:

$$P = 2\rho AV_0^3 a[1 - a]^2 \quad \dots\dots\dots(30)$$

At the same way, the power coefficient can be defined as:

$$C_P = P / [\frac{1}{2}\rho AV_0^3] \quad \dots\dots\dots(31)$$

Then:

$$C_P = 4a[1 - a]^2 \quad \dots\dots\dots(32)$$

To find the maximum thrust coefficient with respect to a :

$$\frac{dC_T}{da} = \frac{d}{da} [4a(1 - a)] = 0 \quad \dots\dots\dots(33)$$

$$a = \frac{1}{2}$$

$$C_{T \max} = 1$$

At the same way, the maximum power coefficient is:

$$\frac{dC_P}{da} = \frac{d}{da} [4a(1 - a)^2] = 0 \quad \dots\dots\dots(34)$$

$$a = [1, \frac{1}{3}]$$

$$C_{P \max} = 0.593$$

This maximum power coefficient is called Betz limit [49] [53].

3.7 Noise sources from wind turbines

The leading theory of aeroacoustics for the past 50 years has been Lighthill's acoustic analogy. His theory is focused on sound generation from an unsteady flow with a low Mach number in an infinite fluid region. The Lighthill equation is derived from the continuity and momentum equations. Generally, there are two main sources of noise due to wind turbines: aerodynamic noise and mechanical noise [27].

3.7.1 Mechanical noise

The mechanical noise is the part of sound generated by the different components in the hub of the turbine, such as the gearbox, generator, cooling fan, yaw drives, and other auxiliary tools. The mechanical noise in modern wind turbines has been addressed over the past few years to

provide insulation and sound dampening materials to reduce the loudness of the internal mechanical components. However, failure or wear of the gear assembly is known to continually cause tonal sounds [54].

3.7.2 Aerodynamic noise

Aerodynamic noise stems from the rotation of the blades. The acoustic energy is easily propagated a far distance due to its large wavelength, which annoys the residents close to wind turbine farms. Noise is related to turbulence through Reynolds stress which is the noise generator term given by the Lighthill wave equation shown in the equation below [27].

$$\frac{\delta^2 \rho}{\delta^2 t} - c^2 \frac{\delta^2 \rho}{\delta x_i \delta x_j} = \frac{\delta^2 T_{ij}}{\delta x_i \delta x_j} \dots\dots\dots(35)$$

$$T_{ij} = \rho u_i u_j + (p - c^2 \rho) \delta_{ij} - T_{ij} \dots\dots\dots(36)$$

Where:

ρ : the density,

c : the sound velocity,

u_i, u_j : the fluid velocity components,

p : the pressure and

T_{ij} : the viscous stress tensor

The turbulence intensity for the air flow around the airfoil can be calculated from the velocity measurements captured by the hot-wire anemometer using equation (37) below.

$$I = \frac{\dot{u}}{U} \dots\dots\dots (37)$$

Where U is the mean velocity at the centerline of the wind tunnel exit and

$$\dot{u} = \sqrt{\frac{1}{3}(\dot{u}_x^2 + \dot{u}_y^2 + \dot{u}_z^2)} = \sqrt{\frac{2}{3}k}$$

Where:

$\dot{u}_{x,y,z}$: are the velocity fluctuation components

k : the turbulence energy

There are three main categories of aerodynamic noise classified according to their generation: low frequency noise, turbulent inflow noise, and airfoil self-noise. The sound is perceived as a swishing or hissing sound and is typically broadband in character.

3.7.2.1 Low frequency noise

This type of noise is usually less than 20 Hz. It occurs when the air flow is forced to move around the cylindrical tower of the wind turbine. This type of noise is not very recognizable because it is below the audible range of human hearing. On the other hand, it may cause vibration in buildings and windows, and this may annoy people [49]. The frequency of this kind of noise is related directly to the blade passing frequency f_B and its harmonic f_n

$$f_B = n_B \cdot f_R \dots\dots\dots (36)$$

and:

$$f_n = n \cdot f_B \dots\dots\dots (37)$$

Where:

f_R is the rotor frequency, n_B the number of blades, $n=1, 2, 3, \dots$

These frequencies appear as peaks on the noise spectrum and usually in the low frequency. The sound pressure level can be high especially in case of downwind turbines as the rotors on these

turbines are allocated at front. Low frequency noise in wind turbines can be affected by the distance and the orientation between the rotor and the tower. Larger distances between the rotor and the tower can cause less sound radiation and vice versa; also, the noise is lower for upwind turbines than downwind ones [55]. Figure (19) shows the flow around a cylindrical wind turbine tower. [49]

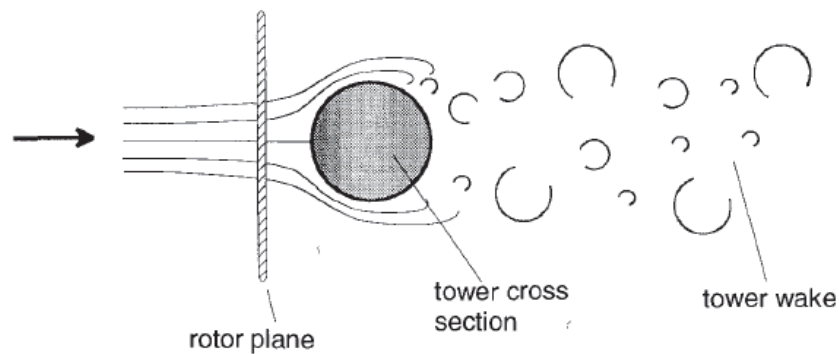


Figure 19. Flow around a cylindrical wind turbine tower

3.7.2.2 Turbulent inflow noise

The second aerodynamic source is turbulent inflow noise that may cause unsteady loading distribution around the blades. This type of noise is generated when the turbulence of the atmosphere encounters the blades of wind turbine and cause broadband noise. The frequency in this type of noise depends on the size of the eddy of the flow turbulence. If the eddy is larger than the airfoil chord length, then the noise frequency will be low and vice versa. This type of noise is not fully understood but is considered one of the main aerodynamic noise sources. This type of noise has a frequency of up to 1,000 Hz and can be described as a swishing noise by people. Figure (20) shows the size of the turbulence eddies and blade loading [30] [56].

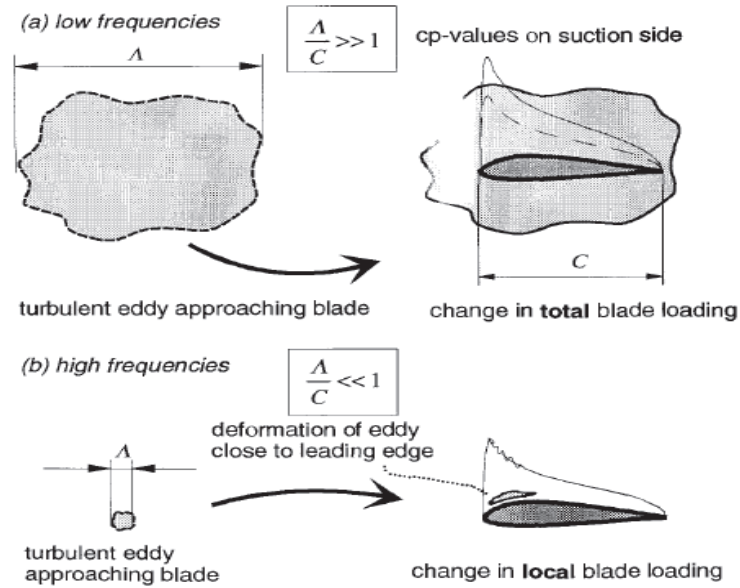


Figure 20. Size of the turbulent eddies and blade loading

3.7.2.3 Airfoil self-noise

The final aerodynamic source from wind turbine noise is airfoil self-noise. This type of noise occurs as a result of interaction between the blades and their boundary layer. There are many types of airfoil self-noise, such as Turbulent Boundary Layer Trailing Edge Noise (TBLTE), Laminar Boundary Layer Vortex Shedding Noise (LBLVS), Tip Vortex Noise (TIP), Separation-Stall Noise (SEP), and Trailing Edge Bluntness Vortex Shedding Noise (TEBVS) [25] [5] [57].

Figure (21) shows the different kinds of airfoil self-noise.

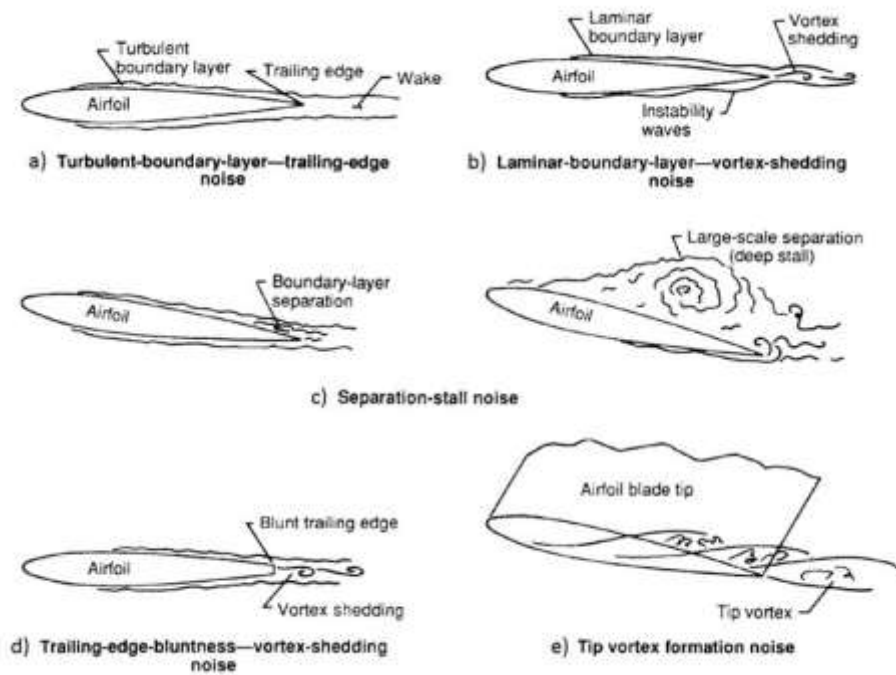


Figure 21. Kind of airfoil self-noise

Paterson et al. showed that the noise field of an airfoil was governed by vortex-shedding at the trailing edge of the airfoil, where the boundary layer measurement was correlated to the microphone noise measurement. Paterson et al. suggested the following formula to quantify the tones emitted by NACA 0012 and NACA 0018 airfoils [51]

$$f = \frac{KU^{1.5}}{(cv)^{0.5}} \dots\dots\dots (38)$$

Where:

f : frequency of acoustic tone,

U : free stream velocity,

c : chord length,

ν : kinematic viscosity,

K : an arbitrary constant.

This chapter covered the mathematical equations of the study, including the acoustics equations, forces equations, and turbulence equations. Some of the sound properties were explained in this chapter to provide clear understanding of noise: how does the noise generate, how does it transfer, and how does the noise affect the people who live close to the wind turbines. Force equations included in this chapter such as the lift coefficient and drag coefficient, because the efficiency of the wind turbines depends on these coefficients. Turbulence equations are included in the chapter because the turbulence fluctuation in the flow around the wind turbines is responsible of the noise generation.

CHAPTER 4

EXPERIMENTAL AND NUMERICAL WORK

4.1 Experimental work

The objective of this chapter is to design and build all the necessary equipment and tools to measure the data. The data that needs to be measured in this chapter includes: noise data, force data, and turbulence data. The experimental work includes:

- Source of flow: the wind tunnel already exists in the fluid dynamic laboratory of the mechanical engineering department, at Western Michigan University WMU.
- To get more accuracy of the noise data, a quiet area is required to be built around the testing area.
- Airfoils with channels need to be designed and printed.
- Equipment to measure the noise data.
- Design a balance to measure and collect force measurements.
- Prepare and collect all the necessary tools to measure the turbulence by hot-wire anemometer technique.

4.1.1 The wind tunnel

To generate flow for aerodynamic noise measurements, the wind tunnel of the fluid dynamic laboratory of the mechanical engineering department was used. This wind tunnel has a flow velocity up to 29 m/s with a circular exit with a diameter of 13 cm. To make acoustics measurements, a quiet environment is required, so a testing area was built around this wind tunnel.

4.1.2 The quiet room designing

ANSYS Fluent is used to simulate the flow inside the testing area. The inlet of the chamber is 13 cm in diameter (the exit diameter of the wind tunnel). There are two factors that may affect the flow inside the chamber that need to be focused on: a) the chamber size, and b) the outlet size. In order to figure out the effects of these two factors on the air flow and the wind velocity, four geometries are simulated using CFD. Code Fluent from ANSYS:

- The first geometry was 1 cubic meter size with a 13 cm diameter outlet.
- The second geometry was 1 cubic meter size with a 26 cm diameter outlet.
- The third geometry was 9 cubic meter size with a 13 cm diameter outlet.
- The fourth geometry was 9 cubic meter size with a 26 cm diameter outlet.

The air was used as an inlet flow with velocity 30 m/s. for the above mentioned geometries, the simulations were carried out and results were presented below:

- a) 1 cubic meter chamber size with 13 and 26 cm diameter outlet

Figure (22) shows the geometry of a 1 cubic meter chamber size with 13 cm (on left) and 26 cm (on right) diameter outlets.

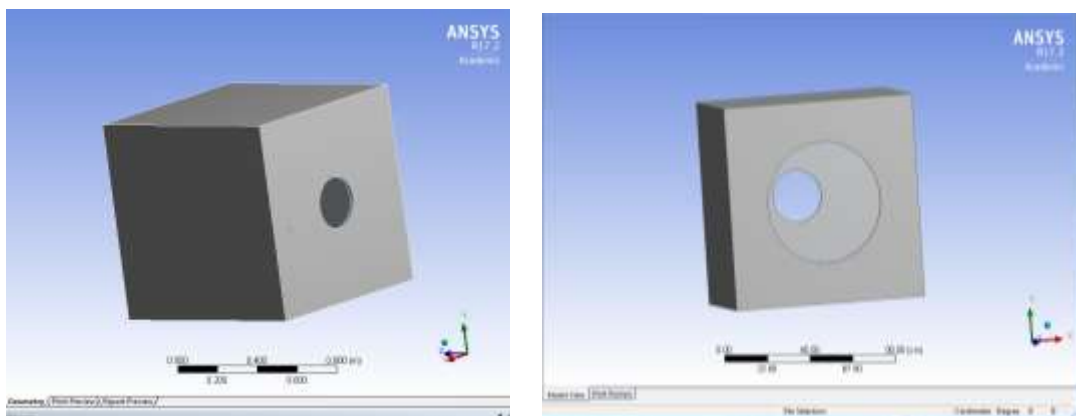


Figure 22. The geometry of 1 cubic meter chamber size with 13 and 26 cm diameter outlet

Figure (23) shows the scholar velocity magnitudes in (m/s) for both of the two chambers. It can be clearly seen that the effects of the increase in the outlet diameters on the wind velocity magnitude. In the first figure on the left, with a 13 cm outlet diameter, the wind keeps maintaining at the same velocity for about 50 cm compared with more than 75 cm in the case of 26 cm of outlet diameter. Therefore, in order to have a steady flow, increasing the outlet diameter is a preferred option.

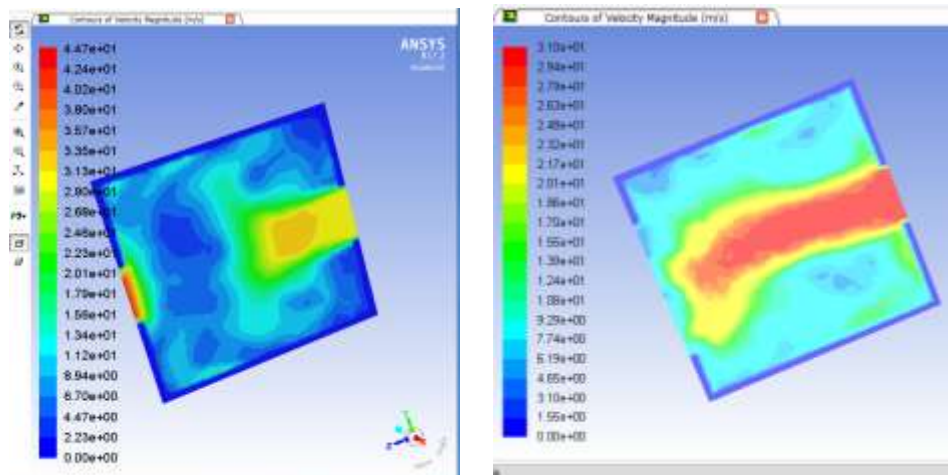


Figure 23. The counter of velocity magnitude in (m/s) for both of the two chambers

Similarly, Figure (24) illustrates the velocity vectors' magnitude for both chambers. The results showed the flow maintained steady state longer for the case of the larger diameter outlet, compared with the smaller one as expected. The recirculations and eddies developments were clearly seen in the small diameter outlet case.

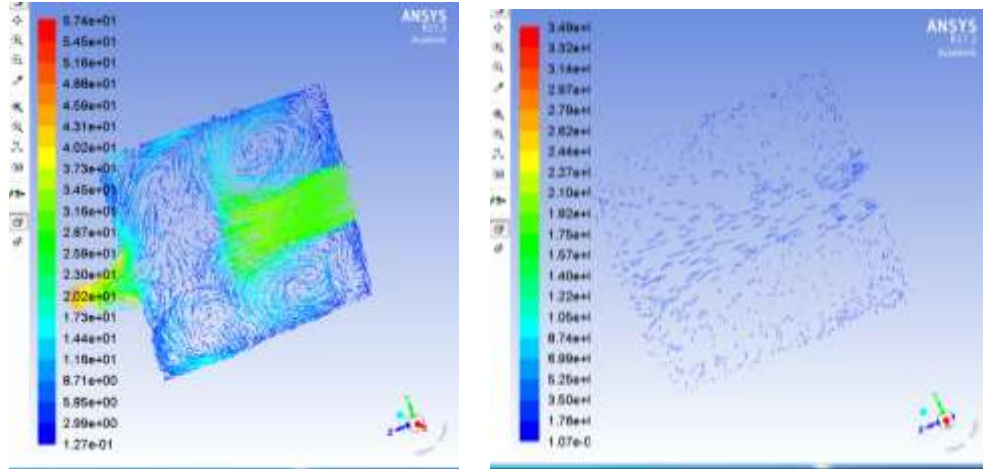


Figure 24. The velocity vectors magnitude for both chambers

b) 9 cubic meter chamber size with 13 and 26 cm diameter outlets

The dimensions increased to be three times larger than the first designed chamber. The geometry of a 9 cubic meter chamber size with 13 cm (on left) and 26 cm (on right) diameter outlets were shown in the Figure (25) below.

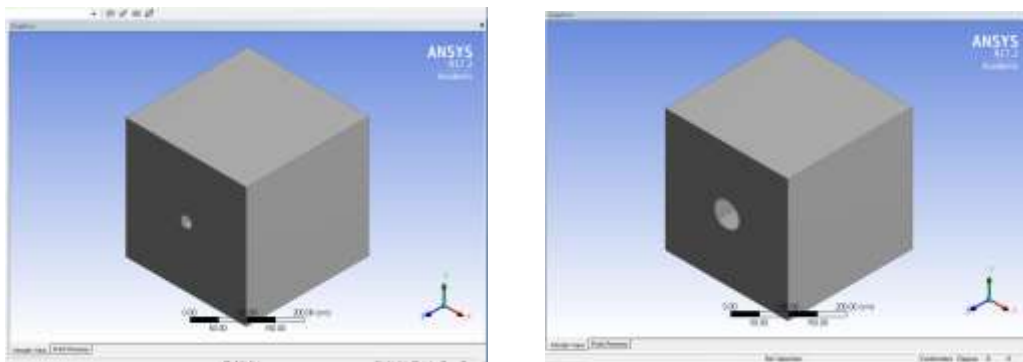


Figure 25. The geometry of 9 cubic meter chamber size with 13 and 26 cm diameter outlet

Figure (26) shows the counter of velocity magnitude in (m/s) for both of the chambers, exactly like the previous case. The effects of the outlet size on the wind velocity magnitude were

very clear. In the first case, with a 13 cm outlet diameter, the wind keeps steady in the same velocity for about 1 m compared with more than 2 m in a 26 cm of outlet diameter.

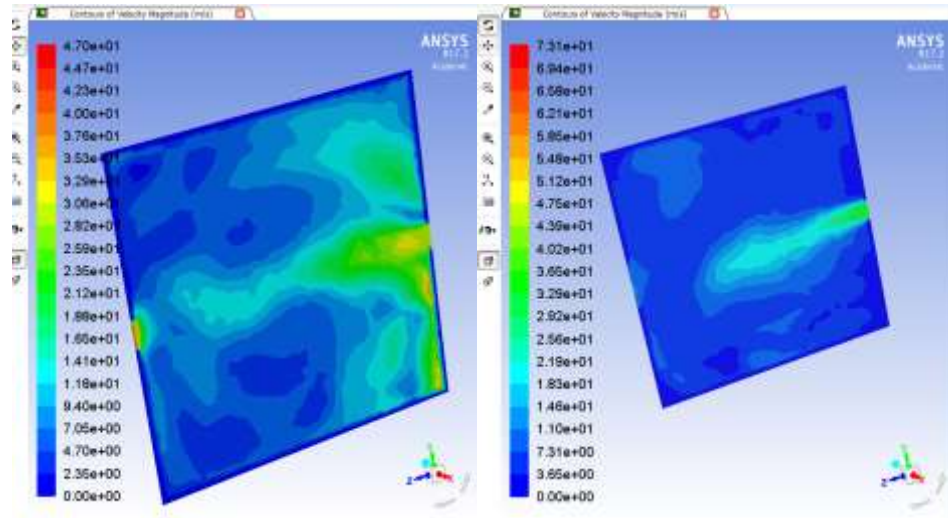


Figure 26. The counter of velocity magnitude in (m/s) for both chambers

Figure (27) shows the velocity vectors magnitude for both of the chambers. The flow looks steady, and there are less recirculations in the chamber with a 26 cm outlet diameter compared with recirculation bubbles or eddies in the chamber with a 13 cm outlet diameter.

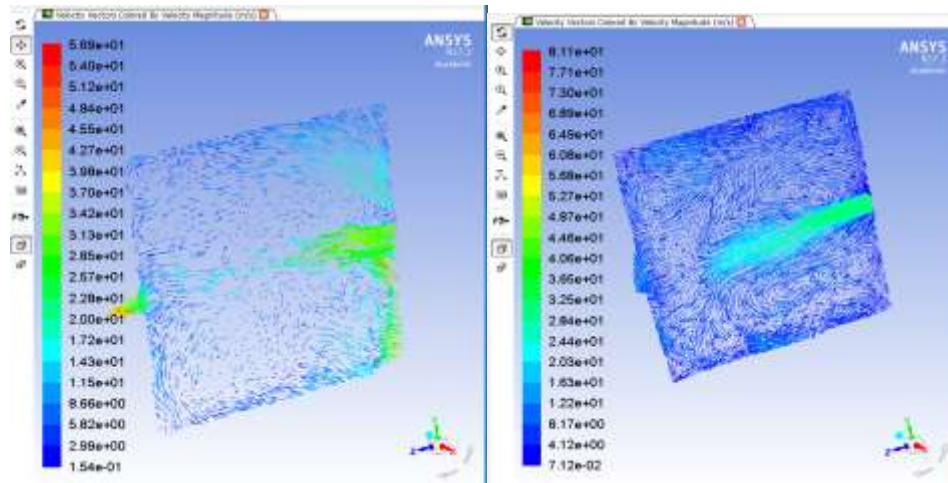


Figure 27. The velocity vectors magnitude for both chambers

As comparing the simulation results, it is decided to build 10 feet long, 10 feet wide, and 9 feet height quiet chamber to produce more speedy flow inside the room.

4.1.3 Wind Tunnel testing area (quiet room)

The wind tunnel testing area, also called the quiet room, was built in the Fluid Dynamics Laboratory on Western Michigan University's College of Engineering and Applied Sciences campus in room G-107. The assembly of the quiet room was an integral component for the research because, to test for aerodynamic noise, the designated area for testing needs to provide an insulated environment that negates outside noise and echo from within. The wind tunnel generator was already provided in the laboratory, and the quiet room was built around the generator's outlet for wind flow.

The first phase for the construction of the quiet room was the design, which is a simple cubicle room that was 10 feet in length, 10 feet in width, and 9 feet in height. Prior to constructing the room, it was first modeled in AutoCAD in 3D and viewed for approval of its structure as shown in Figure (28).



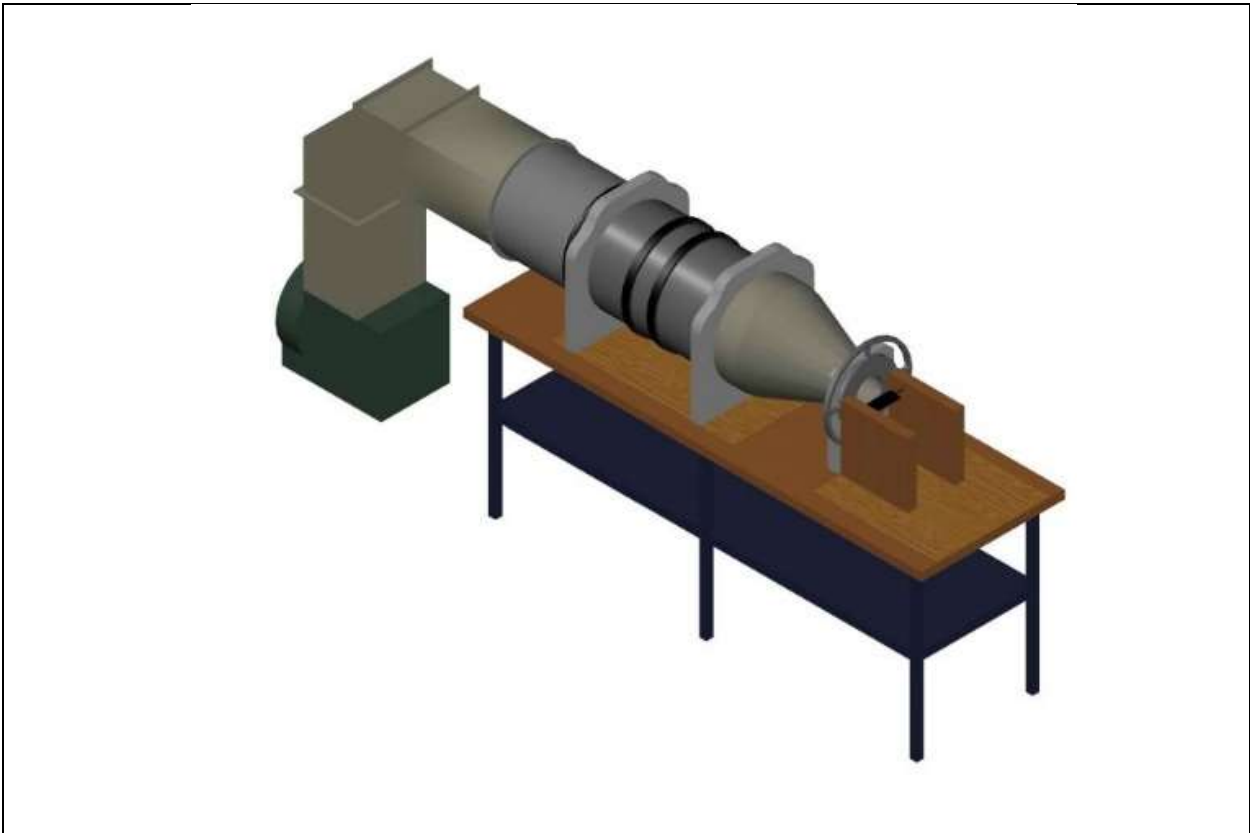
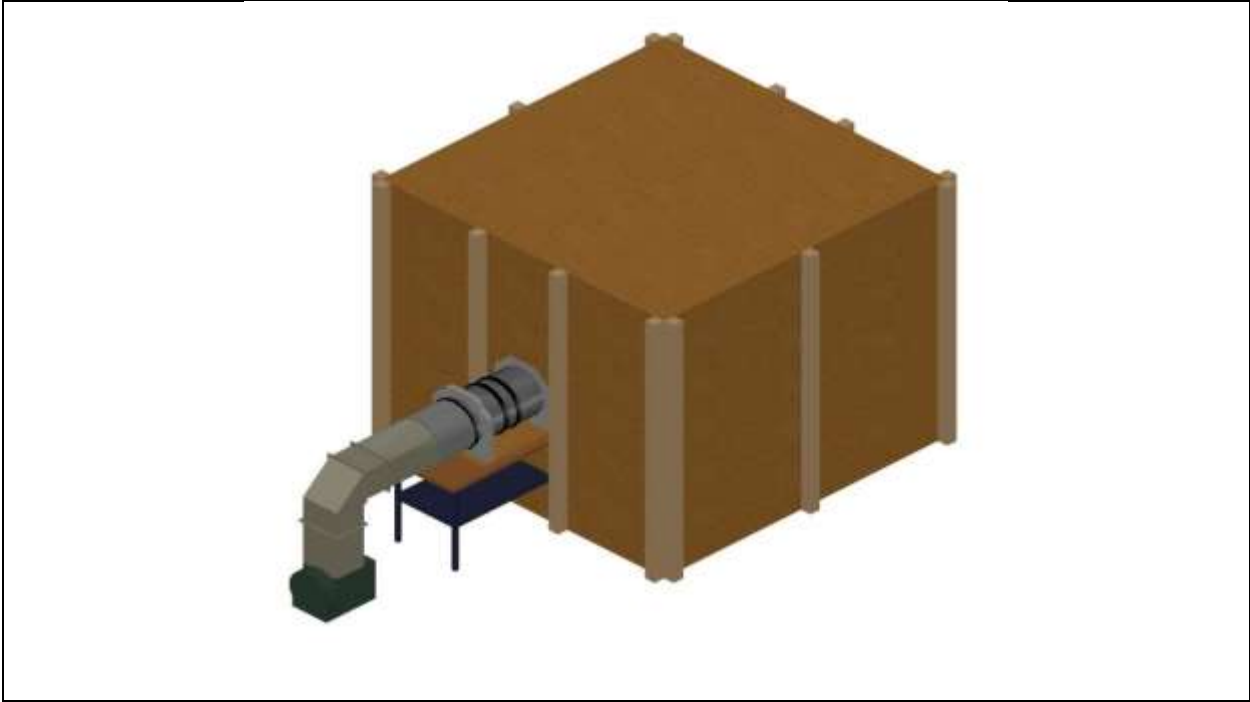


Figure 28. Quiet crea modeled in AutoCAD in 3D

Plywood was used to build the structure of the walls and ceiling; the first phase of construction of the room can be seen below in Figure (29).



Figure 29. The plywood used to build the structure of the walls and ceiling

Also, in Figure (30) the middle opening section was where the wind tunnel generator would be placed. A door was also added for convenient personnel entry.



Figure 30. Middle opening section was where the wind tunnel generator would be placed

The second phase of building the quiet room was outfitting it with three layers of foam. The first foam layer consisted of two layers of $\frac{1}{4}$ inch white foam (Volara Foam) that covered the entirety of the inside of the room (the walls, ceiling, and floor). This foam's purpose was to negate about 50% of exterior noise and reduce vibrations as shown in the Figure (31).



Figure 31. The first layer of foam (Volara Foam)

The second foam used was a 4-inch black foam (Wedge Foam) that was laid over all the white foam. The black foam was to prevent any echo from noise generated within the room as shown in Figure (32). These two foams provided from (Foam N More Company). For more information see the link: (<https://foamforyou.com/noise-control>)



Figure 32. The second layer of foam (Wedge Foam)

Lastly, the third foam was a FOAMULAR® 250 (25 psi) R-15 Extruded Polystyrene Foam Board Insulation 2" x 4' x 8' - Square Edge, bought from Menards that covered the exterior of the quiet room to add further protection from exterior noises as shown in Figure (33).



Figure 33. The third layer of foam to add further protection from exterior noises

An adhesive made for specially foam applications provided by Foam N More Company was used to attach all foams. Upon completion of adding the foam, there were permeable cracks from the purple foam that were sealed off by using caulk for further protection from the outside noise.

The third and final phase was placing the wind tunnel generator within the quiet room. The part of the tunnel with the outflow was placed inside the room, and the other part with the control operations was left outside. The tunnel inside was also outfitted with foam to further reduce vibrations and excess noise. A hole with a diameter of (35cm) was created in the wall at the opposite end of the wind tunnel outflow to give an exit for the wind and prevent it from making contact with the wall and generating undesired noise. The completion of the room can be seen in Figure (34) below.



Figure 34. Quiet room completed

4.1.4 Noise measurements

4.1.4.1 The microphones set up

Four microphones were used to measure the noise around the airfoil; the First one (mic.1) is a low frequency free field microphone with a frequency range of (0.13 to 20000 Hz). The other three microphones (mic.2, mic.3, and mic.4) measure the audible noise (20-20000 Hz).

The microphones were set up as shown in Figure (35). All four microphones were located at the same distance from the samples: mic.1 was located perpendicular to and 6 inches away from the trailing edge; mic.2 was located 6 inches and a 45 degree angle from the trailing edge; mic.3 was located perpendicular to and 6 inches away from the middle point of the chord; and mic.4 was located perpendicular to and 6 inches away from the leading edge. The microphones were connected to the Smart Office application that could read and save the level of noise for all the range of the interested frequencies.

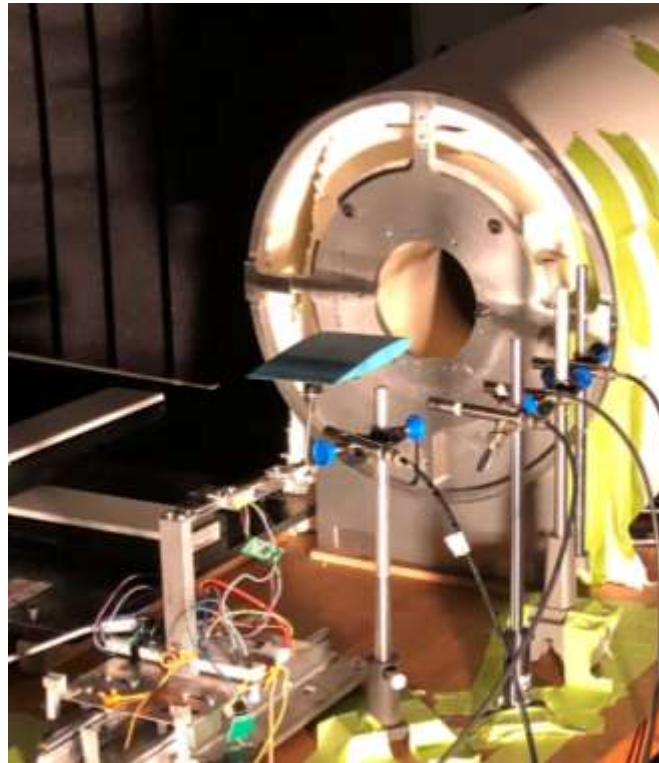


Figure 35. The microphones set up

The four ½-inch free-field polarized microphones were used to measure infrasound at separate points simultaneously. Both are ICP Infrasound Microphone systems manufactured by PCB Piezotronics. The microphone system is composed of the microphone (Model: 377A07), preamplifier (Model: 426E01) and a low-frequency filter adapter (Model: 079A43). The complete system allows for the measurement of noise down to 0.1 Hz. Before testing, all the microphones are calibrated using a Larson Davis CAL200 Precision Acoustic Calibrator. The CAL200 was set to a 94 dB noise source at 1kHz. The sensitivity is altered during calibration so that the output of the microphone is within 0.025% of the 94 dB source. This output is displayed numerically and graphically on a frequency spectrum within the m+p SmartOffice Dynamic Signal Acquisition and Analysis software. To mitigate this effect in measurement readings, the manufacturer has pre-calibrated the microphones to account for themselves [58]. Figure (36) shows the ½ inch Infrasound Microphone System Outline Drawing, and Figure (37) shows ½” Microphones being calibrated by Larson Davis CAL200.

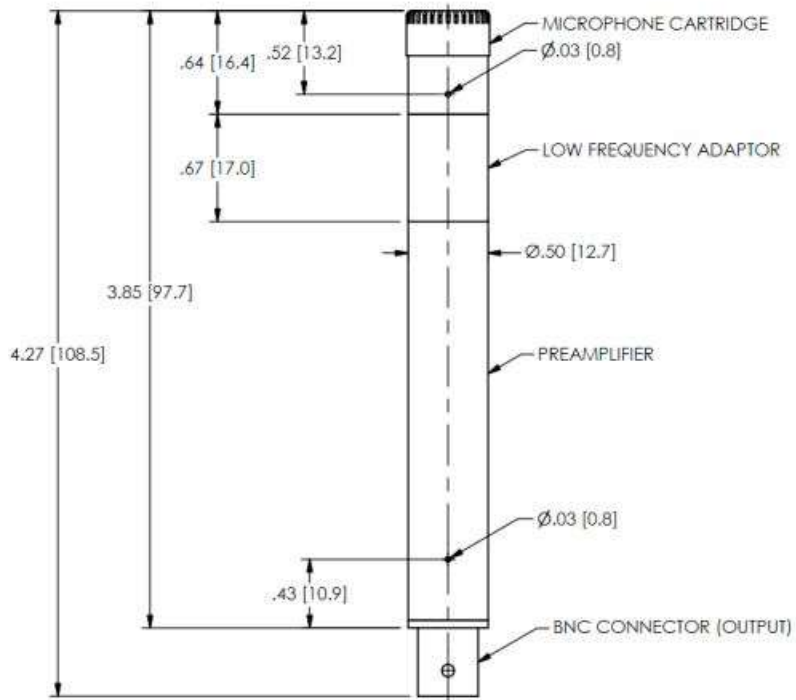


Figure 36. 1/2 inch Infrasound Microphone System Outline Drawing



Figure 37. 1/2" Microphones being calibrated by Larson Davis CAL200

The four microphones are connected via a coaxial cable to a National Instruments C-Series Sound and Vibration Input Module. It can simultaneously measure dynamic signals from all four

of its inputs. The Input Module is connected to a National Instruments CompactDAQ HiSpeed USB Carrier Chassis pictured in Figures (38) and (39). The USB Chassis provides a gateway between the serial port on the input module to the computer running the m+p SmartOffice software using a male USB Type B to male USB Type-A cable. Figure (38) shows NI-9234 C-Series Sound and Vibration Input Module [59], and Figure (39) shows NI-9162 CDAQ USB Chassis [60]



Figure 38. NI-9234 C-series sound and vibration input module



Figure 39. NI-9162 CDAQ USB chassis

4.1.5 Wind tunnel testing procedure

Before the wind tunnel testing can begin, the wind tunnel does not provide actual wind velocity values, so a method was needed to measure the velocity output. A digital manometer, seen below in Figure (41), was used to measure the pressure of the wind when the tunnel was in operation. The measured pressure was then converted into velocity. Density of air was assumed to be 1.225 kg/m^3 . With a valid method to calculate the wind flow speed, then it could easily be controlled to operate at designated speeds of 5, 10, and 15 m/s.



Figure 40. Digital Manometer

4.1.6 Test samples

4.1.6.1 NACA 0012 airfoil

NACA 0012 airfoil was used in this study, and SolidWorks was used to design the samples. The data used to generate a two-dimensional profile was retrieved from <http://airfoiltools.com/airfoil/NACA4digit>. [61] The two-dimensional profile was imported to SolidWorks and extruded to generate the 3D model. The channels were represented by circles with different diameters and then extruded in different angles. The sample's design was already decided and drawn using SolidWorks, so no further changes were made. 12 different samples were generated to show the differences of the noise and forces around the airfoil; the first sample was designed to be with no channel the base case. Channels were generated through the airfoil starting from the leading edge with the length of the airfoil's chord with different sizes and different angles with the chord. Three different channels' diameter sizes (0.05, 0.08, 0.1 inch) were used in every angle between the channels' direction and the chord direction; the distance between channels is

0.25inch. Four different directions of these channels were used between the channels and chord direction (-1, 0, 2, and 3 degrees). Just in the angle (-1), the channel's diameter sizes (0.05, 0.08 inch) were used, and (0.1 inch) was not used due to the designing problem. These 12 samples were sent to a 3D printer to create them. The surface of these samples was not smooth enough, and this may generate more eddies that may cause more turbulence which is responsible for generating aerodynamic noise. To treat this issue, sandpaper was used with 20 different Grit sizes (P60, P80, P100, P120, P150, P180, P240, P280, P320, P360, P400, P500, P600, P800, P1000, P1200, P1500, P2000, P2500, and P3000).

For every sample, measurements were taken in three different angles of attack (5, 10, and 15 degrees) and three different flow speeds (5, 10, and 15 m/s). The Figures (41) and (42) show the unchanneled and A3D0.1 samples designed in SolidWorks in both 3D and 2D views, and Figure (43) shows the picture of NACA 0012 airfoil. For the other nine samples, see the appendix E.

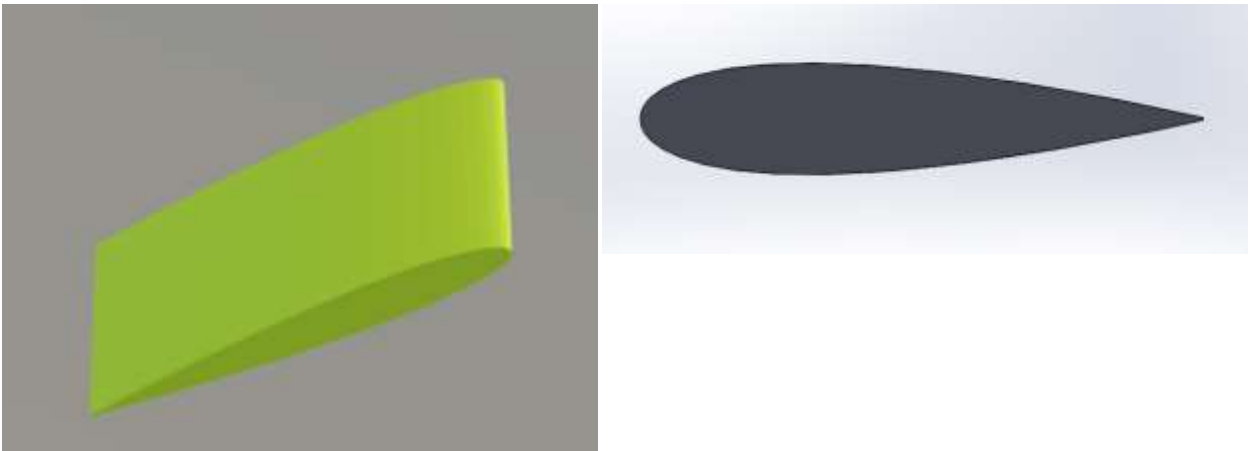


Figure 41. The unchanneled airfoil 3D and 2D views

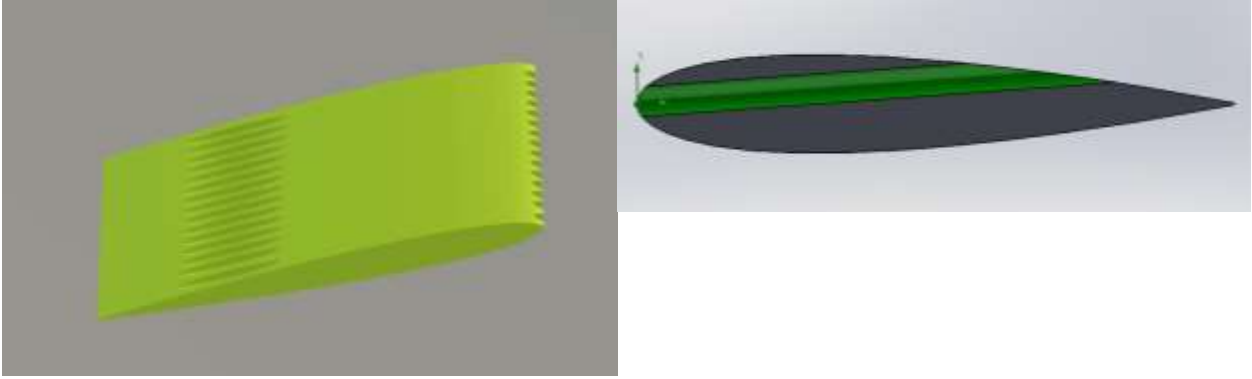


Figure 42. Airfoil with channel direction 3 degrees and diameter size 0.1 inch 3D and 2D views

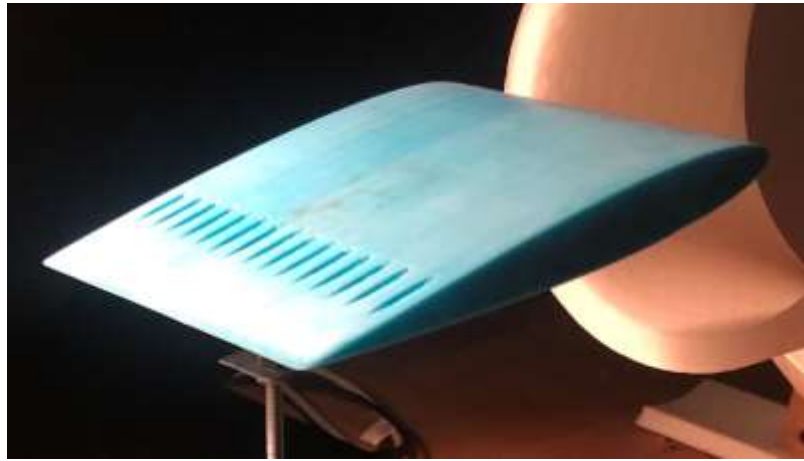


Figure 43. Picture of NACA 0012

4.1.7 Force measurements

4.1.7.1 Force balance

Lift and drag forces need to be measured around the airfoil samples in the wind tunnel where the quiet room was built. For this reason, the force balance was designed and built. The balance was made of four load cells, two of them responsible for measuring the vertical forces (lift force) and the other two to measure the horizontal forces (drag force). The angle of attack was designed to be measured manually. 500 gm capacity load cells of aluminum alloy weighing sensor were used in the balance. These load cells convert the strain forces to voltage. This voltage could be read using Arduino which was connected to the computer. Figure (44) shows the force balance

designed by SolidWorks, Figure (45) shows it after completion, and Figure (46) shows the calibration set up for the forces' balance.

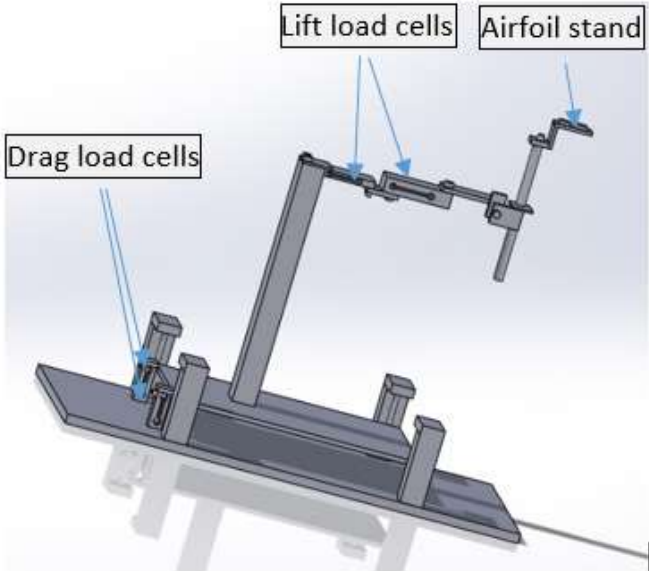


Figure 44. The force balance designed by solid works program

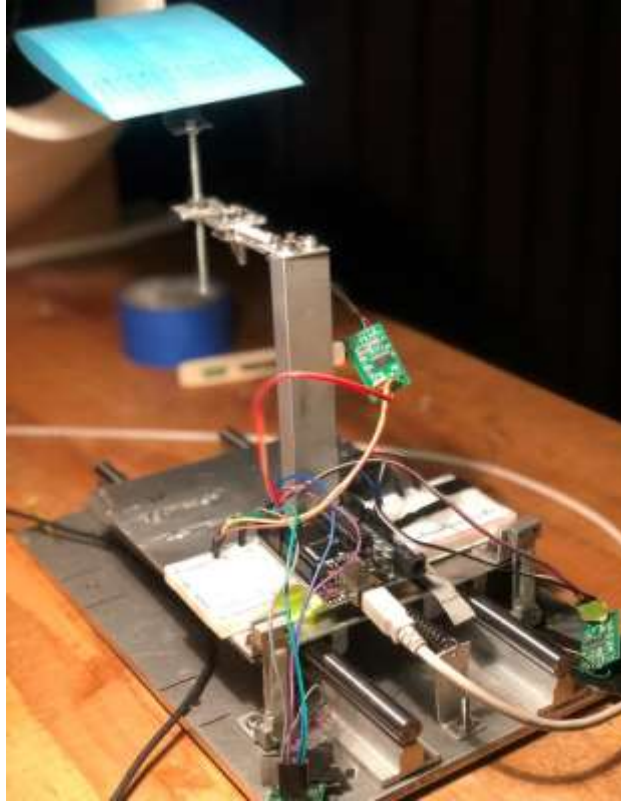


Figure 45. The force balance ready to measure the forces



Figure 46. The calibration set up of the force balance

4.1.8 Velocity and turbulence measurements

4.1.8.1 The hot-wire anemometer

For velocity and turbulence measurements, the hot-wire anemometer is proven to be a feasible method that provides accurate measurements for velocity fluctuations. The hot wire anemometer is capable of capturing the velocity change within a microsecond. Figure (47) shows the constant temperature anemometer used to capture velocity data around the airfoil samples and the linear stages assembly used to mount and control the probe motion. Three Newmark NLS linear stages were integrated with an additional rotary stage to move the probe in three dimensions for turbulence measurements. All stages were controlled using M drive computer software. The wind tunnel was used to calibrate the hot-film probe using a Kiel probe pressure transducer as a reference. The velocity values measured with the Kiel probe were correlated to the voltage captured with the hot-film at the same location. Figure (48) shows the 2D design of the hot wire and microphones set up, while Figure (49) shows the calibration curve for the probe used in the experimental measurements.

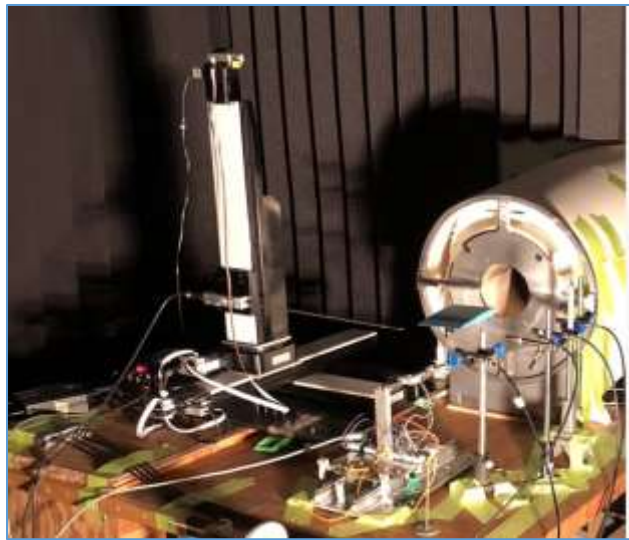


Figure 47. The hot-wire anemometer setup

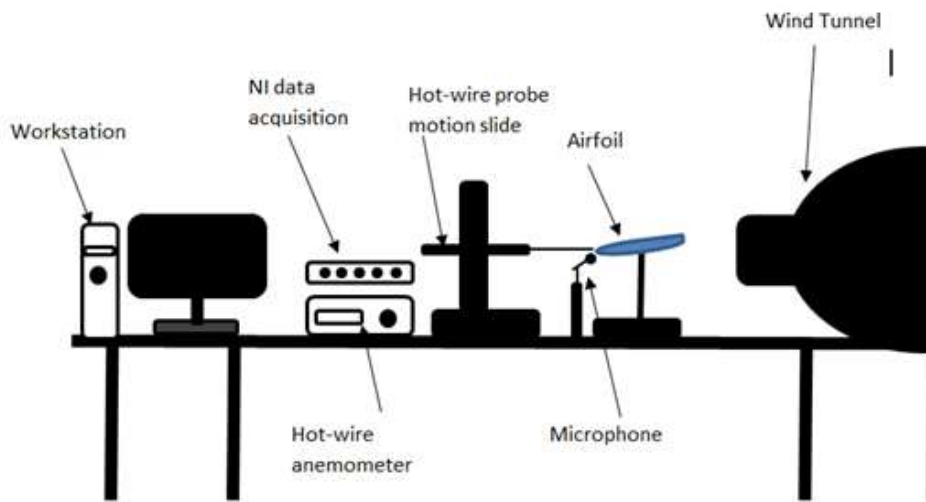


Figure 48. 2D designing of the hot wire and microphones setup

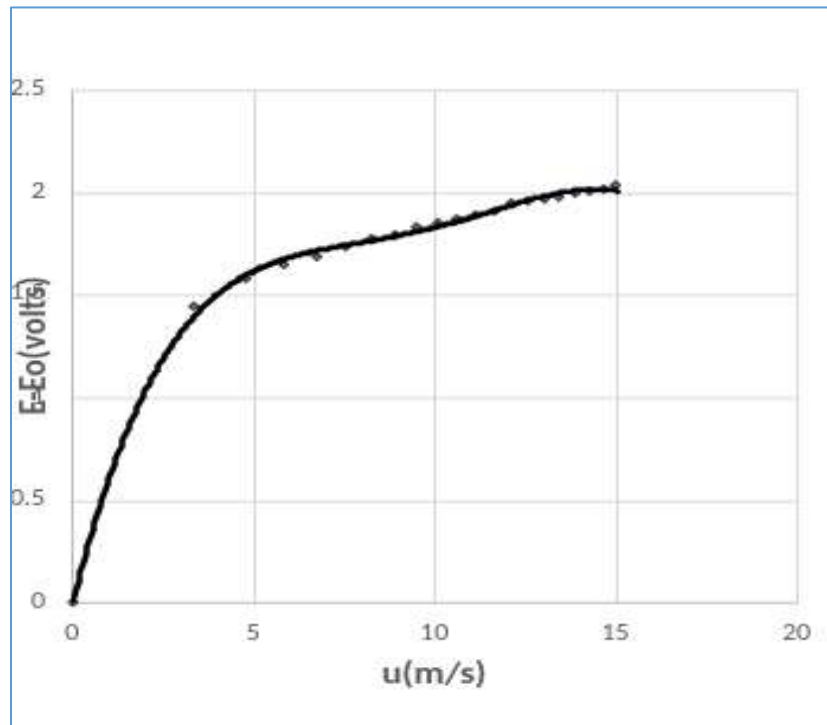


Figure 49. The hot-film calibration curve for the hot-film probe used in the velocity tests

The velocity data have been captured using NI USB 6012 data acquisition hardware aided with a LabVIEW interface. MATLAB along with Microsoft Excel was used to process the data and generate graphs.

4.2 Method of numerical simulation

4.2.1 Computational domains

Five different 2D models for NACA 0012 are considered in the current computations. The primary airfoil is a regular NACA 0012 airfoil with 5.5 inch as a chord length. Three channeled airfoils of 3° inclination, A3, with diameters ($D=0.1, 0.08, 0.05$ inch) were studied as shown in Figure (50) and (51). The figure show the airfoil's geometries and meshes at a 10° angle of attack. The far-field boundaries are set at 18 chords away from the leading edge in front, up, and down directions and 36 chords away in the back direction.

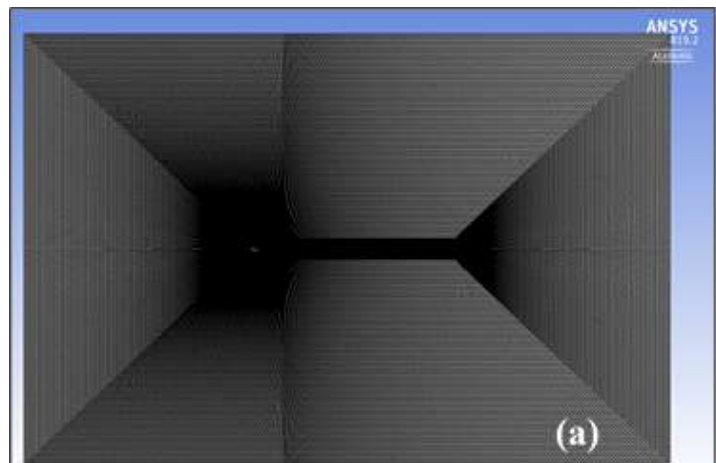


Figure 50. Regular airfoil's entire domain

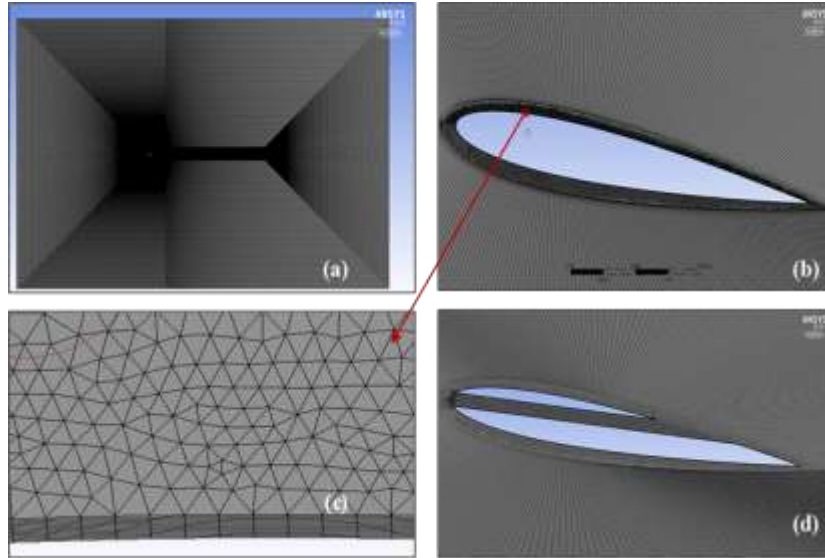


Figure 51. a) Regular airfoil's entire domain. b) Airfoil surface zoomed in. c) Airfoil boundary layer zoomed in. d) Channeled airfoil $D=0.1$ inch.

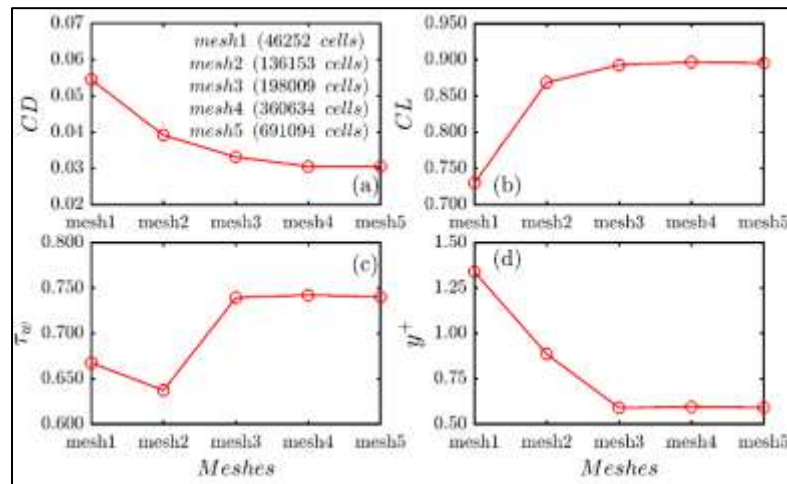


Figure 52. Variation of the flow parameters of all the tested samples

4.2.2 Grid-Independent Convergence (GIC)

Mesh quality has an essential role in achieving accurate simulations. Therefore, it is an important step to run the simulations with suitable meshes for the current study's purposes. The mesh for each airfoil was generated by using ANSYS Meshing 19.2 [62]. Five different meshes with number of elements (46252, 136153, 198009, 360634, and 691094) were considered to test

the mesh quality. To resolve the high intensity of the vorticity near the airfoil wall, inflations of ten quadrilateral mesh layers were applied along the regular airfoil and channeled airfoil edges with a thickness of 1e-2 in with 400 grid points along the airfoil. To ensure that the simulations were mesh independent, four different parameters were monitored in each mesh test. These four parameters were drag coefficient CD, lift coefficient CL, wall shear stress τ_w , and dimensionless wall distance y^+ . Along the airfoil edges, y^+ was kept below one to capture the sharp change in velocity near the wall. Figure (52) shows the converged values of the four monitored parameters at different meshes. It is clear that the variation in each parameter decreases with increasing the number of elements. As the error between mesh 4 and mesh 5 did not exceed 2%, mesh 4 is considered in the current simulations. For the channeled airfoil, the same procedures were followed.

4.2.3 Turbulence model and governing equations

Navier-Stokes and energy equations are solved by using a transient pressure-velocity coupling method of the SIMPLE scheme in FLUENT 19.2. The viscous two-equation pressure based SST k- ω turbulent model was employed for the closure of the Reynolds-Averaged Navier-Stokes (RANS) equations as below [27].

$$\frac{\partial \bar{u}_i}{\partial x_i} = 0 \quad \dots\dots\dots(39)$$

$$\frac{\partial(\rho \bar{u}_i)}{\partial t} + \frac{\partial(\rho \bar{u}_i \bar{u}_j)}{\partial x_j} = -\frac{\partial \bar{p}}{\partial x_i} + \frac{\partial}{\partial x_j} \left[\mu \left(\frac{\partial \bar{u}_i}{\partial x_j} + \frac{\partial \bar{u}_j}{\partial x_i} \right) \right] + \frac{\partial}{\partial x_j} (-\rho \overline{u'_i u'_j}) \quad \dots\dots(40)$$

Where ρ , p , μ represent the working fluid density, pressure, and dynamic viscosity. A scaled residual of 1×10^{-6} is used for all governing equations with 1×10^{-6} as a time step size to achieve a converged stable solution [63]. The SST k- ω model was first founded and proposed by

Menter [64]. This turbulence model is giving more accurate results than other two-equation models as reported by Wilcox [65] and Menter [64] [66].

To validate the numerical results of ANSYS Fluent, Fluent Validation Guide shows different examples to compare the prediction of Fluent with the experimental data. Table (3) shows a comparison between the numerical predictions of the lift coefficients, and the drag coefficients with the experimental values of Cook et al. [67] the lift coefficient was predicted within 2.5% of the experimental results while the drag coefficient was predicted within 2.9% of the experimental results [68].

Table 3. Comparison of the Predictions of Lift and Drag Coefficients

Mesh	model	Lift (CL)	Drag (CD)
	experiment	0.803	0.0168
Quadrilateral	Realizable k- ϵ	0.828	0.0181
	SST k- ω	0.782	0.0163
	Spalart-Allmaras	0.817	0.0170

The numerical results for the regular NACA 0012 in this study match the previous studies [40] [69] [70] and match the results from www.airfoiltools.com [61].

Summary

This chapter included all the experimental and numerical work. The experimental work started by designing the quiet chamber and explaining the steps of building this chamber to provide a quiet environment for acoustic measurements. The acoustic data were measured by four microphones connected to acoustic software to read and save the noise data. The force balance was used to measure the force measurements. Designing and printing the airfoil samples were

explained, one of these airfoils was regular and eleven other samples have different channels sizes and directions. The turbulence measurements were taken by hot-wire technique, a computer software was used to provide 3D movements for probe. Data acquisition hardware aided with a LabVIEW interface, and MATLAB, along with Microsoft Excel, was used to process the data and generate graphs. Numerical simulation was explained in this chapter, and ANSYS Fluent software was used to predict the noise and force measurements.

CHAPTER 5

THE RESULTS

This chapter will discuss three types of results: sound results which is related to the aerodynamic noise emitted from the airfoils, force results which is related to aerodynamic performance, and turbulence intensity which is related to the aerodynamic turbulence around the airfoils.

5.1 Noise results

Acoustic equipment, including the microphones and smart office, were used to calculate the noise around the airfoils. This section studied all the factors that affect the noise such as the flow velocity, angle of attack, and exists of channels. Tonal noise is also one of the noise sources of wind turbines included in this study.

5.1.1 Background noise

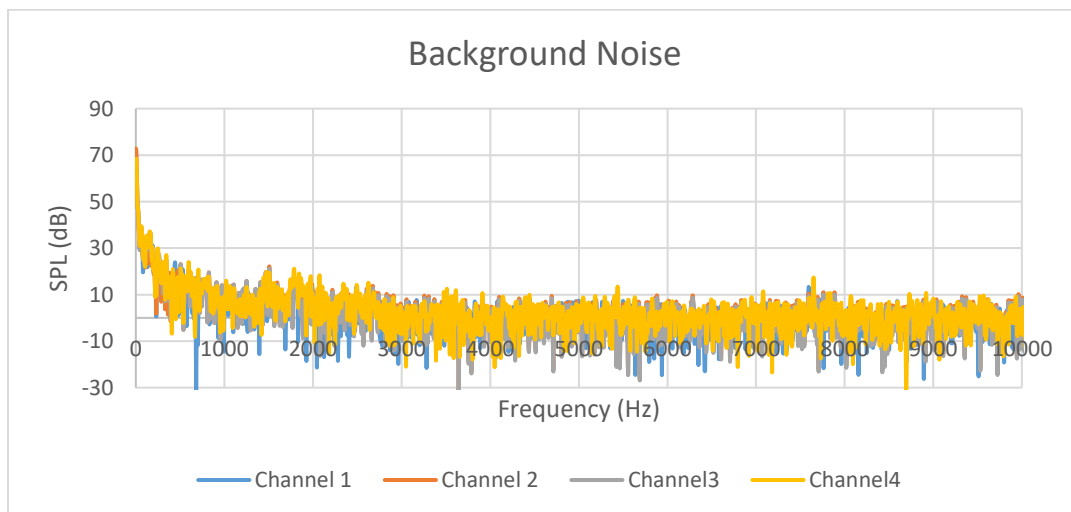


Figure 53. The background noise with no airflow for the different location of microphones

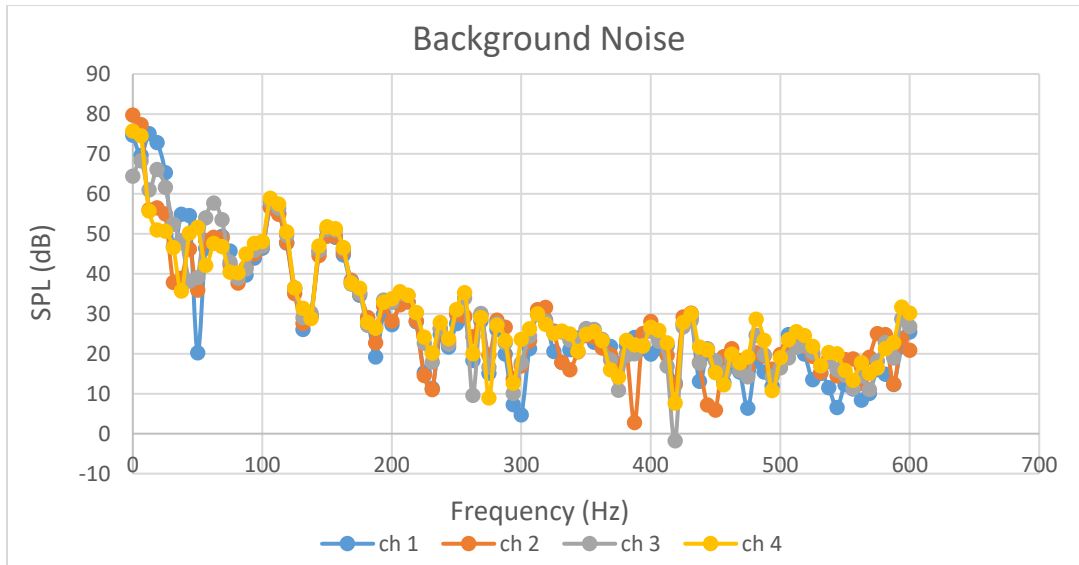


Figure 54. The background noise with 5 m/s flow velocity for the different location of microphones for unchanneled sample

From the preliminary results, the range of frequencies measured from the airfoil section was 20 Hz to 12 kHz. The results indicate that the noise of interest will be within 0-500 Hz range. Figures (53) and (54) show the measurement of background noise with no airflow and 5 m/s flow velocity for the different locations of microphones. The background noise level for the different microphones looks similar for all four microphones, so the results of microphone 1 was used. This microphone is different than the other three microphones because it is a low frequency microphone and reads noise with frequencies starting from 0.13 Hz compared to the other microphones that can record noise with frequencies more than 20 Hz (audible noise).

5.1.2 Velocity influence

Figures (55) through (66) show the relation between sound pressure level and flow velocity. It is very clear from the figures that when the wind velocity gets larger, the noise gets higher. Generally, we can see that when the velocity increases by an increment of 5 m/s, the noise gets larger by an average amount of 10 dB as shown in Table (3). These results match the previous studies [19].

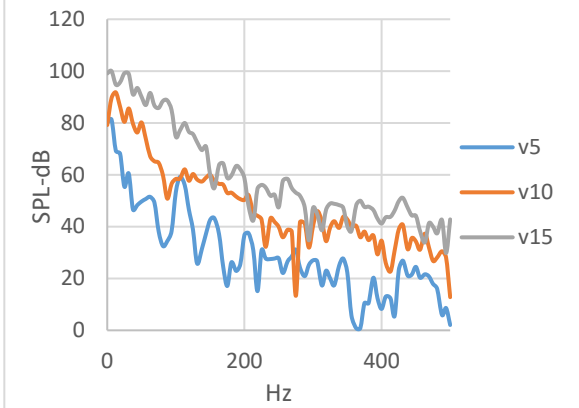


Figure 55. SPL vs. Freq. for Unchanneled sample for Velocities 5, 10, 15 m/s

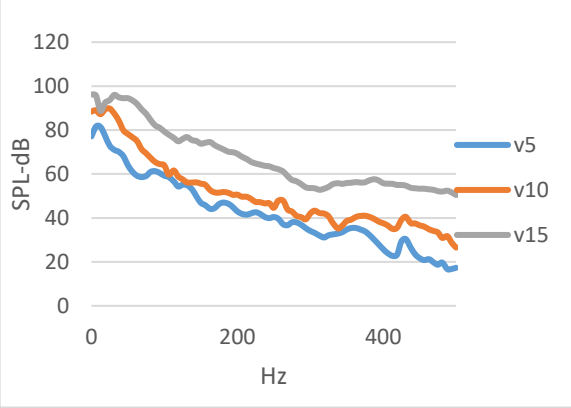


Figure 56. SPL vs. Freq. for A0 D0.05 sample for Velocities 5, 10, 15 m/s

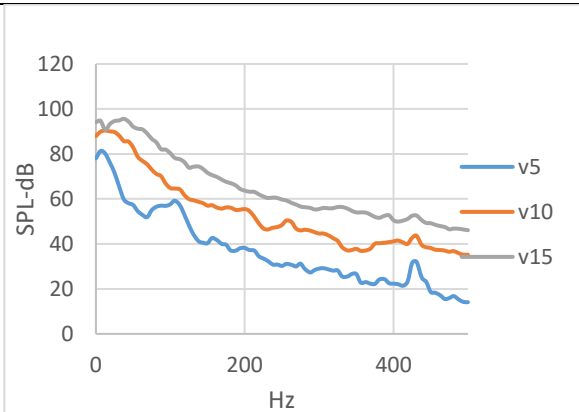


Figure 57. SPL vs. Freq. for A0 D0.08 sample for Velocities 5, 10, 15 m/s

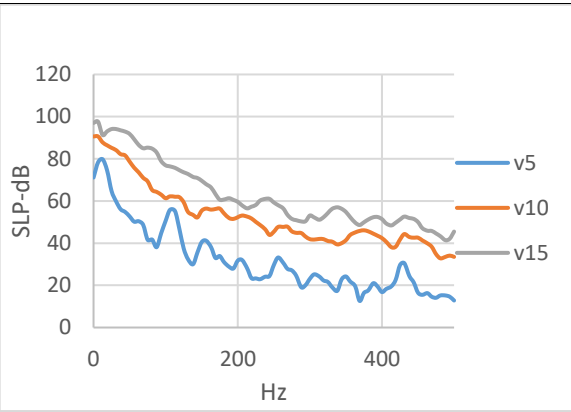


Figure 58. SPL vs. Freq. for A0 D0.01 sample for Velocities 5, 10, 15 m/s

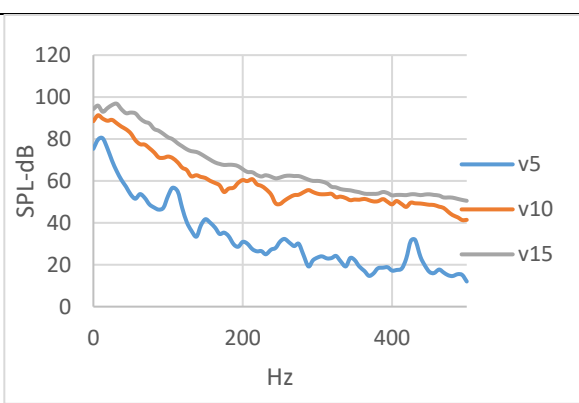


Figure 59. SPL vs. Freq. for A-1 D0.05 sample for Velocities 5, 10, 15 m/s

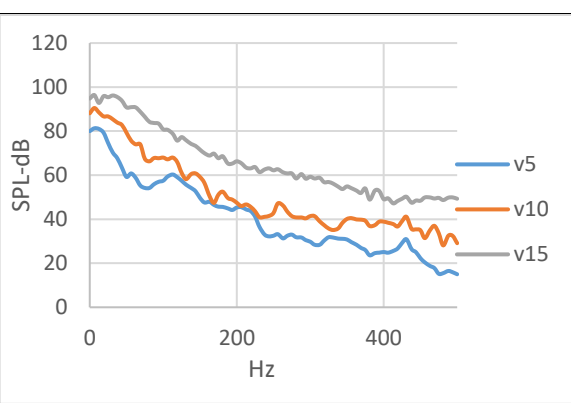


Figure 60. SPL vs. Freq. for A-1 D0.08 sample for Velocities 5, 10, 15 m/s

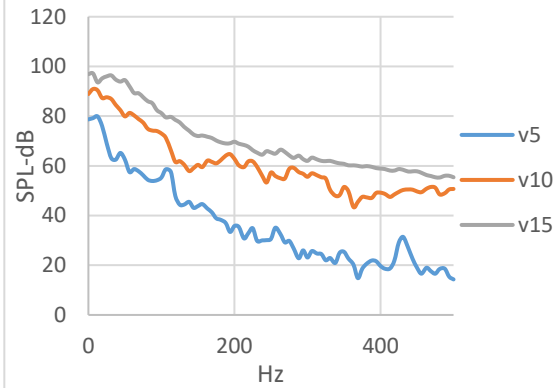


Figure 61. SPL vs. Freq. for A2 D0.05 sample for Velocities 5, 10, 15 m/s

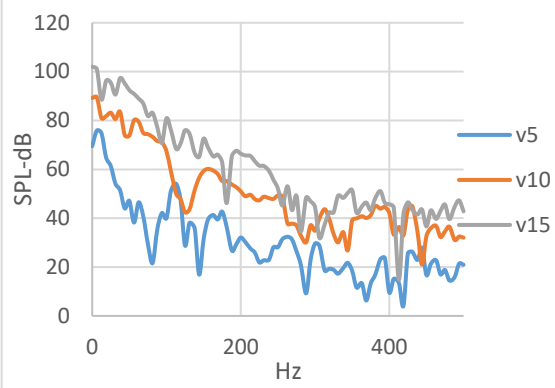


Figure 62. SPL vs. Freq. for A2 D0.08 sample for Velocities 5, 10, 15 m/s

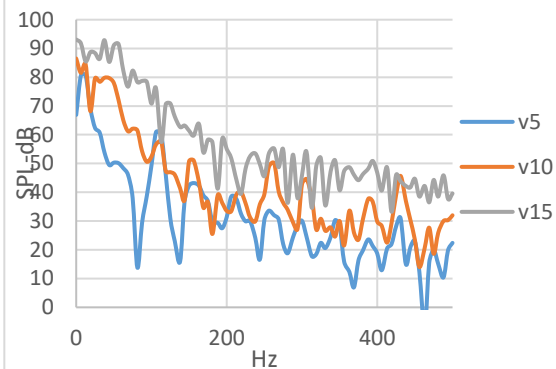


Figure 63. SPL vs. Freq. for A2 D0.01 sample for Velocities 5, 10, 15 m/s

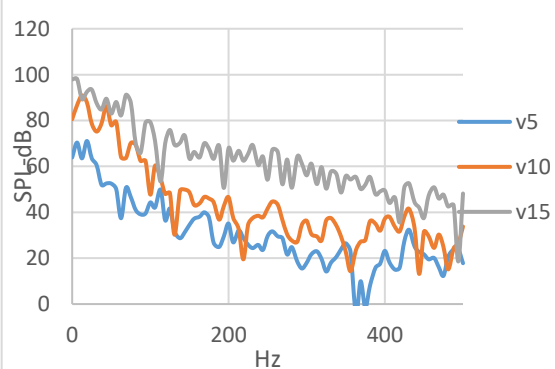


Figure 64. SPL vs. Freq. for A3 D0.05 sample for Velocities 5, 10, 15 m/s

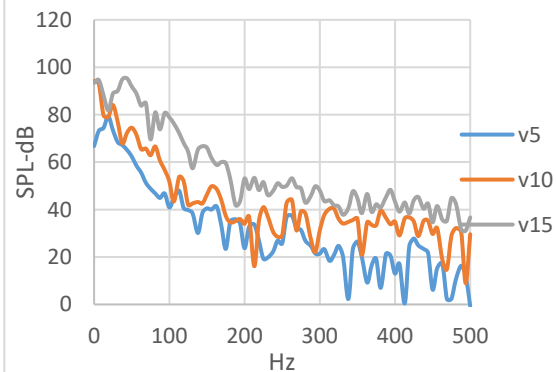


Figure 65. SPL vs. Freq. for A3 D0.08 sample for Velocities 5, 10, 15 m/s

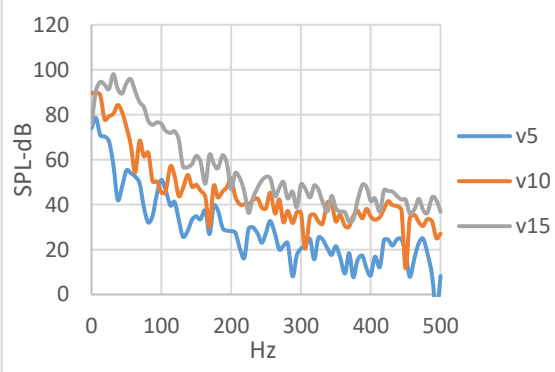


Figure 66. SPL vs. Freq. for A3 D0.1 sample for Velocities 5, 10, 15 m/s

Tables (4) to (6) show sound pressure level in (dBA) for the velocities 5, 10, 15 m/s in order. Table (4) shows A-weighting adjustments for one octave center frequencies for all the samples in flow velocity 15 m/s. The overall sound pressure level is measured by the equation:

$$\text{Overall (dBA)} = 10 * \log\left[\left(10\right)^{\frac{S_1}{10}} + \left(10\right)^{\frac{S_2}{10}} + \dots + \left(10\right)^{\frac{S_n}{10}}\right] \dots\dots\dots (41)$$

Where: S1, S2 Sn are the sound pressure level in A-weighting adjustments for one-octave center frequencies starting with 31.5 Hz to 8,000 Hz.

Table 4. A-weighting adjustments for one octave center frequencies for all the samples in flow velocity 15 m/s.

X [Hz]	Unch.	a3 d0.08	a3 d0.05	a3 d0.1	a2 d0.08	a2 d0.05	a2 d0.1	a-1 d0.08	a-1 d0.05	a0 d0.08	a0 d0.05	a0 d0.1
31.5	43.89	42.59	44.13	44.67	48.23	46.97	46.00	45.80	47.44	45.49	46.64	46.68
63	49.56	47.60	46.03	44.32	48.75	53.06	46.23	44.63	49.60	44.70	45.65	50.42
125	45.81	43.30	47.84	42.91	46.87	51.40	44.80	51.17	48.95	47.78	49.83	47.48
250	28.43	35.04	45.57	37.80	41.55	46.84	36.99	53.55	52.96	51.07	54.13	50.71
500	27.93	33.52	38.97	33.64	39.58	52.21	36.38	46.06	47.31	42.94	47.25	42.26
1000	29.80	46.46	37.56	37.41	34.61	44.38	40.66	43.41	41.56	41.32	45.13	41.68
2000	15.59	37.99	27.36	35.33	21.52	36.28	30.60	32.99	35.68	36.30	37.85	36.03
4000	11.99	24.37	28.12	26.48	-1.10	26.66	25.07	27.81	28.91	25.21	27.37	28.48
8000	0.85	12.67	11.01	9.22	14.36	17.36	15.37	16.43	16.08	16.46	17.07	13.84
Overall (dBA)	51.91	51.86	52.49	49.71	53.36	58.04	51.29	56.90	56.95	54.63	57.24	55.64

Tables (5) and (6) show the A-weighting adjustments for one-octave center frequencies for all the samples in flow velocities 10 and 5 m/s in order and AOA 10°, and overall (dBA) were measured in the same way. The entire acoustic results are shown in the appendix A.

Table 5. A-weighting adjustments for one octave center frequencies for all the samples in flow velocity 10 m/s AOA 10°.

X [Hz]	unch.	a3 d0.08	a3 d0.05	a3 d0.1	a2 d0.08	a2 d0.05	a2 d0.1	a-1 d0.08	a-1 d0.05	a0 d0.08	a0 d0.05	a0 d0.1
31.5	38.19	37.68	35.83	38.03	39.20	40.52	36.96	38.98	38.08	38.70	41.10	40.69
63	34.03	35.74	37.94	35.39	33.64	39.14	35.33	37.84	41.30	40.67	40.78	37.44
125	31.49	26.45	32.83	27.68	25.34	43.78	30.89	44.08	39.73	36.77	40.45	40.03
250	31.34	28.40	34.28	29.85	29.66	40.66	30.65	34.21	38.41	33.82	39.02	31.75
500	19.65	23.35	30.55	23.95	26.83	31.54	28.78	25.94	36.23	32.96	33.25	30.31
1000	28.02	23.46	29.38	17.41	25.30	29.67	22.28	28.45	31.44	30.03	27.72	29.45
2000	26.43	7.71	17.74	19.19	17.56	22.96	14.76	22.76	22.96	22.64	23.24	23.91
4000	13.37	5.38	-7.12	12.23	9.67	10.91	12.45	13.23	14.24	11.60	13.40	11.66
8000	-2.20	-4.42	-2.91	9.25	-0.83	5.11	6.35	1.39	3.87	2.19	3.02	1.80
Overall (dBA)	41.2	40.5	42.2	40.7	41.1	47.6	40.7	46.4	46.2	44.7	46.7	44.9

Table6. A-weighting adjustments for one octave center frequencies for all the samples in flow velocity 5 m/s.

X [Hz]	unchan	a3 d0.08	a3 d0.05	a3 d0.1	a2 d0.08	a2 d0.05	a2 d0.1	a-1 d0.08	a-1 d0.05	a0 d0.08	a0 d0.05	a0 d0.1
31.5	25.10	26.10	25.10	23.20	24.70	23.70	27.30	30.90	28.20	26.00	24.60	30.40
63	30.30	29.40	21.20	30.30	30.30	32.50	24.20	29.60	31.50	26.70	33.00	30.20
125	25.70	23.70	25.50	23.20	12.70	28.30	28.90	31.40	24.30	32.20	35.00	21.40
250	22.20	17.10	21.00	18.90	19.50	22.00	26.80	23.90	27.40	21.60	31.80	21.00
500	-1.14	-3.88	14.60	5.03	17.70	11.10	19.20	11.80	8.80	10.90	14.10	19.60
1,000	5.57	18.60	16.80	15.70	11.70	15.00	18.50	19.30	16.40	16.30	15.10	15.30
2,000	1.04	11.70	14.90	4.73	22.30	8.56	4.84	9.67	9.44	10.70	11.09	8.49
4,000	-12.30	-1.37	-10.60	2.52	-1.72	2.26	-5.91	-0.18	1.77	1.25	1.36	2.60
8,000	5.32	10.10	8.12	9.10	11.20	4.91	2.67	4.54	1.74	4.72	5.56	5.05
Overall (dBA)	32.88	32.21	30.21	32.10	32.39	34.63	33.45	35.89	34.71	34.38	38.47	34.06

Table (7) shows overall SPL for all samples in flow velocities 5, 10, 15 m/s AOA 10.

Table 7. Overall SPL (dBA) for all samples in flow velocities 5, 10, 15 m/s

Flow velocity	unchan	a3 d0.08	a3 d0.05	a3 d0.1	a2 d0.08	a2 d0.05	a2 d0.1	a-1 d0.08	a-1 d0.05	a0 d0.08	a0 d0.05	a0 d0.1
5 m/s	32.88	32.21	30.21	32.10	32.39	34.63	33.45	35.89	34.71	34.38	38.47	34.06
10 m/s	41.2	40.5	42.2	40.7	41.1	47.6	40.7	46.4	46.2	44.7	46.7	44.9
15 m/s	51.91	51.86	52.49	49.71	53.36	58.04	51.29	56.90	56.95	54.63	57.24	55.64

5.1.3 Angle of attack influence

The results of noise showed a direct relation between aerodynamic noise results and the angle of attack of the samples. Figures (67) through (78) show this relation between Sound Pressure Level (SPL) and Angle Of Attack (AOA). The figures show an increase in sound pressure level when angle of attack increases.

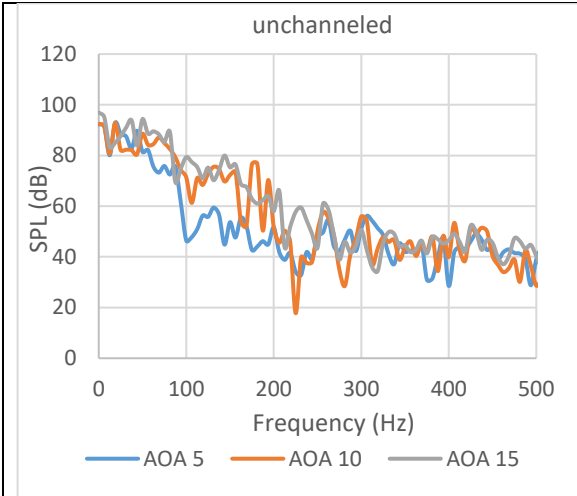


Figure 67 SPL vs. Freq. for Unchanneled sample for AOA 5,10, 15

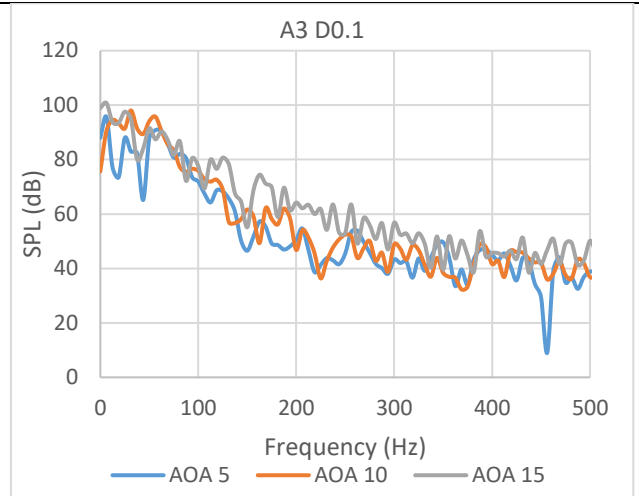


Figure 68 SPL vs. Freq. for A3 D0.1 sample for AOA 5,10, 15

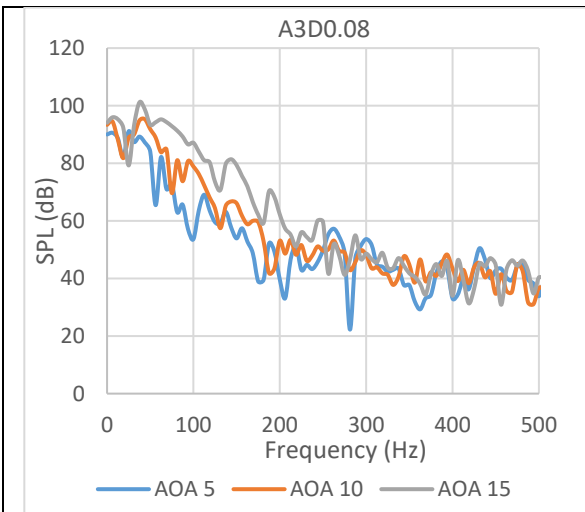


Figure 69 SPL vs. Freq. for A3 D0.08 sample for AOA 5,10, 15

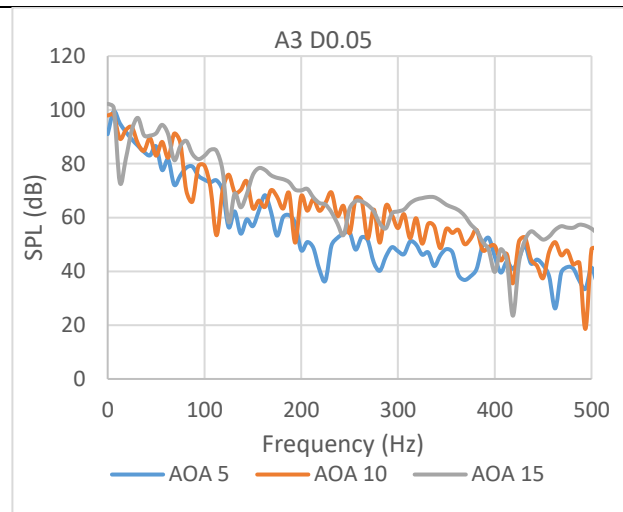


Figure 70 SPL vs. Freq. for A3 D0.05 sample for AOA 5,10, 15

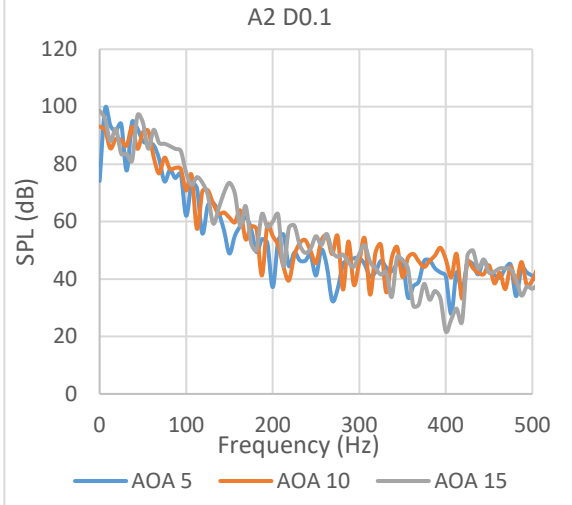


Figure 71 SPL vs. Freq. for A2 D0.1 sample for AOA 5,10, 15

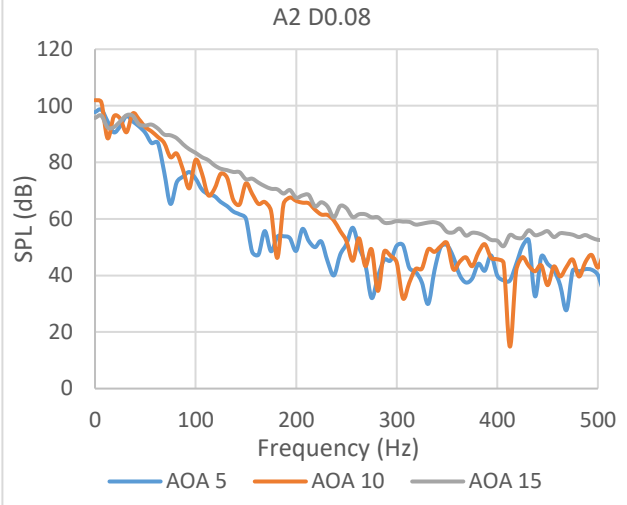


Figure 72 SPL vs. Freq. for A2D0.08 sample for AOA 5,10, 15

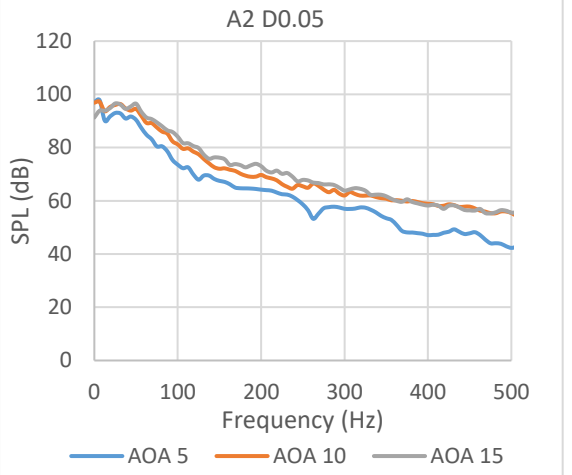


Figure 73 SPL vs. Freq. for A2 D0.05 sample for AOA 5,10, 15

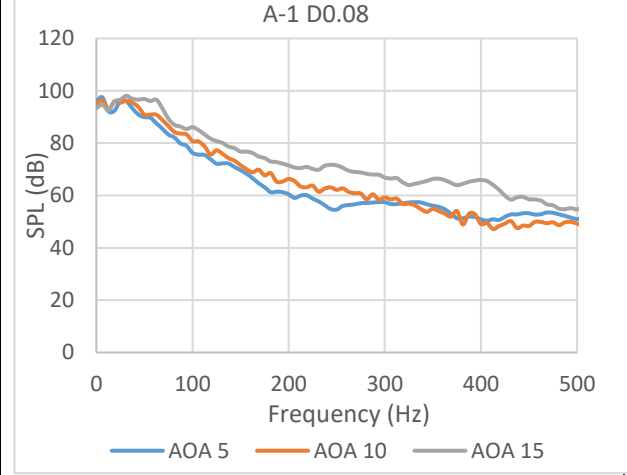


Figure 74 SPL vs. Freq. for A-1D0.08 sample for AOA 5,10, 15

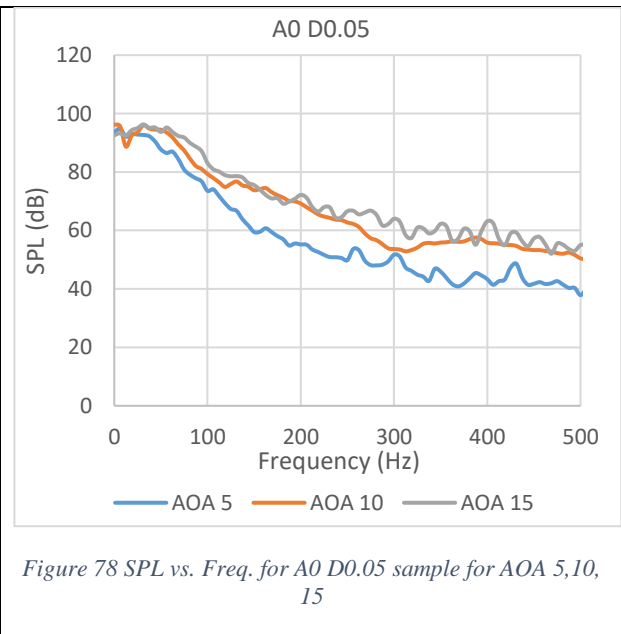
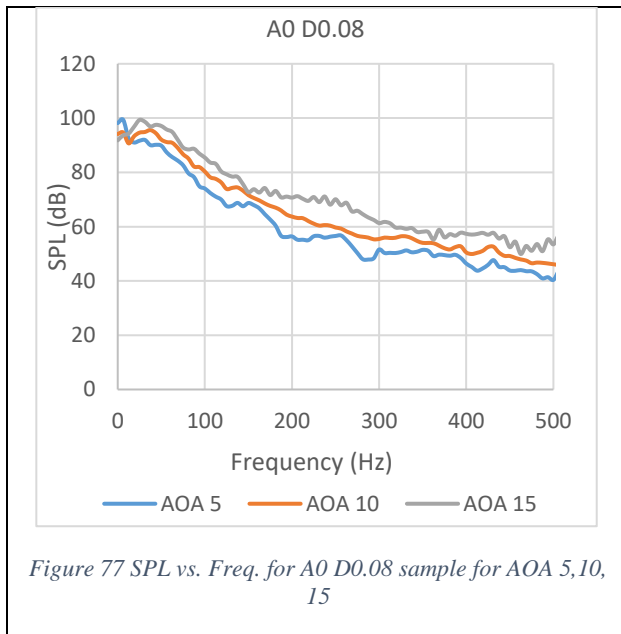
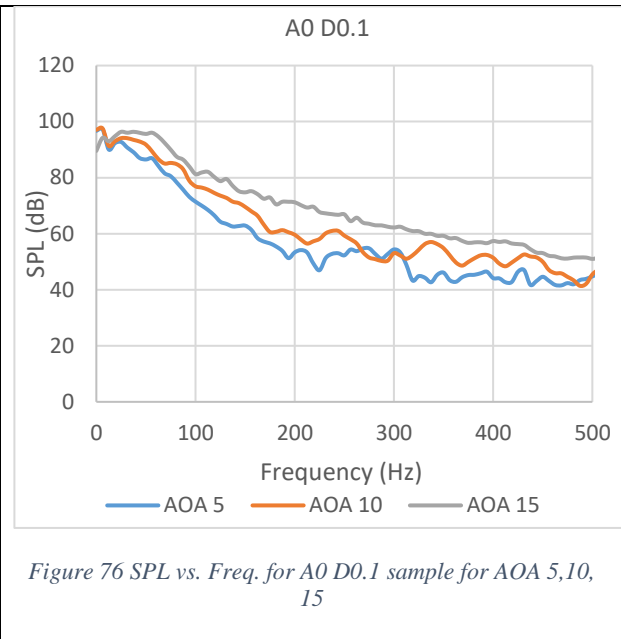
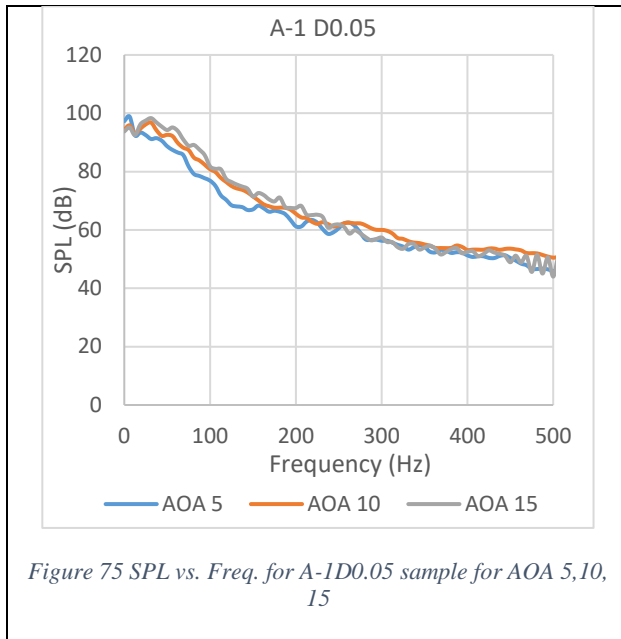


Table (8) shows overall sound pressure level for the different samples. Overall SPL increases between (1-4 dBA) when angle of attack increases from 5-10 degrees, while there is an increase from (1-6 dBA) when angle of attack increases from 10-15 degrees. Figure (79) shows overall sound pressure level for different angles of attack for all samples.

Table 8 overall SPL (dBA) for all samples for AOA 5, 10 15 V 10 m/s

AOA	Unch.	a3 d0.08	a3 d0.05	a3 d0.1	a2 d0.08	a2 d0.05	a2 d0.1	a-1 d0.08	a-1 d0.05	a0 d0.08	a0 d0.05	a0 d0.1
5.00	40.11	40.11	40.52	38.91	39.72	44.56	40.32	45.18	44.94	43.87	42.77	42.99
10.00	41.16	40.51	42.21	40.74	41.07	47.63	40.69	46.40	46.18	44.72	46.65	44.94
15.00	43.26	41.88	47.11	43.06	47.36	49.86	40.85	51.18	46.02	50.76	47.82	47.06

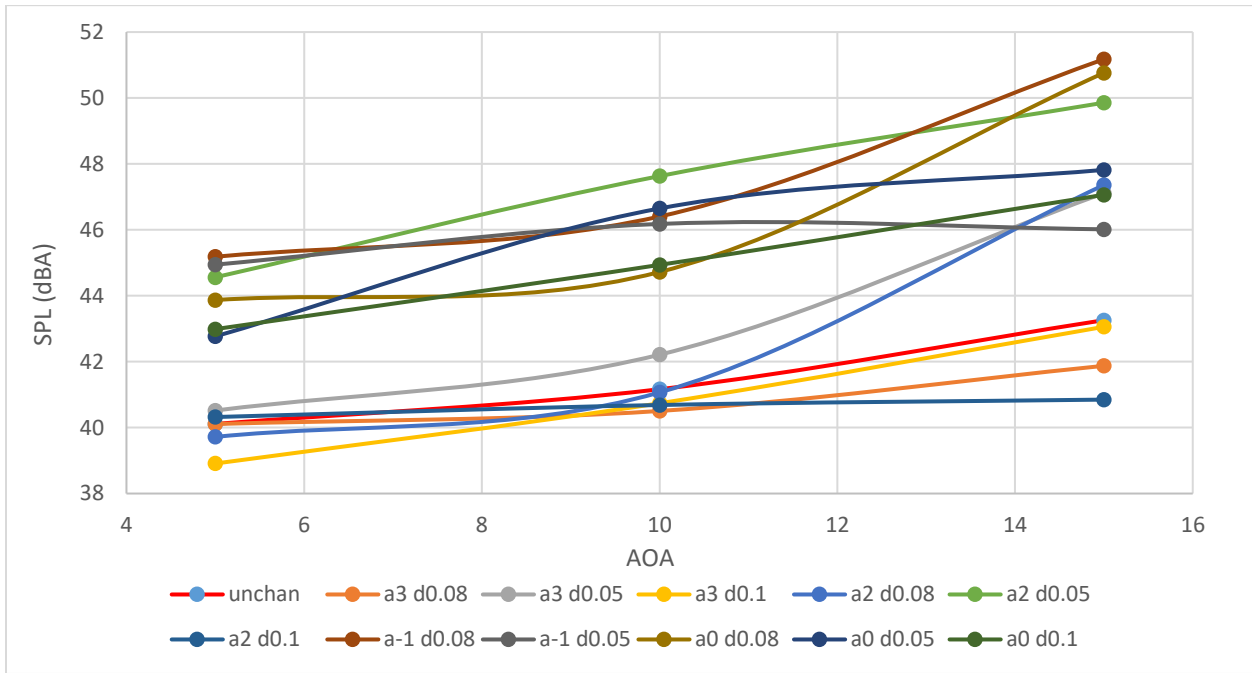


Figure 79 Overall sound level for all samples vs. AOA

5.1.4 Channel influence

According to Brian Fite [15], trailing edge blowing is a technique used to reduce the wake momentum deficit of the fan blade. Their study showed reduction in the overall sound power level, broadband noise, and tone noise. In this study, the channels carried the flow from leading edge all the way to the section side of the airfoils A3 and A2, to the pressure side of the airfoils A-1, and to the trailing edge of the airfoils A0. These channels were injecting the flow at the trailing edge or near the trailing edge on one of the airfoil sides, and this worked as a wake filling strategy.

5.1.4.1 Channel direction influence

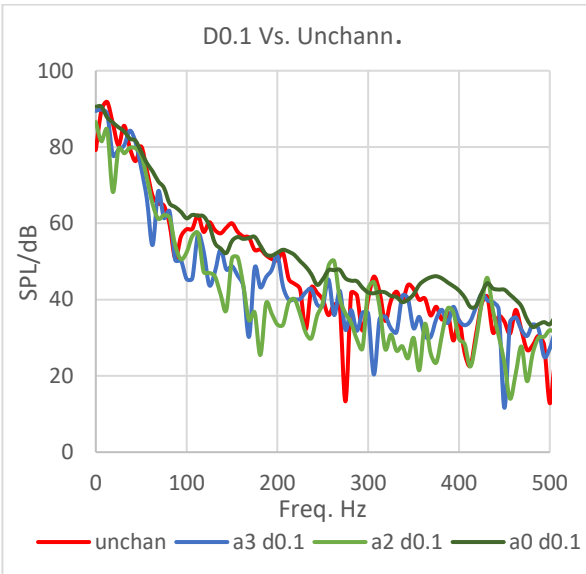


Figure 80. SPL vs. Freq. for D0.1 sample for different Angles at 10 m/s velocity

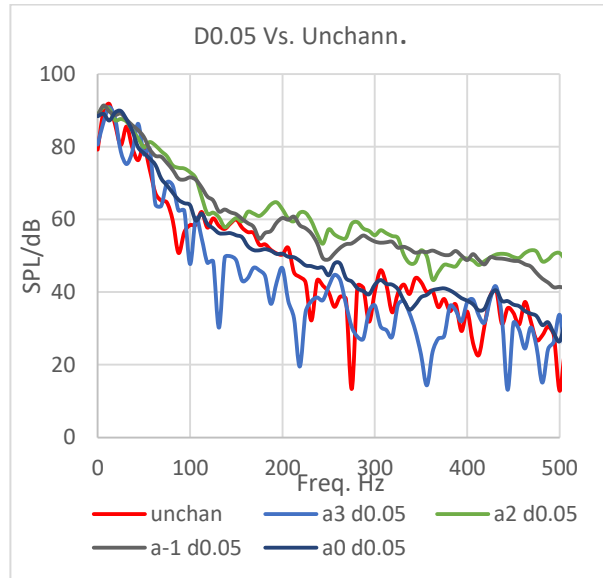


Figure 81. SPL vs. Freq. for D0.05 sample for different Angles at 10 m/s velocity

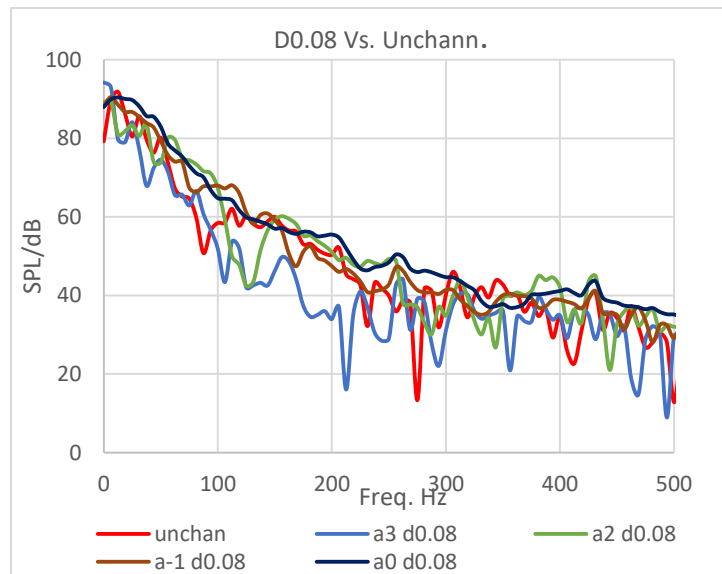


Figure 82. SPL vs. Freq. for D0.08 sample for different Angles at 10 m/s velocity

Figure (80) shows the noise spectrum for frequencies 0-600 Hz, which is the range where aerodynamic noise is mostly located. The figure shows the noise in the sample D0.1 for three

different directions, A3, A2, and A0. We noticed that the samples A2 and A3 produced less noise than the unchanneled sample. However, the sample A0 showed a higher level of noise than the unchanneled sample. In Figure (81), the samples with a diameter of 0.05 inches, D0.05, generated a high level of noise compared to the unchanneled sample for all angles except for sample A3. In Figure (82), the samples with a diameter of 0.08 inches, D0.08, showed similar behavior with that of samples with D0.05, Figure (81). In conclusion, the sample that produces the least amount of noise, regardless of the size of the channel, is the channel with an inclination of 3 degrees, the A3 channel. The flow in this sample goes to the suction surface where the most turbulence happens. The flow in sample A3 helps wake momentum deficit and reduces the pressure fluctuation and eventually reduces the noise that is generated by this fluctuation.

5.1.4.2 Diameter size Influence

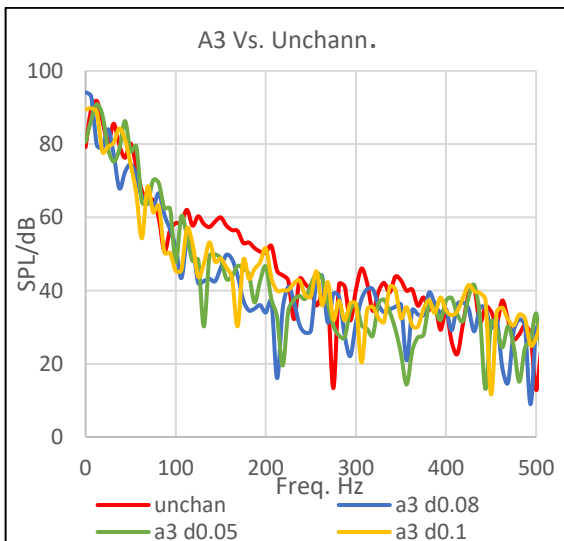


Figure 83. SPL vs. Freq. for A3 sample for different Diameters at 10 m/s velocity

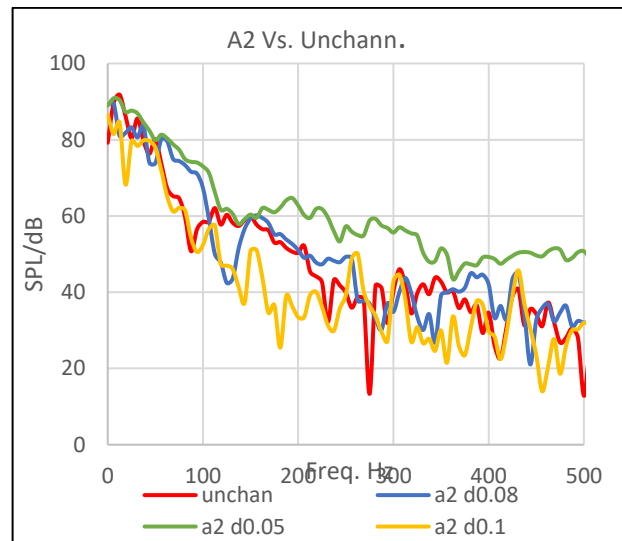


Figure 84. SPL vs. Freq. for A2 sample for different Diameters at 10 m/s velocity

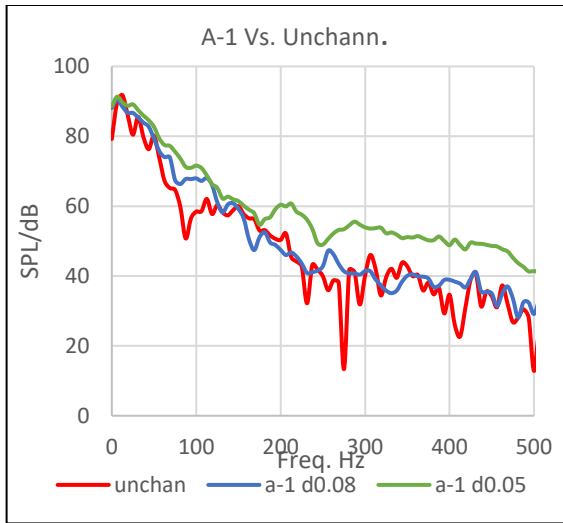


Figure 85. SPL vs. Freq. for A-1 sample for different Diameters at 10 m/s velocity

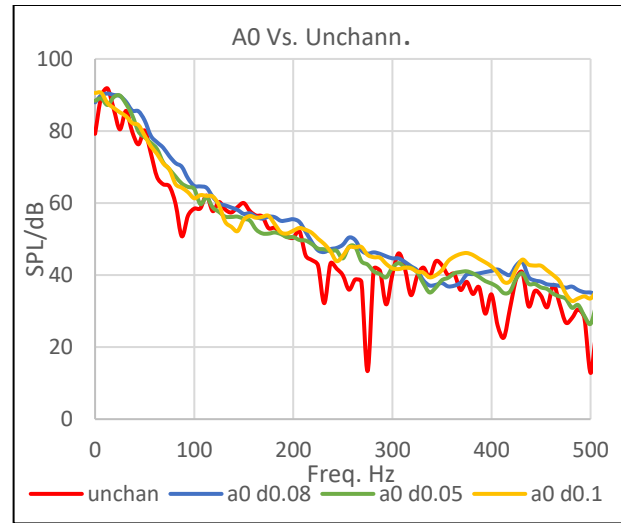


Figure 86. SPL vs. Freq. for A0 sample for different Diameters at 10 m/s velocity

Figures (83) to (86) showed the noise spectrum for frequencies 0-600 Hz for different channel sizes. In this section, the influence of size of channels on the aerodynamic noise needs to be studied for all the different samples. The results showed that similarly the samples with (D0.1) are the quieter samples than the samples (D0.08) and the samples (D0.05) that showed more noise. As a conclusion, the size of channels has significant influence on the aerodynamic noise, and as the channel size gets smaller, the noise gets higher.

5.1.5 Tonal noise

Figures (87) to (91) showed tonal noise of the sound spectrum in log scale of the frequency up to 10,000 Hz. All samples showed a peak at 930 Hz, which means that different channels have no effect on the tone noise. This specific tone comes from the wind tunnels' engine itself because the background spectrum did not show this peak when the engine was off.

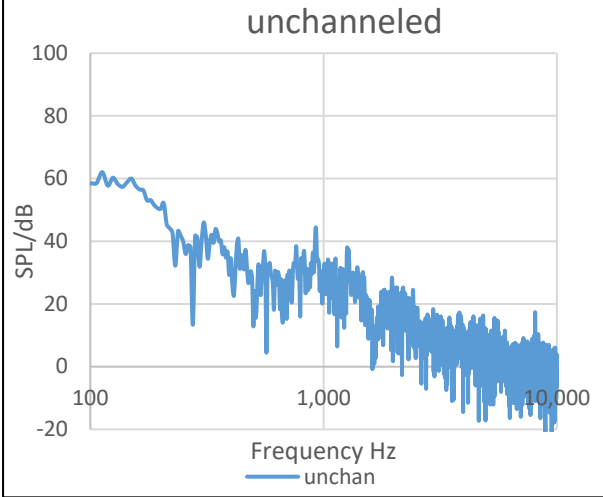


Figure 87. noise spectrum for unchanneled sample

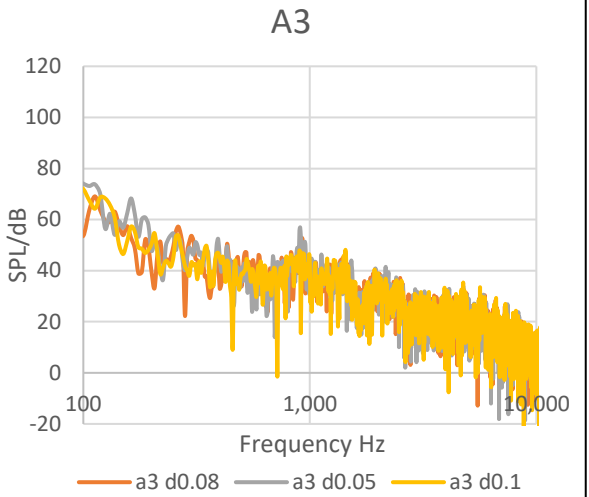


Figure 88. noise spectrum for the sample A3

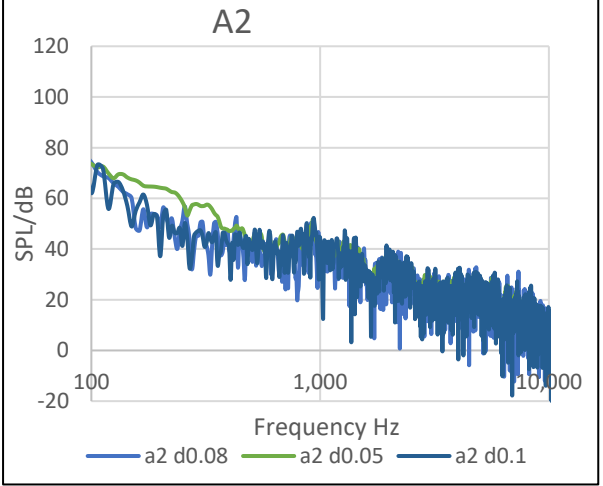


Figure 89. noise spectrum for the sample A2

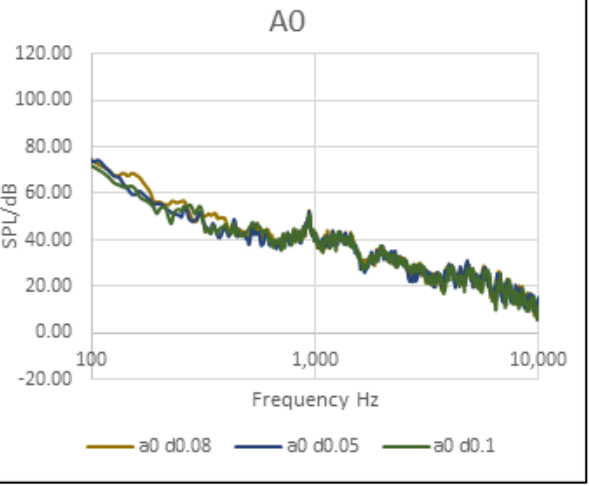
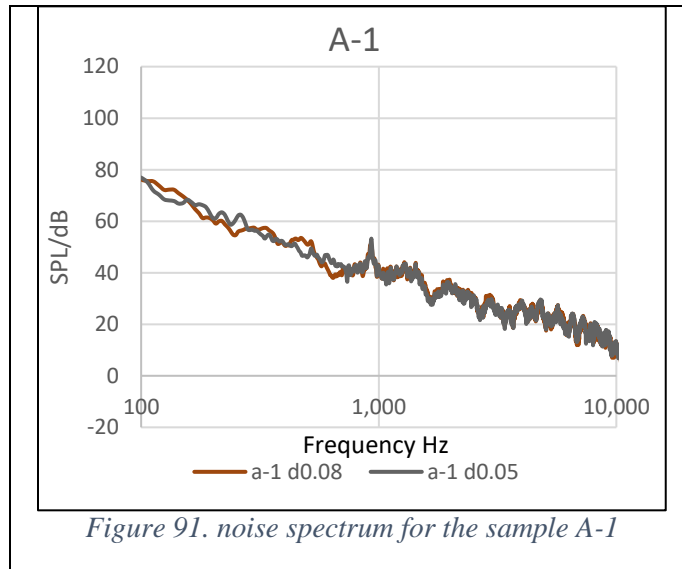


Figure 90. noise spectrum for the sample A0



5.2 Force results

Aerodynamic performance is directly related to the aerodynamic force results. This section is devoted to the force results. Lift and drag forces were measured by the balance that was mentioned in Chapter 4. Three flow velocities were calculated: the results of 5 m/s will be studied in this section, and the other two velocities, 10 m/s and 15 m/s, are shown in appendix B.

5.2.1 Calibration setup

To start using the balance built to measure the forces, calibration needs to be done first. To calibrate the balance that was mentioned in Figure (46) in Chapter 3, four different weights are used (0.005, 0.01, 0.05, 0.1 kg). For drag calibration, the weights hung horizontally were used, and for lift calibration, weights hung vertically were used. This data was recorded and saved in a computer. Tables (9) and (10) showed the results of calibration for both lift and drag, respectively.

Table9. The result of lift calibration

lift		
weight kg	voltage	weight/voltage
0.005	0.514	0.009728
0.01	1.145	0.008734
0.05	5.057	0.009887
0.1	10.541	0.009487

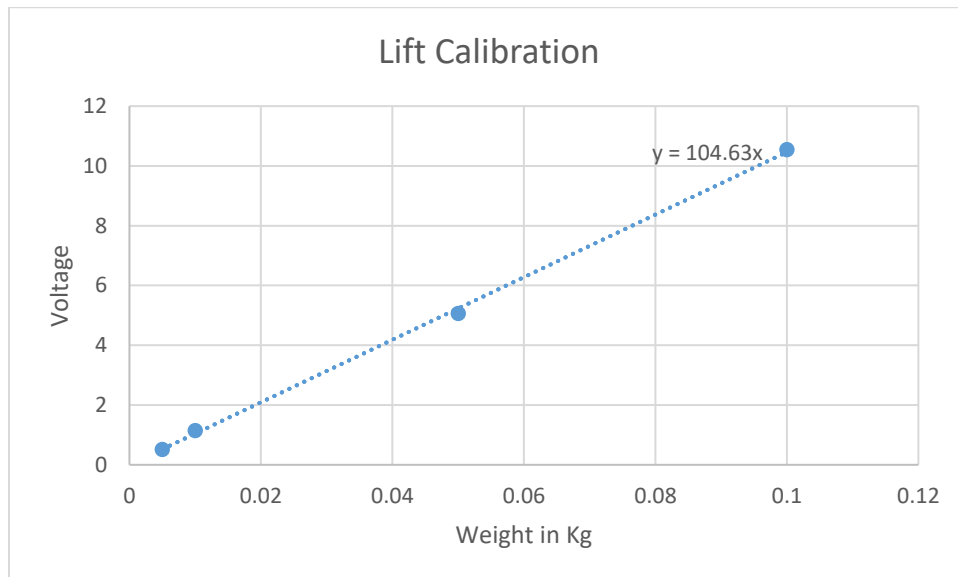


Figure 92. The calibration data of the lift forces

Table10. The result of drag calibration

Drag (Drag1+Drag2)		
weight kg	voltage	weight/voltage
0.005	1.945	0.002571
0.01	4.128	0.002422
0.05	17.026	0.002937
0.1	35.237	0.002838

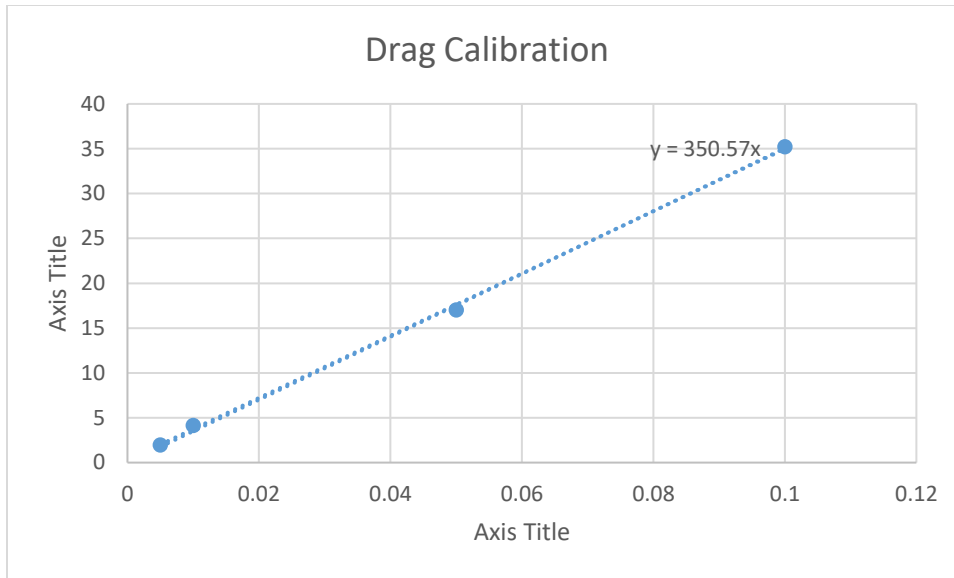


Figure 93. The calibration data of the drag forces

After calibration setup was done, the balance is ready to take data for both drag and lift forces. The force results were taken in three different flow velocities 5 m/s, 10 m/s and 15 m/s, and in three different angles of attack (AOA) 5, 10, and 15 degrees. Table (11) showed the results of drag coefficients and lift coefficients for different samples in flow velocity 5 m/s. The results of drag coefficients and lift coefficients in flow velocities 10 m/s and 15 m/s were shown in the Appendix B.

Table11. The results of drag and lift coefficients for different samples in flow velocity 5 m/s

V= 5m/s	Experimental					
	C _D			C _L		
	aoa 5	aoa 10	aoa 15	aoa 5	aoa 10	aoa 15
Unchanneled	0.067	0.097	0.119	0.257	0.474	0.595
A3 D0.08	0.068	0.098	0.123	0.225	0.459	0.557
A3 D0.05	0.066	0.097	0.121	0.225	0.465	0.575
A3 D0.1	0.070	0.099	0.125	0.236	0.428	0.547
A2 D0.08	0.073	0.100	0.126	0.255	0.430	0.557
A2 D0.05	0.070	0.101	0.127	0.233	0.416	0.545
A2 D0.1	0.074	0.101	0.125	0.225	0.405	0.525
A-1 D0.08	0.081	0.111	0.135	0.245	0.455	0.555
A-1 D0.05	0.081	0.105	0.131	0.254	0.465	0.575
A0 D0.08	0.080	0.109	0.132	0.239	0.461	0.575
A0 D0.05	0.074	0.105	0.133	0.255	0.475	0.585
A0 D0.1	0.083	0.111	0.133	0.251	0.446	0.565

5.2.2 Lift results

5.2.2.1 Influence of the channel direction

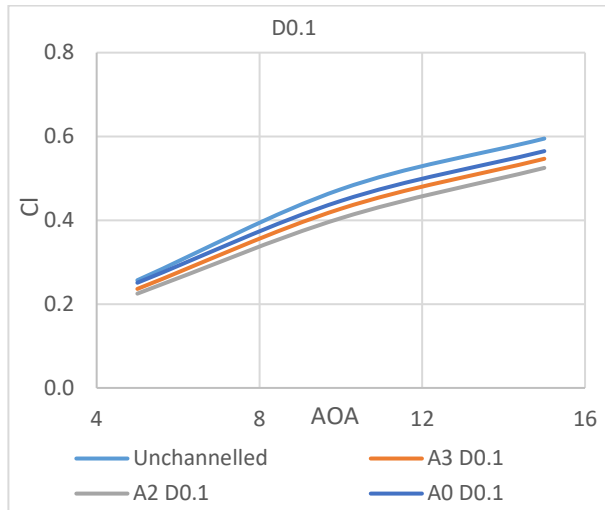


Figure 94. Cl vs. AOA for D0.1 samples for different angle directions

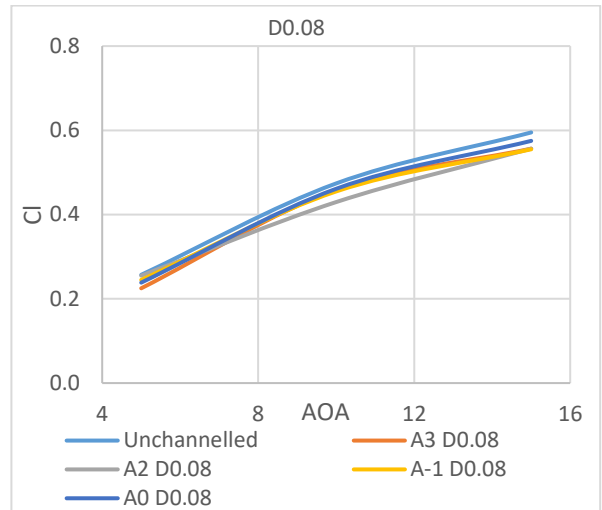


Figure 95. Cl vs. AOA for D0.08 samples for different angle directions

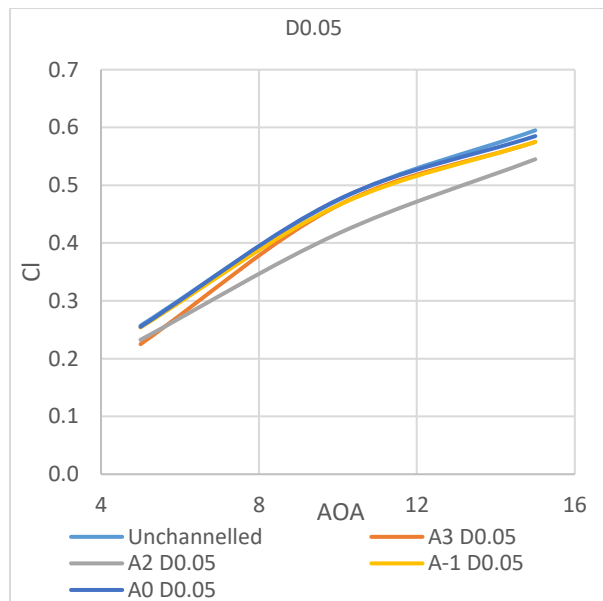


Figure 96. Cl vs. AOA for D0.05 samples for different angle directions

Figures (94) through (96) showed the effect of channel direction on lift coefficients for flow velocity of 5 m/s and for three different angle of attacks 5, 10, and 15 degrees. The data

showed that the presence of channels causes a decrease in the lift coefficients for all types of samples. Specifically, the A2 channel caused the largest decrease, while the A0 and A-1 caused the least decrease.

5.2.2.2 Influence of channels size

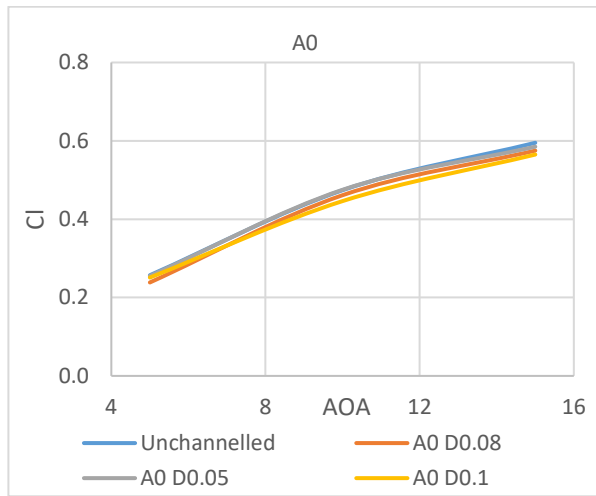


Figure 97. *Cl vs. AOA for A0 sample for different Diameters*

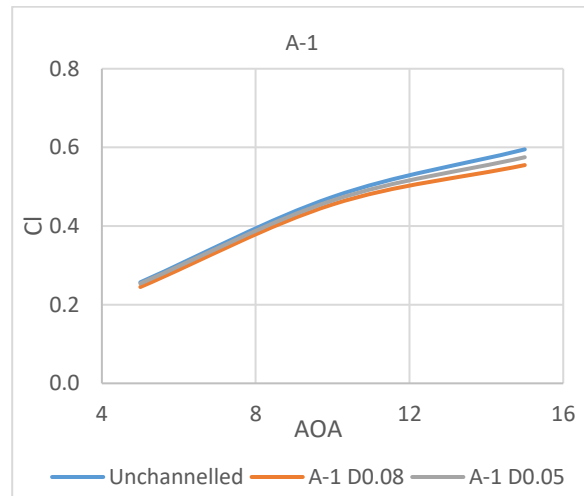


Figure 98. *Cl vs. AOA for A-1 sample for different Diameters*

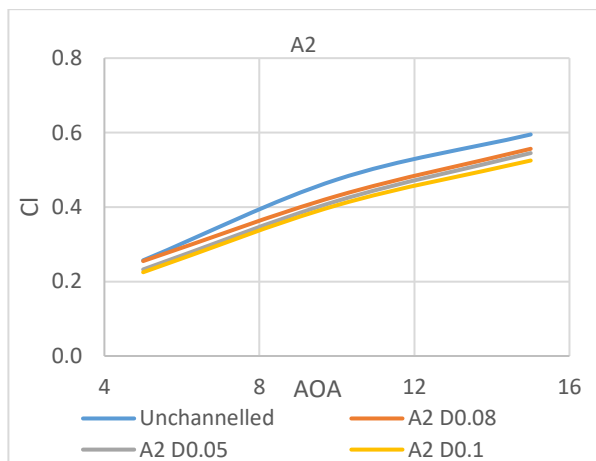


Figure 99. *Cl vs. AOA for A2 sample for different Diameters*

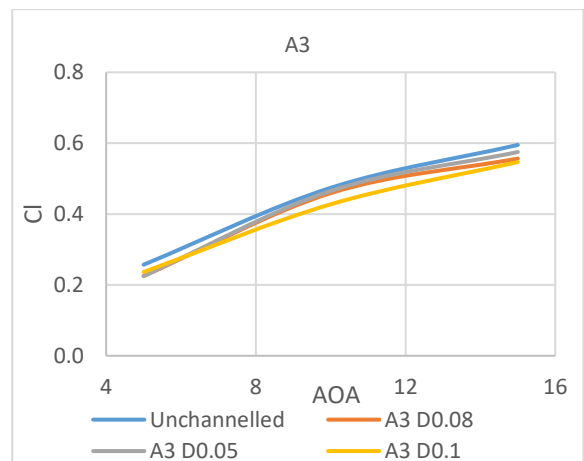


Figure 100. *Cl vs. AOA for A3 sample for different Diameters*

Figures (97) through (100) showed the effect of channel sizes on lift coefficients for three different angles of attack, 5, 10, and 15 degrees. The results showed that presence of channels caused a decrease on lift coefficients for all samples. Specifically, D0.1 channel caused the largest

decrease in lift coefficients, while the D0.05 channel caused the least decrease. Generally, an increase in channel size leads to a decrease in lift coefficients, so the relation between the channel size and the lift coefficient is of an inverse nature.

5.2.3 Drag

5.2.3.1 Influence of the channel angle

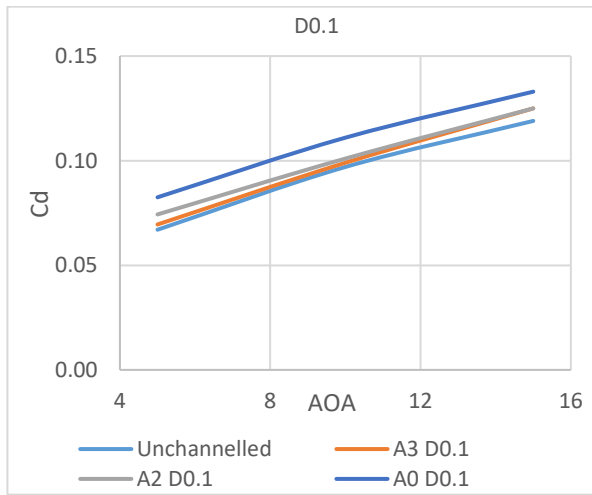


Figure 101. Cd vs. AOA for D0.1 sample for different angles

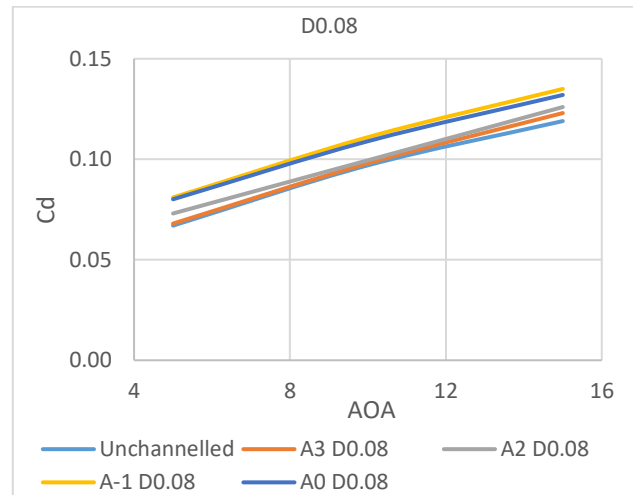


Figure 102. Cd vs. AOA for D0.08 sample for different angles

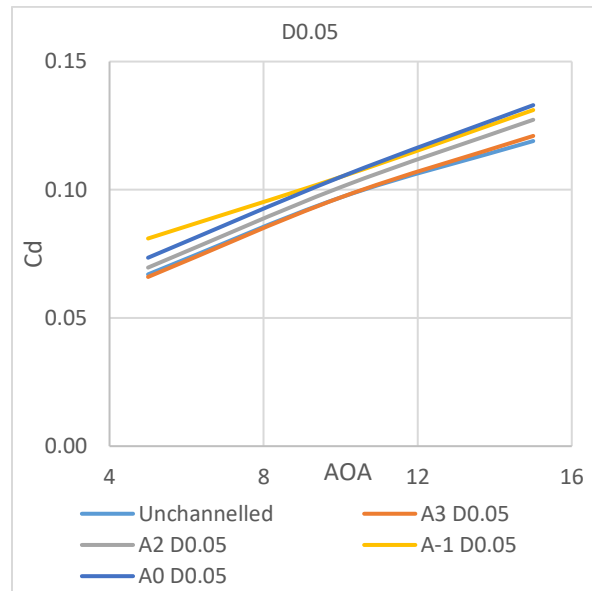


Figure 103. Cd vs. AOA for D0.05 sample for different angles

Figures (101) through (103) showed the effect of channel direction on drag coefficients for flow velocity of 5 m/s and for three different angle of attacks 5, 10, and 15 degrees. As in the lift case, the data showed that the presence of channels affects the aerodynamic forces. However, in this case, it caused an increase in the drag coefficients for all types of samples. Specifically, the A0 and A-1 channels caused the largest increase, while the A3 caused the least increase.

5.2.3.2 Influence of diameter size

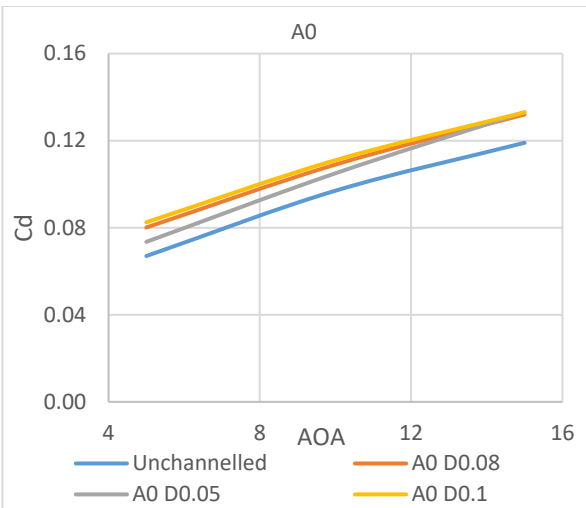


Figure 104. Cd vs. AOA for A0 sample for different Diameters

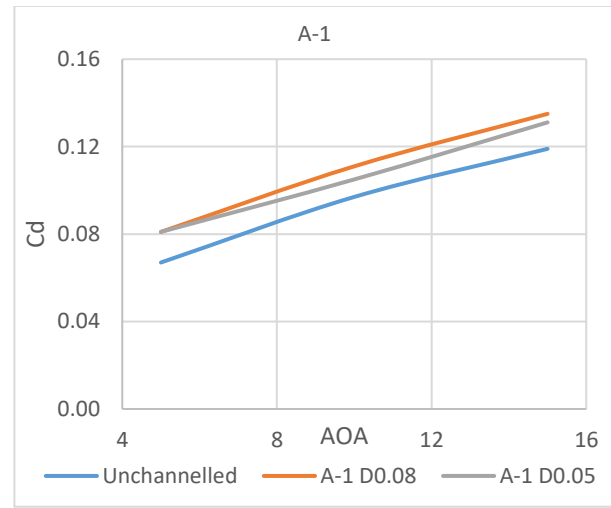


Figure 105. Cd vs. AOA for A-1 sample for different Diameters

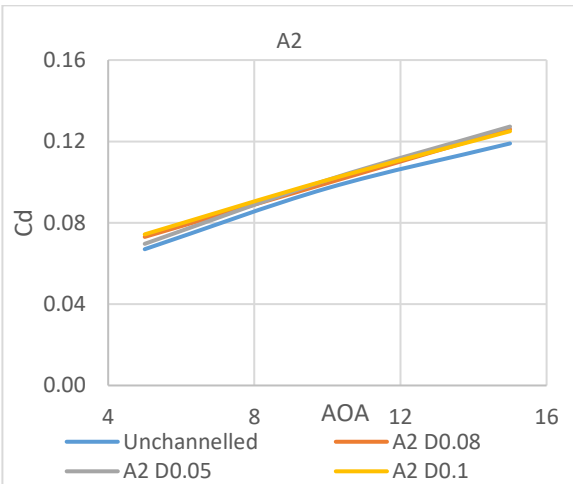


Figure 106. Cd vs. AOA for A2 sample for different Diameters

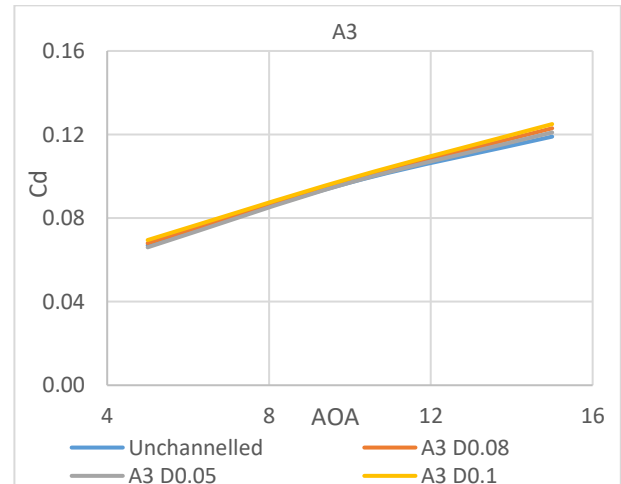


Figure 107. Cd vs. AOA for A3 sample for different Diameters

Figures (104) through (107) showed the effect of channel sizes on drag coefficients for three different angles of attack, 5, 10, and 15 degrees. They show that presence of channels causes an increase in drag coefficients for all samples, as mentioned earlier. Specifically, D0.1 channel causes the largest increase in drag coefficients, while the D0.05 channel causes the least increase. Generally, an increase in channel size leads to an increase in drag coefficients, so the relation between the channel size and the drag coefficient is directly proportional.

5.2.4 Lift/drag

5.2.4.1 Influence of the channel angle

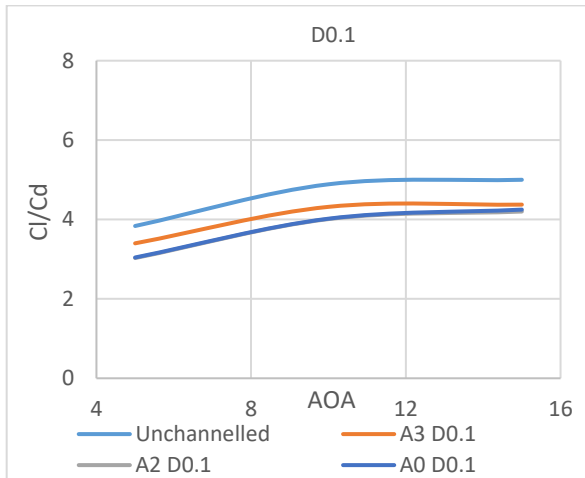


Figure 108. Cl/Cd vs. AOA for D0.1 sample for different angles

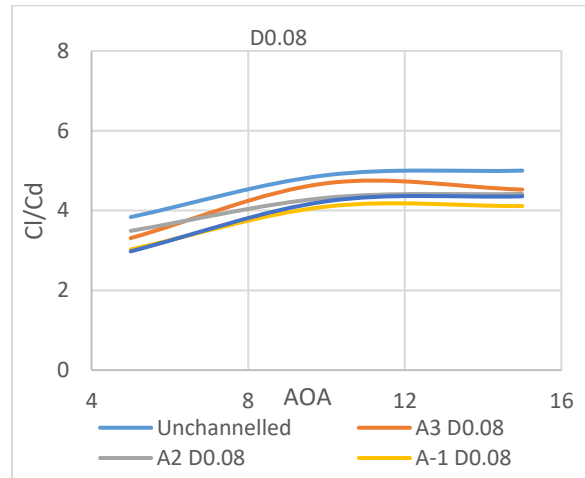


Figure 109. Cl/Cd vs. AOA for D0.08 sample for different angles

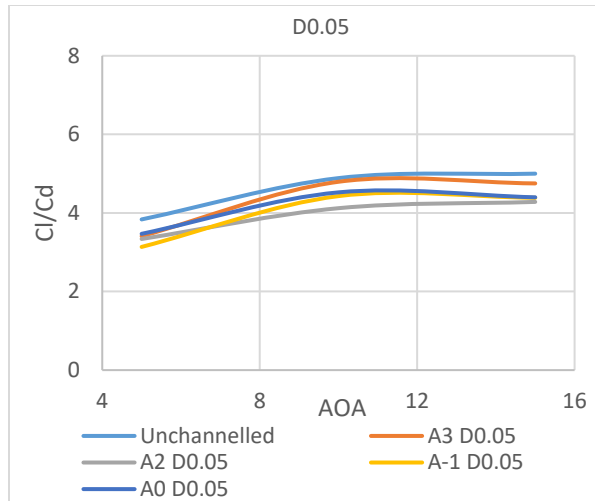


Figure 110. Cl/Cd vs. AOA for D0.05 sample for different angles

5.2.4.2 Influence of diameter size

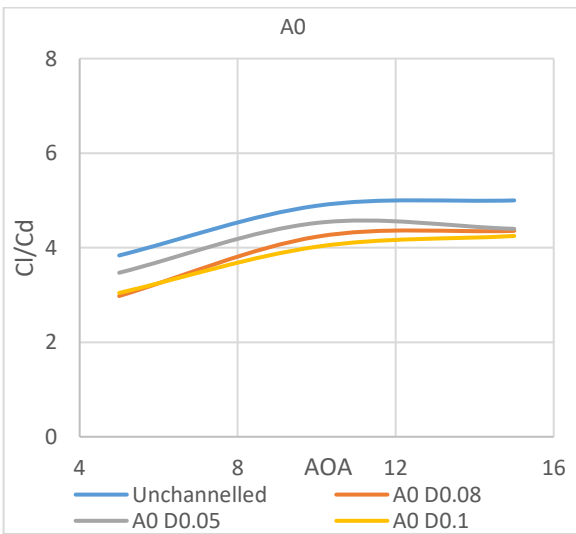


Figure 111. Cl/Cd vs. AOA for A0 sample for different Diameters

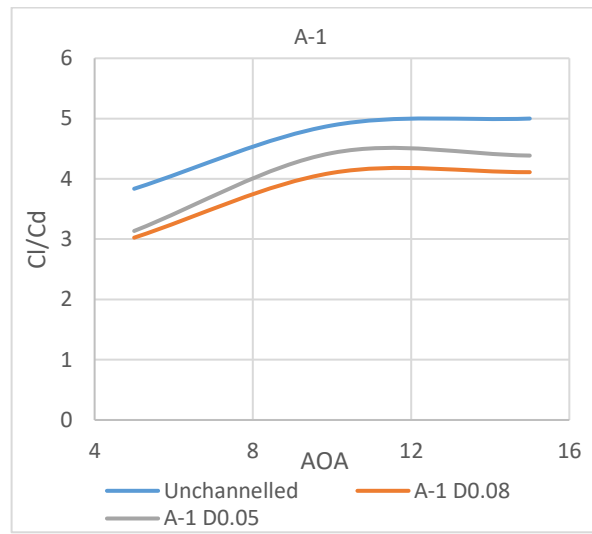


Figure 112. Cl/Cd vs. AOA for A-1 sample for different Diameters

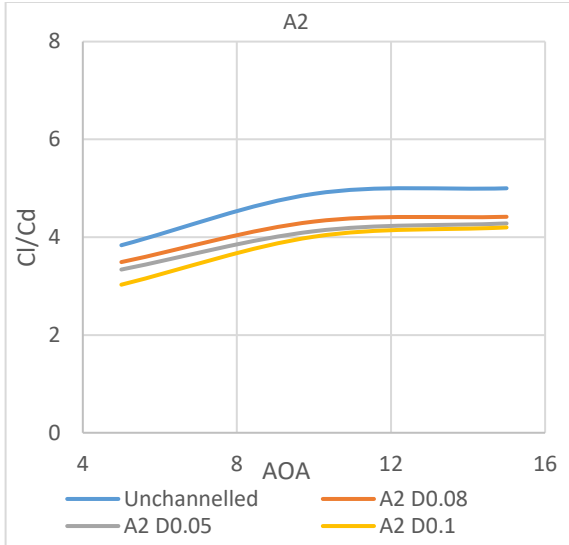


Figure 113. *Cl/Cd vs. AOA for A2 sample for different Diameters*

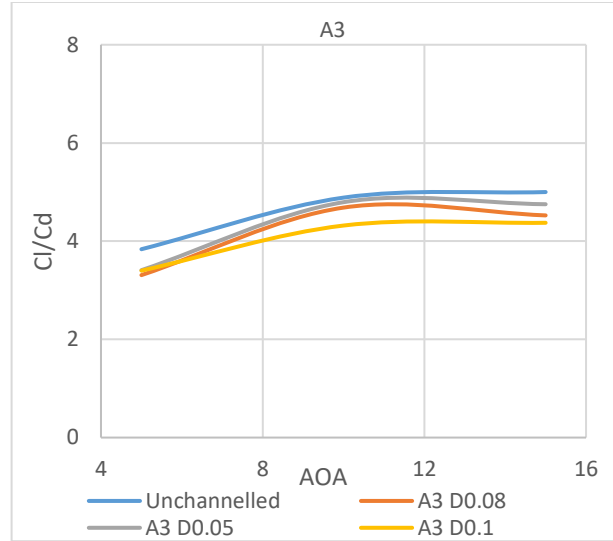


Figure 114. *Cl/Cd vs. AOA for A3 sample for different Diameters*

Figures (108) through (114), show the relation between the efficiency (Cl/Cd) and angle of attack for all types of samples. It can be seen that the presence of channels of any size or any direction reduces the ratio, Cl/Cd . Figures (108) through (110) showed that there was a loss in the ratio for any channel direction. However, the loss was minimal for the channel A3. Figures (111) through (114) showed that with increasing sizes, there was a larger loss in the efficiency. However, the loss was minimal for the channel D0.05, and the loss was maximal for the channel D0.1. As a result, an increase in channel size leads to a decrease in the efficiency, so the relation between the channel size and the efficiency is of an inverse nature.

Increasing percentages in drag coefficient and decreasing percentages in lift coefficient for channelled airfoils compared with the unchannelled airfoil at velocity (5 m/s) are tabulated below, table (12). The table shows that, in general, the presence of the channels increases drag coefficients and decreases lift coefficients, and those changes are different from one sample to another.

In the drag section of the table, and for the sample A3 D0.05 highlighted in yellow, the drag coefficient increased between (0 – 2 %), which was the best among all other samples. However, for the two samples, A-1 D0.08 and A0 D0.1, the drag coefficient increased the most, (12 - 23%), which was the worst among all other samples.

In the lift section of the table, and for the sample A0 D0.05 highlighted in yellow, the lift coefficient decreased between (0 – 2 %), which was the best among all other samples. However, for the sample, A2 D0.1, the lift coefficient decreased the most, (12 - 15%), which was the worst among all other samples.

In general, the results showed that the channels decrease the lift and increase the drag. In contrast with supersonic flow where the pressure drag is dominant, the channels decreased the drag, and eventually, it decreased the ratio (L/D). In our study with subsonic flow, the skin friction drag (viscous drag) was going to be the dominant, with absence of pressure drag, and this was why the drag was getting larger with the channels because the channels gave more skin friction area (wetted area) compared to the airfoil without channels [34].

The results for velocities 10 m/s and 15 m/s showed similar behavior for the velocity 5 m/s and they shown in the appendix B.

Table 12. The losing percentage in drag and lift channeled airfoils comparing to regular (V=5 m/s)

	Cd			CL		
	aoa 5	aoa 10	aoa 15	aoa 5	aoa 10	aoa 15
Unchanneled	0	0	0	0	0	0
A3 D0.08	0.01	0.01	0.03	0.12	0.03	0.06
A3 D0.05	-0.01	0.00	0.02	0.12	0.02	0.03
A3 D0.1	0.04	0.02	0.05	0.08	0.10	0.08

A2 D0.08	0.09	0.03	0.06	0.01	0.09	0.06
A2 D0.05	0.04	0.04	0.07	0.10	0.12	0.08
A2 D0.1	0.11	0.04	0.05	0.12	0.15	0.12
A-1 D0.08	0.21	0.14	0.13	0.05	0.04	0.07
A-1 D0.05	0.21	0.08	0.10	0.01	0.02	0.03
A0 D0.08	0.20	0.12	0.11	0.07	0.03	0.03
A0 D0.05	0.10	0.08	0.12	0.01	0.00	0.02
A0 D0.1	0.23	0.14	0.12	0.02	0.06	0.05

5.3 Turbulence measurements

This section is focused on the turbulence measurements. Velocity fluctuation was captured by the hot wire, and turbulence intensity was calculated from the velocity data. The goal of turbulence intensity measurements is to clarify the relation between the noise data and turbulence data as the aerodynamic noise generated by turbulence fluctuation.

5.3.1 Hot wire levels

The hot-wire probe was mounted on 3 linear stage to allow the motion in 3 dimensions. But the data of the velocity and turbulence intensity was recorded in 2 dimensions only because the behavior of the turbulence was expected to be consistent through the third dimension. The data was recorded in eight levels. Two of these levels were under the pressure side of the airfoils, one level was at the same horizontal level of the trailing edge, and the other five levels were on the suction side of the airfoils. The data got captured from a distance of 4 cm away from the trailing edge, and the hot-wire probe recorded the data at every 5 mm. The distance between each level was 5 mm as well. The levels were named from under to up as Z-2, Z-1 for the two levels under the pressure side, Z=0 for the level at the same horizontal level of the trailing edge, and Z+1, Z+2,

Z+3, Z+4, Z+5 for the levels on the suction side of the airfoils. Figure (115) shows the levels of the set of data measured around the airfoil.

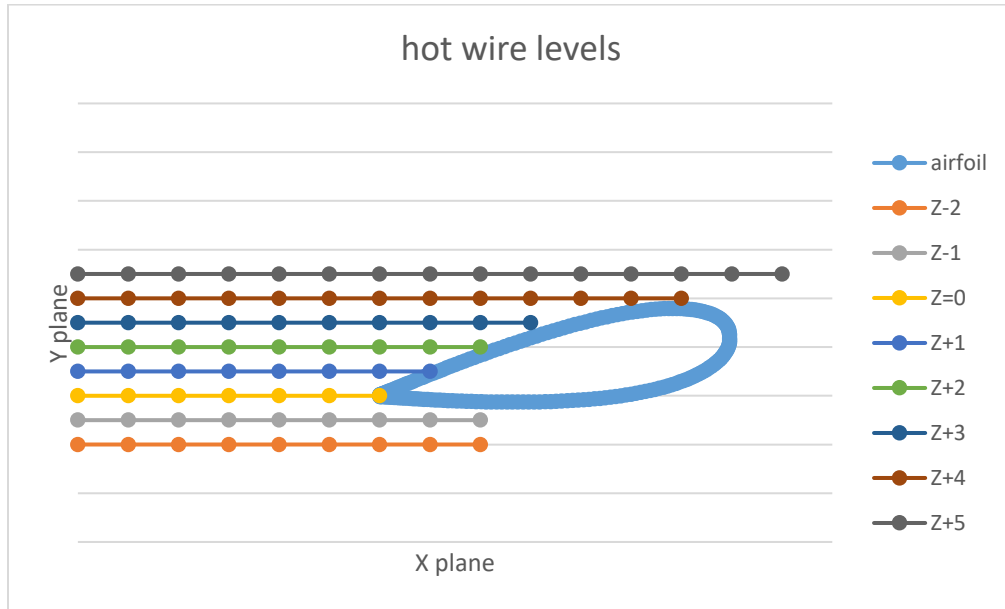


Figure 115. The levels of the set of data measured around the airfoil.

5.3.2 Turbulence Intensity measurements

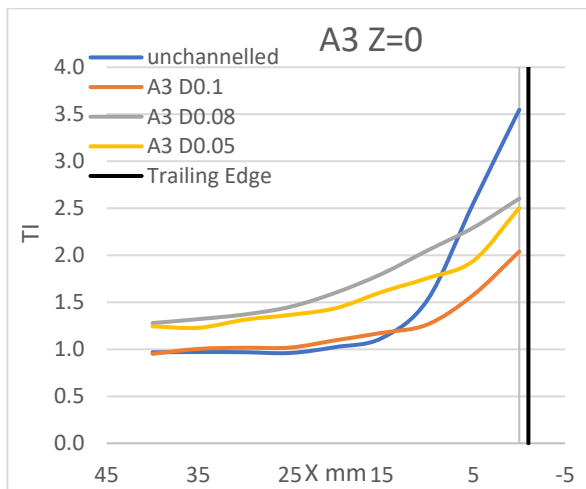


Figure 116. Turbulence intensity for samples A3 at Z=0

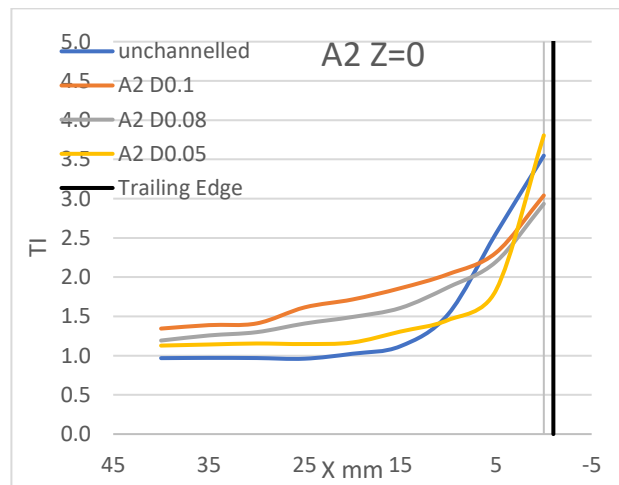


Figure 117. Turbulence intensity for samples A2 at Z=0

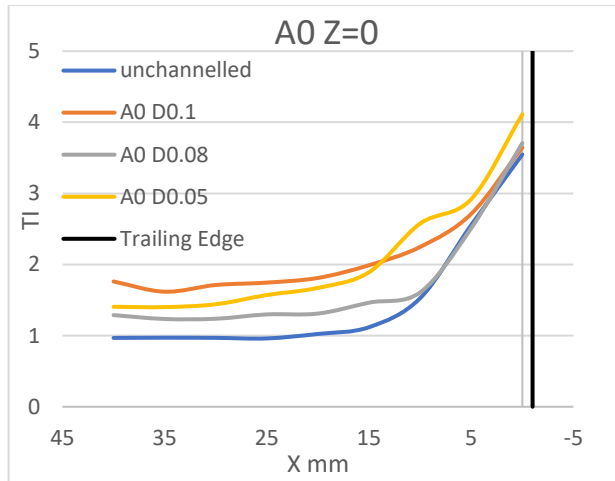


Figure 118. Turbulence intensity for samples A0 at Z=0

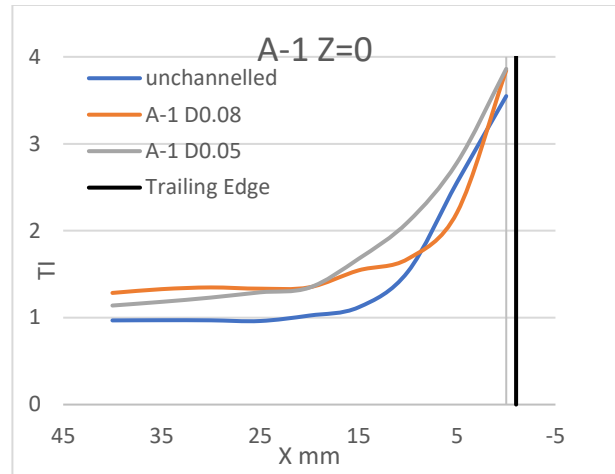


Figure 119. Turbulence intensity for samples A-1 at Z=0

Figures (116) through (119) show the turbulence intensity in the level ($Z=0$) for all the samples compared to the unchannelled one. All figures show an increase in the turbulence intensity closer to the trailing edge. All figures show that the unchannelled airfoil has less turbulence intensity in distances more than 1 cm. In Figure (116), the turbulence intensity for the sample A3 show less turbulence intensity than the unchannelled sample close to the trailing edge for all the channel sizes. In Figure (117), samples A2, D0.1 and D0.08, showed less turbulence intensity than the unchannelled sample close to the trailing edge. In Figure (118) and (119), none of the diameters showed any reduction in the turbulence intensity compared to the unchannelled sample. It has been

shown in this work that the noise level is directly correlated with turbulence intensity at the trailing edge of the airfoil. These results match with previous studies [56] [30].

The results of the other levels are attached in the appendix C.

5.4 Comparison between experimental and numerical results

5.4.1 Noise results

Table (13) shows the experimental results of the overall noise for all the samples and the numerical results of the overall noise for four samples: unchanneled, A3 D0.1, A3 D0.08, and A3 D0.05 in the velocity 15 m/s. The experimental results were close to the numerical results for the samples unchanneled and A3 D0.08. The error in these two samples 4% and 7% in order. However, there was noticeable difference in the results for the samples A3 D0.1 and A3 D0.05 within 15% and 28% error in order.

Table 13. Experimental and numerical results for overall SPL (dBA)

Flow velocity 15 m/s	Unchan.	A3 d0.08	a3 d0.05	a3 d0.1	a2 d0.08	a2 d0.05	a2 d0.1	a-1 d0.08	a-1 d0.05	a0 d0.08	a0 d0.05	a0 d0.1
experimental	51.91	51.86	52.49	49.71	53.36	58.04	51.29	56.90	56.95	54.63	57.24	55.64
simulation	49.5	48.1	44.5	35.6								
Error	0.04	0.07	0.15	0.28								

5.4.2 Force results

Table (14) showed the comparison between experimental and numerical results of Lift and Drag coefficients for some samples. The experimental results were generally higher for Cd and lower for the Cl as expected as the experimental data have 3D, surface smoothness, limitation on measurement accuracy, and other effects which were not considered in the simulation. However, the error can be considered within the experimental errors.

Table 14. Experimental and numerical results of lift and drag coefficients for some samples

Cases	A	AOA	V	CD		CL	
				Exp	Num	Exp	Num
Regular		10°	5	0.09	0.07	0.47	0.58
		10°	15	0.054	0.03	0.64	0.89
D=0.05	3°	10°	15	0.055	0.061	0.63	0.73
D=0.08	3°	10°	15	0.058	0.075	0.61	0.61
D=0.1	3°	10°	15	0.063	0.078	0.57	0.58
D=0.1	3°	10°	5	0.09	0.019	0.43	0.054
	3°	10°	10	0.071	0.082	0.52	0.589
	3°	10°	15	0.063	0.078	0.57	0.58
	3°	5°	15	0.047	0.03	0.315	0.317
D=0.08	-1°	10°	15	0.075	0.23	0.58	2.06
	3°	10°	15	0.058	0.075	0.61	0.61

5.5 Pressure fluctuation

Many studies focused on the extraction of pressure from velocity field [71] [72] [73] [74]. The extraction of pressure from the PIV time-resolved velocity field was reviewed by [71] [73]. The authors mentioned that the pressure values can be calculated from the momentum equation assuming negligible viscous effects with dominant acceleration term for incompressible flow. This study recommended using Lagrangian method over Eulerian for the more accuracy obtained from Lagrangian since the latter allows the increase of time step which reduces the error. While the

viscous and unsteadiness effects were considered in [72] to evaluate the deviation from Bernoulli's integral to obtain more accurate results for pressure calculations.

The influence of a fluctuating velocity field on the surface pressure has been experimentally investigated by [74] for a jet fin cross flow. A high frequency pressure sensor was used to measure the pressure. The results proved that the pressure fluctuation is strongly related to the PIV measured velocity fluctuation in the main flow direction where the high pressure is located at the lower velocity position and vice versa according to Bernoulli equation. Based on this research Bernoulli equation was used to predict the pressure from the measured velocity. The noise is related directly to the pressure fluctuation. However, pressure fluctuation is related to the kinetic energy velocity fluctuation as well. According to Bernoulli's equation, the relationship between pressure and velocity by neglecting the elevation can be described as:

$$P_1 + \frac{1}{2}\rho V_1^2 = P_2 + \frac{1}{2}\rho V_2^2 \dots\dots\dots (41)$$

From this equation, the pressure is inversely proportional to the square of the velocity. The effect of channels on the pressure fluctuation needs to be calculated. The values of the inverse of the square of the velocity can be considered as an approximate pressure value for comparing. Figures from (120) to (130) show the fluctuation of the value of $(1/v^2)$ which represents the pressure fluctuation for 100 measurements for the different samples compared to the unchanneled one. The results show low values of $(1/v^2)$ for the all the samples A3 and high values of $(1/v^2)$ for the samples A-1 and samples A0. As we will see in the next section, these results show similarity with the acoustic results collected by microphones.

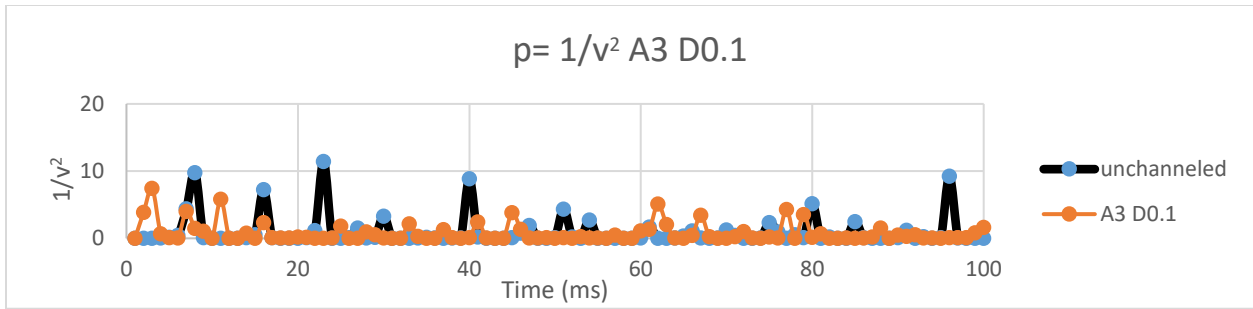


Figure 120. Fluctuation of $(1/v^2)$ for the sample A3 D0.1 vs. unchanneled

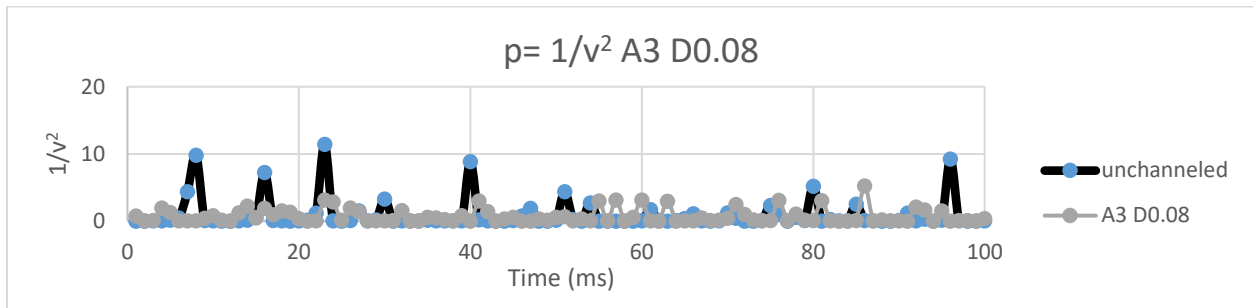


Figure 121. Fluctuation of $(1/v^2)$ for the sample A3 D0.08 vs. unchanneled

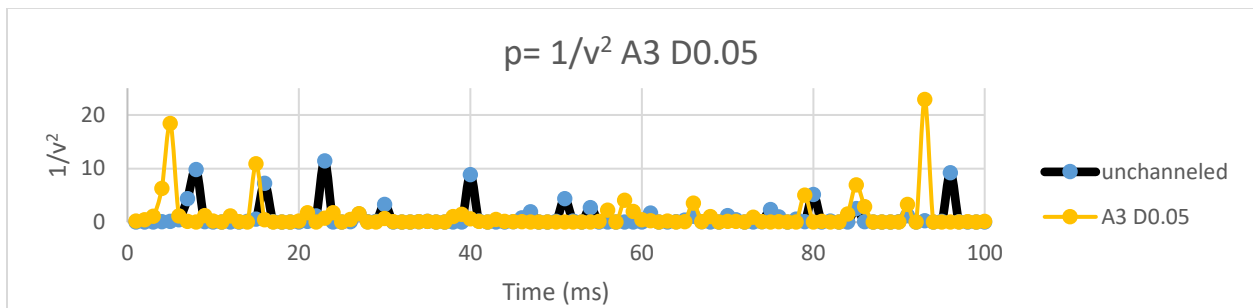


Figure 122. Fluctuation of $(1/v^2)$ for the sample A3 D0.05 vs. unchanneled

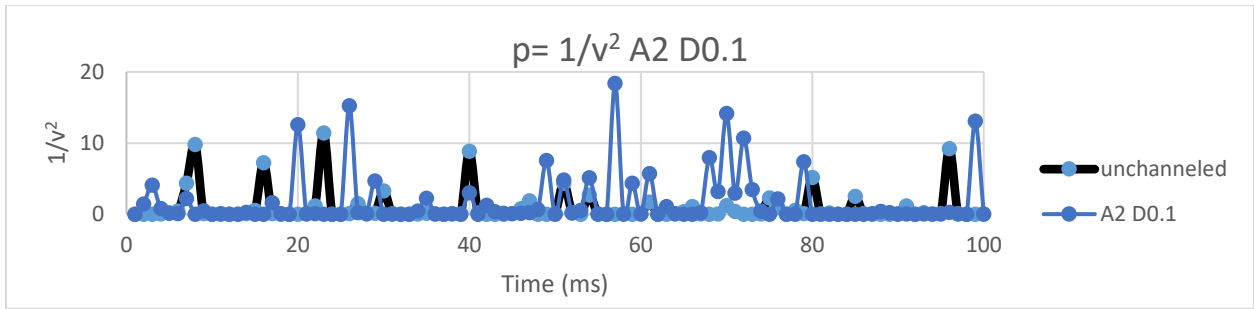


Figure 123. Fluctuation of $(1/v^2)$ for the sample A2 D0.1 vs. unchanneled

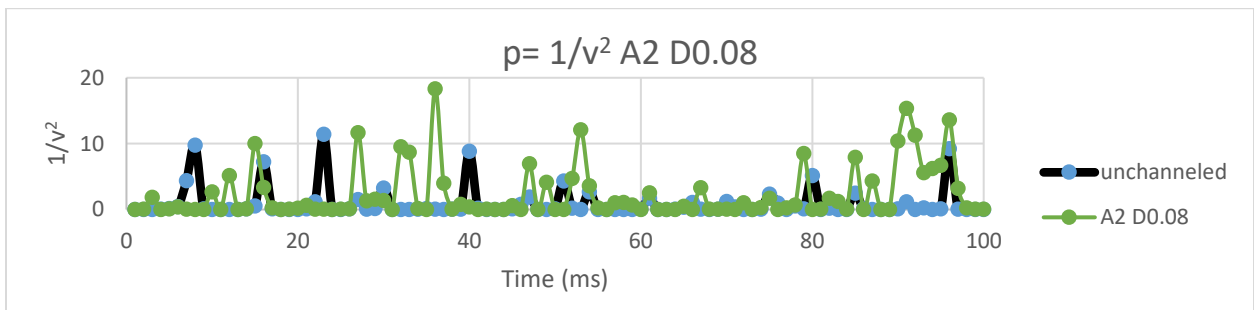


Figure 124. Fluctuation of $(1/v^2)$ for the sample A2 D0.08 vs. unchanneled

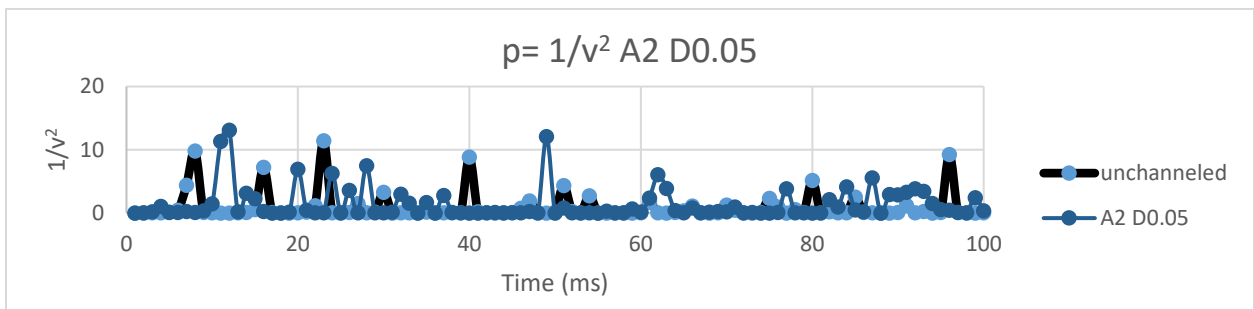


Figure 125. Fluctuation of $(1/v^2)$ for the sample A2 D0.05 vs. unchanneled

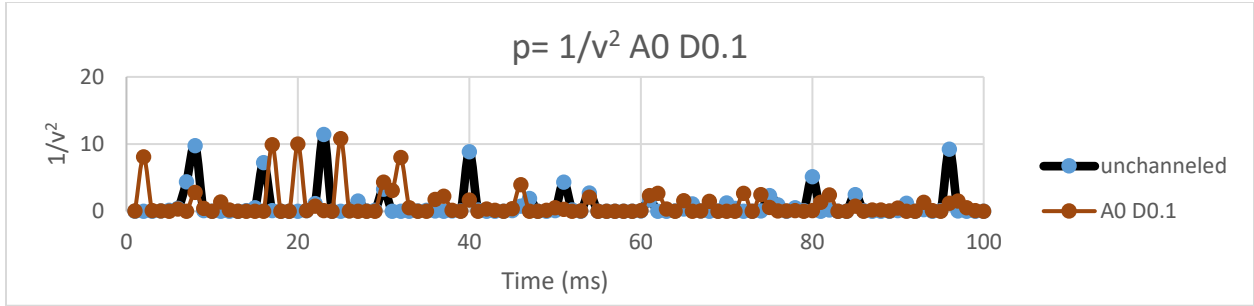


Figure 126. Fluctuation of $(1/v^2)$ for the sample A0 D0.1 vs. unchanneled

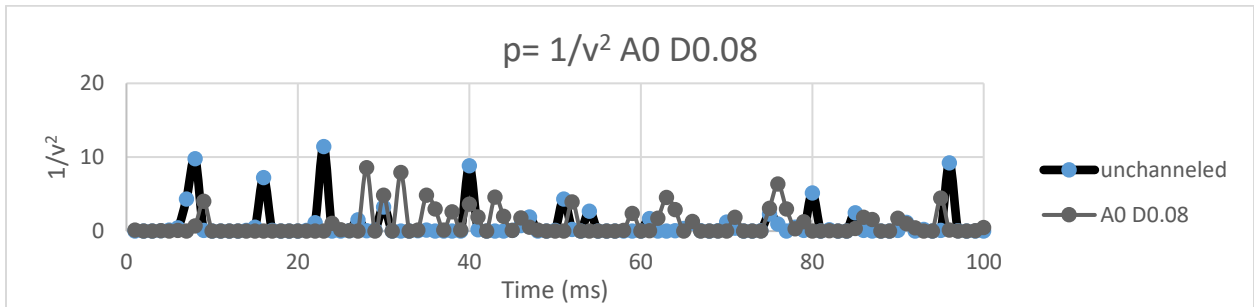


Figure 127. Fluctuation of $(1/v^2)$ for the sample A0 D0.08 vs. unchanneled

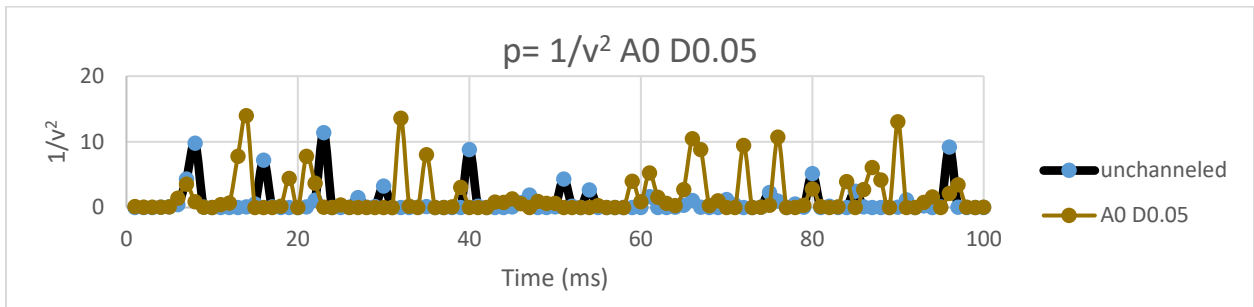


Figure 128. Fluctuation of $(1/v^2)$ for the sample A0 D0.05 vs. unchanneled

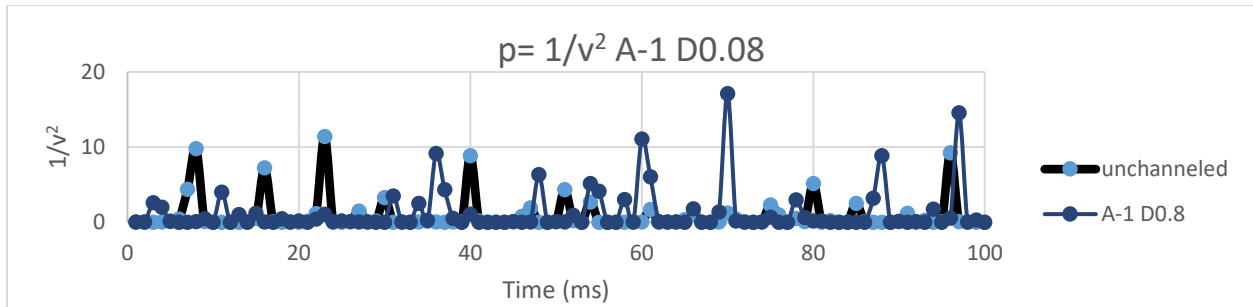


Figure 129. Fluctuation of $(1/v^2)$ for the sample A-1 D0.08 vs. unchanneled

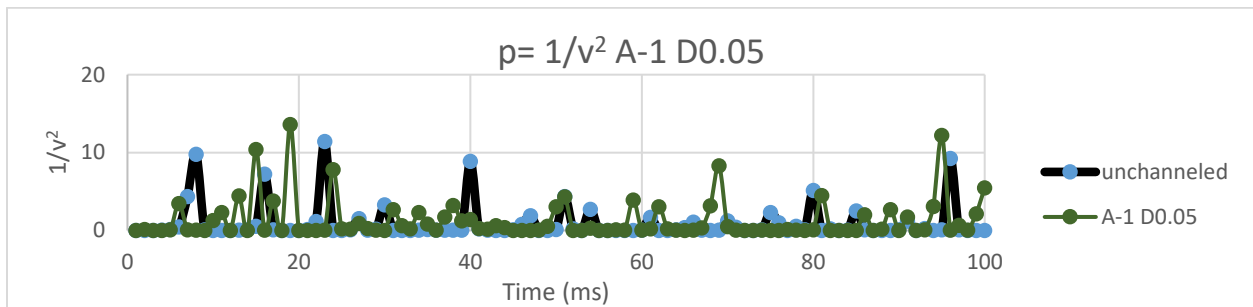


Figure 130. Fluctuation of $(1/v^2)$ for the sample A-1 D0.05 vs. unchanneled

5.6 The correlation between the noise and turbulence intensity

5.6.1 The correlation between the noise from microphone and turbulence intensity

A low frequency microphone with a frequency range of (1 to 20000 Hz) was used to measure the noise around the airfoil. The microphone was located 6 inches from the trailing edge, see Figure (35). The microphone was connected to a smart office application that could read and save the level of noise for all the range of the interested frequencies.

For velocity and turbulence measurements, the hot-wire anemometer was proven to be a feasible method that provided accurate measurements for velocity fluctuations. The hot wire anemometer is capable of capturing the velocity change within a micro second. Figure (37) showed

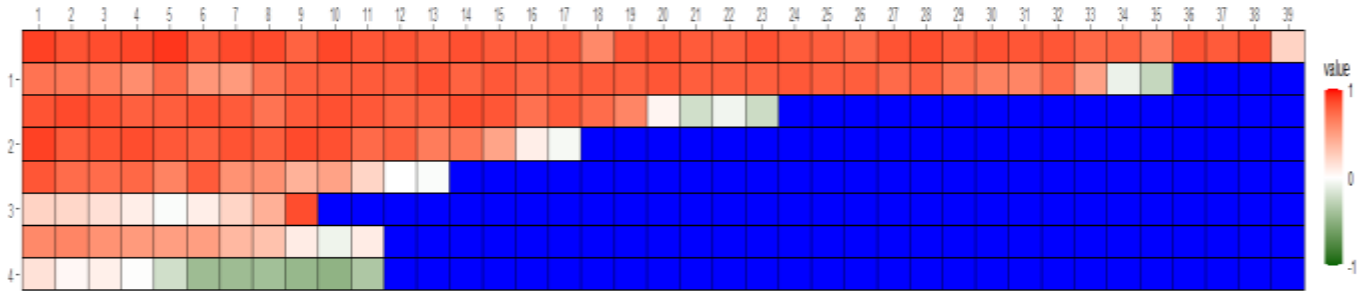


Figure 131 visualization for the correlation between the turbulence and the overall noise (0-10000Hz)

The visualization figures shows a high correlation between the turbulence intensity and the overall of spectrum of sound (0-10,000). The figure shows a high correlation in the area far from the airfoil where the flow is mostly laminar, and high correlation in both the leading edge and trailing edge as well, while the correlation was low in the levels down the airfoil and most of the points close to the airfoil surface.

5.6.2 The correlation between the data ($1/v^2$) and turbulence intensity

The sound pressure level data that was measured in the microphone has been correlated to the turbulence intensity in the last section. In this section, the correlation between the sound pressure level and the turbulence intensity will be repeated but in a different way. This time, the noise data will be taken from the pressure fluctuation that comes from the velocity fluctuation as explained previously. Table (16) shows the correlation values between the turbulence intensity and the noise data that comes from the pressure fluctuation ($1/v^2$), and Figure (132) shows the visualization of this correlation. The correlation in this section shows similarity to the correlation in the last section. So, the method used could be a reasonable tool to correlate and analyze the data in future.

CHAPTER 6

CONCLUSION AND FUTURE STUDIES

6.1 Conclusion

A new technique was used in this study in order to reduce the aerodynamic noise that is generated as a result of different sources around the airfoils. This new technique is creating channels with different sizes and directions inside the airfoils to study the influence of these channels on the aerodynamic noise in addition to the influence of these channels on the aerodynamic performance were carried out. Three sets of data were collected: noise data, collected directly from the microphones; force data, collected from the balance that was designed to measure the horizontal and vertical forces to calculate eventually the lift and drag forces; and turbulence data, collected by the hot wire technique.

The results could be concluded to:

- 1- The noise data showed that most of the emitted noise was found on the low frequency spectrum where it does not have serious effects on human hearing because it is close to the infrasound frequencies. This range of frequency has less attenuation, so it spreads farther.
- 2- The velocity of air flow directly influences aerodynamic noise; when the velocity increases by an increment of 5 m/s, the noise gets larger by an average amount of 10 dB.
- 3- Angle of Attack (AOA) of the airfoil directly influences aerodynamic noise; the increase of AOA from 5-10 degrees leads to an increase in the overall aerodynamic noise by an average of (1-3) dB, depending on the sample.

- 4- The different angles of channels inside the airfoil have different influences on the aerodynamic noise. Among the different angles tested, the sample A3 has the best influence and showed improvement in the reduction of aerodynamic noise more than the other cases.
- 5- The different diameter sizes of channels have different influences on the aerodynamic noise. The results showed a direct relation between the channel size and the aerodynamic noise; as the channel size gets smaller, the noise gets higher.
- 6- The results showed a tonal noise at a frequency of 928 Hz for all samples. This peak could be generated from external sources such as the wind tunnel engine.
- 7- The results showed a direct relation between sound pressure level and turbulence intensity at the trailing edge area.
- 8- The study showed a high correlation between the noise data and turbulence intensity data for most of the area not close enough to the airfoil surface where the flow does not have high turbulence intensity.
- 9- The study showed that the channels had a significant influence on the aerodynamic performance for most of the airfoil samples.
- 10- The channels increased the drag coefficients and decreased the lift coefficients for all the airfoil samples.
- 11- The study concluded that the influence of the channels was not equal for all the samples.
- 12- The force results showed in the drag section that the sample A3 D0.05 was the best among all other samples, while the sample A0 D0.05 was the best among all other samples in the lift section.
- 13- The noise results were close for both the data collected experimentally and numerically.

14- The force results were not close enough for both data collected experimentally and numerically.

15- The experimental data had 3D, surface smoothness, limitation on measurement accuracy, and other effects which were not considered in the simulation. However, the error, generally, can be considered within the experimental errors.

6.2 Recommendations and future studies

According to this study, there are some recommendations for possible future studies:

- 1- As the results showed different influences of different channels on the aerodynamic noise, it will be recommended to investigate more channel kinds, such as different sizes, directions and curved channels.
- 2- To display the turbulence around the airfoil and to explain the effect of the channels on the aerodynamic noise, Particle Image Velocimetry (PIV) technique could be used to show the turbulence around the airfoils and to justify the results clearly.
- 3- Repeat the same experiments with a larger scale. Larger wind tunnels and larger samples of airfoil will make the experimental results more accurate.
- 4- Use different kinds of airfoil (asymmetric preferred) other than NACA0012. In this case, the aerodynamic performance could be increased.

REFERENCES

- [1] Michaelides and E. E. Stathis, *Alternative energy sources*, Fort Worth, TX: Springer Science & Business Media, 2012.
- [2] G. A. Karim, *Fuels, energy, and the environment*, Crc Press, 2012.
- [3] G. Dolf, F. Boshell, D. Saygin, M. D. Bazilian, N. Wagner and R. Gorini, "The role of renewable energy in the global energy transformation," *Energy Strategy Reviews*, vol. 24, pp. 38-50, 2019.
- [4] A. Kumar, S. Ogita and Y. Y. Yau, *Biofuels: greenhouse gas mitigation and global warming: next generation biofuels and role of biotechnology*, New Delhi, India: Springer, 2018.
- [5] W. Tong, *Fundamentals of wind energy* (Vol. 44, p. 112), Southampton, UK: WIT Press, 2010.
- [6] J. Lee and F. Zhao, "GLOBAL WIND REPORT 2021," GWEC, Brussels, Belgium, 25 March 2021.
- [7] W. Siegfried, R. Bareiß and G. Guidati, "Noise mechanisms of wind turbines," in *Wind Turbine Noise*, Berlin, Heidelberg, Springer, 1996, pp. 67-92.
- [8] Y. Zhou, A. D. Lucey, Y. Liu and L. Huang, "Fluid-structure-sound interactions and control," in *In Proceedings of the 3rd Symposium on Fluid-Structure-Sound Interactions and Control*, Heidelberg, Germany., Springer, 2016.
- [9] H. Møller and C. S. Pedersen, "Low-frequency noise from large wind turbines.," *The Journal of the Acoustical Society of America*, vol. 129(6), pp. 3727-3744, 2011.
- [10] S. Buck, S. Oerlemans and S. Palo., "Experimental validation of a wind turbine turbulent inflow noise prediction code," *AIAA Journal*, vol. 56, no. 4, pp. 1495-1506, 2018.
- [11] K. W. Van Treuren and A. W. Hays, "A Study of Noise Generation on the E387, S823, NACA 0012, and NACA 4412 Airfoils for Use on Small-Scale Wind Turbines in the Urban Environment," *Journal of Energy Resources Technology*, vol. 139, no. 5, 2017.
- [12] E. Sarradj, C. Fritzsche and T. Geyer, "Silent owl flight: bird flyover noise measurements," *AIAA journal*, vol. 49, no. 4, pp. 769-779, 2011.

- [13] M. Muthuramalingam, E. Talboys, H. Wagner and C. Bruecker, "Flow turning effect and laminar control by the 3D curvature of leading edge serrations from owl wing," *Bioinspiration & Biomimetics*, vol. 16, no. 2, p. 026010, 2020.
- [14] K. Chen, Q. Liu, G. Liao, Y. Yang, L. Ren, H. Yang and X. Chen, "The sound suppression characteristics of wing feather of owl (*Bubo bubo*)," *Journal of Bionic Engineering*, vol. 9, no. 2, pp. 192-199, 2012.
- [15] E. Fite, R. Woodward and G. Podboy, "Effect of trailing edge flow injection on fan noise and aerodynamic performance," in *3rd AIAA flow control conference*, San Francisco, California, 2006.
- [16] T. Nakano, N. Fujisawa, Y. Oguma, Y. Takagi and S. Lee., "Experimental study on flow and noise characteristics of NACA0018 airfoil," *Journal of Wind Engineering and Industrial Aerodynamics*, vol. 95, no. 7, pp. 511-531, 2007.
- [17] T. Geyer and E. Sarradj, "Trailing edge noise of partially porous airfoils," in *20th AIAA/CEAS aeroacoustics conference*, Atlanta, 2014.
- [18] T. Chong, P. Joseph and M. Gruber, "Airfoil self noise reduction by non-flat plate type trailing edge serrations," *Applied Acoustics*, vol. 74, no. 4, pp. 607-613, 2013.
- [19] V. Katinas, M. Marčiukaitis and M. Tamašauskienė, "Analysis of the wind turbine noise emissions and impact on the environment," *Renewable and Sustainable Energy Reviews*, vol. 58, pp. 825-831, 2016.
- [20] R. G. Berger, P. Ashtiani, C. A. Ollson, M. Whitfield Aslund, L. C. McCallum, G. Leventhall and L. D. Knopper, "Health-based audible noise guidelines account for infrasound and low-frequency noise produced by wind turbines.," *Frontiers in public health*, p. 31, 24 February 2015.
- [21] F. A. Fernandez, R. A. Burdisso and J. P. Arenas, "Indoor simulation of amplitude modulated wind turbine noise," *Wind Energy*, vol. 20, no. 3, pp. 507-519, 2017.
- [22] C. H. Chiu, S. C. C. Lung, N. Chen, J. S. Hwang and M. C. M. Tsou, "Effects of low-frequency noise from wind turbines on heart rate variability in healthy individuals. Scientific reports, 11(1), 1-12.," 2021.
- [23] J. Pohl, J. Gabriel and G. Hübner, "Understanding stress effects of wind turbine noise—The integrated approach," *Energy Policy*, vol. 112, pp. 119-128, 2018.
- [24] S. A. Stansfeld and M. P. Matheson, "Noise pollution: non-auditory effects on health," *British medical bulletin*, vol. 68(1), pp. 243-257, (2003).

- [25] G. Leventhall, S. Benton and D. Robertson, "Coping strategies for low frequency noise," *Journal of low frequency noise, vibration and active control*, vol. 27(1), pp. 35-52, 2008.
- [26] D. Shepherd, D. McBride, D. Welch, K. N. Dirks and E. M. Hill, "Evaluating the impact of wind turbine noise on health-related quality of life," *Noise and Health*, vol. 13(54), p. 333, 2011.
- [27] M. J. Lighthill, "On sound generated aerodynamically I. General theory," *Proceedings of the Royal Society of London. Series A. Mathematical and Physical Sciences*, vol. 211, no. 1107, pp. 564-587., 1952.
- [28] S. W. Li, S. Wang, J. P. Wang and J. C. Mi, "Effect of turbulence intensity on airfoil flow: numerical simulations and experimental measurements," *Applied Mathematics and Mechanics*, vol. 32(8), p. 1029, 2011.
- [29] T. P. Chong, P. F. Joseph and P. O. A. L. Davies, "Design and performance of an open jet wind tunnel for aero-acoustic measurement," *Applied acoustics*, vol. 70, no. 4, pp. 605-614., 2009.
- [30] S. Buck, S. Oerlemans and S. Palo, "Experimental characterization of turbulent inflow noise on a full-scale wind turbine," *Journal of Sound and Vibration*, vol. 385, pp. 219-238, 2016.
- [31] H. Cao, Aerodynamics analysis of small horizontal axis wind turbine blades by using 2D and 3D CFD modelling (Doctoral dissertation, University of Central Lancashire)., 2011.
- [32] T. M. Young, Performance of the Jet Transport Airplane: Analysis Methods, Flight Operations, and Regulations, John Wiley & Sons., 2017.
- [33] S. M. Ruffin, A. Gupta and D. Marshall, "Supersonic channel airfoils for reduced drag," *AIAA journal*, vol. 38, no. 3, pp. 480-486, 2000.
- [34] A. Gupta, S. M. Ruffin, M. E. Newfield and L. Yates, "Aerothermodynamic performance enhancement of sphere-cones using the artificially blunted leading-edge concept," *Journal of Spacecraft and Rockets*, vol. 37, no. 2, pp. 235-241, 2000.
- [35] A. & R. S. M. Gupta, "Optimal artificially blunted leading-edge airfoils for enhanced aerothermodynamic performance," *Journal of spacecraft and rockets*, vol. 36, no. 4, pp. 499-506, 1999.
- [36] D. Giles and D. Marshall, "Aerodynamic Performance Enhancement of a NACA 66-206 Airfoil Using Supersonic Channel Airfoil Design.," in *46th AIAA Aerospace Sciences Meeting and Exhibit (p. 300)*, 2008.

- [37] T. Rao, T. Mahapatra and S. Mangavelli, "Enhancement of lift-drag characteristics of NACA 0012," *Materials Today*, vol. 5, no. 2, pp. 5328-5337, 2018.
- [38] R. Huang and H. Lee, " Effects of freestream turbulence on wing-surface flow and aerodynamic performance," *Journal of aircraft*, vol. 36, no. 6, pp. 965-972, 1999.
- [39] R. Arunraj, K. Logesh, V. Balaji, T. Ravichandran and G. Yuvasree, "Experimental investigation of lift enhancement by suction-assisted delayed separation of the boundary layer on NACA 0012 airfoil," *International Journal of Ambient Energy*, vol. 40, no. 3, pp. 243-247, 2019.
- [40] L. H. Feng, T. N. Jukes, K. S. Choi and J. J. Wang, "Flow control over a NACA 0012 airfoil using dielectric-barrier-discharge plasma actuator with a Gurney flap," *Experiments in fluids*, vol. 52, no. 6, pp. 1533-1546, 2012.
- [41] A. Shoja-Sani, E. Roohi, M. Kahrom and S. Stefanov, "Investigation of aerodynamic characteristics of rarefied flow around NACA 0012 airfoil using DSMC and NS solvers," *European Journal of Mechanics-B/Fluids*, vol. 48, pp. 59-74, 2014.
- [42] D. H. Kim, J. W. Chang and J. Chung, "Low-Reynolds-number effect on aerodynamic characteristics of a NACA 0012 airfoil," *Journal of aircraft*, vol. 48, no. 4, pp. 1212-1215, 2011.
- [43] M. Friman, Directivity of sound from wind turbines: A study on the horizontal sound radiation pattern from a wind turbine, Stockholm: Master's Thesis, Kungliga Tekniska högskolan, 2011.
- [44] E. Son, H. Kim, H. Kim, W. Choi and S. Lee, "Integrated numerical method for the prediction of wind turbine noise and the long range propagation," *Current Applied Physics*, vol. 10, no. 2, pp. S316-S319, 2010.
- [45] A. Huskey and J. Van Dam, "Wind turbine generator system acoustic noise test report for the ARE 442 wind turbine (No. NREL/TP-5000-49179)," in *National Renewable Energy Lab (NREL)*, Golden, CO (United States)., 2010.
- [46] F. Vanek and L. Albright, *Energy Systems Engineering: Evaluation & Implementation*, McGraw-Hill, 2008.
- [47] D. R. Raichel, *The science and applications of acoustics*, Springer Science & Business Media, 2006.
- [48] M. Hansen, *Aerodynamics of Wind Turbines—2nd edn*, London, Sterling, VA: Earthscan, 2008.
- [49] P. Dijkstra, *Rotor noise and aero-acoustic optimization of wind turbine airfoils.*, 2015.

- [50] H. Lord, W. Gatley and H. Evensen, *Noise Control for Engineers*, New York City: McGraw-Hill Book Company, 1980.
- [51] R. W. Paterson, P. G. Vogt, M. R. Fink and C. L. Munch, "Vortex noise of isolated airfoils," *Journal of Aircraft*, vol. 10, no. 5, pp. 296-302, 1973.
- [52] T. M. Young, *Performance of the Jet Transport Airplane: Analysis Methods, Flight Operations, and Regulations*, John Wiley & Sons., 2017.
- [53] A. Betz, *Introduction to the theory of flow machines*, Elsevier, 2014.
- [54] R. Tonin, *SOURCES OF WIND TURBINE NOISE AND SOUND PROPAGATION 40(1)*, Australia: Acoustics Australia, 2012.
- [55] S. Wagner, R. Bareiß and G. Guidati, "Noise mechanisms of wind turbines," in *Wind Turbine Noise*, Berlin, Heidelberg, Springer, 1996, pp. 67-92.
- [56] S. Buck, S. Oerlemans and S. Palo, "Experimental validation of a wind turbine turbulent inflow noise prediction code," *AIAA Journal*, vol. 56, no. 4, pp. 1495-1506, 2018.
- [57] T. F. Brooks, D. S. Pope and M. A. Marcolini, *Airfoil self-noise and prediction (Vol. 1218)*, Washington, DC: National Aeronautics and Space Administration, Office of Management, Scientific and Technical Information Division, 1989.
- [58] "PCB Piezotronics, ICP Infrasound Microphone System Installation and Operating Manual, Depew, New York, 2009".
- [59] "National Instruments, "NI-9234 C Series Sound and Vibration Input Module," 29 November 2016. [Online]. Available: <https://www.ni.com/en-us/support/model.ni-9234.html>."
- [60] "National Instruments, "USB-9162 CompactDAQ Chassis," 11 November 2016. [Online]. Available: <https://www.ni.com/en-us/support/model.usb-9162.html>."
- [61] "Airfoil Tools," [Online]. Available: <http://www.airfoiltools.com/airfoil/details?airfoil=n0012-il>.
- [62] "FLUENT, A. (2016). ANSYS FLUENT User's Guide, Release 17.1".
- [63] "S. M. Jalil, "Experimental and numerical investigation of axial heat transfer enhancement by oscillatory flows," *International Journal of Thermal Sciences*, vol. 137, pp. 352-364, 2019."
- [64] F. R. Menter, "Two-equation eddy-viscosity turbulence models for engineering applications," *AIAA journal*, vol. 32, no. 8, pp. 1598-1605, 1994.

- [65] D. C. Wilcox, "Multiscale model for turbulent flows," *AIAA journal*, vol. 26, no. 11, pp. 1311-1320., 1988.
- [66] S. H. Peng, L. Davidson and S. Holmberg, "The two-equation turbulence $k-\omega$ model applied to recirculating ventilation flows," Dept. of Thermo and Fluid Dynamics, Chalmers University of Technology, Gothenburg, 1996.
- [67] P. Cook, M. McDonald and M. Firmin, "Aerofoil RAE 2822-Pressure distributions, and boundary layer and wake measurements," Experimental data base for computer program assessment., AGARD Report AR-138., 1979.
- [68] FLUENT, "FLUENT 6.3 VALIDATION GUIDE," Fluent Inc, Lebanon, NH, 2006.
- [69] Y. Amini, M. Liravi and E. Izadpanah, "The effects of Gurney flap on the aerodynamic performance of NACA 0012 airfoil in the rarefied gas flow," *Computers & Fluids*, vol. 170, pp. 93-105, 2018.
- [70] M. W. Al-Jibory and H. A. A. Shinan, "Numerical Study of the Boundary Layer Separation Control on the NACA 0012 Airfoil using Triangular Rib," in *IOP Conference Series: Materials Science and Engineering (Vol. 671, No. 1, p. 012144)*. IOP Publishing., 2020.
- [71] J. J. Charonko, C. V. King, B. L. Smith and P. P. Vlachos, "Assessment of pressure field calculations from particle image velocimetry measurements," *Measurement Science and technology*, vol. 21, no. 10, p. 105401, 2010.
- [72] Z. Cai, Y. Liu, T. Chen and T. Liu, "Variational method for determining pressure from velocity in two dimensions," *Experiments in Fluids*, vol. 61, no. 5, pp. 1-26, 2020.
- [73] B. W. Van Oudheusden, "PIV-based pressure measurement," *Measurement Science and Technology*, vol. 24, no. 3, p. 032001, 2013.
- [74] S. J. Beresh, J. F. Henfling, R. W. Spillers and B. Pruett, "Influence of the fluctuating velocity field on the surface pressures in a jet/fin interaction," *Journal of Spacecraft and Rockets*, vol. 55, no. 5, pp. 1098-1110, 2018.
- [75] E. E. S. Michaelides, *Alternative energy sources.*, Springer Science & Business Media., 2012.

APPENDICES

A: Noise results

This appendix contains the noise results; Sound Pressure Level (SPL) in both dB and dBA in one octave band for all samples for different velocities and different Angle Of Attack (AOA):

1- Overall Sound Pressure Level (SPL) for velocity 5 m/s and AOA 15°

X [Hz]	Unch.	A3 D0.08	A3 D0.05	A3 D0.1	A2 D0.08	A2 D0.05	A2 D0.1	A-1 D0.08	A-1 D0.05	A0 D0.08	A0 D0.05	A0 D0.1
31.25	66.54	48.77	55.88	63.09	74.20	71.56	66.92	66.98	72.65	73.11	69.64	73.13
62.50	65.67	52.61	46.27	47.09	69.46	60.85	54.63	56.15	64.48	58.42	59.30	62.37
125	46.92	31.83	34.67	44.62	41.99	48.18	42.06	41.07	52.73	45.81	50.86	52.86
250	35.35	29.85	33.88	35.51	48.01	35.78	31.10	30.93	35.13	35.20	33.79	37.48
500	27.04	15.82	12.81	8.45	20.70	16.51	16.27	15.02	15.92	16.50	17.38	16.79
1000	17.14	14.11	10.41	5.48	9.30	14.64	15.85	15.91	16.79	17.06	16.93	16.75
2000	12.82	11.82	5.17	4.11	1.74	9.65	15.06	9.01	8.02	9.17	7.53	8.06
4000	-9.89	3.64	1.64	4.10	3.12	0.48	-3.70	0.31	0.97	-0.21	-2.29	1.22
8000	1.56	10.67	8.48	9.26	6.49	2.39	3.79	6.62	4.66	7.03	7.39	4.40
12500	-3.91	-3.93	-2.46	-5.43	-0.21	-2.79	-3.46	-2.69	-0.17	-3.49	-2.38	-2.51
Overall dB	69.16	54.15	56.39	63.27	75.46	71.93	67.19	67.34	73.31	73.26	70.08	73.52

2- Overall Sound Pressure Level (SPL) A- weighted for velocity 5 m/s and AOA 15°

X [Hz]	Unch.	A3 D0.08	A3 D0.05	A3 D0.1	A2 D0.08	A2 D0.05	A2 D0.1	A-1 D0.08	A-1 D0.05	A0 D0.08	A0 D0.05	A0 D0.1
31.25	27.14	9.37	16.48	23.69	34.80	32.16	27.52	27.58	33.25	33.71	30.24	33.73
62.50	39.47	26.41	20.07	20.89	43.26	34.65	28.43	29.95	38.28	32.22	33.10	36.17
125	30.82	15.73	18.57	28.52	25.89	32.08	25.96	24.97	36.63	29.71	34.76	36.76
250	26.75	21.25	25.28	26.91	39.41	27.18	22.50	22.33	26.53	26.60	25.19	28.88
500	23.84	12.62	9.61	5.25	17.50	13.31	13.07	11.82	12.72	13.30	14.18	13.59
1000	17.14	14.11	10.41	5.48	9.30	14.64	15.85	15.91	16.79	17.06	16.93	16.75
2000	14.02	13.02	6.37	5.31	2.94	10.85	16.26	10.21	9.22	10.37	8.73	9.26
4000	-8.89	4.64	2.64	5.10	4.12	1.48	-2.70	1.31	1.97	0.79	-1.29	2.22
8000	0.46	9.57	7.38	8.16	5.39	1.29	2.69	5.52	3.56	5.93	6.29	3.30
12500	-10.51	-10.53	-9.06	-12.03	-6.81	-9.39	-10.06	-9.29	-6.77	-10.09	-8.98	-9.11
Overall dBA	40.55	28.40	27.69	31.98	45.24	38.30	32.87	33.26	41.45	37.40	38.14	40.83

3- Overall Sound Pressure Level (SPL) for velocity 10 m/s and AOA 15°

X [Hz]	Unch.	A3 D0.08	A3 D0.05	A3 D0.1	A2 D0.08	A2 D0.05	A2 D0.1	A-1 D0.08	A-1 D0.05	A0 D0.08	A0 D0.05	A0 D0.1
31.25	77.64	76.45	81.05	79.95	80.82	83.94	78.94	84.78	79.98	80.07	80.37	82.97
62.50	64.04	65.04	69.64	65.42	67.13	68.60	60.85	70.90	68.54	71.00	68.91	67.41
125	50.93	47.06	51.56	38.74	59.55	62.95	30.58	63.14	54.72	63.75	57.89	57.02
250	42.20	39.58	45.22	31.15	45.71	41.35	24.04	50.18	41.37	50.43	49.67	40.83
500	35.95	13.10	39.79	17.41	30.99	29.90	19.52	36.20	32.08	38.25	33.58	31.08
1000	30.67	7.54	24.30	15.34	20.14	17.57	14.26	20.48	29.88	25.22	21.65	18.08
2000	15.62	20.78	31.14	16.64	22.15	22.73	17.22	21.58	25.06	24.16	21.54	20.96
4000	7.77	2.30	10.73	11.92	8.86	7.84	12.75	9.57	15.36	8.34	9.19	9.76
8000	4.48	0.22	5.38	3.16	3.09	4.26	7.20	2.98	2.80	4.47	2.96	3.09
12500	-9.78	-6.43	1.07	1.01	-1.10	-2.70	-3.28	-2.45	-2.69	-1.27	-3.35	-1.33
Overall dB	77.84	76.76	81.36	80.10	81.03	84.10	79.01	84.99	80.29	80.67	80.70	83.10

4- Overall Sound Pressure Level (SPL) A- weighted for velocity 10 m/s and AOA 15°

X [Hz]	Unch.	A3 D0.08	A3 D0.05	A3 D0.1	A2 D0.08	A2 D0.05	A2 D0.1	A-1 D0.08	A-1 D0.05	A0 D0.08	A0 D0.05	A0 D0.1
31.25	38.24	37.05	41.65	40.55	41.42	44.54	39.54	45.38	40.58	40.67	40.97	43.57
62.50	37.84	38.84	43.44	39.22	40.93	42.40	34.65	44.70	42.34	44.80	42.71	41.21
125	34.83	30.96	35.46	22.64	43.45	46.85	14.48	47.04	38.62	47.65	41.79	40.92
250	33.60	30.98	36.62	22.55	37.11	32.75	15.44	41.58	32.77	41.83	41.07	32.23
500	32.75	9.90	36.59	14.21	27.79	26.70	16.32	33.00	28.88	35.05	30.38	27.88
1000	30.67	7.54	24.30	15.34	20.14	17.57	14.26	20.48	29.88	25.22	21.65	18.08
2000	16.82	21.98	32.34	17.84	23.35	23.93	18.42	22.78	26.26	25.36	22.74	22.16
4000	8.77	3.30	11.73	12.92	9.86	8.84	13.75	10.57	16.36	9.34	10.19	10.76
8000	3.38	-0.88	4.28	2.06	1.99	3.16	6.10	1.88	1.70	3.37	1.86	1.99
12500	-16.38	-13.03	-5.53	-5.59	-7.70	-9.30	-9.88	-9.05	-9.29	-7.87	-9.95	-7.93
Overall dB	43.26	41.88	47.11	43.06	47.36	49.86	40.85	51.18	46.02	50.76	47.82	47.06

5- Overall Sound Pressure Level (SPL) for velocity 15 m/s and AOA 15°

X [Hz]	Unch.	A3 D0.08	A3 D0.05	A3 D0.1	A2 D0.08	A2 D0.05	A2 D0.1	A-1 D0.08	A-1 D0.05	A0 D0.08	A0 D0.05	A0 D0.1
31.3	97.54	93.18	92.03	92.90	96.64	96.15	93.61	98.07	98.34	98.62	96.31	96.03
62.5	92.57	90.26	90.95	88.35	91.96	91.30	91.94	96.62	93.89	94.90	93.67	94.65
125	55.79	73.57	58.29	80.73	77.73	79.81	69.28	80.78	76.44	79.27	78.51	78.76
250	45.72	59.71	63.32	52.93	63.79	67.86	54.91	71.51	61.89	70.10	66.60	66.91
500	37.20	40.38	55.88	50.16	52.59	55.55	36.64	54.65	44.00	53.47	55.00	51.00
1000	35.76	43.09	47.19	43.21	43.95	46.37	36.88	46.68	44.63	45.34	41.54	41.00
2000	31.40	36.43	24.09	36.15	34.04	35.11	37.62	37.83	34.73	36.57	34.13	34.58
4000	23.98	22.08	6.84	24.96	22.46	26.27	22.28	24.55	21.04	21.58	21.74	25.58
8000	17.13	14.73	11.59	15.91	16.39	15.88	7.37	15.98	14.01	16.16	16.80	14.22
12500	4.89	8.23	6.53	6.69	4.61	3.72	9.73	6.02	4.92	5.12	4.01	7.55
Overall dB	98.74	95.00	94.54	94.40	97.95	97.46	95.88	100.47	99.69	100.19	98.25	98.45

6- Overall Sound Pressure Level (SPL) A- weighted for velocity 15 m/s and AOA 15°

X [Hz]	Unch.	A3 D0.08	A3 D0.05	A3 D0.1	A2 D0.08	A2 D0.05	A2 D0.1	A-1 D0.08	A-1 D0.05	A0 D0.08	A0 D0.05	A0 D0.1
31.3	58.14	53.78	52.63	53.50	57.24	56.75	54.21	58.67	58.94	59.22	56.91	56.63
62.5	66.37	64.06	64.75	62.15	65.76	65.10	65.74	70.42	67.69	68.70	67.47	68.45
125	39.69	57.47	42.19	64.63	61.63	63.71	53.18	64.68	60.34	63.17	62.41	62.66
250	37.12	51.11	54.72	44.33	55.19	59.26	46.31	62.91	53.29	61.50	58.00	58.31
500	34.00	37.18	52.68	46.96	49.39	52.35	33.44	51.45	40.80	50.27	51.80	47.80
1000	35.76	43.09	47.19	43.21	43.95	46.37	36.88	46.68	44.63	45.34	41.54	41.00
2000	32.60	37.63	25.29	37.35	35.24	36.31	38.82	39.03	35.93	37.77	35.33	35.78
4000	24.98	23.08	7.84	25.96	23.46	27.27	23.28	25.55	22.04	22.58	22.74	26.58
8000	16.03	13.63	10.49	14.81	15.29	14.78	6.27	14.88	12.91	15.06	15.70	13.12
12500	-1.71	1.63	-0.07	0.09	-1.99	-2.88	3.13	-0.58	-1.68	-1.48	-2.59	0.95
Overall dBA	67.00	65.44	65.70	66.87	67.92	68.53	66.31	72.26	69.03	70.75	69.35	70.02

7- Overall Sound Pressure Level (SPL) for velocity 5 m/s and AOA 10°

	Unch.	A3 D0.08	A3 D0.05	A3 D0.1	A2 D0.08	A2 D0.05	A2 D0.1	A-1 D0.08	A-1 D0.05	A0 D0.08	A0 D0.05	A0 D0.1
31.30	64.50	65.50	64.50	62.60	64.10	63.10	66.70	70.30	67.60	65.40	64.00	69.80
62.50	56.50	55.60	47.40	56.50	56.50	58.70	50.40	55.80	57.70	52.90	59.20	56.40
125	41.80	39.80	41.60	39.30	28.80	44.40	45.00	47.50	40.40	48.30	51.10	37.50
250	30.80	25.70	29.60	27.50	28.10	30.60	35.40	32.50	36.00	30.20	40.40	29.60
500	2.06	-0.68	17.80	8.23	20.90	14.30	22.40	15.00	12.00	14.10	17.30	22.80
1000	5.57	18.60	16.80	15.70	11.70	15.00	18.50	19.30	16.40	16.30	15.10	15.30
2000	-0.16	10.50	13.70	3.53	21.10	7.36	3.64	8.47	8.24	9.50	9.89	7.29
4000	-13.30	-2.37	-11.60	1.52	-2.72	1.26	-6.91	-1.18	0.77	0.25	0.36	1.60
8000	6.42	11.20	9.22	10.20	12.30	6.01	3.77	5.64	2.84	5.82	6.66	6.15
12500	-20.90	-7.18	-0.13	-1.52	-2.65	-0.94	-2.02	-0.11	-1.37	-1.65	-0.46	-1.11
Overall dB	65.16	65.93	64.61	63.57	64.80	64.49	66.83	70.47	68.03	65.72	65.42	70.00

8- Overall Sound Pressure Level (SPL) A- weighted for velocity 5 m/s and AOA 10°

X [Hz]	Unch.	A3 D0.08	A3 D0.05	A3 D0.1	A2 D0.08	A2 D0.05	A2 D0.1	A-1 D0.08	A-1 D0.05	A0 D0.08	A0 D0.05	A0 D0.1
31.3	25.10	26.10	25.10	23.20	24.70	23.70	27.30	30.90	28.20	26.00	24.60	30.40
62.5	30.30	29.40	21.20	30.30	30.30	32.50	24.20	29.60	31.50	26.70	33.00	30.20
125	25.70	23.70	25.50	23.20	12.70	28.30	28.90	31.40	24.30	32.20	35.00	21.40
250	22.20	17.10	21.00	18.90	19.50	22.00	26.80	23.90	27.40	21.60	31.80	21.00
500	-1.14	-3.88	14.60	5.03	17.70	11.10	19.20	11.80	8.80	10.90	14.10	19.60
1,000	5.57	18.60	16.80	15.70	11.70	15.00	18.50	19.30	16.40	16.30	15.10	15.30
2,000	1.04	11.70	14.90	4.73	22.30	8.56	4.84	9.67	9.44	10.70	11.09	8.49
4,000	-12.30	-1.37	-10.60	2.52	-1.72	2.26	-5.91	-0.18	1.77	1.25	1.36	2.60
8,000	5.32	10.10	8.12	9.10	11.20	4.91	2.67	4.54	1.74	4.72	5.56	5.05
12,500	-27.50	-13.78	-6.73	-8.12	-9.25	-7.54	-8.62	-6.71	-7.97	-8.25	-7.06	-7.71
Overall dBA	32.88	32.21	30.21	32.10	32.39	34.63	33.45	35.89	34.71	34.38	38.47	34.06

9- Overall Sound Pressure Level (SPL) for velocity 10 m/s and AOA 10°

	Unch.	A3 D0.08	A3 D0.05	A3 D0.1	A2 D0.08	A2 D0.05	A2 D0.1	A-1 D0.08	A-1 D0.05	A0 D0.08	A0 D0.05	A0 D0.1
31.25	77.59	77.08	75.23	77.43	78.60	79.92	76.36	78.38	77.48	78.10	80.50	80.09
62.50	60.23	61.94	64.14	61.59	59.84	65.34	61.53	64.04	67.50	66.87	66.98	63.64
125	47.59	42.55	48.93	43.78	41.44	59.88	46.99	60.18	55.83	52.87	56.55	56.13
250	39.94	37.00	42.88	38.45	38.26	49.26	39.25	42.81	47.01	42.42	47.62	40.35
500	22.85	26.55	33.75	27.15	30.03	34.74	31.98	29.14	39.43	36.16	36.45	33.51
1000	28.02	23.46	29.38	17.41	25.30	29.67	22.28	28.45	31.44	30.03	27.72	29.45
2000	25.23	6.51	16.54	17.99	16.36	21.76	13.56	21.56	21.76	21.44	22.04	22.71
4000	12.37	4.38	-8.12	11.23	8.67	9.91	11.45	12.23	13.24	10.60	12.40	10.66
8000	-1.10	-3.32	-1.81	10.35	0.27	6.21	7.45	2.49	4.97	3.29	4.12	2.90
12500	-1.12	-2.05	-4.96	-17.58	2.88	-1.00	-0.12	-0.84	-1.56	-0.73	-1.56	-1.20
Overall dB	77.67	77.21	75.57	77.55	78.66	80.11	76.51	78.60	77.93	78.43	80.70	80.21

10- Overall Sound Pressure Level (SPL) A- weighted for velocity 10 m/s and AOA 10°

X [Hz]	Unch.	A3 D0.08	A3 D0.05	A3 D0.1	A2 D0.08	A2 D0.05	A2 D0.1	A-1 D0.08	A-1 D0.05	A0 D0.08	A0 D0.05	A0 D0.1
31.3	38.19	37.68	35.83	38.03	39.20	40.52	36.96	38.98	38.08	38.70	41.10	40.69
62.5	34.03	35.74	37.94	35.39	33.64	39.14	35.33	37.84	41.30	40.67	40.78	37.44
125	31.49	26.45	32.83	27.68	25.34	43.78	30.89	44.08	39.73	36.77	40.45	40.03
250	31.34	28.40	34.28	29.85	29.66	40.66	30.65	34.21	38.41	33.82	39.02	31.75
500	19.65	23.35	30.55	23.95	26.83	31.54	28.78	25.94	36.23	32.96	33.25	30.31
1000	28.02	23.46	29.38	17.41	25.30	29.67	22.28	28.45	31.44	30.03	27.72	29.45
2000	26.43	7.71	17.74	19.19	17.56	22.96	14.76	22.76	22.96	22.64	23.24	23.91
4000	13.37	5.38	-7.12	12.23	9.67	10.91	12.45	13.23	14.24	11.60	13.40	11.66
8000	-2.20	-4.42	-2.91	9.25	-0.83	5.11	6.35	1.39	3.87	2.19	3.02	1.80
12500	-7.72	-8.65	-11.56	-24.18	-3.72	-7.60	-6.72	-7.44	-8.16	-7.33	-8.16	-7.80
Overall dBA	41.2	40.5	42.2	40.7	41.1	47.6	40.7	46.4	46.2	44.7	46.7	44.9

11- Overall Sound Pressure Level (SPL) for velocity 15 m/s and AOA 10°

X [Hz]	Unch.	A3 D0.08	A3 D0.05	A3 D0.1	A2 D0.08	A2 D0.05	A2 D0.1	A-1 D0.08	A-1 D0.05	A0 D0.08	A0 D0.05	A0 D0.1
31.3	83.29	81.99	83.53	84.07	87.63	86.37	85.40	85.20	86.84	84.89	86.04	86.08
62.5	75.76	73.80	72.23	70.52	74.95	79.26	72.43	70.83	75.80	70.90	71.85	76.62
125	61.91	59.40	63.94	59.01	62.97	67.50	60.90	67.27	65.05	63.88	65.93	63.58
250	37.03	43.64	54.17	46.40	50.15	55.44	45.59	62.15	61.56	59.67	62.73	59.31
500	31.13	36.72	42.17	36.84	42.78	55.41	39.58	49.26	50.51	46.14	50.45	45.46
1000	29.80	46.46	37.56	37.41	34.61	44.38	40.66	43.41	41.56	41.32	45.13	41.68
2000	14.39	36.79	26.16	34.13	20.32	35.08	29.40	31.79	34.48	35.10	36.65	34.83
4000	10.99	23.37	27.12	25.48	-2.10	25.66	24.07	26.81	27.91	24.21	26.37	27.48
8000	1.95	13.77	12.11	10.32	15.46	18.46	16.47	17.53	17.18	17.56	18.17	14.94
12500	-4.99	-0.47	6.55	-5.34	5.87	5.41	-4.02	6.58	5.75	5.21	7.19	5.00
Overall dB	84.02	82.63	83.89	84.27	87.88	87.20	85.63	85.45	87.21	85.10	86.26	86.57

12- Overall Sound Pressure Level (SPL) A- weighted for velocity 15 m/s and AOA 10°

X [Hz]	Unch.	A3 D0.08	A3 D0.05	A3 D0.1	A2 D0.08	A2 D0.05	A2 D0.1	A-1 D0.08	A-1 D0.05	A0 D0.08	A0 D0.05	A0 D0.1
31.3	43.89	42.59	44.13	44.67	48.23	46.97	46.00	45.80	47.44	45.49	46.64	46.68
62.5	49.56	47.60	46.03	44.32	48.75	53.06	46.23	44.63	49.60	44.70	45.65	50.42
125	45.81	43.30	47.84	42.91	46.87	51.40	44.80	51.17	48.95	47.78	49.83	47.48
250	28.43	35.04	45.57	37.80	41.55	46.84	36.99	53.55	52.96	51.07	54.13	50.71
500	27.93	33.52	38.97	33.64	39.58	52.21	36.38	46.06	47.31	42.94	47.25	42.26
1000	29.80	46.46	37.56	37.41	34.61	44.38	40.66	43.41	41.56	41.32	45.13	41.68
2000	15.59	37.99	27.36	35.33	21.52	36.28	30.60	32.99	35.68	36.30	37.85	36.03
4000	11.99	24.37	28.12	26.48	-1.10	26.66	25.07	27.81	28.91	25.21	27.37	28.48
8000	0.85	12.67	11.01	9.22	14.36	17.36	15.37	16.43	16.08	16.46	17.07	13.84
12500	-11.59	-7.07	-0.05	-11.94	-0.73	-1.19	-10.62	-0.02	-0.85	-1.39	0.59	-1.60
Overall dBA	51.91	51.86	52.49	49.71	53.36	58.04	51.29	56.90	56.95	54.63	57.24	55.64

13- Overall Sound Pressure Level (SPL) for velocity 5 m/s and AOA 5°

X [Hz]		Unch.	A3 D0.08	A3 D0.05	A3 D0.1	A2 D0.08	A2 D0.05	A2 D0.1	A-1 D0.08	A-1 D0.05	A0 D0.08	A0 D0.05	A0 D0.1
31.3	31	56.80	55.31	58.50	54.46	55.05	60.74	54.83	55.97	60.43	66.61	67.91	65.21
62.5	63	53.67	53.74	50.70	54.13	47.87	54.24	66.97	50.69	52.17	55.66	55.41	57.36
125	125	36.13	41.63	40.78	33.65	40.26	45.49	45.43	38.52	39.05	42.83	48.21	39.59
250	250	27.54	33.69	20.91	32.90	29.30	30.45	36.40	29.45	27.84	32.04	37.90	28.96
500	500	19.60	14.05	13.86	13.05	5.01	13.66	17.57	12.43	12.45	11.75	14.56	14.57
1000	1000	15.67	12.99	14.84	7.08	11.06	16.85	19.93	17.61	16.45	17.54	15.87	14.73
2000	2000	13.03	11.40	9.50	13.43	2.68	9.88	4.05	9.54	7.17	7.69	8.49	6.32
4000	4000	-2.84	-2.13	2.83	-1.81	4.70	0.70	-1.86	0.34	-0.34	0.91	-0.52	-0.26
8000	8000	-3.51	9.24	12.30	9.77	7.24	3.74	7.28	4.34	3.39	5.47	5.80	5.66
12500	12500	-0.38	-4.36	0.56	-3.38	-6.94	-1.45	-3.34	-1.24	-1.20	-1.44	-1.05	-1.32
Overall dB		58.55	57.73	59.23	57.34	55.94	61.73	67.26	57.16	61.06	66.96	68.20	65.88

14- Overall Sound Pressure Level (SPL) A- weighted for velocity 5 m/s and AOA 5°

X [Hz]	Unch.	A3 D0.08	A3 D0.05	A3 D0.1	A2 D0.08	A2 D0.05	A2 D0.1	A-1 D0.08	A-1 D0.05	A0 D0.08	A0 D0.05	A0 D0.1
31.3	17.40	15.91	19.10	15.06	15.65	21.34	15.43	16.57	21.03	27.21	28.51	25.81
62.5	27.47	27.54	24.50	27.93	21.67	28.04	40.77	24.49	25.97	29.46	29.21	31.16
125	20.03	25.53	24.68	17.55	24.16	29.39	29.33	22.42	22.95	26.73	32.11	23.49
250	18.94	25.09	12.31	24.30	20.70	21.85	27.80	20.85	19.24	23.44	29.30	20.36
500	16.40	10.85	10.66	9.85	1.81	10.46	14.37	9.23	9.25	8.55	11.36	11.37
1000	15.67	12.99	14.84	7.08	11.06	16.85	19.93	17.61	16.45	17.54	15.87	14.73
2000	14.23	12.60	10.70	14.63	3.88	11.08	5.25	10.74	8.37	8.89	9.69	7.52
4000	-1.84	-1.13	3.83	-0.81	5.70	1.70	-0.86	1.34	0.66	1.91	0.48	0.74
8000	-4.61	8.14	11.20	8.67	6.14	2.64	6.18	3.24	2.29	4.37	4.70	4.56
12500	-6.98	-10.96	-6.04	-9.98	-13.54	-8.05	-9.94	-7.84	-7.80	-8.04	-7.65	-7.92
Overall dBA	29.54	31.29	28.71	30.13	27.68	32.72	41.33	28.48	29.38	33.38	36.11	33.17

15- Overall Sound Pressure Level (SPL) for velocity 10 m/s and AOA 5°

	Unch.	A3 D0.08	A3 D0.05	A3 D0.1	A2 D0.08	A2 D0.05	A2 D0.1	A-1 D0.08	A-1 D0.05	A0 D0.08	A0 D0.05	A0 D0.1
31	78.48	78.30	77.94	76.66	77.24	79.94	78.53	78.93	79.93	80.37	79.78	80.54
63	51.76	54.09	52.09	55.30	53.41	61.82	58.02	62.31	64.79	63.48	60.97	61.35
125	31.91	26.75	41.17	40.31	45.65	55.06	43.65	57.83	54.34	50.72	48.46	43.98
250	37.03	30.89	38.34	36.49	36.71	44.25	30.00	43.69	45.28	42.26	38.52	38.57
500	21.13	26.44	31.03	8.61	30.75	33.33	25.09	29.11	28.91	30.02	33.07	27.10
1000	29.80	31.45	32.39	17.08	28.06	29.53	20.46	30.60	28.91	28.03	30.50	32.00
2000	14.39	16.76	18.56	27.34	9.06	20.29	14.46	21.67	20.79	21.13	21.29	21.33
4000	10.99	13.13	14.16	3.90	-10.48	12.41	14.21	13.78	11.42	10.90	12.86	11.48
8000	1.95	0.00	2.28	0.49	-18.70	7.87	2.67	4.13	4.06	3.44	2.60	2.77
12500	-4.99	-0.94	-2.00	-1.71	-11.43	-2.66	-7.99	-1.31	-1.05	-1.98	-2.64	-1.00
Overall dB	78.49	78.32	77.95	76.69	77.26	80.02	78.57	79.06	80.07	80.47	79.84	80.59

16- Overall Sound Pressure Level (SPL) A- weighted for velocity 10 m/s and AOA 5°

X [Hz]	Unch.	A3 D0.08	A3 D0.05	A3 D0.1	A2 D0.08	A2 D0.05	A2 D0.1	A-1 D0.08	A-1 D0.05	A0 D0.08	A0 D0.05	A0 D0.1
31.3	39.08	38.90	38.54	37.26	37.84	40.54	39.13	39.53	40.53	40.97	40.38	41.14
62.5	25.56	27.89	25.89	29.10	27.21	35.62	31.82	36.11	38.59	37.28	34.77	35.15
125	15.81	10.65	25.07	24.21	29.55	38.96	27.55	41.73	38.24	34.62	32.36	27.88
250	28.43	22.29	29.74	27.89	28.11	35.65	21.40	35.09	36.68	33.66	29.92	29.97
500	17.93	23.24	27.83	5.41	27.55	30.13	21.89	25.91	25.71	26.82	29.87	23.90
1000	29.80	31.45	32.39	17.08	28.06	29.53	20.46	30.60	28.91	28.03	30.50	32.00
2000	15.59	17.96	19.76	28.54	10.26	21.49	15.66	22.87	21.99	22.33	22.49	22.53
4000	11.99	14.13	15.16	4.90	-9.48	13.41	15.21	14.78	12.42	11.90	13.86	12.48
8000	0.85	-1.10	1.18	-0.61	-19.80	6.77	1.57	3.03	2.96	2.34	1.50	1.67
12500	-11.59	-7.54	-8.60	-8.31	-18.03	-9.26	-14.59	-7.91	-7.65	-8.58	-9.24	-7.60
Overall dBA	40.11	40.11	40.52	38.91	39.72	44.56	40.32	45.18	44.94	43.87	42.77	42.99

17- Overall Sound Pressure Level (SPL) for velocity 15 m/s and AOA 5°

X [Hz]	Unch.	A3 D0.08	A3 D0.05	A3 D0.1	A2 D0.08	A2 D0.05	A2 D0.1	A-1 D0.08	A-1 D0.05	A0 D0.08	A0 D0.05	A0 D0.1
31	91.51	91.10	89.03	87.97	92.76	92.99	93.92	96.20	92.51	91.66	92.81	92.72
63	82.19	65.44	77.66	80.81	86.81	87.42	87.20	89.67	87.44	87.35	86.51	86.90
125	56.25	63.62	70.03	68.69	68.05	69.88	55.85	73.84	70.32	69.98	69.33	66.58
250	37.28	45.67	53.93	41.58	47.33	60.23	48.26	54.79	59.19	56.31	50.56	53.03
500	27.40	38.22	33.50	36.89	42.02	42.93	42.23	51.51	46.50	41.37	40.33	43.88
1000	38.95	43.66	30.85	46.46	32.75	39.43	44.89	43.09	42.91	41.76	43.06	41.61
2000	34.05	30.50	35.48	33.33	33.70	35.58	33.56	34.20	34.97	34.37	36.31	34.52
4000	21.24	22.54	21.16	23.54	29.12	27.71	18.59	28.77	29.01	27.02	26.68	27.48
8000	15.44	9.35	-1.15	18.55	15.09	15.32	7.19	12.56	15.20	14.89	15.74	15.63
12500	11.90	-3.33	-1.97	2.41	-5.89	7.82	-4.01	6.21	5.43	8.63	7.78	4.56
Overall dB	92.00	91.12	89.39	88.77	93.76	94.07	94.76	97.09	93.71	93.05	93.74	93.74

18- Overall Sound Pressure Level (SPL) A- weighted for velocity 15 m/s and AOA 5°

X [Hz]	Unch.	A3 D0.08	A3 D0.05	A3 D0.1	A2 D0.08	A2 D0.05	A2 D0.1	A-1 D0.08	A-1 D0.05	A0 D0.08	A0 D0.05	A0 D0.1
31	52.11	51.70	49.63	48.57	53.36	53.59	54.52	56.80	53.11	52.26	53.41	53.32
63	55.99	39.24	51.46	54.61	60.61	61.22	61.00	63.47	61.24	61.15	60.31	60.70
125	40.15	47.52	53.93	52.59	51.95	53.78	39.75	57.74	54.22	53.88	53.23	50.48
250	28.68	37.07	45.33	32.98	38.73	51.63	39.66	46.19	50.59	47.71	41.96	44.43
500	24.20	35.02	30.30	33.69	38.82	39.73	39.03	48.31	43.30	38.17	37.13	40.68
1000	38.95	43.66	30.85	46.46	32.75	39.43	44.89	43.09	42.91	41.76	43.06	41.61
2000	35.25	31.70	36.68	34.53	34.90	36.78	34.76	35.40	36.17	35.57	37.51	35.72
4000	22.24	23.54	22.16	24.54	30.12	28.71	19.59	29.77	30.01	28.02	27.68	28.48
8000	14.34	8.25	-2.25	17.45	13.99	14.22	6.09	11.46	14.10	13.79	14.64	14.53
12500	5.30	-9.93	-8.57	-4.19	-12.49	1.22	-10.61	-0.39	-1.17	2.03	1.18	-2.04
Overall dBA	57.65	53.91	57.16	57.74	61.89	62.93	62.05	65.36	62.92	62.55	61.91	61.93

B: Force results

This appendix contains the force results (lift coefficients and drag coefficients) in flow velocities 10 m/s and 15 m/s and the effects of channel's size and direction on these coefficients.

Flow Velocity 10 m/s:

This table shows the force results for the 12 samples in flow velocity 10 m/s.

	V=10 m/s		Experimental			
			Cd		CL	
		aoa 5	aoa 10	aoa 15	aoa 5	aoa 10
Unchanneled	0.045	0.069	0.085	0.305	0.574	0.708
A3 D0.08	0.048	0.071	0.091	0.275	0.520	0.631
A3 D0.05	0.047	0.070	0.088	0.295	0.573	0.694
A3 D0.1	0.051	0.071	0.092	0.275	0.515	0.625
A2 D0.08	0.054	0.076	0.096	0.299	0.495	0.627
A2 D0.05	0.062	0.083	0.104	0.264	0.495	0.635
A2 D0.1	0.065	0.083	0.106	0.255	0.465	0.595
A-1 D0.08	0.062	0.085	0.108	0.295	0.497	0.615
A-1 D0.05	0.063	0.081	0.105	0.312	0.515	0.625
A0 D0.08	0.063	0.083	0.106	0.298	0.545	0.655
A0 D0.05	0.059	0.078	0.102	0.305	0.555	0.673
A0 D0.1	0.065	0.085	0.109	0.298	0.535	0.635

The force results for the 12 samples in flow velocity 10 m/s

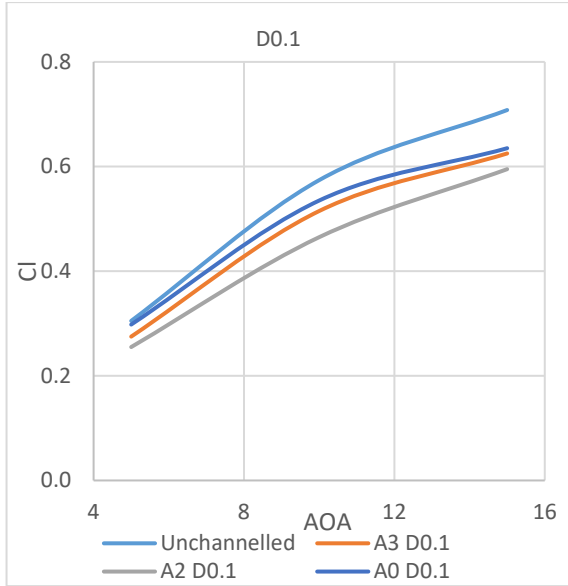
This table shows the losing percentage in drag and lift channeled airfoils comparing to regular (V=10 m/s)

	Cd			CL		
	aoa 5	aoa 10	aoa 15	aoa 5	aoa 10	aoa 15
Unchanneled						
A3 D0.08	0.07	0.03	0.07	0.10	0.09	0.11
A3 D0.05	0.04	0.01	0.04	0.03	0.00	0.02
A3 D0.1	0.13	0.03	0.08	0.10	0.10	0.12
A2 D0.08	0.20	0.10	0.13	0.02	0.14	0.11
A2 D0.05	0.38	0.21	0.22	0.14	0.14	0.10
A2 D0.1	0.44	0.20	0.25	0.16	0.19	0.16
A-1 D0.08	0.38	0.23	0.27	0.03	0.13	0.13
A-1 D0.05	0.40	0.17	0.24	-0.02	0.10	0.12
A0 D0.08	0.40	0.20	0.25	0.02	0.05	0.07
A0 D0.05	0.31	0.13	0.20	0.00	0.03	0.05
A0 D0.1	0.44	0.23	0.28	0.02	0.07	0.10

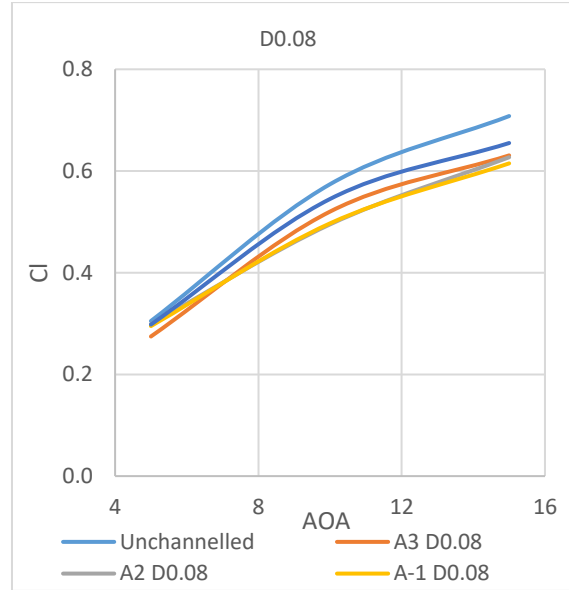
The losing percentage in drag and lift channeled airfoils comparing to regular (V=10 m/s)

Lift:

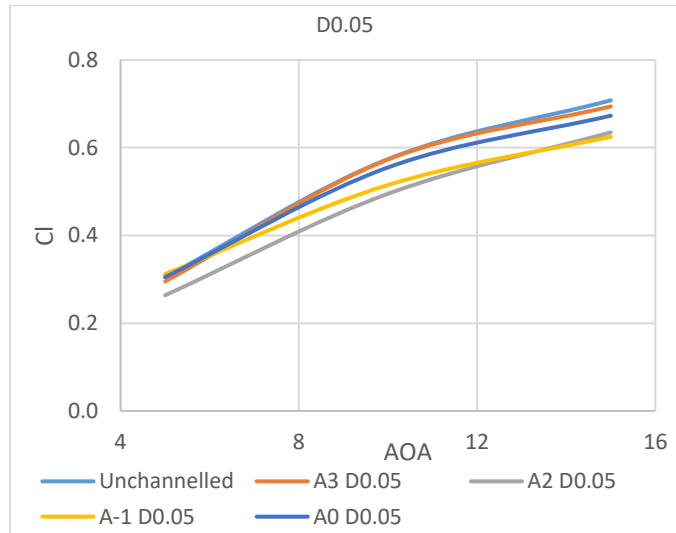
Influence of the Channel angle:



Cl vs. AOA for D0.1 sample for different angles

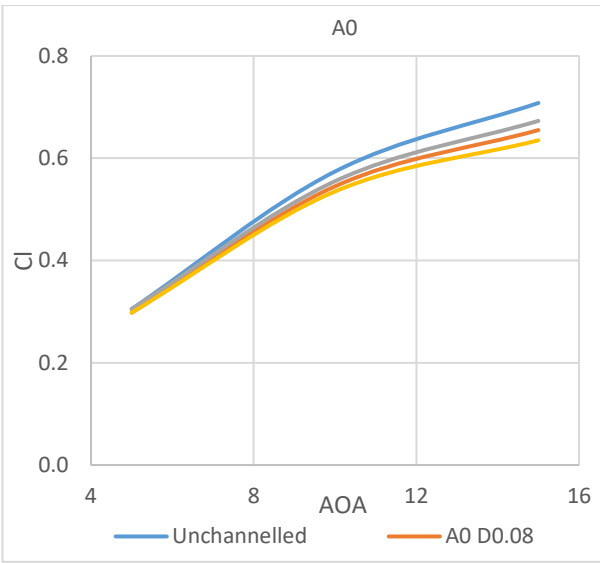


Cl vs. AOA for D0.08 sample for different angles

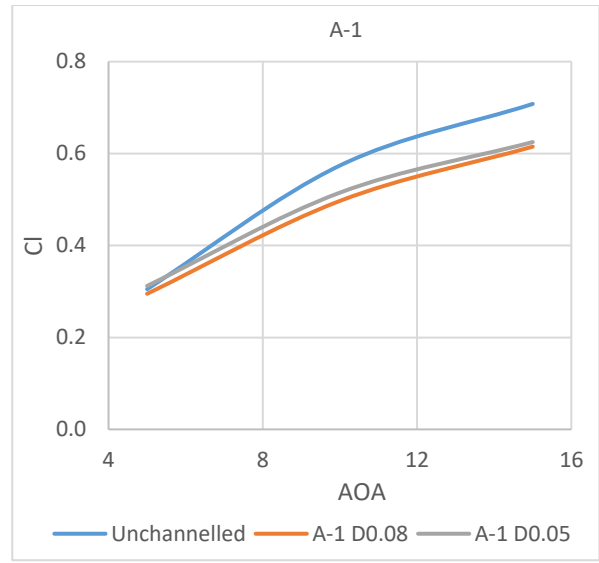


Cl vs. AOA for D0.05 sample for different angles

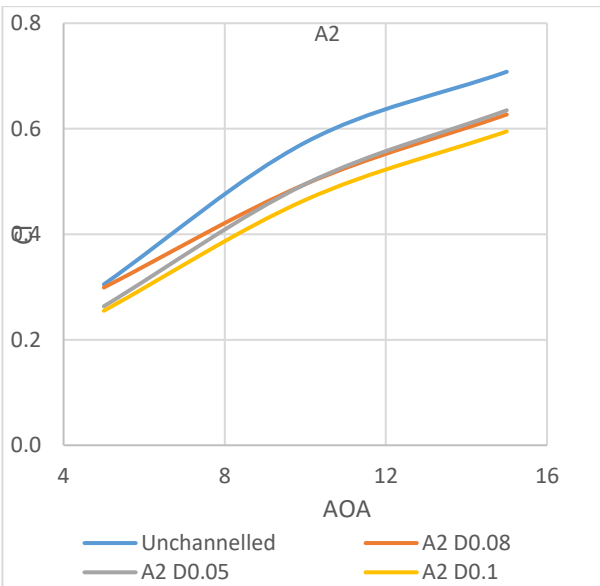
Influence of diameter size:



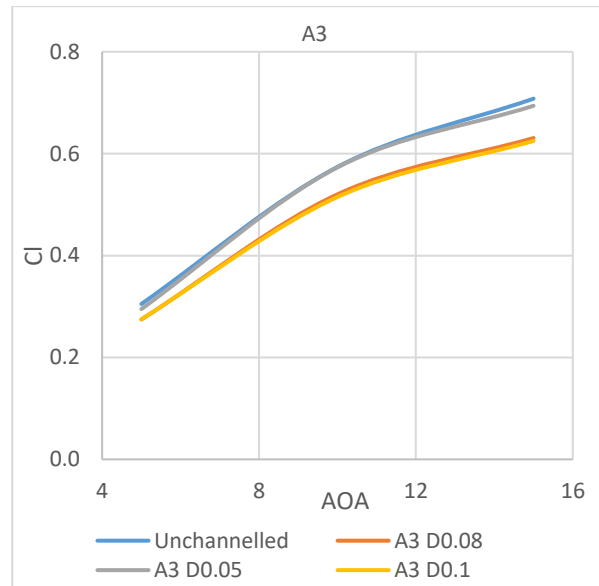
Cl vs. AOA for A0 sample for different Diameters



Cl vs. AOA for A-1 sample for different Diameters



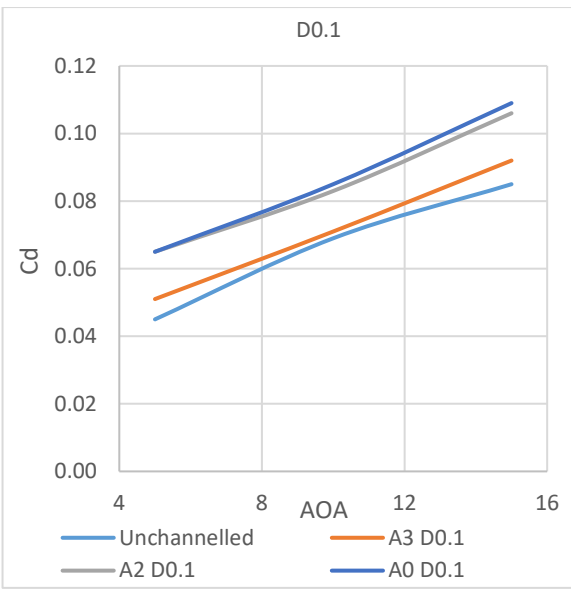
Cl vs. AOA for A2 sample for different Diameters



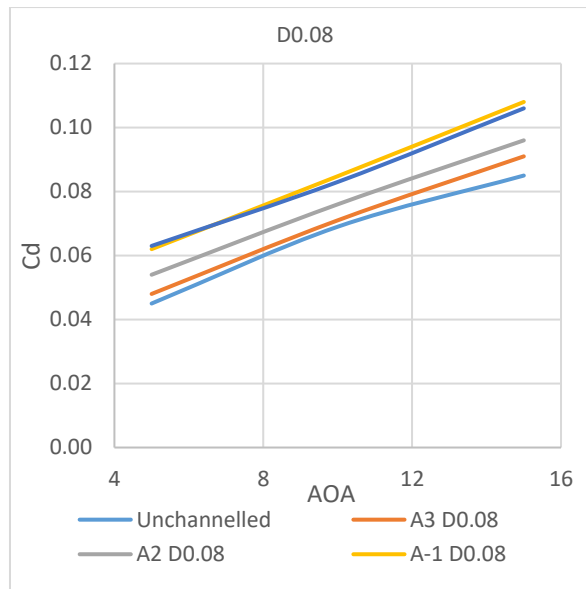
Cl vs. AOA for A3 sample for different Diameters

Drag:

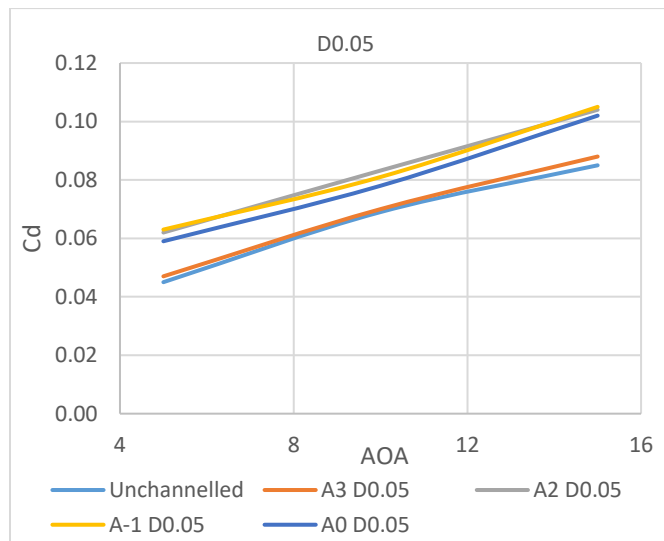
Influence of the Channel angle:



Cd vs. AOA for D0.1 sample for different angles

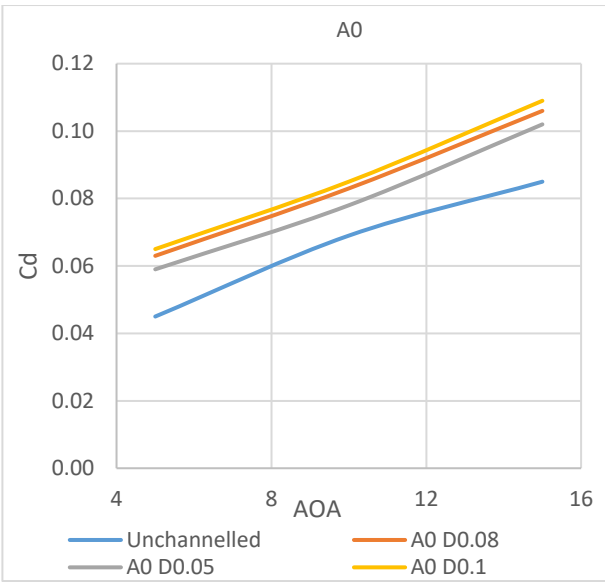


Cd vs. AOA for D0.08 sample for different angles

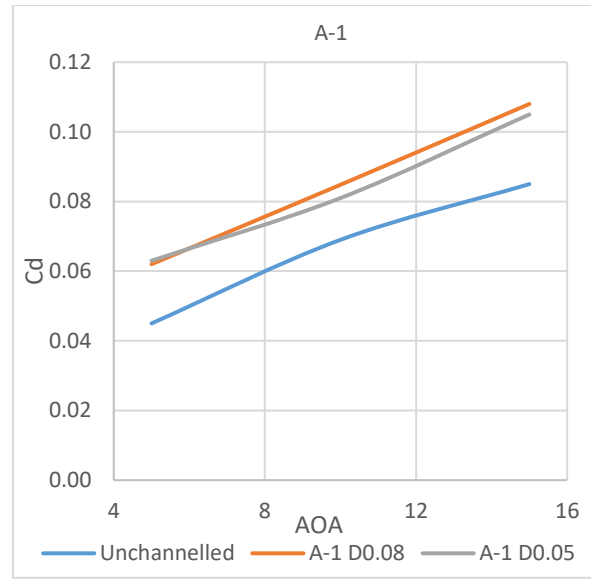


Cd vs. AOA for D0.05 sample for different angles

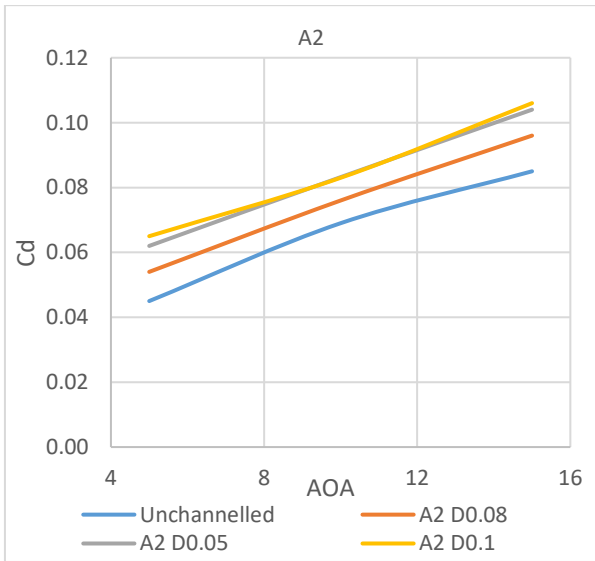
Influence of diameter size:



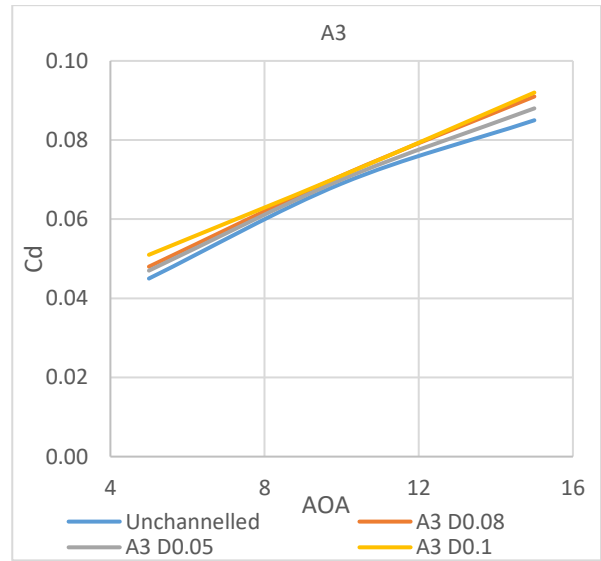
Cd vs. AOA for A0 sample for different Diameters



Cd vs. AOA for A-1 sample for different Diameters



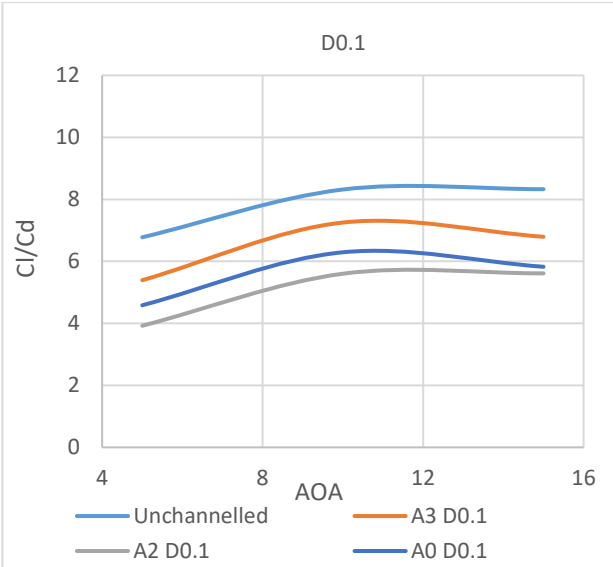
Cd vs. AOA for A2 sample for different Diameters



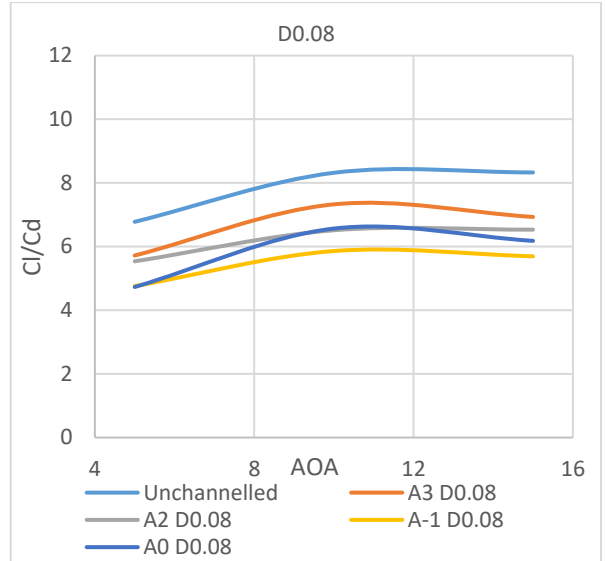
Cd vs. AOA for A3 sample for different Diameters

Drag/lift

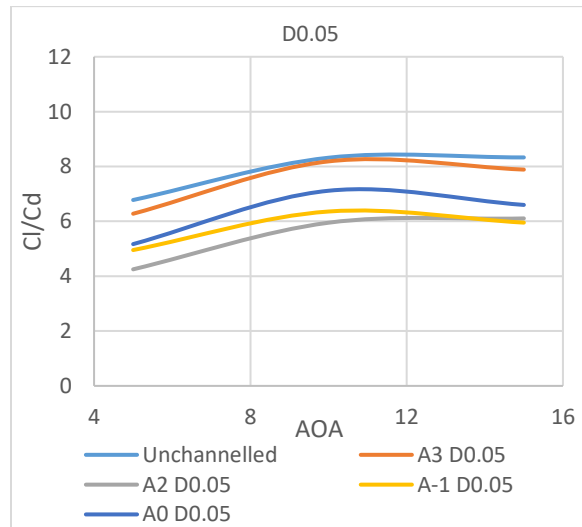
Influence of the channel angle:



Cl/Cd vs. AOA for D0.1 sample for different angles

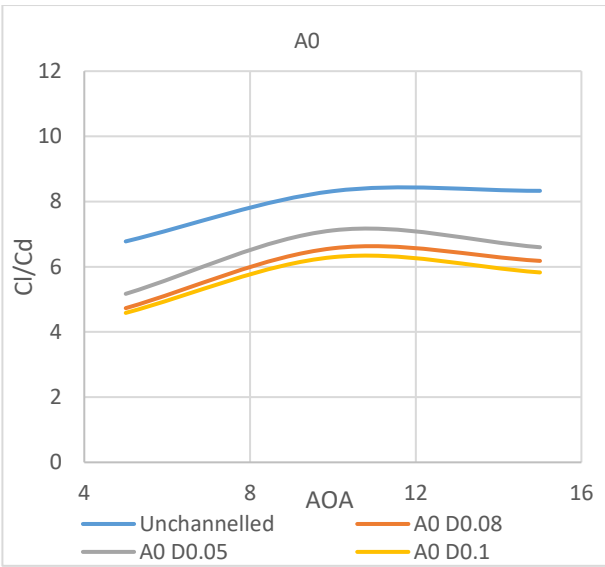


Cl/Cd vs. AOA for D0.08 sample for different angles

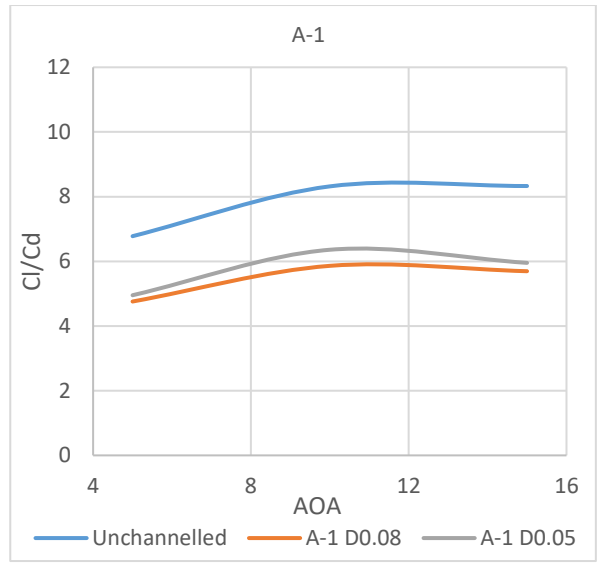


Cl/Cd vs. AOA for D0.05 sample for different angles

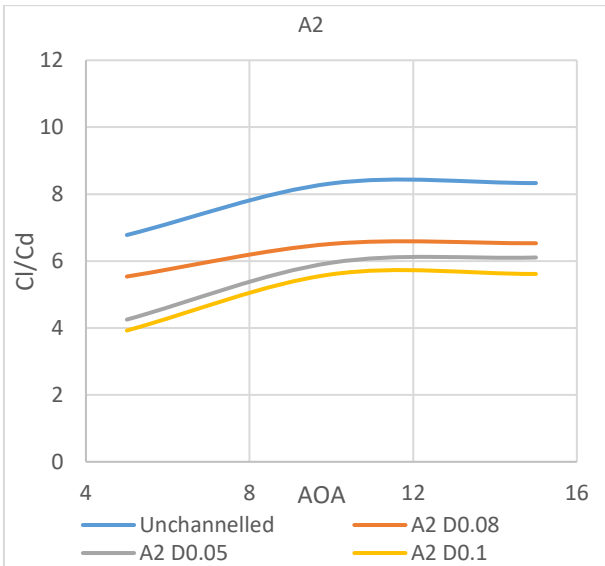
Influence of diameter size:



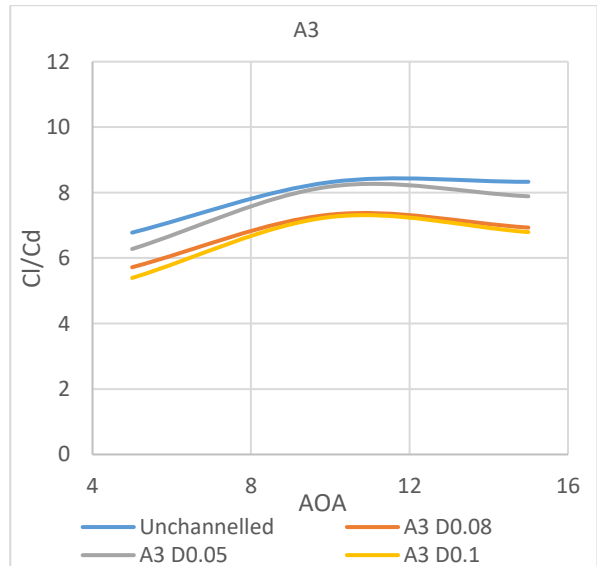
Cl/Cd vs. AOA for A0 sample for different Diameters



Cl/Cd vs. AOA for A-1 sample for different Diameters



Cl/Cd vs. AOA for A2 sample for different Diameters



Cl/Cd vs. AOA for A3 sample for different Diameters

Flow Velocity 15 m/s:

This table shows the force results for the 12 samples in flow velocity 10 m/s.

	V=15 m/s					
	Cd			Exparimental		
	aoa 5	aoa 10	aoa 15	aoa 5	aoa 10	aoa 15
Unchanneled	0.039	0.054	0.072	0.343	0.642	0.824
A3 D0.08	0.041	0.058	0.078	0.323	0.612	0.742
A3 D0.05	0.039	0.055	0.073	0.337	0.625	0.747
A3 D0.1	0.047	0.063	0.083	0.315	0.57	0.729
A2 D0.08	0.0487	0.063	0.082	0.34	0.573	0.742
A2 D0.05	0.0481	0.064	0.081	0.31	0.555	0.733
A2 D0.1	0.05	0.066	0.088	0.287	0.529	0.679
A-1 D0.08	0.056	0.0754	0.097	0.339	0.582	0.759
A-1 D0.05	0.0514	0.07	0.0874	0.312	0.545	0.73
A0 D0.08	0.0534	0.0703	0.0908	0.318	0.615	0.763
A0 D0.05	0.0493	0.069	0.0909	0.341	0.637	0.798
A0 D0.1	0.055	0.072	0.0872	0.318	0.595	0.751

The force results for the 12 samples in flow velocity 15 m/s.

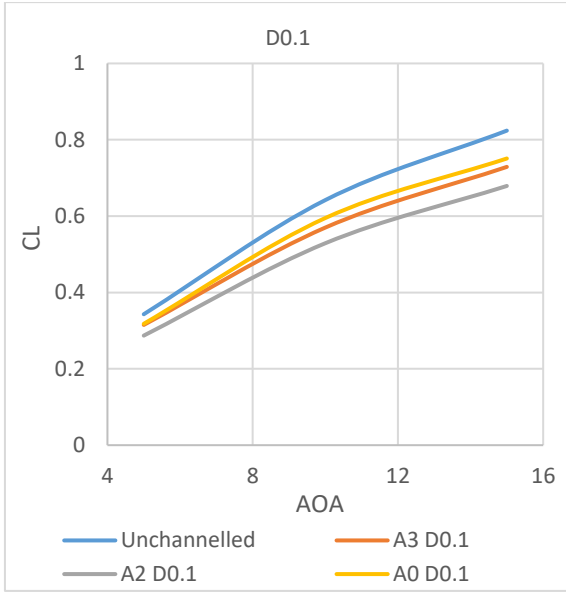
This table shows the losing percentage in drag and lift channeled airfoils comparing to regular (V=10 m/s)

	Cd			CL		
	aoa 5	aoa 10	aoa 15	aoa 5	aoa 10	aoa 15
Unchanneled						
A3 D0.08	0.05	0.07	0.08	0.06	0.05	0.10
A3 D0.05	0.00	0.02	0.01	0.02	0.03	0.09
A3 D0.1	0.21	0.17	0.15	0.08	0.11	0.12
A2 D0.08	0.25	0.17	0.14	0.01	0.11	0.10
A2 D0.05	0.23	0.19	0.13	0.10	0.14	0.11
A2 D0.1	0.28	0.22	0.22	0.16	0.18	0.18
A-1 D0.08	0.44	0.40	0.35	0.01	0.09	0.08
A-1 D0.05	0.32	0.30	0.21	0.09	0.15	0.11
A0 D0.08	0.37	0.30	0.26	0.07	0.04	0.07
A0 D0.05	0.26	0.28	0.26	0.01	0.01	0.03
A0 D0.1	0.41	0.33	0.21	0.07	0.07	0.09

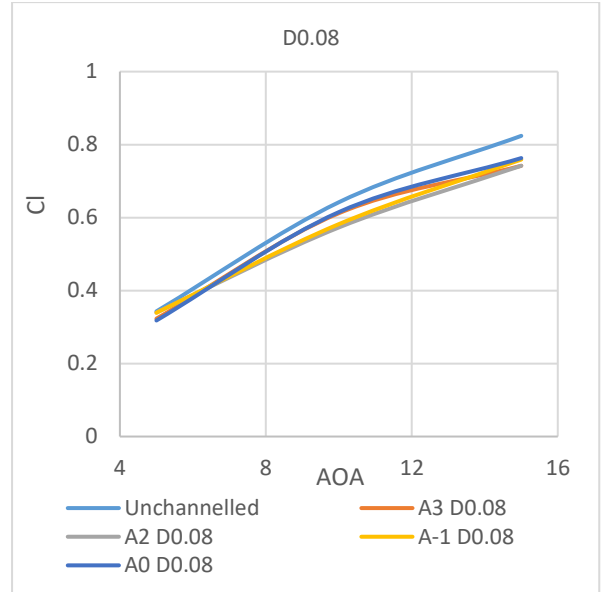
Losing percentage in drag and lift channeled airfoils comparing to regular (V=15m/s)

Lift:

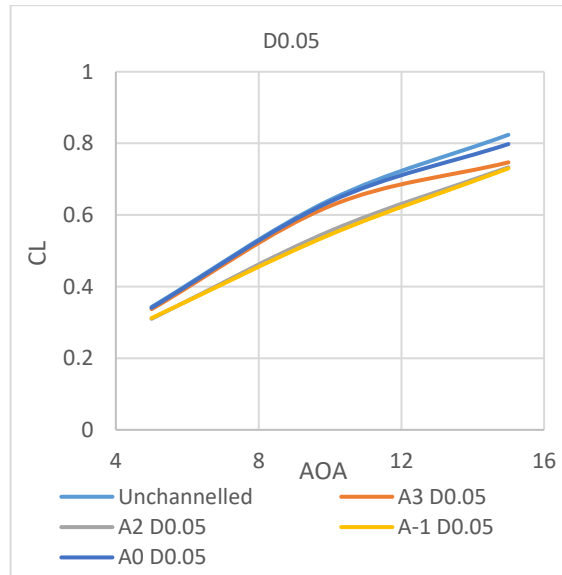
Influence of the channel angle:



Cl vs. AOA for D0.1 sample for different angles

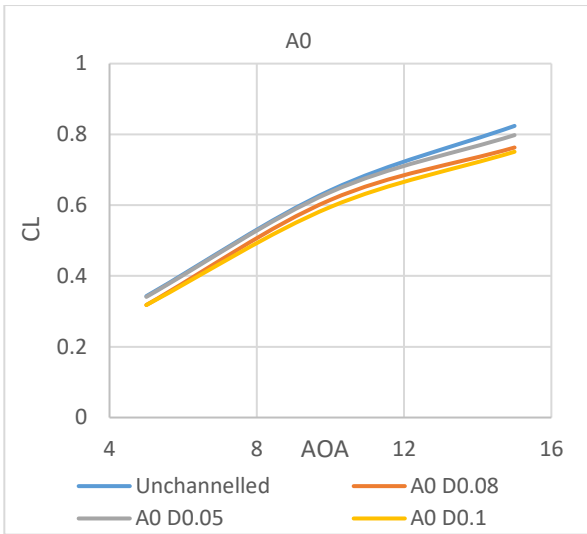


Cl vs. AOA for D0.08 sample for different angles

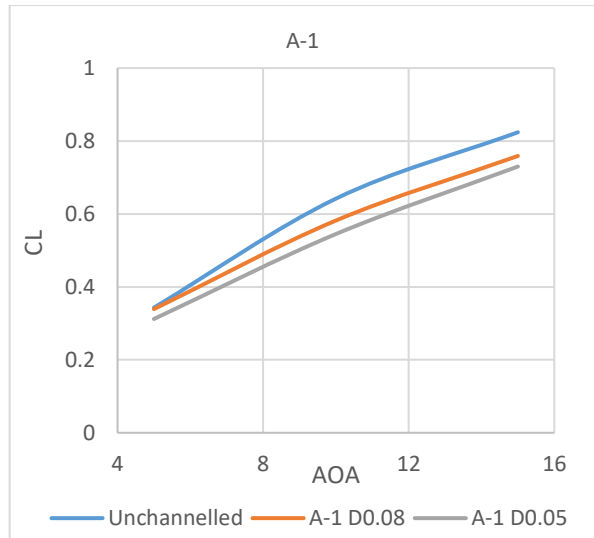


Cl vs. AOA for D0.05 sample for different angles

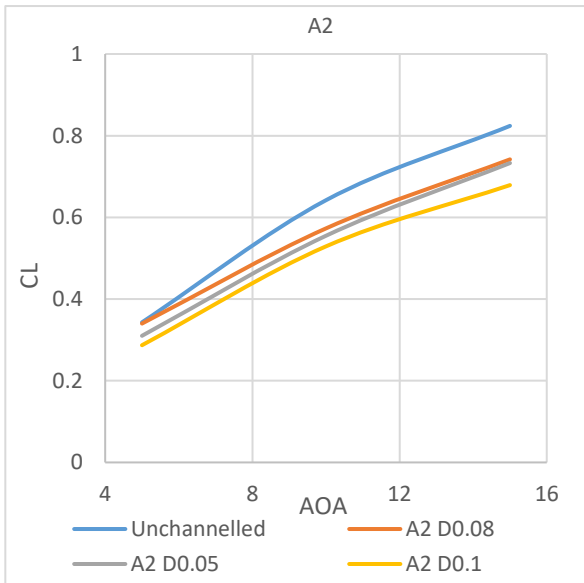
Influence of diameter size:



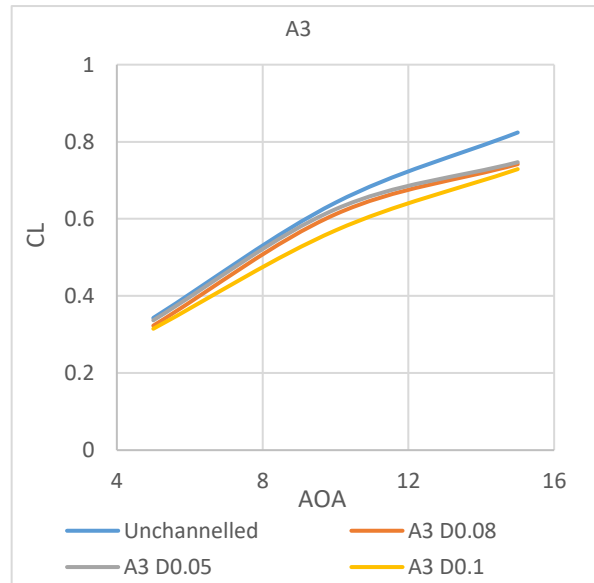
Cl vs. AOA for A0 sample for different Diameters



Cl vs. AOA for A-1 sample for different Diameters



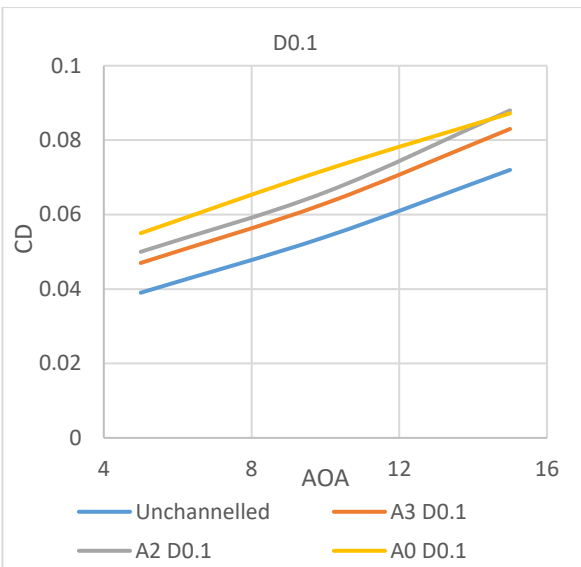
Cl vs. AOA for A2 sample for different Diameters



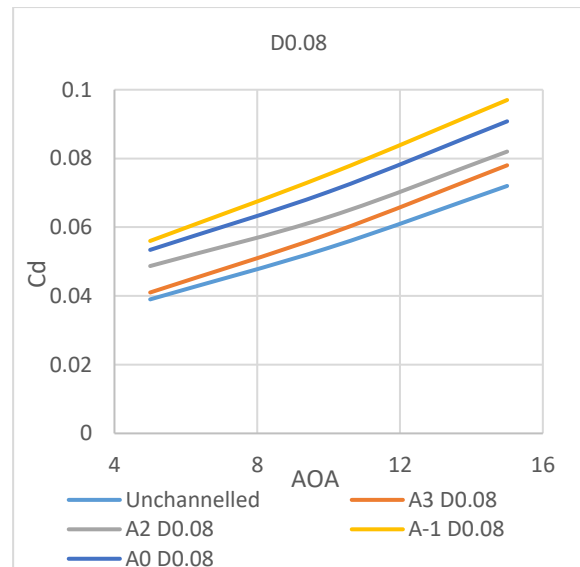
Cl vs. AOA for A3 sample for different Diameters.

Drag:

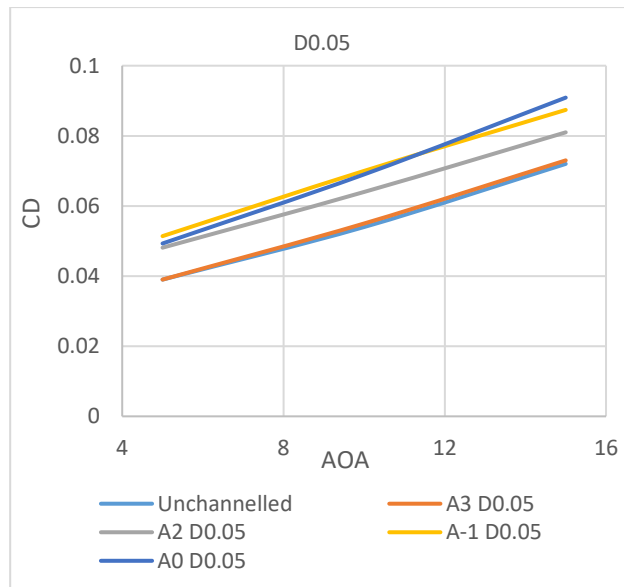
Influence of the Channel angle:



Cd vs. AOA for D0.1 sample for different angles

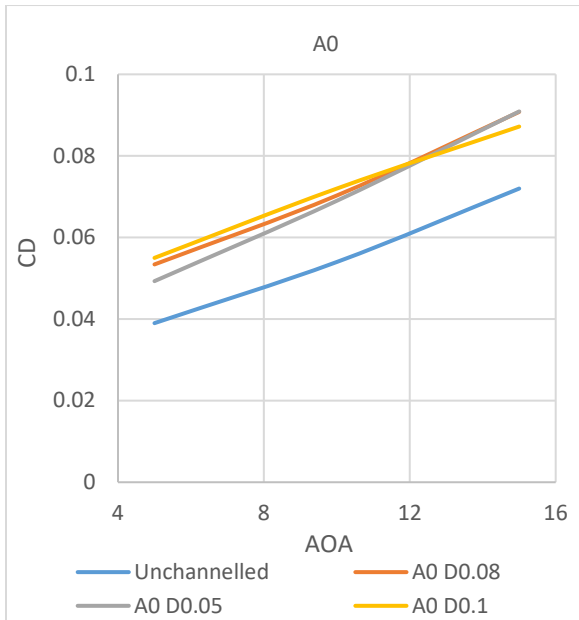


Cd vs. AOA for D0.08 sample for different angles

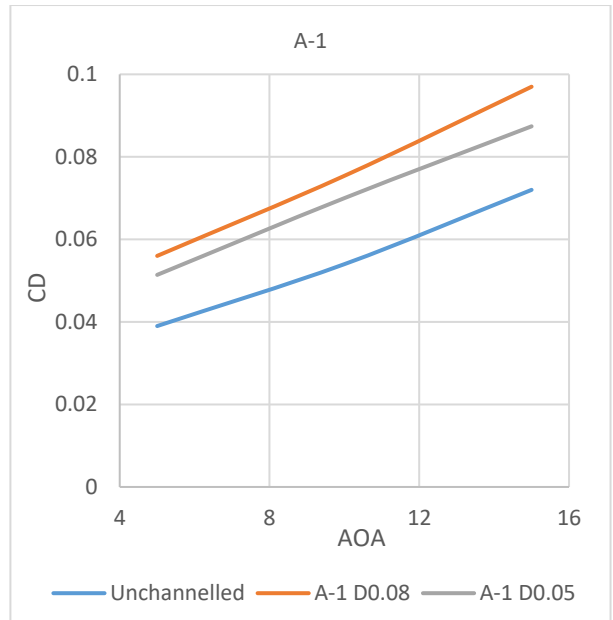


Cd vs. AOA for D0.05 sample for different angles

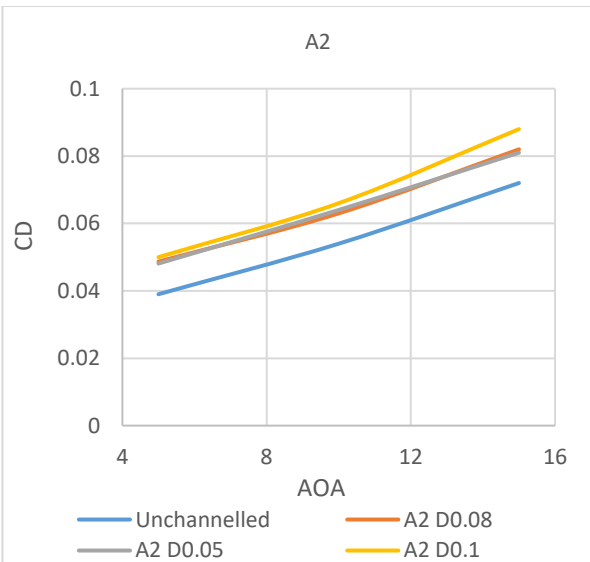
Influence of diameter size:



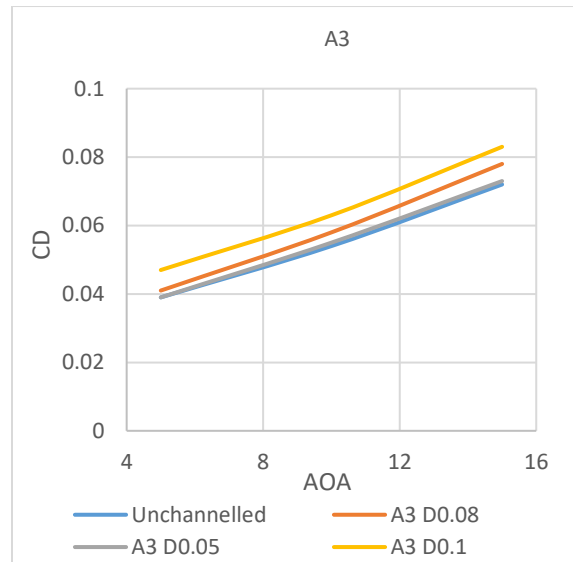
Cd vs. AOA for A0 sample for different Diameters



Cd vs. AOA for A-1 sample for different Diameters



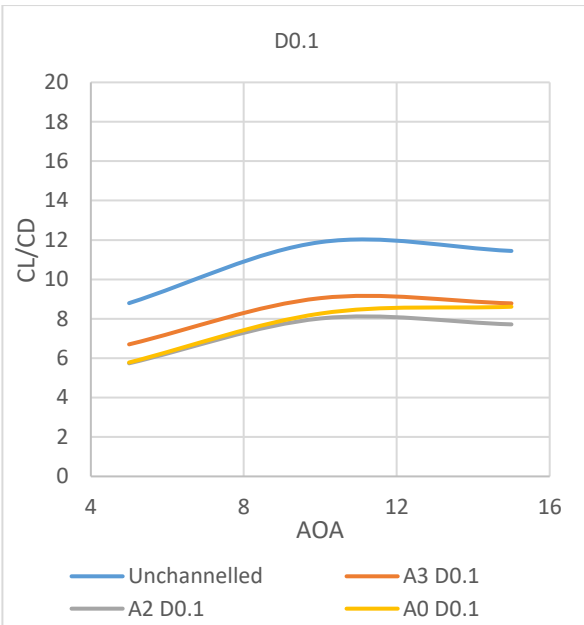
Cd vs. AOA for A2 sample for different Diameters



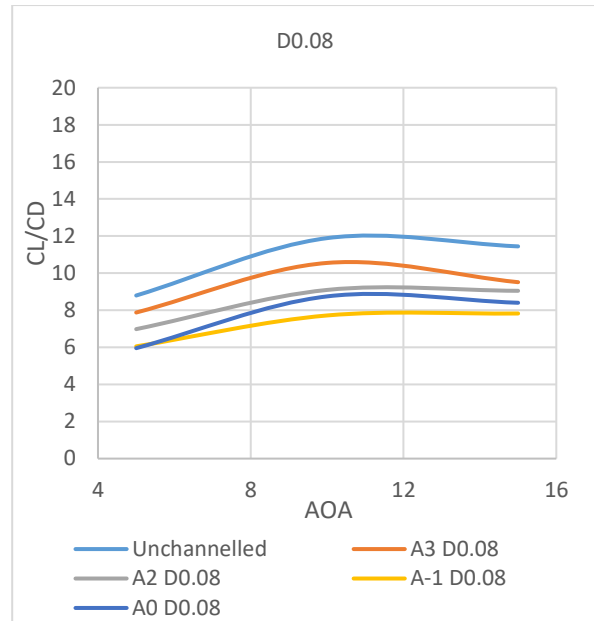
Cd vs. AOA for A3 sample for different Diameters

Drag/Lift

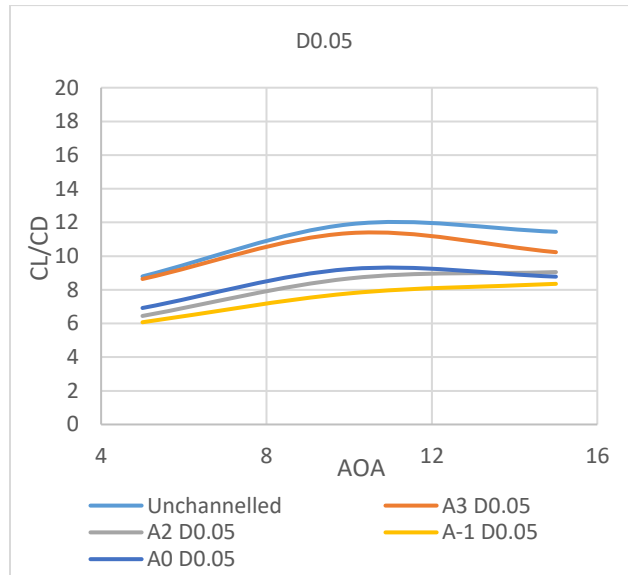
Influence of the Channel angle:



CL/Cd vs. AOA for D0.1 sample for different angles

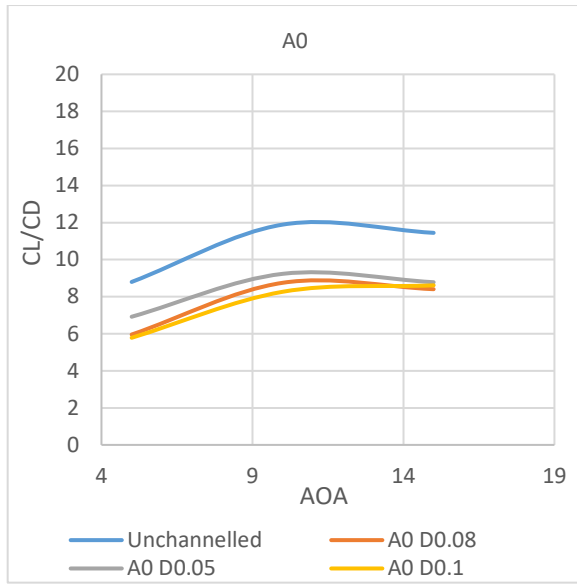


CL/Cd vs. AOA for D0.08 sample for different angles

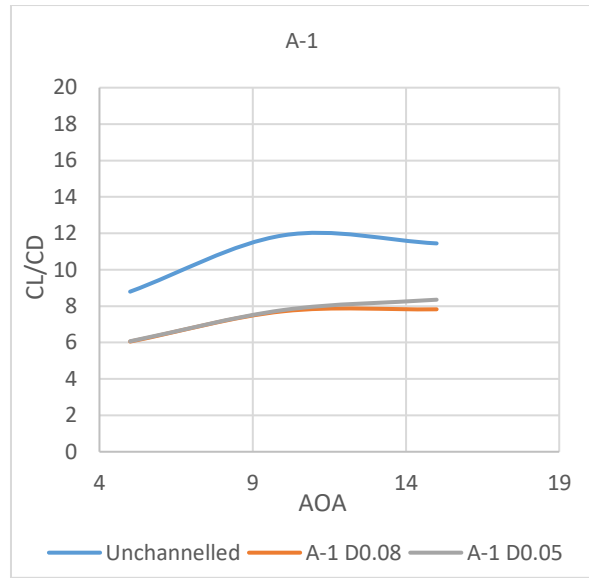


CL/Cd vs. AOA for D0.05 sample for different angles

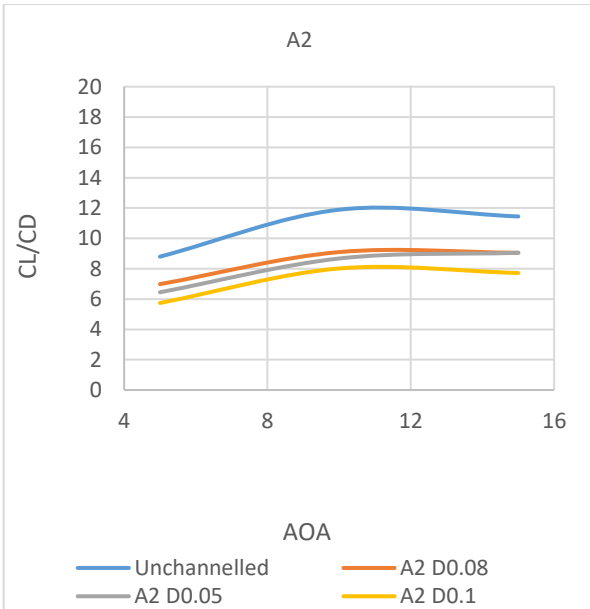
Influence of diameter size:



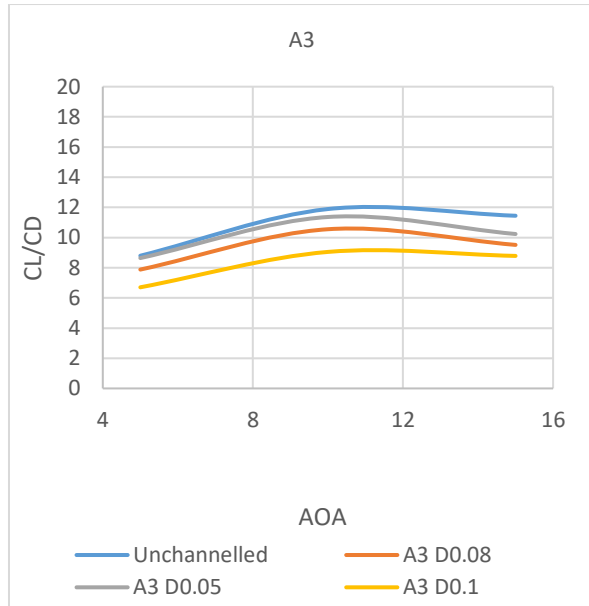
Cl/Cd vs. AOA for A0 sample for different Diameters



Cl/Cd vs. AOA for A-1 sample for different Diameters



Cl/Cd vs. AOA for A2 sample for different Diameters



Cl/Cd vs. AOA for A3 sample for different Diameters

C: Turbulence results:

This appendix contain the turbulence intensity for all samples in different levels as explained in turbulence section in the chapter four. The data was recorded in eight different levels, these levels are:

1- Level Z-2

	Unch.	A0 D0.1	A0 D0.08	A0 D0.05	A-1 D0.08	A-1 D0.05	A2 D0.1	A2 D0.08	A2 D0.05	A3 D0.1	A3 D0.08	A3 D0.05
0	1.19	1.91	1.46	1.52	1.75	1.32	1.58	1.48	1.25	1.08	1.51	1.67
5	1.19	1.97	1.57	1.49	1.74	1.29	1.63	1.58	1.28	1.14	1.62	1.79
10	1.19	1.97	1.59	1.52	1.83	1.35	1.55	1.53	1.32	1.28	1.71	1.79
15	1.21	1.92	1.57	1.67	1.88	1.32	1.57	1.48	1.23	1.22	1.89	2.02
20	1.30	1.65	1.51	1.51	1.66	1.35	1.46	1.50	1.20	1.20	1.94	2.12
25	1.33	1.63	1.31	1.35	1.46	1.30	1.42	1.52	1.10	1.21	1.97	2.06
30	1.36	1.58	1.23	1.24	1.53	1.25	1.40	1.36	1.12	1.21	1.77	1.91
35	1.31	1.41	1.27	1.24	1.42	1.19	1.31	1.34	1.12	1.19	1.73	1.79
40	1.44	1.37	1.21	1.23	1.36	1.15	1.25	1.31	1.15	1.14	1.80	1.72
45	1.37	1.39	1.12	1.23	1.31	1.13	1.30	1.27	1.11	1.11	1.69	1.75
50	1.33	1.29	1.20	1.18	1.31	1.15	1.14	1.25	1.08	1.05	1.64	1.72

2- Level Z-1

	Unch.	A0 D0.1	A0 D0.08	A0 D0.05	A-1 D0.08	A-1 D0.05	A2 D0.1	A2 D0.08	A2 D0.05	A3 D0.1	A3 D0.08	A3 D0.05
0	1.20	1.58	1.62	1.72	1.56	1.29	1.59	1.40	1.26	1.17	1.03	1.12
5	1.19	1.65	1.77	1.79	1.65	1.39	1.65	1.55	1.27	1.18	1.03	1.05
10	1.19	1.77	1.77	1.94	1.86	1.43	1.84	1.65	1.31	1.35	1.03	1.04
15	1.18	1.95	2.08	2.07	2.03	1.56	2.03	1.71	1.41	1.52	1.08	1.42
20	1.21	2.02	2.14	2.10	2.28	1.73	2.02	1.94	1.58	1.66	1.54	1.61
25	1.22	2.23	2.14	2.10	2.49	1.84	2.02	1.90	1.63	1.86	1.58	1.54
30	1.25	2.43	1.94	2.14	2.37	1.97	2.10	2.17	1.69	1.85	1.82	1.60
35	1.35	2.49	2.00	1.92	2.45	1.89	1.90	2.03	1.69	1.84	1.85	1.84
40	1.47	2.39	1.74	1.84	2.32	1.84	1.87	1.95	1.46	1.65	2.03	1.90
45	1.62	2.32	1.81	1.74	2.19	1.69	1.96	1.97	1.48	1.38	2.19	2.07
50	1.46	2.27	1.81	1.81	2.07	1.61	1.79	1.90	1.88	1.30	2.04	2.36

3- Level Z=0

	Unch.	A0 D0.1	A0 D0.08	A0 D0.05	A-1 D0.08	A-1 D0.05	A2 D0.1	A2 D0.08	A2 D0.05	A3 D0.1	A3 D0.08	A3 D0.05
0	1.12	1.76	1.29	1.41	1.28	1.14	1.34	1.19	1.13	0.95	1.28	1.24
5	1.14	1.62	1.23	1.40	1.33	1.18	1.39	1.26	1.14	1.00	1.32	1.23
10	1.16	1.71	1.24	1.44	1.35	1.23	1.41	1.30	1.15	1.02	1.37	1.31
15	1.28	1.75	1.30	1.57	1.33	1.29	1.61	1.41	1.15	1.02	1.45	1.37
20	1.29	1.81	1.31	1.67	1.35	1.35	1.72	1.49	1.17	1.10	1.60	1.44
25	1.41	1.99	1.46	1.89	1.54	1.68	1.86	1.61	1.31	1.17	1.80	1.61
30	1.74	2.25	1.61	2.58	1.68	2.10	2.04	1.87	1.45	1.26	2.05	1.76
35	2.56	2.71	2.51	2.92	2.21	2.78	2.31	2.20	1.83	1.58	2.29	1.94
40	3.55	3.65	3.71	4.11	3.85	3.86	3.04	2.93	3.81	2.04	2.60	2.50

4- Level Z+1

	Unch.	A0 D0.1	A0 D0.08	A0 D0.05	A-1 D0.08	A-1 D0.05	A2 D0.1	A2 D0.08	A2 D0.05	A3 D0.1	A3 D0.08	A3 D0.05
0	1.02	1.17	1.17	1.24	1.25	1.12	1.09	1.10	1.11	0.97	0.98	1.04
5	1.02	1.24	1.15	1.21	1.22	1.13	1.09	1.09	1.09	0.97	1.01	1.05
10	1.01	1.20	1.14	1.22	1.18	1.11	1.09	1.13	1.08	0.97	1.01	1.02
15	1.01	1.15	1.21	1.17	1.18	1.08	1.10	1.09	1.10	0.98	1.06	1.01
20	1.01	1.18	1.12	1.23	1.17	1.16	1.14	1.09	1.09	0.96	1.05	1.10
25	1.01	1.16	1.16	1.22	1.18	1.16	1.08	1.10	1.10	0.96	1.06	1.05
30	1.02	1.14	1.13	1.21	1.17	1.10	1.13	1.12	1.10	0.95	1.13	1.09
35	1.06	1.13	1.16	1.18	1.14	1.10	1.13	1.10	1.10	0.94	1.11	1.10
40	1.09	1.15	1.13	1.20	1.14	1.15	1.12	1.10	1.08	0.96	1.20	1.11
45	1.11	1.13	1.17	1.16	1.23	1.13	1.09	1.14	1.13	0.93	1.16	1.19
50	1.14	1.20	1.15	1.18	1.27	1.12	1.15	1.22	1.15	0.93	1.29	1.23
55	1.17	1.38	1.25	1.28	0.98	1.14	1.18	1.21	1.23	0.96	1.48	1.28
60	1.17	1.37	1.15	1.44	1.00	1.15	1.29	1.25	1.43	1.00	1.62	1.38

5- Level Z+2

	Unch.	A0 D0.1	A0 D0.08	A0 D0.05	A-1 D0.08	A-1 D0.05	A2 D0.1	A2 D0.08	A2 D0.05	A3 D0.1	A3 D0.08	A3 D0.05
0	1.06	1.18	1.20	1.26	1.20	1.18	1.09	1.10	1.13	1.01	0.96	0.99
5	1.06	1.18	1.15	1.24	1.18	1.15	1.08	1.08	1.07	1.02	0.96	1.00
10	1.06	1.15	1.15	1.23	1.15	1.16	1.08	1.08	1.08	1.03	0.96	0.98
15	1.05	1.15	1.12	1.23	1.15	1.16	1.05	1.06	1.09	1.01	0.96	0.98
20	1.05	1.17	1.14	1.18	1.12	1.14	1.05	1.10	1.08	1.02	0.95	0.98
25	1.05	1.14	1.13	1.15	1.17	1.14	1.06	1.10	1.05	1.01	0.96	0.97
30	1.05	1.13	1.10	1.18	1.12	1.18	1.07	1.07	1.10	1.02	0.99	0.99
35	1.05	1.12	1.09	1.21	1.12	1.11	1.07	1.08	1.07	1.03	0.97	0.97
40	1.05	1.09	1.10	1.16	1.12	1.12	1.05	1.08	1.09	1.02	0.95	0.99
45	1.04	1.09	1.11	1.14	1.14	1.10	1.06	1.06	1.09	1.03	0.97	0.98
50	1.06	1.08	1.08	1.10	1.11	1.11	1.07	1.07	1.06	1.02	0.97	0.96
55	1.04	1.09	1.10	1.14	1.09	1.09	1.06	1.07	1.08	1.03	1.00	1.00
60	1.05	1.09	1.12	1.11	1.12	1.09	1.09	1.11	1.05	1.00	1.01	1.00
65	1.04	1.10	1.12	1.13	1.13	1.09	1.07	1.10	1.07	1.00	1.08	1.00
70	1.05	1.09	1.13	1.10	1.17	1.10	1.08	1.13	1.05	0.99	1.13	1.02
75	1.06	1.11	1.20	1.13	1.25	1.09	1.11	1.33	1.09	0.94	1.42	1.07
80	1.08	1.18	1.41	1.18	1.52	1.08	1.25	1.83	1.10	0.94	1.84	1.15

6- Level Z+3

	Unch.	A0 D0.1	A0 D0.08	A0 D0.05	A-1 D0.08	A-1 D0.05	A2 D0.1	A2 D0.08	A2 D0.05	A3 D0.1	A3 D0.08	A3 D0.05
0	1.10	1.13	1.16	1.28	1.15	1.15	1.05	1.05	1.09	1.08	0.95	0.99
5	1.11	1.15	1.18	1.25	1.16	1.16	1.05	1.06	1.09	1.07	0.96	0.99
10	1.11	1.14	1.17	1.21	1.15	1.19	1.08	1.09	1.10	1.07	0.95	0.95
15	1.11	1.13	1.11	1.20	1.14	1.14	1.07	1.07	1.06	1.05	0.95	0.97
20	1.11	1.13	1.12	1.17	1.13	1.14	1.07	1.10	1.09	1.07	0.96	0.97
25	1.11	1.13	1.11	1.16	1.13	1.12	1.06	1.06	1.11	1.05	0.95	0.97
30	1.11	1.11	1.10	1.13	1.12	1.11	1.06	1.08	1.07	1.03	0.96	0.98
35	1.10	1.12	1.10	1.12	1.08	1.11	1.05	1.08	1.08	1.07	0.94	0.95
40	1.10	1.09	1.08	1.13	1.10	1.11	1.07	1.06	1.06	0.95	0.97	0.98
45	1.10	1.07	1.10	1.10	1.11	1.13	1.06	1.07	1.08	0.95	0.94	0.96
50	1.10	1.10	1.12	1.13	1.09	1.10	1.06	1.08	1.06	0.95	0.94	0.98
55	1.11	1.10	1.10	1.11	1.09	1.13	1.07	1.07	1.05	0.96	0.93	0.97
60	1.11	1.10	1.09	1.09	1.11	1.12	1.05	1.09	1.06	0.95	0.95	0.98
65	1.11	1.10	1.10	1.14	1.10	1.11	1.07	1.07	1.11	0.95	0.94	0.97
70	1.11	1.09	1.11	1.10	1.10	1.12	1.04	1.06	1.04	0.95	0.96	0.96
75	1.10	1.10	1.11	1.12	1.10	1.09	1.09	1.08	1.04	0.94	0.96	0.97
80	1.10	1.08	1.09	1.09	1.10	1.09	1.06	1.06	1.08	0.93	0.98	0.99
85	1.11	1.08	1.08	1.12	1.12	1.09	1.05	1.07	1.06	0.93	1.06	0.98
90	1.12	1.09	1.08	1.11	1.12	1.09	1.07	1.08	1.07	0.93	1.09	0.98
95	1.11	1.09	1.08	1.14	1.09	1.10	1.07	1.08	1.08	0.94	1.44	0.99
100	1.14	1.09	1.10	1.16	1.10	1.06	1.06	1.10	1.06	0.97	1.76	1.11
105	1.17	1.10	1.30	1.20	1.09	1.09	1.06	1.08	1.08	1.02	1.48	1.28
110	1.17	1.30	1.44	1.19	1.11	1.10	1.08	1.14	1.08	1.23	1.55	1.41

7- Level Z+4

	Unch.	A0 D0.1	A0 D0.08	A0 D0.05	A-1 D0.08	A-1 D0.05	A2 D0.1	A2 D0.08	A2 D0.05	A3 D0.1	A3 D0.08	A3 D0.05
0	1.05	1.15	1.15	1.18	1.17	1.14	1.07	1.10	1.10	1.04	1.07	1.11
5	1.04	1.14	1.15	1.17	1.20	1.14	1.08	1.08	1.09	1.05	1.09	1.07
10	1.06	1.15	1.14	1.19	1.18	1.13	1.06	1.08	1.08	1.05	1.11	1.10
15	1.05	1.11	1.11	1.15	1.18	1.14	1.07	1.08	1.06	1.05	1.08	1.10
20	1.05	1.11	1.13	1.15	1.18	1.14	1.06	1.07	1.08	1.04	1.08	1.04
25	1.05	1.11	1.13	1.12	1.17	1.09	1.08	1.05	1.06	0.91	1.09	1.11
30	1.05	1.12	1.11	1.13	1.12	1.11	1.07	1.07	1.06	0.93	1.10	1.09
35	1.05	1.11	1.09	1.14	1.14	1.12	1.05	1.08	1.05	0.93	1.05	1.04
40	1.04	1.12	1.11	1.12	1.12	1.11	1.07	1.08	1.06	0.93	0.96	0.96
45	1.05	1.10	1.08	1.14	1.17	1.11	1.05	1.10	1.05	0.93	0.96	0.96
50	1.04	1.10	1.09	1.12	1.15	1.10	1.06	1.05	1.05	0.92	0.96	0.98
55	1.05	1.09	1.09	1.12	1.15	1.11	1.06	1.09	1.07	0.92	0.95	0.97
60	1.05	1.09	1.10	1.11	1.11	1.11	1.04	1.06	1.06	0.94	0.97	0.97
65	1.05	1.10	1.07	1.13	1.14	1.09	1.06	1.08	1.05	0.92	0.96	0.97
70	1.05	1.09	1.10	1.10	1.14	1.07	1.05	1.06	1.07	0.94	0.97	0.97
75	1.05	1.10	1.10	1.10	1.15	1.08	1.07	1.07	1.05	0.92	0.97	0.97
80	1.05	1.10	1.09	1.13	1.13	1.10	1.07	1.07	1.06	0.93	0.95	0.96
85	1.05	1.10	1.10	1.10	1.13	1.10	1.06	1.09	1.07	0.92	0.94	0.97
90	1.05	1.10	1.10	1.12	1.12	1.06	1.07	1.07	1.07	0.92	0.95	0.97
95	1.05	1.10	1.09	1.10	1.13	1.10	1.04	1.06	1.06	0.92	0.96	0.98
100	1.06	1.08	1.08	1.11	1.12	1.10	1.06	1.07	1.04	0.93	0.94	0.97
105	1.05	1.09	1.09	1.12	1.14	1.08	1.06	1.07	1.06	0.94	0.96	0.97
110	1.06	1.12	1.11	1.10	1.13	1.10	1.06	1.06	1.05	0.93	0.93	0.96
115	1.08	1.10	1.09	1.12	1.13	1.08	1.05	1.06	1.06	0.91	0.96	0.97
120	1.06	1.09	1.11	1.10	1.13	1.08	1.08	1.07	1.08	0.93	0.94	0.97
125	1.08	1.09	1.10	1.09	1.12	1.10	1.06	1.06	1.06	0.91	0.95	0.97
130	1.14	1.11	1.08	1.11	1.12	1.08	1.07	1.09	1.08	0.92	0.95	0.96
135	1.15	1.10	1.09	1.11	1.12	1.09	1.07	1.07	1.09	0.92	0.93	0.96
140	1.19	1.08	1.10	1.10	1.13	1.09	1.07	1.06	1.06	0.90	0.95	0.97
145	1.19	1.09	1.08	1.11	1.05	1.09	1.06	1.07	1.06	0.92	0.94	0.96
150	1.18	1.11	1.11	1.06	1.06	1.09	1.05	1.08	1.06	0.93	0.94	0.96
155	1.18	1.10	1.11	1.10	1.09	1.10	1.05	1.05	1.05	1.00	0.92	0.95
160	1.19	1.10	1.14	1.12	1.08	1.10	1.05	1.07	1.06	1.16	0.94	0.94
165	1.18	1.09	1.10	1.11	1.06	1.12	1.05	1.05	1.05	1.34	1.11	0.96
170	1.27	1.08	1.09	1.10	1.10	1.11	1.04	1.06	1.08	1.73	1.15	0.96

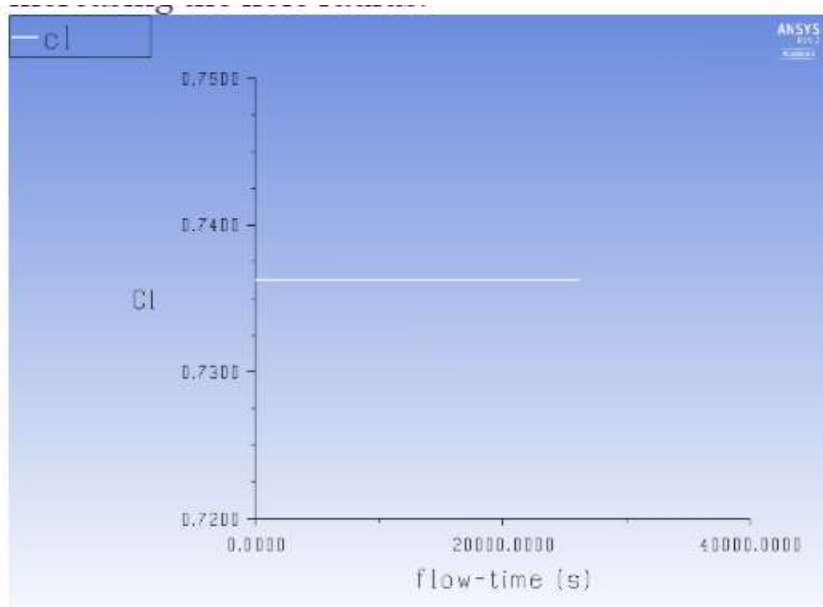
8- Level Z+5

	Unch.	A0 D0.1	A0 D0.08	A0 D0.05	A-1 D0.08	A-1 D0.05	A2 D0.1	A2 D0.08	A2 D0.05	A3 D0.1	A3 D0.08	A3 D0.05
0	1.04	1.11	1.16	1.17	1.17	1.16	1.06	1.06	1.08	0.95	0.95	0.97
5	1.05	1.09	1.13	1.21	1.12	1.16	1.07	1.08	1.06	0.94	0.95	0.99
10	1.05	1.10	1.16	1.22	1.15	1.16	1.07	1.05	1.05	0.94	0.95	0.96
15	1.05	1.09	1.15	1.16	1.16	1.11	1.07	1.08	1.09	0.94	0.96	0.97
20	1.04	1.09	1.12	1.17	1.14	1.12	1.05	1.03	1.12	0.94	0.95	0.97
25	1.05	1.09	1.11	1.14	1.13	1.12	1.07	1.07	1.05	0.94	0.95	0.96
30	1.05	1.09	1.10	1.14	1.12	1.11	1.03	1.10	1.08	0.93	0.97	0.98
35	1.05	1.07	1.09	1.13	1.14	1.12	1.06	1.06	1.08	0.94	0.95	0.96
40	1.04	1.09	1.09	1.11	1.16	1.10	1.07	1.07	1.06	0.94	0.95	0.97
45	1.04	1.09	1.09	1.14	1.13	1.13	1.05	1.07	1.08	0.93	0.96	0.96
50	1.04	1.08	1.09	1.12	1.14	1.09	1.06	1.05	1.05	0.92	0.95	0.97
55	1.04	1.07	1.11	1.11	1.11	1.11	1.04	1.08	1.06	0.92	0.96	0.98
60	1.05	1.08	1.08	1.09	1.12	1.10	1.06	1.06	1.05	0.93	0.96	0.97
65	1.04	1.06	1.10	1.11	1.12	1.10	1.05	1.07	1.06	0.93	0.94	0.97
70	1.04	1.10	1.09	1.10	1.12	1.09	1.06	1.07	1.08	0.94	0.95	0.96
75	1.04	1.08	1.09	1.10	1.10	1.09	1.05	1.06	1.05	0.94	0.94	0.96
80	1.05	1.09	1.08	1.11	1.11	1.11	1.06	1.06	1.07	0.93	0.95	0.96
85	1.05	1.10	1.09	1.12	1.13	1.09	1.06	1.21	1.04	0.94	0.95	0.96
90	1.06	1.10	1.11	1.14	1.11	1.11	1.05	1.04	1.03	0.94	0.94	0.96
95	1.05	1.09	1.10	1.12	1.12	1.11	1.05	1.06	1.05	0.94	0.93	0.96
100	1.06	1.09	1.10	1.10	1.12	1.12	1.07	1.08	1.08	0.94	0.94	0.95
105	1.06	1.08	1.10	1.12	1.11	1.10	1.07	1.09	1.07	0.92	0.96	0.95
110	1.06	1.10	1.10	1.11	1.14	1.11	1.06	1.07	1.09	0.93	0.96	0.95
115	1.06	1.11	1.10	1.11	1.10	1.11	1.06	1.06	1.06	0.93	0.95	0.96
120	1.05	1.10	1.11	1.09	1.11	1.11	1.05	1.08	1.06	0.93	0.94	0.96
125	1.07	1.08	1.08	1.10	1.12	1.10	1.06	1.10	1.05	0.92	0.94	0.95
130	1.06	1.08	1.09	1.10	1.12	1.10	1.06	1.05	1.07	0.94	0.93	0.96
135	1.07	1.07	1.12	1.10	1.12	1.10	1.05	1.06	1.07	0.92	0.94	0.96
140	1.07	1.09	1.09	1.10	1.12	1.12	1.07	1.05	1.06	0.92	0.95	0.96
145	1.08	1.10	1.12	1.12	1.11	1.11	1.04	1.06	1.06	0.91	0.94	0.96
150	1.09	1.09	1.12	1.10	1.12	1.09	1.05	1.05	1.05	0.92	0.93	0.95
155	1.10	1.09	1.12	1.11	1.11	1.10	1.05	1.07	1.06	0.93	0.93	0.96
160	1.15	1.10	1.09	1.09	1.11	1.09	1.05	1.05	1.07	1.01	0.94	0.93
165	1.09	1.10	1.07	1.09	1.12	1.10	1.05	1.07	1.05	0.95	0.92	0.94
170	1.07	1.09	1.10	1.12	1.11	1.12	1.04	1.03	1.06	1.13	0.96	0.96
175	1.05	1.10	1.10	1.10	1.08	1.10	1.04	1.04	1.06	0.98	0.93	0.95
180	1.08	1.09	1.09	1.09	1.12	1.10	1.08	1.05	1.07	0.98	0.95	0.97
185	1.08	1.08	1.09	1.11	1.11	1.11	1.05	1.05	1.06	0.98	0.97	0.96
190	1.13	1.09	1.10	1.09	1.11	1.10	1.04	1.05	1.04	0.97	0.98	0.97

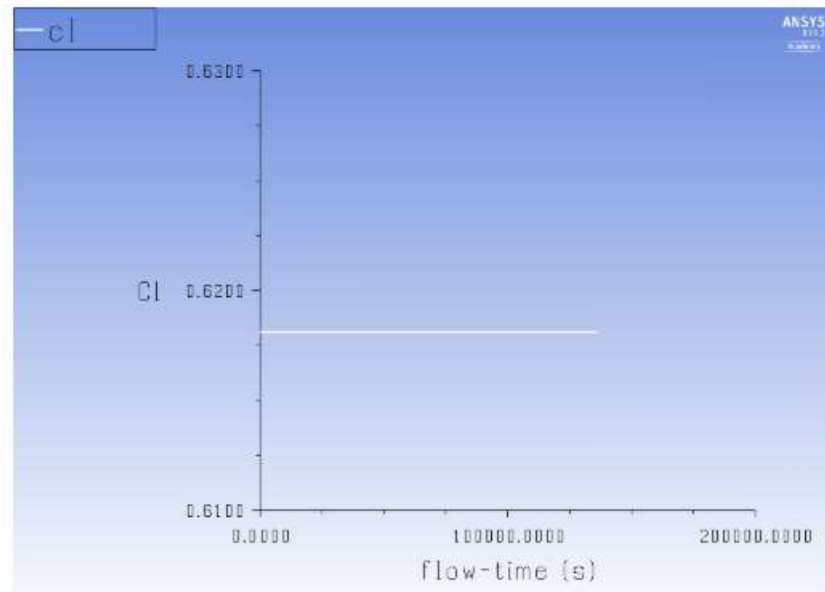
D: Numerical results

These figures show the force results for four samples (unchanneled, A3D0.05, A3D0.08, and A3D0.1) in order. For each case Cl and Cd converged results:

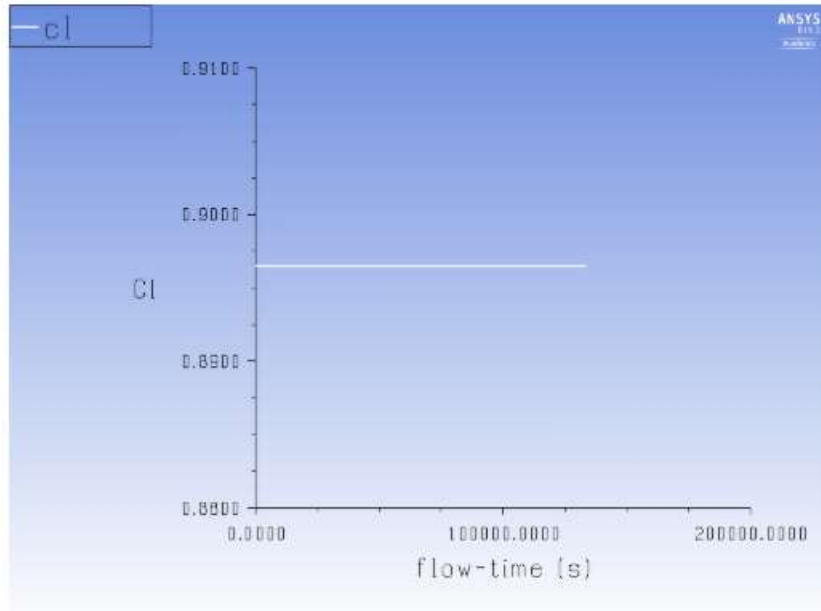
Converged Cl for unchanneled sample:



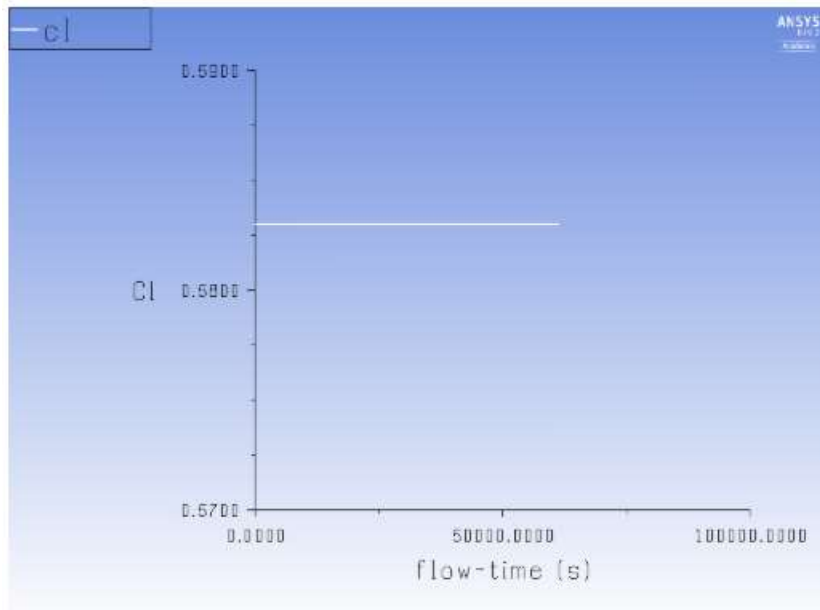
Converged Cl for A3D0.05 sample:



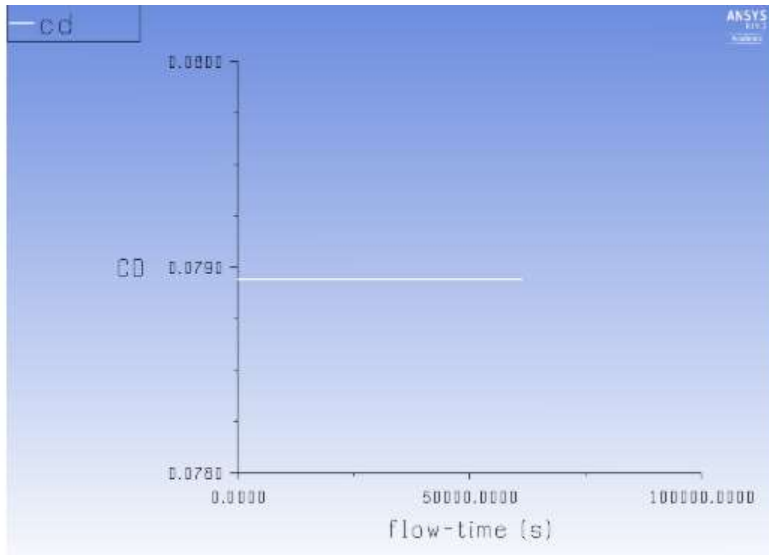
Converged Cl for A3D0.08 sample:



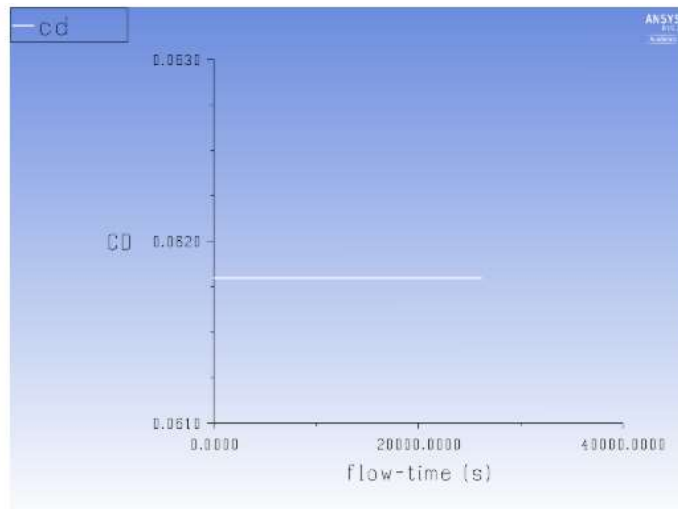
Converged Cl for A3D0.1 sample:



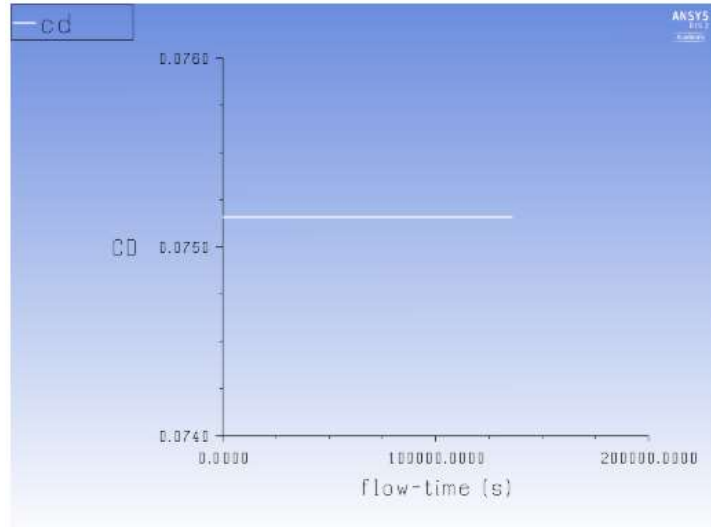
Converged Cd for unchanneled sample:



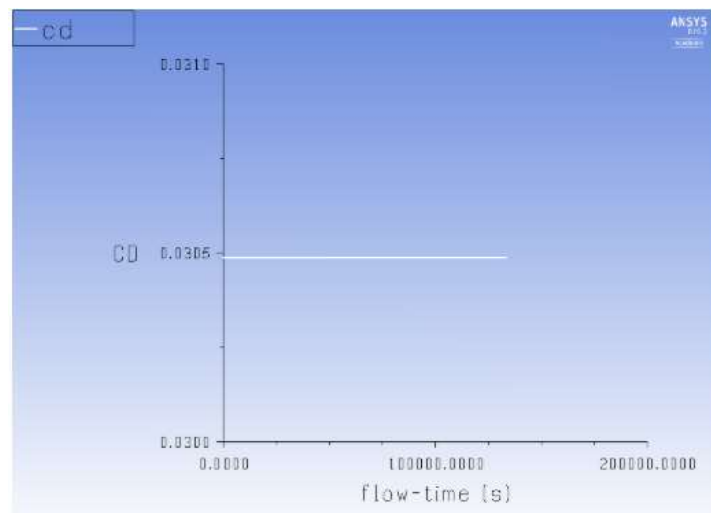
Converged Cd for A3D0.05 sample:



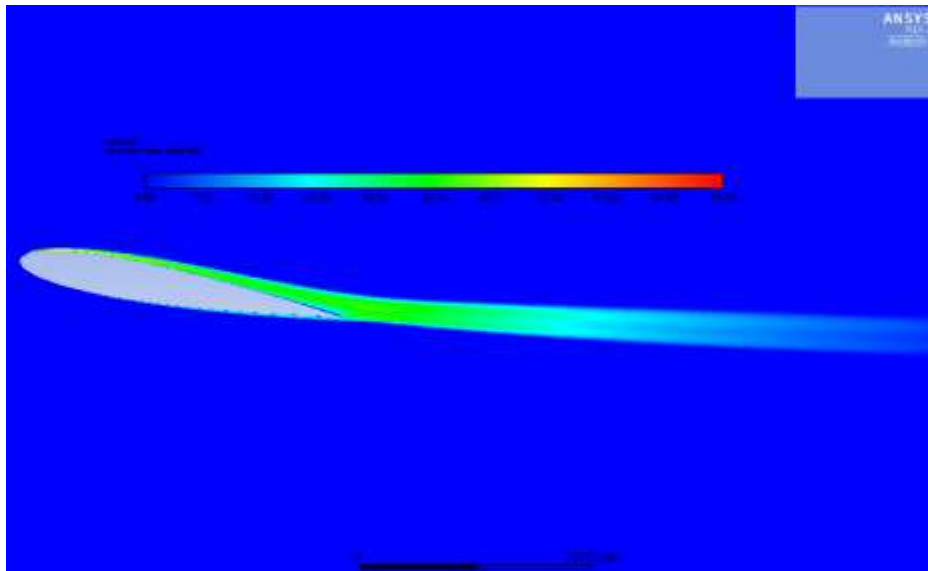
Converged Cd for A3D0.08 sample:



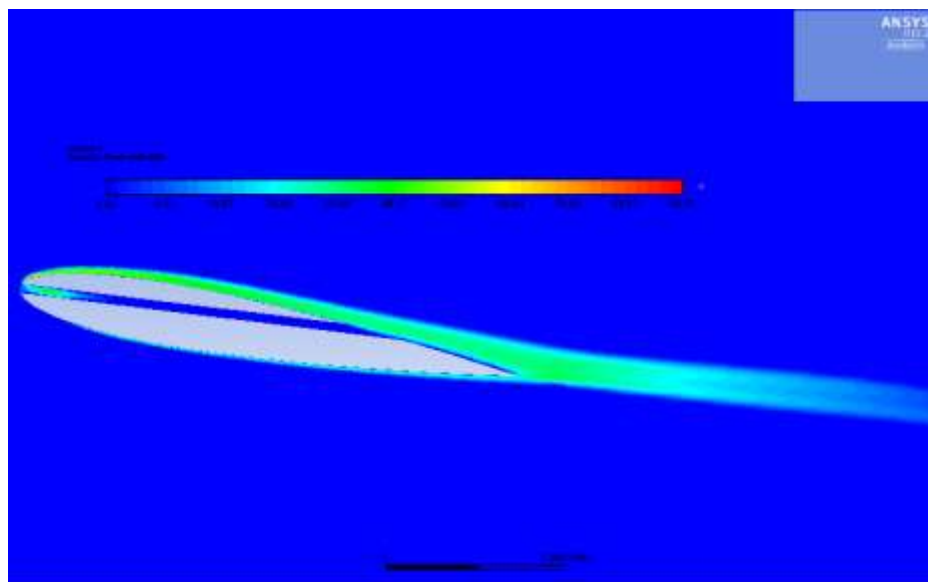
Converged CI for A3D0.1 sample:



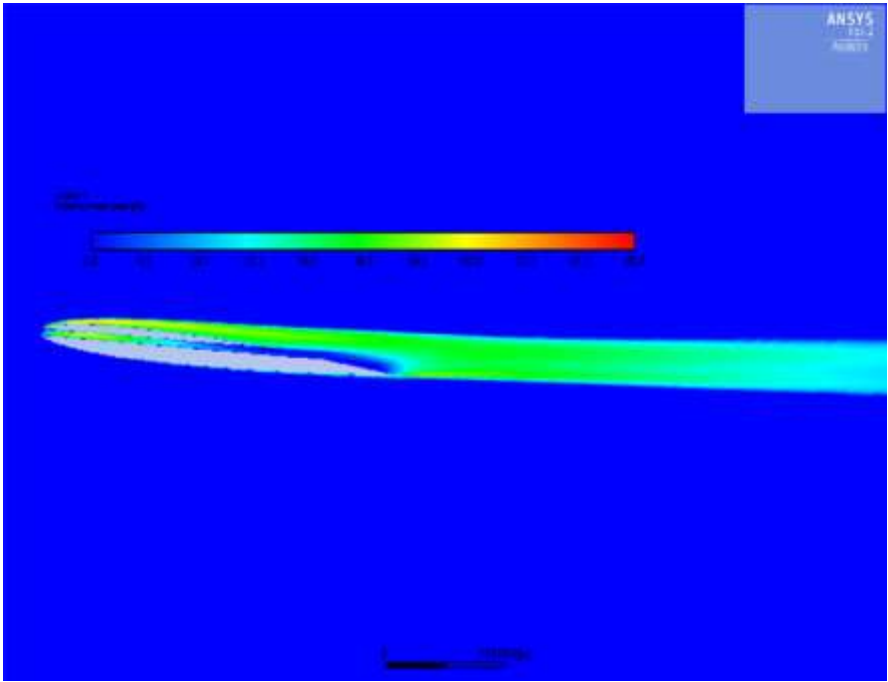
Acoustic power counter for unchanneled airfoil with flow velocity 15 m/s and 10 AOA



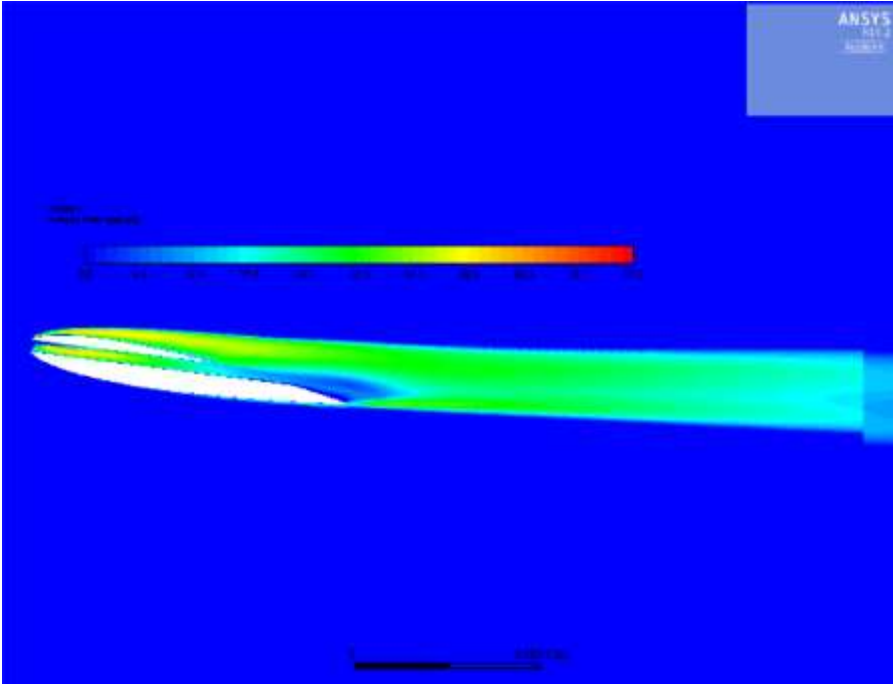
Acoustic power counter for A3 D0.05 airfoil with flow velocity 15 m/s and 10 AOA



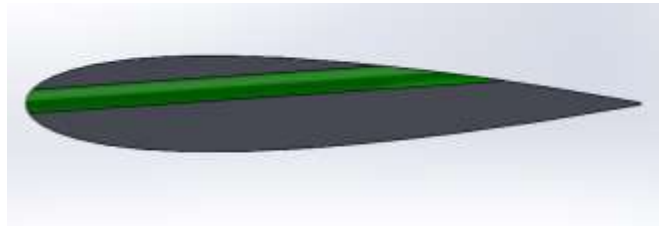
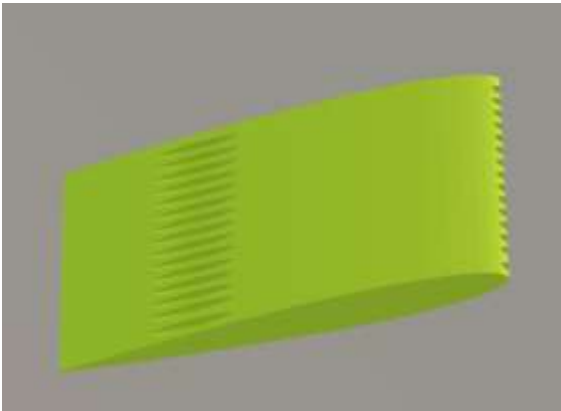
Acoustic power counter for A3 D0.08 airfoil with flow velocity 15 m/s and 10 AOA



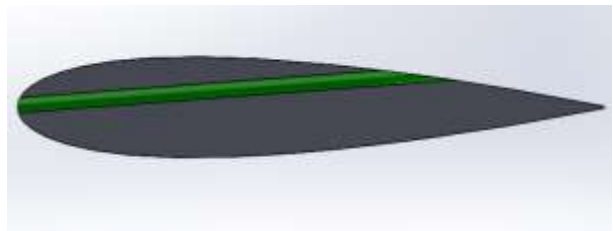
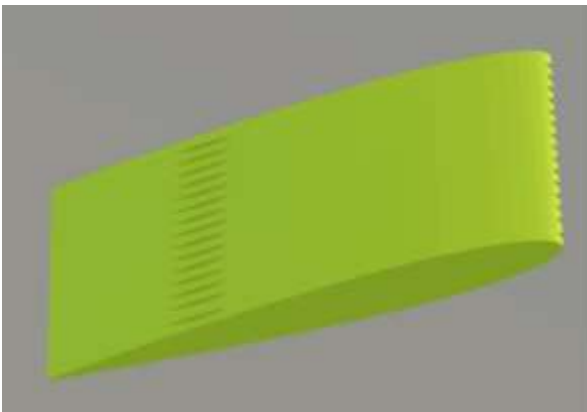
Acoustic power counter for A3 D0.1 airfoil with flow velocity 15 m/s and 10 AOA



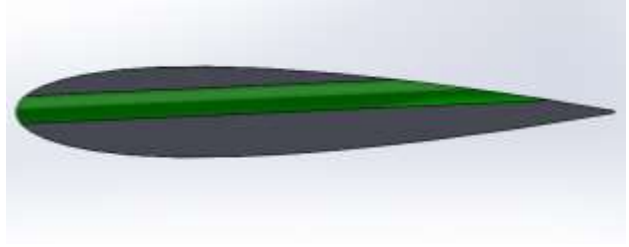
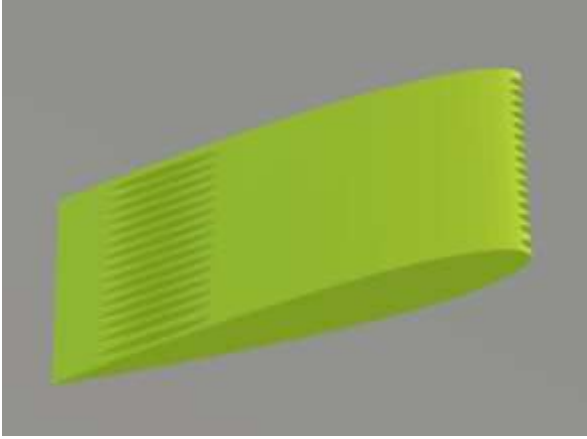
E: Airfoil design



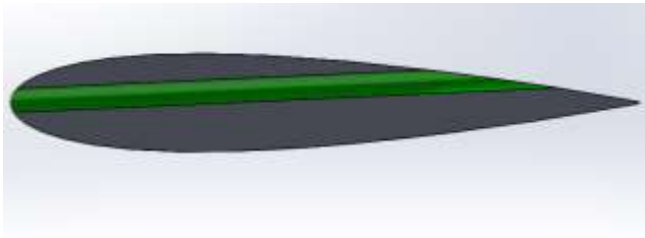
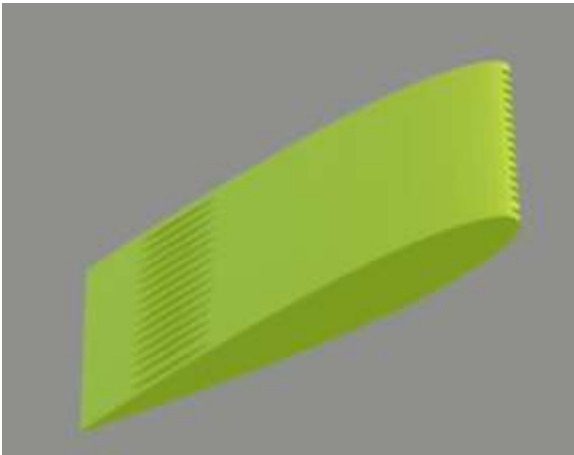
Airfoil with channel direction 3 degrees and diameter size 0.08 inch 3D and 2D views



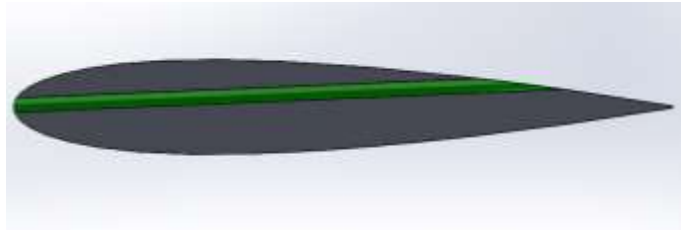
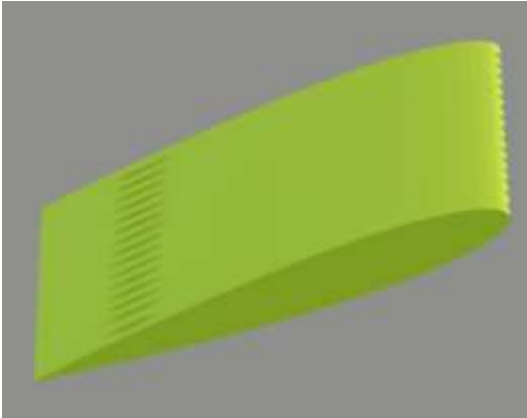
Airfoil with channel direction 3 degrees and diameter size 0.05 inch 3D and 2D views



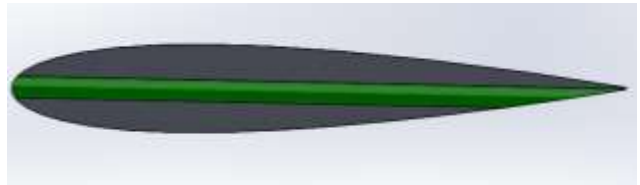
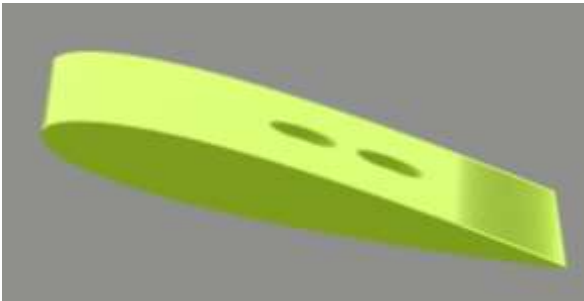
Airfoil with channel direction 2 degrees and diameter size 0.1 inch 3D and 2D views



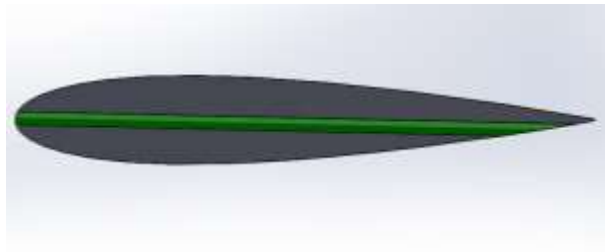
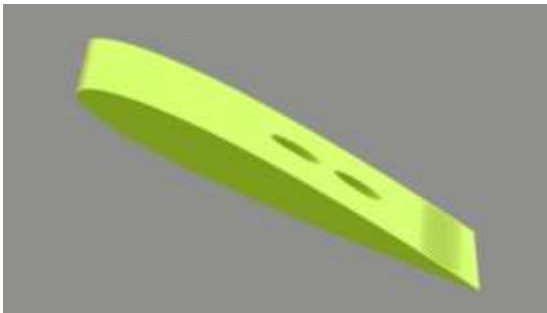
Airfoil with channel direction 2 degrees and diameter size 0.08 inch 3D and 2D views



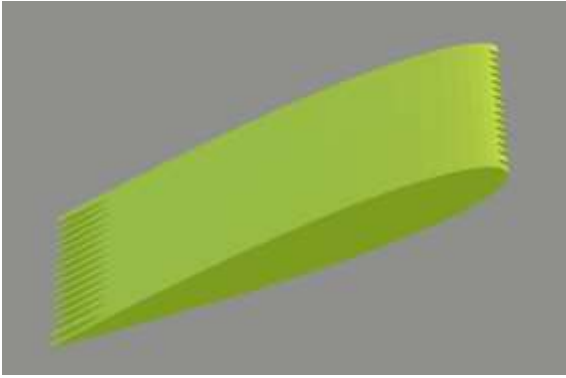
Airfoil with channel direction 2 degrees and diameter size 0.05 inch 3D and 2D views



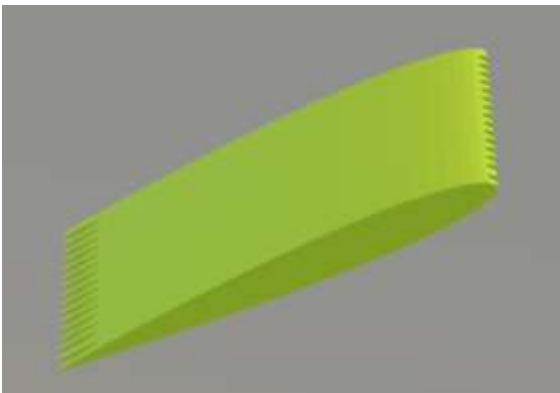
Airfoil with channel direction -1 degrees and diameter size 0.08 inch 3D and 2D views



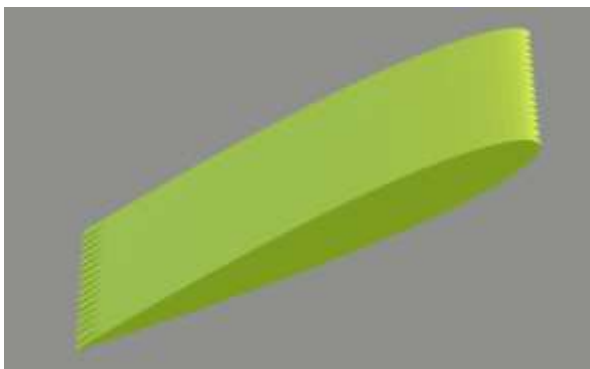
Airfoil with channel direction -1 degrees and diameter size 0.05 inch 3D and 2D views



Airfoil with channel direction 0 degrees and diameter size 0.1 inch 3D and 2D views

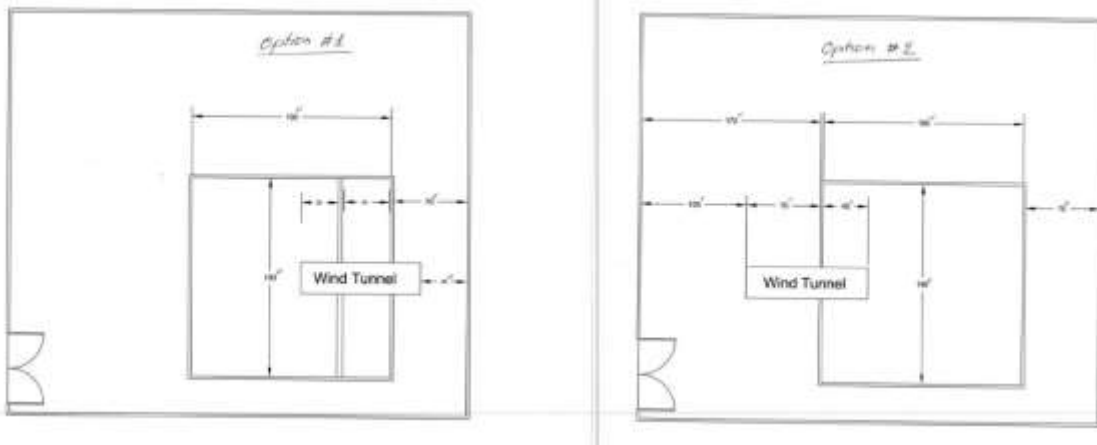


Airfoil with channel direction 0 degrees and diameter size 0.08 inch 3D and 2D views



Airfoil with channel direction 0 degrees and diameter size 0.05 inch 3D and 2D views

F: 2D design of the wind tunnel and quiet chamber



G: Arduino code

```
#include "HX711.h" //You must have this library in your arduino library folder

#define DOUT1 3
#define CLK1 2
#define DOUT2 5
#define CLK2 4
#define DOUT3 7
#define CLK3 6
#define DOUT4 8
#define CLK4 9

HX711 scaleOne(DOUT1, CLK1);
HX711 scaleTwo(DOUT2, CLK2);
HX711 scaleThree(DOUT3, CLK3);
HX711 scaleFour(DOUT4, CLK4);

//Change this calibration factor as per your load cell once it is found you many need to vary it in
thousands
float calibration_factor = 177650; //-106600 worked for my 40Kg max scale setup

//=====
//=====
//          SETUP
//=====
//=====

void setup() {
  Serial.begin(9600);
  //Serial.println("Press T to tare");
  scaleOne.set_scale(calibration_factor); //Calibration Factor obtained from first sketch
```

```

scaleOne.tare();          //Reset the scale to 0
scaleTwo.set_scale(calibration_factor); //Calibration Factor obtained from first sketch
scaleTwo.tare();          //Reset the scale to 0
scaleThree.set_scale(calibration_factor); //Calibration Factor obtained from first sketch
scaleThree.tare();
scaleFour.set_scale(calibration_factor); //Calibration Factor obtained from first sketch
scaleFour.tare();        //Reset the scale to 0
}

//=====
//
//          LOOP
//=====
void loop() {
  Serial.print("  Right Drag: ");
  Serial.print(scaleThree.get_units(), 3); //Up to 3 decimal points
  Serial.print(" volts"); //Change this to kg and re-adjust the calibration factor if you follow lbs
  Serial.print("  Left Drag: ");
  Serial.print(scaleFour.get_units(), 3); //Up to 3 decimal points
  Serial.print(" volts"); //Change this to kg and re-adjust the calibration factor if you follow lbs
  Serial.print("  Base Lift: ");
  Serial.print(scaleOne.get_units(), 3); //Up to 3 decimal points
  Serial.print(" volts"); //Change this to kg and re-adjust the calibration factor if you follow lbs
  Serial.print("  Front Lift: ");
  Serial.print(scaleTwo.get_units(), 3); //Up to 3 decimal points
  Serial.println(" volts"); //Change this to kg and re-adjust the calibration factor if you follow lbs
  if(Serial.available())

```

```
{  
  char temp = Serial.read();  
  if(temp == 't' || temp == 'T')  
    scaleOne.tare(); //Reset the scale to zero  
  //=====
```

H: Airfoil NACA0012 points from airfoil tools generator

1	0	5.5	0	0
1	1	5.4986415	0.000198	0
1	2	5.4945715	0.0007865	0
1	3	5.4877955	0.001771	0
1	4	5.4783135	0.003146	0
1	5	5.466142	0.0049005	0
1	6	5.451292	0.00704	0
1	7	5.433769	0.0095535	0
1	8	5.413606	0.01243	0
1	9	5.3908085	0.0156695	0
1	10	5.365404	0.0192555	0
1	11	5.33742	0.023188	0
1	12	5.306884	0.027445	0
1	13	5.2738235	0.032021	0
1	14	5.238277	0.036905	0
1	15	5.2002665	0.0420805	0
1	16	5.1598415	0.0475365	0
1	17	5.1170405	0.053262	0
1	18	5.071902	0.059235	0
1	19	5.02447	0.06545	0
1	20	4.974794	0.0718905	0
1	21	4.922929	0.07854	0
1	22	4.8689135	0.0853765	0
1	23	4.812808	0.0924	0
1	24	4.754662	0.099583	0
1	25	4.6945415	0.106909	0
1	26	4.632507	0.1143725	0

1	27	4.568608	0.1219515	0
1	28	4.502916	0.1296295	0
1	29	4.435497	0.1373955	0
1	30	4.3664115	0.1452275	0
1	31	4.295731	0.153109	0
1	32	4.2235215	0.1610345	0
1	33	4.1498655	0.1689765	0
1	34	4.0748235	0.176924	0
1	35	3.9984725	0.184855	0
1	36	3.920895	0.192764	0
1	37	3.842157	0.200629	0
1	38	3.762341	0.208428	0
1	39	3.6815295	0.21615	0
1	40	3.599794	0.223773	0
1	41	3.517228	0.231286	0
1	42	3.4338975	0.238667	0
1	43	3.349896	0.245894	0
1	44	3.2653005	0.252956	0
1	45	3.1801935	0.259831	0
1	46	3.0946685	0.2665025	0
1	47	3.008797	0.272943	0
1	48	2.9226725	0.279147	0
1	49	2.8363775	0.2850815	0
1	50	2.75	0.290741	0
1	51	2.6636225	0.2960925	0
1	52	2.5773275	0.3011195	0
1	53	2.491203	0.305811	0
1	54	2.4053315	0.310145	0

1	55	2.3198065	0.314094	0
1	56	2.2346995	0.3176525	0
1	57	2.150104	0.320793	0
1	58	2.0661025	0.3235045	0
1	59	1.982772	0.325765	0
1	60	1.900206	0.3275635	0
1	61	1.8184705	0.3288835	0
1	62	1.737659	0.3297085	0
1	63	1.657843	0.330033	0
1	64	1.579105	0.3298405	0
1	65	1.5015275	0.3291255	0
1	66	1.4251765	0.327877	0
1	67	1.3501345	0.326084	0
1	68	1.2764785	0.3237465	0
1	69	1.204269	0.320859	0
1	70	1.1335885	0.317416	0
1	71	1.064503	0.313423	0
1	72	0.997084	0.3088745	0
1	73	0.931392	0.303776	0
1	74	0.867493	0.298133	0
1	75	0.8054585	0.2919565	0
1	76	0.745338	0.285241	0
1	77	0.687192	0.278003	0
1	78	0.6310865	0.270259	0
1	79	0.577071	0.262009	0
1	80	0.525206	0.2532695	0
1	81	0.47553	0.244057	0
1	82	0.428098	0.2343825	0

1	83	0.3829595	0.224268	0
1	84	0.3401585	0.2137245	0
1	85	0.2997335	0.2027685	0
1	86	0.261723	0.1914165	0
1	87	0.2261765	0.1796905	0
1	88	0.193116	0.1676015	0
1	89	0.16258	0.1551715	0
1	90	0.134596	0.1424115	0
1	91	0.1091915	0.1293435	0
1	92	0.086394	0.115984	0
1	93	0.066231	0.1023385	0
1	94	0.048708	0.088429	0
1	95	0.033858	0.0742665	0
1	96	0.0216865	0.059862	0
1	97	0.0122045	0.0452265	0
1	98	0.0054285	0.0303655	0
1	99	0.0013585	0.0152845	0
1	100	0	0	0
1	101	0.0013585	-0.0152845	0
1	102	0.0054285	-0.0303655	0
1	103	0.0122045	-0.0452265	0
1	104	0.0216865	-0.059862	0
1	105	0.033858	-0.0742665	0
1	106	0.048708	-0.088429	0
1	107	0.066231	-0.1023385	0
1	108	0.086394	-0.115984	0
1	109	0.1091915	-0.1293435	0
1	110	0.134596	-0.1424115	0

1	111	0.16258	-0.1551715	0
1	112	0.193116	-0.1676015	0
1	113	0.2261765	-0.1796905	0
1	114	0.261723	-0.1914165	0
1	115	0.2997335	-0.2027685	0
1	116	0.3401585	-0.2137245	0
1	117	0.3829595	-0.224268	0
1	118	0.428098	-0.2343825	0
1	119	0.47553	-0.244057	0
1	120	0.525206	-0.2532695	0
1	121	0.577071	-0.262009	0
1	122	0.6310865	-0.270259	0
1	123	0.687192	-0.278003	0
1	124	0.745338	-0.285241	0
1	125	0.8054585	-0.2919565	0
1	126	0.867493	-0.298133	0
1	127	0.931392	-0.303776	0
1	128	0.997084	-0.3088745	0
1	129	1.064503	-0.313423	0
1	130	1.1335885	-0.317416	0
1	131	1.204269	-0.320859	0
1	132	1.2764785	-0.3237465	0
1	133	1.3501345	-0.326084	0
1	134	1.4251765	-0.327877	0
1	135	1.5015275	-0.3291255	0
1	136	1.579105	-0.3298405	0
1	137	1.657843	-0.330033	0
1	138	1.737659	-0.3297085	0

1	139	1.8184705	-0.3288835	0
1	140	1.900206	-0.3275635	0
1	141	1.982772	-0.325765	0
1	142	2.0661025	-0.3235045	0
1	143	2.150104	-0.320793	0
1	144	2.2346995	-0.3176525	0
1	145	2.3198065	-0.314094	0
1	146	2.4053315	-0.310145	0
1	147	2.491203	-0.305811	0
1	148	2.5773275	-0.3011195	0
1	149	2.6636225	-0.2960925	0
1	150	2.75	-0.290741	0
1	151	2.8363775	-0.2850815	0
1	152	2.9226725	-0.279147	0
1	153	3.008797	-0.272943	0
1	154	3.0946685	-0.2665025	0
1	155	3.1801935	-0.259831	0
1	156	3.2653005	-0.252956	0
1	157	3.349896	-0.245894	0
1	158	3.4338975	-0.238667	0
1	159	3.517228	-0.231286	0
1	160	3.599794	-0.223773	0
1	161	3.6815295	-0.21615	0
1	162	3.762341	-0.208428	0
1	163	3.842157	-0.200629	0
1	164	3.920895	-0.192764	0
1	165	3.9984725	-0.184855	0
1	166	4.0748235	-0.176924	0

1	167	4.1498655	-0.1689765	0
1	168	4.2235215	-0.1610345	0
1	169	4.295731	-0.153109	0
1	170	4.3664115	-0.1452275	0
1	171	4.435497	-0.1373955	0
1	172	4.502916	-0.1296295	0
1	173	4.568608	-0.1219515	0
1	174	4.632507	-0.1143725	0
1	175	4.6945415	-0.106909	0
1	176	4.754662	-0.099583	0
1	177	4.812808	-0.0924	0
1	178	4.8689135	-0.0853765	0
1	179	4.922929	-0.07854	0
1	180	4.974794	-0.0718905	0
1	181	5.02447	-0.06545	0
1	182	5.071902	-0.059235	0
1	183	5.1170405	-0.053262	0
1	184	5.1598415	-0.0475365	0
1	185	5.2002665	-0.0420805	0
1	186	5.238277	-0.036905	0
1	187	5.2738235	-0.032021	0
1	188	5.306884	-0.027445	0
1	189	5.33742	-0.023188	0
1	190	5.365404	-0.0192555	0
1	191	5.3908085	-0.0156695	0
1	192	5.413606	-0.01243	0
1	193	5.433769	-0.0095535	0
1	194	5.451292	-0.00704	0

1	195	5.466142	-0.0049005	0
1	196	5.4783135	-0.003146	0
1	197	5.4877955	-0.001771	0
1	198	5.4945715	-0.000786	0
1	199	5.4986415	-0.000198	0
1	0	5.5	0	0